Author:
Whiteley, Jim

Title:
Geophysical indicators of slope stability

towards improved early warning of moisture-induced landslide hazards

GEOPHYSICAL INDICATORS OF SLOPE STABILITY: TOWARDS IMPROVED EARLY WARNING OF MOISTURE-INDUCED LANDSLIDE HAZARDS

James S. Whiteley

Supervisors: J. M. Kendall, J. E. Chambers & J. Wookey

A dissertation submitted to the University of Bristol in accordance with the requirements for award of the degree of Doctor of Philosophy in the Faculty of Science

School of Earth Sciences

22/06/2022

Word count:

54.807

Abstract

Landslide hazards pose risks to human life and economic activities across the world. The evolving conditions that precede moisture-induced destabilisation can be monitored, providing early warning of slope failure. To understand the spatial and temporal subsurface heterogeneity that governs stability, tools that acquire information at the appropriate scales and resolutions are needed. Near-surface geophysical methods provide a non-invasive, rapid and spatially complete means to achieve this.

The sensitivity of seismic refraction measurements to the geomechanical properties of the ground complements the hydrogeological information acquired by electrical resistivity. I develop the application of seismic refraction as an integrated tool for hazard monitoring and ground characterisation in landslide early warning systems.

Firstly, I coordinate a 33-month monitoring campaign, comprising of 16 seismic surveys of a landslide in the UK. I address issues in time-varying landslide topography by developing a novel pseudo-time-lapse inversion approach. Analysis of the effect of topographic variations on inverted models shows that up to a quarter of the model values can contain errors of ±10%, masking genuine temporal variations in velocity of the same order. The time-series of velocity tracks the saturation content of the sliding layer at the site.

Secondly, I conduct a combined electrical resistivity and seismic refraction survey at the same landslide. Using a machine learning algorithm, I produce a ground model that identifies discontinuities of the landslide subsurface through analysing non-spatial relationships in the datasets. The model is produced without manual integration of individual inverted models by expert analysis and opinion, and provides a robust and repeatable means of slope-scale investigation of landslide structure.

Finally, I synthesise the geophysical research undertaken at the landslide, including the work in this thesis. I highlight spatiotemporal resolution, petrophysical elaboration, and remote seismic imaging capabilities as important to the continued development of landslide early warning systems.

Author’s declaration

I declare that the work in this dissertation was carried out in accordance with the requirements of the University's Regulations and Code of Practice for Research Degree Programmes and that it has not been submitted for any other academic award. Except where indicated by specific reference in the text, the work is the candidate's own work. Work done in collaboration with, or with the assistance of, others, is indicated as such. Any views expressed in the dissertation are those of the author.

Acknowledgements

This thesis was funded by a NERC GW4+ UK Doctoral Training Partnership Studentship (Grant NE/L002434/1) and the BGS University Funding Initiative (S337). I would like to acknowledge the funded extension to these grants provided by NERC due to the impact of Covid-19.

First and foremost, my sincere thanks go to my supervisors, Mike Kendall from Oxford University (formerly University of Bristol), Jon Chambers from BGS and James Wookey from University of Bristol who has filled in for Mike since his departure. From the start, working with you all has been collaborative and fun, and I am grateful for the freedom and support you afforded me to indulge in ideas and themes of my choosing for this thesis. It has been a privilege to be mentored by academics who are highly regarded in their field, but who still have the patience and enthusiasm to nurture the less-developed seedlings of ideas in to scientific output. I would also like to thank Jon for believing in my abilities enough to lobby for my continued involvement at BGS, and for sharing his eagerness for Hollin Hill and the vanilla slices at the Terrington Village Store.

My fellow BGS PhD students Mihai Cimpoiasu, Jess Holmes, Jimmy Boyd, Tom Bott, Luke Hawley-Sibbett and Title Sujitapan have made this PhD particularly enjoyable. Being part of a cohesive team of enthusiastic researchers has been a highlight; that, and the post-publication curries. I was lucky to be a student ensconced within the Shallow Geophysics team at BGS. Being in a team with such technically-diverse members who deliver consistently impactful, applied science has been both daunting and motivating, and I would like to thank Oliver Kuras, Paul Wilkinson, Phil Meldrum, Arnaud Watlet, Cornelia Inauen, Russell Swift and Harry Harrison for their professional, scientific and pastoral guidance. A special thanks goes to Arnaud Watlet, and former BGS colleague Seb Uhlemann, who between them have borne the brunt of my PhD ramblings and fumblings, and who have always made the time to help, be it with writing Python code, or sampling the best (British) beers in Malton.

I would like to thank my friends at TerraDat; my six years as part of a team of keen field geophysicists allowed me to jump straight in to acquiring data for this project in the first few weeks. I would like to especially thank Simon Hughes for his early encouragement in pursuing this PhD opportunity. Furthermore, I would not have the curiosity and drive to keep pursuing education if it weren't for my parents; your enthusiasm for lifelong learning must have rubbed off on me somewhere, although I think I'll probably stop going back to university now.

I am most grateful to those who have made this journey a pleasure in the face of occasional adversity; my wife Leila, my children, and my dog Kaepa, the latter of whom ceaselessly wagged her tail at me with an infectious enthusiasm for life. Leila, you've supported me all the way with kindness, encouragement and love, as always. It has been wonderful to have both you and our children by my side throughout this project. Watching our children, learn, try, misstep, recover, assess, retry, succeed, master, grow and beam joyously at the end of it all has been our privilege, and a reminder that we are all always learning. To my children, I hope that you will one day appreciate the wonder of the natural world, and that you never lose that sense of achievement gained from overcoming the obstacles you face. I dedicate this thesis to you.

Personal reflections

"I am not a geophysicist" was how I introduced myself to the room when I first presented part of my work from this thesis at the Symposium on the Application of Geophysics to Engineering and Environmental Problems (SAGEEP) in Oregon, US in 2019. Despite having spent the six years prior to my PhD studies working as a geophysicist for a geophysics consultancy, my background in applied environmental geology, which had very little formal academic training in the field of geophysics, had always left me feeling like I was a geologist playing with geophysics; "Far more *geo* than *physics*" I would tell people. It's not say I couldn't do my job to a high standard or that I didn't enjoy it; I would (and still do) get a genuine thrill out of processing field data in the anticipation of finding out what it might tell me (or not tell me) about the ground. It was in part a desire to remedy this 'imposter syndrome' that underpinned the decision to pursue this PhD project. The other, much larger part of that decision was driven by seeing the opportunity to marry my enthusiasm for surface processes and soil mechanics with geophysics, a well-resourced DTP scholarship, and affiliation with two prestigious centres of research. Deciding to leave a job that I enjoyed, and in my early thirties, to pursue full-time education again wasn't an easy decision. Before the PhD commenced, I had visions of myself having the freedom and funding to pursue training opportunities of my own choosing, expand my academic interests in to fringe topics that touched on slope stability and geophysics, and meet and work with people with a similar enthusiasm for learning and applied research. To say these expectations have been met would be an understatement, and I conclude this project with a sense of contentment at having made a right decision.

During my studies, I have had numerous opportunities to learn through training courses, often in far-flung and fantastic locations. In 2017, I attended the LARAM 'Landslide and Risk Assessment and Mitigation' International School for two weeks in Salerno, Italy, where I learnt the basics of landslide risk theory. It was here that I was introduced to the concept of a slope-scale early warning system, which has become a key theme in my research. In 2018, I won a place at a NERC-funded 24-hour 'Interdisciplinary Pressure Cooker Event on Risk Communication' as part of the Understanding Risk Forum in Mexico City, Mexico. The event was attended by a range of early-career researchers and professionals working in the field of disaster risk reduction, social sciences, journalism, communication and environmental sciences from across the world, and showed me how interdisciplinary science, when executed and communicated well, can be far more than the sum of its parts. Later that year, I attended the two-week iRALL 'International Research Association on Large Landslides' School in Chengdu, China, where I spent a week studying a handful of the 15,000 landslides triggered by the 2008 Wenchuan earthquake. After each of these events I have left feeling like part of a network, and am still in regular contact with many of the people I met. One of the highlights of these meetings has been the subsequent co-authorship of two publications in *Earth-Science Reviews* with two groups of highly regarded international researchers I met at these training events. In addition to course-based learning, I've expanded my skills in other areas enormously. In particular, I arrived at this project with no prior knowledge of coding, and can now manipulate open-source Python codes to process and present geophysical data, a process that I have no shame in saying was (and continuous to be) a very steep learning curve, but something that has unlocked totally new ways of working with data.

This thesis has felt like a continual work in progress (something I increasingly realise is true of most research), and I have had the opportunity to present it to many people, some willingly, some less-so, during the various stages of its evolution. Highlights have included presenting at the EGU General Assembly in Vienna, Austria in 2018, which was my first experience of a large conference, and some of the more specialist meetings such as SAGEEP in 2019, or the Near Surface Geoscience meeting in The Hague, Netherlands, also in 2019. At the AGU Fall meeting in San Francisco, US in 2019 I was able to present my work as well as co-convene a session on landslide characterisation and monitoring which was well attended and thoroughly enjoyable. The digital conferences forced by Covid-19 recently, such as the EGU General Assembly in 2020 have been less sociable, but where the social elements have been lacking the science has flourished.

One of the most enjoyable aspects of this project has been the opportunity to spend ample time at a particularly beautiful and serene landslide in North Yorkshire. Although spread over several years, the amount of time spent on Hollin Hill collecting data for this project totals over a month, and it has been fascinating to see the hillside change throughout the seasons. I feel very proud to have contributed a modest amount of research to the reams of papers, theses and reports on the site, and I have no doubt that it will continue to produce world-class interdisciplinary research for many years to come. The site has recently been instrumented with a DAS system, which was one of the technologies identified in this work as having huge potential for bridging the spatial-temporal gap in seismic monitoring. Combined with the newly installed PRIME resistivity system at the site, we are now moving ever closer to getting high spatiotemporal resolution images of the subsurface to support landslide early warning systems.

I've learnt a huge amount during this project, but perhaps the most important thing I've realised is not to do a PhD if you want to try and cure imposter syndrome. That said, after this experience developing new skills, learning new concepts and collaborating with others, I am ready to revise my introduction from SAGEEP talk; I am not *just* a geophysicist.

Contents

Figures

Tables

1 Introduction

"One obstacle to a simple definition of a 'landslide' is the erroneous assumption that a landslide is, simply, a slide of land. A similar linguistic analysis would suggest that a cowboy is a male calf."

D. M. Cruden (1991)

The Hollin Hill Landslide Observatory in North Yorkshire, UK

This thesis explores and develops novel geophysical methods as a means of characterising and monitoring slopes at risk of destabilisation by increases in ground moisture. This introductory section aims to set this research within the context of landslide risk, and the use of slope-scale early warning systems to mitigate landslide hazards. Firstly, the big picture of landslide occurrence at the global scale is presented, highlighting the need for effective and globally accessible ways of mitigating the impacts of landslide hazards. The concepts of landslide characterisation and monitoring are introduced, alongside the rationale for using geophysical methods to improve upon existing observational and intrusive approaches. In particular, two geophysical tomographic techniques, electrical resistivity (ER) and seismic refraction (SR) are identified as being of particular importance due to their sensitivity to key slope stability parameters. The basic principles of these two methods are presented, along with a discussion of the main challenges that currently inhibit their further use as a tool in slope-scale early warning systems. The presence of systematic and random errors combined with data uncertainty within geophysical approaches is one of the main areas in which improvements are required to exploit geophysical methods for slope-scale monitoring. Following this, a summary of past research undertaken in this area at a field observatory site, the Hollin Hill Landslide Observatory (HHLO), is presented, setting the research context for the work contained within this thesis. Finally, the key research questions in this thesis are posed, along with a summary of the thesis structure.

1.1 The inequality of landslide distribution, occurrence and risk

Landslides are forms of geological mass wasting that occur at a wide range of scales and speeds, in different material types and at many locations (Hungr et al., 2014). Consequently, their classification is complex and dependent on many variables (Cruden, 1991, Cruden and Varnes, 1996). Nonetheless, the common problem they present to society is that the volumes of material mobilised downslope by landslide processes pose hazards to people and infrastructure across the world. Their triggers are associated with cascading hazard chains, in particular earthquakes, intense rainfall events and floods (Gill and Malamud, 2014).

Seismically-induced landslides associated with earthquakes, volcanic activity and other sources of ground vibration are not considered in this thesis. Landslides triggered by increases in ground moisture are most commonly referred to as 'rainfall-induced' in the literature. However, the term 'moisture-induced' is used in this thesis. This term captures the concept that it is not necessarily rainfall alone that triggers landslides directly, but the complex interactions of antecedent soil moisture, infiltration patterns, and intensity and duration of rainfall, flood or snow-melt events. Moreover, the geophysical methods used to monitor slope condition discussed in this thesis are, strictly speaking, sensitive to changes in ground moisture rather than rainfall. Where the term 'rainfall-induced' is used, it is in specific reference to sources or datasets that use this term. Unless specified otherwise, the landslides discussed in this thesis are moisture-induced.

In the past, the number of fatalities associated with landslides globally has been severely underestimated, often due to the attributing of deaths to the triggering event (e.g., earthquake, tropical storm) rather than the landslide itself (Froude and Petley, 2018, Kirschbaum et al., 2015, Petley, 2012). In part to address this underreporting, and with a focus on landslides triggered by rainfall events, NASA's Global Landslide Catalog (GLC) is a global landslide inventory which semi-automatically records literary and real-time reports of landslide events

(Kirschbaum et al., 2010, Kirschbaum et al., 2015) (Figure 1.1). The GLC is supplemented by the Cooperative Open Online Landslide Repository (COOLR), which comprises of entries of landslide events submitted by the public (Juang et al., 2019). The GLC and COOLR list 13,050 landslide events with known dates (and an additional 1476 events with no known date) ranging between 1915 and 2021, with a total of 63,566 recorded fatalities (complete entries for 2019 – 2021 had not been updated by NASA in to the GLC at the time of writing).

Figure 1.1: Global occurrences of fatal and non-fatal landslides triggered by increased ground moisture as recorded in the Global Landslide Catalog (GLC) and Cooperative Open Online Landslide Repository (COOLR) until 2019 (Kirschbaum et al., 2010). Source: Esri, Maxar, GeoEye, Earthstar Geographics, CNES/Airbus DS, USDA, USGS, AeroGRID, IGN, and the GIS User Community.

The number of landslides and associated fatalities vary significantly across years, in part due to the continued reporting omissions associated with a catalogue operating at a global scale (van Westen et al., 2006), but also due to temporal variability in landslide occurrence (Figure 1.2). Nevertheless, data in the GLC and COOLR indicates an average of 2.5 people have been killed per reported rainfall-induced landslide globally between 2010 and 2020; even in years with fewer fatalities, the rate of deaths per rainfall-triggered landslide remains above 1. When landslides triggered by earthquakes are also included, they are shown to be responsible for 17% of all deaths associated with natural hazards (Lacasse et al., 2005).

The spatial distribution and temporal occurrence of rainfall-induced landslide hazards are not distributed evenly across the planet, which is a natural function of i) the geological and geographical characteristics of the Earth's surface, and ii) predisposition of these areas to the meteorological conditions and occurrence of the conditions that trigger landslides. Moreover, within these landslide susceptible areas, the risks to human health and

economic activities presented by these hazards are also not distributed equally. Data in the GLC from 1988 to 2016 shows that countries that are less economically developed according to the Organisation for Economic Co-operation and Development (OECD) experience higher rates of fatalities associated with landslides (Figure 1.3). In nations that the OECD describes as 'least developed', there are on average 7.9 deaths per landslide recorded in the GLC; conversely, in OECD member countries, one death is recorded for every four landslide events. The disparities in reporting of landslide events between countries are known, if not well expressed within the GLC and COOLR datasets; many OECD member countries have well-established and organised landslide databases, such as in the UK (Pennington et al., 2015) and US (Spiker and Gori, 2003). Conversely, developing countries may have no such reporting system, and instead the visibility of major landslide events in the GLC is dependent on a minimum threshold of magnitude and number of fatalities that may draw public and media attention to major events.

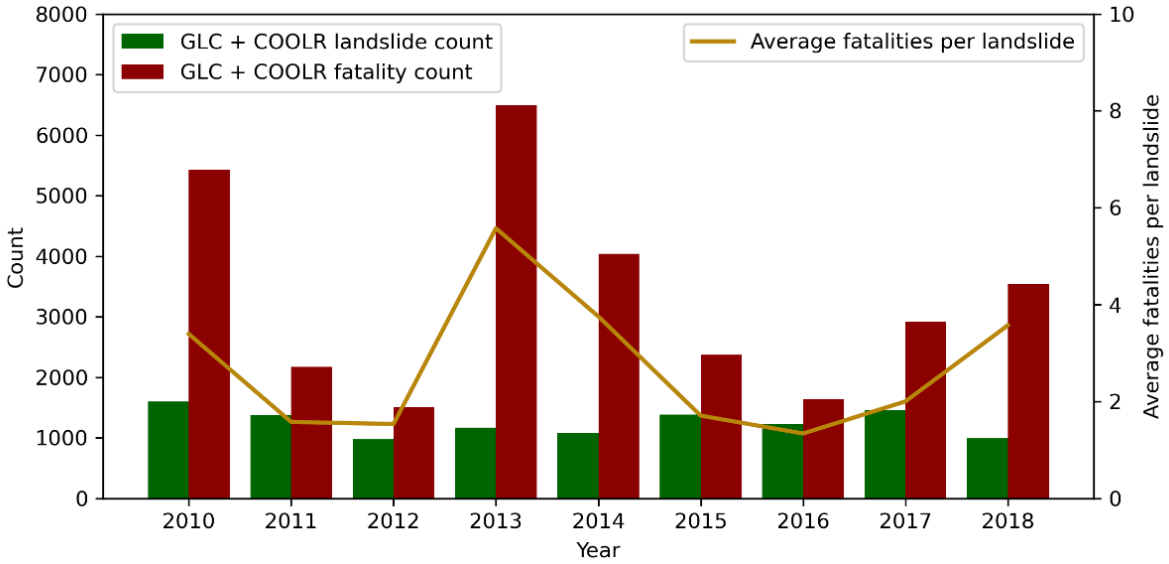

Figure 1.2: Annual counts of landslide occurrences and associated fatalities from the GLC and COOLR between 2010 and 2018 (Juang et al., 2019, Kirschbaum et al., 2010).

In addition to their immediate threat to life, economic losses caused by landslides are significant (Dilley, 2005). A summary by Klose et al. (2016) shows that annual economic losses caused by landslides is in the region of USD$ 20 billion, equivalent to approximately 17% of the total annual economic losses caused by natural hazards worldwide. The impacts of a changing climate are set to usher in greater uncertainties surrounding the timing and magnitude of landslide events, with potential greater losses of life and economic costs associated with landslide hazards in the future (Dijkstra and Dixon, 2010, Gariano and Guzzetti, 2016).

Regardless of whether slope failures threaten life, infrastructure or economic activities, landslides are a significant global hazard that require investigation and mitigation to protect many and various elements at risk from damage and harm. Mitigation of landslide hazards at the slope-scale tends to come in two forms; reduction of the intensity or frequency of the landslide hazard through intervening engineering approaches, or reduction of

the vulnerability of an element at risk, typically by increasing resilience and preparedness (Pecoraro et al., 2019). In either scenario, geoscientific knowledge of the landslide underpins assessment of risk and contributes to informed decision-making when designing and implementing effective mitigation strategies. This thesis looks to develop novel, low-cost and non-intrusive geophysical methodologies for use in early warning systems operating at the slope-scale, henceforth referred to as Local Landslide Early Warning Systems (LoLEWS).

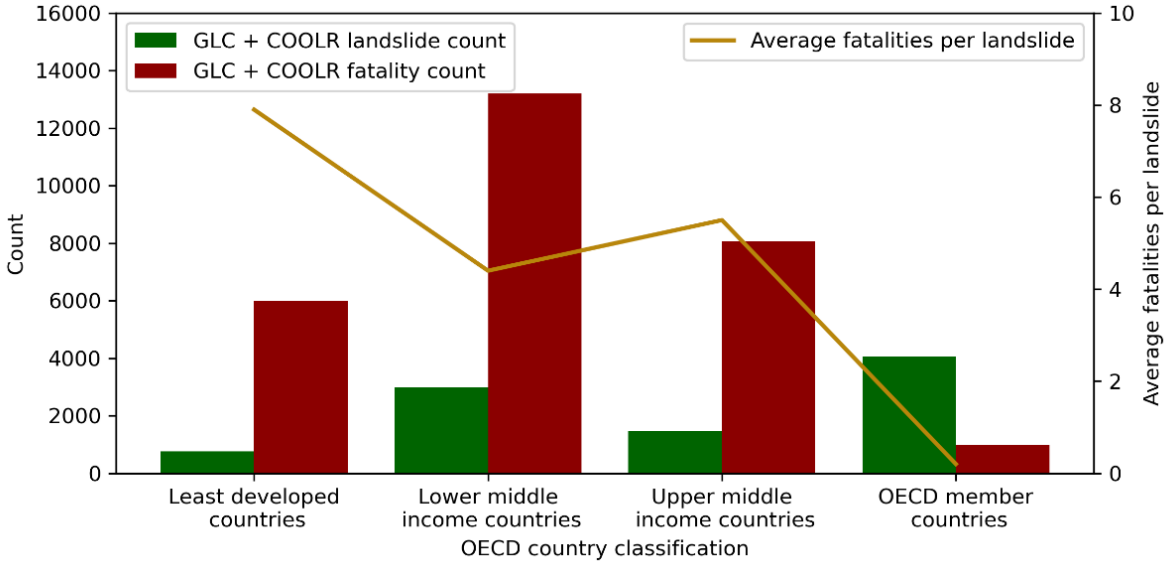

Figure 1.3: Counts of landslide events and fatalities recorded in the GLC and COOLR between 1988 and 2016, classified according to OECD economic designations.

1.2 Landslide characterisation and monitoring for early warning of failure

In order to determine an effective mitigation strategy for a single landslide, the kinematics, hydrology and environmental conditions contributing to slope failure conditions must be understood through site investigation and monitoring studies (Angeli et al., 2000, van Asch et al., 2007b). This is typically achieved using combinations of desk studies and site walkovers (e.g., Jenkins et al., 2005), remotely sensed surface observations (e.g., Handwerger et al., 2013), sensor installations (e.g., Uhlemann et al., 2016b), and subsurface geotechnical observations and measurements (e.g., Agostini et al., 2014). Given that landslides are complex, heterogeneous subsurface features that can react rapidly to variations in environmental conditions, the use of these landslide assessment methods, or even combinations thereof (e.g., Rabby and Li, 2019), may not provide information at the appropriate resolutions and scales. For example, temporal features such as the initiation of surface displacements may not be captured by sporadic site walkovers or from remotely sensed satellite observations, with the latter still tending to offer revisit times of several days or longer (Bovenga et al., 2018, Wasowski and Bovenga, 2014). Conversely, sensor installations or intrusive investigations may not provide detailed information at the spatial scale required to provide a more complete geoscientific understanding of the subsurface without the need for interpolation of sparse data.

The need to understand the processes driving landslide failure at the appropriate spatiotemporal resolutions is imperative when developing an understanding of a landslide system. It is even more crucial when implementing a mitigation approach that places the monitoring of an unstable slope at the centre of an effort to warn of, or even predict, possible future landslide failures (Intrieri et al., 2012). Such LoLEWS are an increasingly common means of mitigating the risk of future landslide events. This is primarily due to their reduced cost of operation and potential for allowing cost-effective implementation of pre-failure mitigation works, which are typically much less costly than post-failure remediation (Glendinning et al., 2009, Pecoraro et al., 2019) or issuing an early-warning of impending failure (Intrieri et al., 2013).

Typically, operational LoLEWS tend to measure deformation and rainfall as the main inputs from which to establish conditions of failure, and issue subsequent warnings (Pecoraro et al., 2019). However, there can be poor relationships between rainfall and landslide initiation from increased saturation, due to the poorly understood impacts of evapotranspiration and preferential infiltration (Bogaard and Greco, 2016, Bogaard and Greco, 2018). Additionally, slope displacement may only become measurable once a landslide has moved toward a critical state of failure. For LoLEWS to provide meaningful lead times from warning to landslide failure, thresholds at which failure occurs need to be established, based on a holistic understanding of landslide stability. This necessitates a comprehensive understanding of the subsurface conditions and processes preceding failure.

1.2.1 Landslide characterisation using geophysical tomography

It is therefore appropriate to look for tools that can provide subsurface information at the spatiotemporal resolutions at which processes driving landslides occur. Near-surface geophysical techniques, in particular tomographic methods, have long been recognised as being beneficial for landslide investigations due to their ability to acquire subsurface data rapidly, non-invasively and at high spatial resolutions (Hack, 2000, Jongmans et al., 2009, McCann and Forster, 1990). Tomographic geophysical techniques (i.e., methods that image the ground in section) are particularly useful for the investigation of heterogeneous subsurface environments (Hack, 2000, Jongmans and Garambois, 2007, Pazzi et al., 2019, Perrone et al., 2014, Schrott and Sass, 2008). Measurements of this kind are typically made in 2D as cross-sections, and individually acquired 2D sections can be compiled to create 3D fence diagrams (e.g., Bichler et al., 2004, Uhlemann et al., 2016a) or volumetric models of the subsurface (e.g., Friedel et al., 2006). Alternatively, 3D measurements can be made by more extensive array deployments in order to acquire measurements in several orientations across a site (e.g., Bièvre et al., 2021, Chambers et al., 2011, Samyn et al., 2012). With these array-based approaches, the spatial resolution of measurements is controlled by the spacing between the individual sensors in an array for 2D measurements, and by the distance between individual arrays for 3D measurements.

Until fairly recently, the main application of geophysical tomography to landslide investigations was for the production of high spatial resolution geophysical models. Typically, the aim of these surveys was the reconnaissance of newly investigated landslides (e.g., Bichler et al., 2004), or to provide subsurface data between geotechnical investigation locations (e.g., Merritt et al., 2013). Such geotechnical investigations typically provide a small number of detailed observations and measurements, between which information must be extrapolated or inferred. Geophysical surveys are typically used to characterise the landslide in terms of its lithology, structure

and hydrology. In reconnaissance surveys, detailed knowledge is typically less of a focus of the survey; instead, the aim is the establishment of a broad baseline of geological understanding from which decisions about the use of more detailed and targeted investigations can be made (Gunn et al., 2013, McCann and Forster, 1990, Rahimi et al., 2021). In more detailed surveys, the geophysical models can be compared to and calibrated with geotechnical observations, in order to extrapolate known material properties or hydrological conditions across the subsurface (e.g., Boon et al., 2015).

1.2.2 Landslide monitoring using geophysical tomography

A major development in the field of landslide geophysics has been the implementation of repeated data acquisition to produce time-lapse geophysical models of the subsurface (e.g., Jomard et al., 2007, Lehmann et al., 2013, Springman et al., 2013, Supper et al., 2014, Travelletti et al., 2012). With this development, landslide geophysics has moved from primarily bringing benefits in the acquisition of high spatial resolution information (i.e., characterisation), to providing temporal resolution too (i.e., monitoring) (Perrone et al., 2014). For the purposes of monitoring landslides at risk of failure, geophysical techniques can broadly be split into two groups; those with high temporal resolution, and those with high spatial resolution. Passive seismology is the predominant high temporal resolution geophysical method used for monitoring landslides. In a typical deployment, near-continuous seismic waveforms are recorded from a sparse number of sensors deployed across a landslide surface (Brückl et al., 2013, Le Breton et al., 2021, Walter et al., 2013). Although the cost and power demands of passive seismic sensors is decreasing, the number of seismometers deployed is typically limited by financial and logistical costs, which in turn limits the spatial resolution of the array despite offering near-continuous temporal monitoring.

On the other hand, high spatial resolution geophysical methods acquire data using dense 2D or 3D sensor arrays in which many measurements are acquired during a single deployment. The main aim in high spatial resolution geophysical methods is to produce images of the subsurface. Acquiring repeated measurements using high spatial resolution geophysical methods can produce time-lapse images of the subsurface, providing a means of both characterising a landslide system, and monitoring its changes over time. Due to the large number of readings required to acquire a complete dataset from which an image of the subsurface can be produced, high spatial resolution methods tend to have lower temporal resolution than high temporal resolution methods; conversely, images produced from high temporal resolution methods (e.g., using methods such ambient noise tomography) tend to have lower spatial resolution.

The development of high spatial resolution geophysical monitoring approaches for landslide applications has occurred relatively recently and at pace, initially stemming from practice of acquiring repeated measurements in the field using mobile equipment with large time periods between surveys (e.g., Bièvre et al., 2012, Friedel et al., 2006). More recently, this has evolved in to the development of bespoke geophysical systems designed to be permanently deployed in the field, with remote access to the system to program schedules and retrieve data facilitated by telemetry (e.g., Holmes et al., 2020, Kuras et al., 2009, Supper et al., 2012, Tresoldi et al., 2020). These developments have mainly occurred in the field of electrical resistivity (ER) studies, in part owing to the

sensitivity of ER measurements to changes in subsurface hydrology that are known to drive slope destabilisations, but also due to the ease in automating ER measurements and systems.

The success of ER applied to monitoring landslides has paved the way for similar innovations in other methods. Seismic refraction (SR), which can produce P- and S-wave velocity models of the subsurface, presents a logical next target for time-lapse implementation for landslide monitoring. The two main reasons for this are: i) seismic velocities are sensitive to the elastic (i.e., mechanical) properties of materials which is one of the main parameters governing slope stability (Terzaghi, 1943), and ii) they are acquired with comparable array geometries and spatial resolutions to ER measurements. This presents opportunities for SR measurements to be integrated with ER measurements, reducing uncertainty in the interpretation of results (e.g., Bièvre et al., 2012, Grandjean et al., 2009).

The recent developments in geophysical monitoring not only provide opportunities for providing better spatial and temporal understanding for the planning and implementation of mitigation strategies, they also open the door for geophysical monitoring to become part of the mitigation solution itself (Holmes et al., 2020). The contribution that ER monitoring has made to slope stability assessment and mitigation is significant despite the nascence of the field. The concurrent development of other geophysical monitoring strategies, such as SR, can only bring further benefits in the form of reduced uncertainties in interpretation. Using multiple geophysical methods provides multiple lines of evidence for the changing conditions of the subsurface that may precede a slope failure.

Consequently, the development of low-cost, non-invasive geophysical monitoring methods for integration into LoLEWS stands to make a real contribution to reducing the impact of landslide hazards across the world. Hence, one aim of this thesis is to develop SR as a monitoring tool for understanding landslide processes. However, in order for a novel methodology to have utility in real-world applications, understanding of the method and its associated errors and uncertainties is required.

1.3 ER and SR surveying

ER and SR are the most common tomographic techniques used to investigate the character of landslides (Hack, 2000, Jongmans and Garambois, 2007, Pazzi et al., 2019). In ER surveys, an array of electrodes is deployed along the ground surface, typically with a regular spacing between electrodes. In SR surveys, geophones are used instead of electrodes. In 2D surveys, the electrode or geophone array tends to comprise of a single linear deployment, while 3D surveys comprise several parallel lines forming a grid. However, parallel lines of 2D acquired data can be processed simultaneously to produce 3D models of the subsurface. The similarity in survey deployment between ER and SR makes them well suited to co-located data acquisition and interpretation.

1.3.1 Principles of ER surveying

The aim of ER surveying is to produce a resistivity model of the subsurface. Apparent resistivity (ρ_a) measurements are made by injecting a current (I) in to the subsurface and measuring potential (i.e., voltage) difference (ΔV) (Kearey et al., 2001). For flat, homogenous ground, this is given by

$$\rho_a = k\frac{\Delta V}{I} \qquad \text{Equation 1.1}$$

where k is a geometric factor dependent on the arrangement of the injection (source and sink) electrodes relative to the potential electrodes (Figure 1.4). These arrangements are referred to as electrode arrays, and have different spatial sensitivities, depths of penetration and vertical and lateral resolution, suited to different aims of investigation (Dahlin and Zhou, 2004, Szalai and Szarka, 2008). The most common of these electrode arrays include the Wenner, Wenner-Schlumberger, Pole-Dipole, Dipole-Dipole, Pole-Pole, and Multiple Gradient arrays (Figure 1.4). Most ER surveys tend to utilise four-point (i.e., quadrupole) measurements (i.e., the Wenner, Wenner-Schlumberger, Dipole-Dipole and Multiple Gradient arrays).

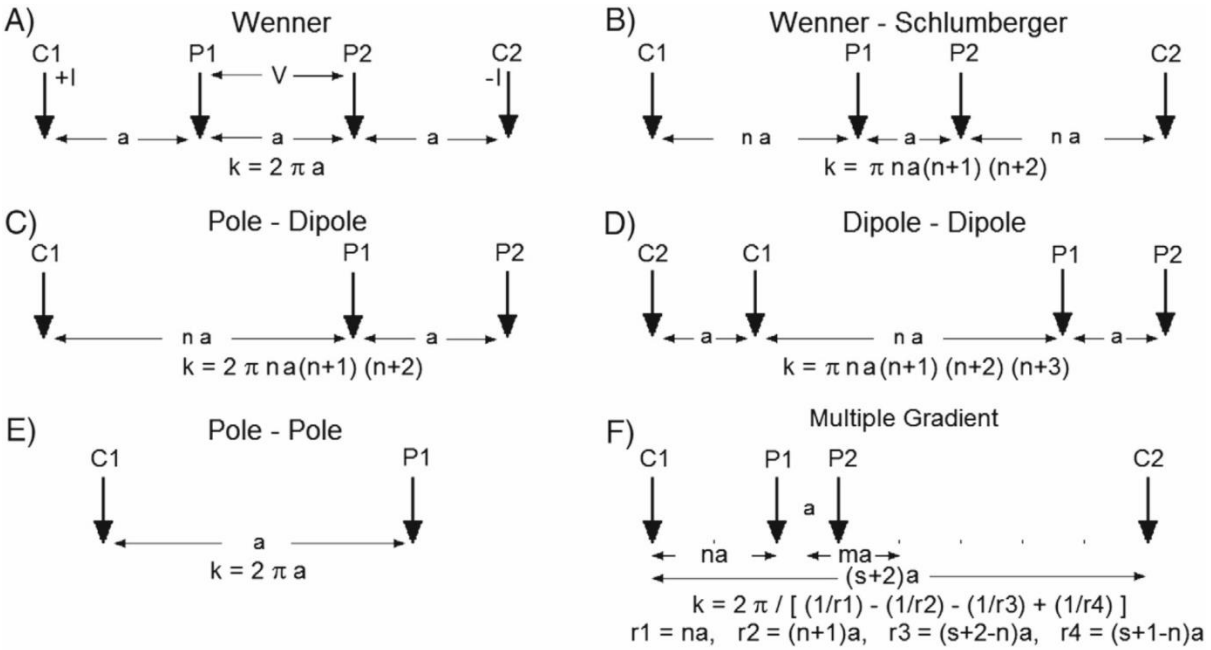

Figure 1.4: Common electrode arrays used in electrical resistivity surveying, showing the relative positons of the current electrodes (Cx), potential electrodes (Px) and the electrode separation (a) used to calculate the geometric factor (k). Modified from Loke et al. (2013).

Current propagates through the subsurface via electronic, dielectric and electrolytic conduction. Electronic conduction occurs in conductive materials that contain free electrons, such as native metals and graphite. Dielectric conduction occurs where the electrons of a poor conductor are marginally displaced relative to their nuclei, separating the positive and negative charge, producing an electrical current. In the majority of cases,

electronic and dielectric conduction play little or no role in the propagation of current through the subsurface. As the majority of soil and rock minerals are insulators or poor conductors, electrical current is transmitted through electrolytic conductivity via ions contained within pore waters. Of all the common near-surface geophysical techniques, the resistivity of materials shows the greatest range relative to other properties, varying over 20 order of magnitude (Table 1.1) (Merritt, 2014, Telford et al., 1990).

Table 1.1: Resistivity values of common geological materials (after Telford et al., 1990)

Common rock types	**Resistivity range (Ωm)**
Granite porphyry	$4.5x10^3$ (wet) - $1.3x10^6$ (dry)
Gabbro	10^3 - 10^6
Slates	$6x10^2$ – $4x10^7$
Consolidated shales	20 – $2x10^3$
Conglomerates	$2x10^3$ - 10^4
Sandstones	1 – $6.4x10^8$
Limestones	50 – 10^7
Unconsolidated wet clay	20
Clays	1 - 100
Common sedimentary rocks at specific moisture contents	**Resistivity value (Ωm)**
Siltstones (54% water)	$1.5x10^4$
Siltstones (38% water)	$5.6x10^8$
Coarse sandstone (39% water)	$9.6x10^5$
Coarse sandstone (18% water)	10^8
Medium sandstone (100% water)	$4.2x10^3$
Medium sandstone (10% water)	$1.4x10^8$

In addition to the dissolved salts in pore waters that conduct current efficiently, certain mineral crystals sorb ions on to their surface in an exchangeable state. The Electrical Double Layer surrounding a mineral particle comprises the Stern Layer (containing water molecules and oppositely charge ions) and the Electrical Diffuse Layer (made up of partially mobilised ions). In particular, the plate-like structure of clay minerals provides a large surface area on which ions and water molecules can be sorbed. Current is transmitted through the mobile ions contained in the Electrical Double Layer, providing a second means of electrolytic conduction in addition to current transmission through pore fluids. Hence, soils and rocks with higher clay-mineral contents have lower bulk apparent resistivity than clay-mineral deficient materials.

In two-dimensional multi-electrode surveys, electrodes (typically metal spikes) are deployed at shallow (10 – 20 cm) depths along the ground surface at a uniform spacing. A resistivity meter connected to the electrodes via multi-cored cable controls the injection of current, measuring the potential difference according to a pre-determined measurement schedule designed for the needs of the survey. For a typical deployment of several tens of electrodes, several hundreds of measurements using different positional combinations of injection and potential electrodes can be made to build up a 2D pseudo-section of apparent resistivity. Some electrode arrays, including the Dipole-Dipole and Multiple Gradient arrays are suitable for use with multi-channel systems, where the current is injected through a pair of electrodes and the arising field measured by multiple combinations of potential electrode arrangements, which can decrease surveying time.

In a homogenous medium, the distribution of current flow paths create hemispheric equipotential surfaces (Figure 1.5). However, variations in the resistivity of soils and rocks caused by changes in pore fluid composition and quantity, porosity and clay-content cause perturbations in the electric field. Hence, the measurement of resistivity from a quadrupole can only be considered a bulk measurement of resistivity at that point in the ground. It is for this reason that the measurements made in ER surveys are referred to as 'apparent' resistivity. Field measurements of apparent resistivity are typically repeated and averaged (a process called stacking) to reduce the impact of background noise and improve the signal-to-noise ratio. The resulting apparent resistivity data are inverted to produce a modelled profile of resistivity distribution (see Chapter 1.3.4 for more detail on data inversion).

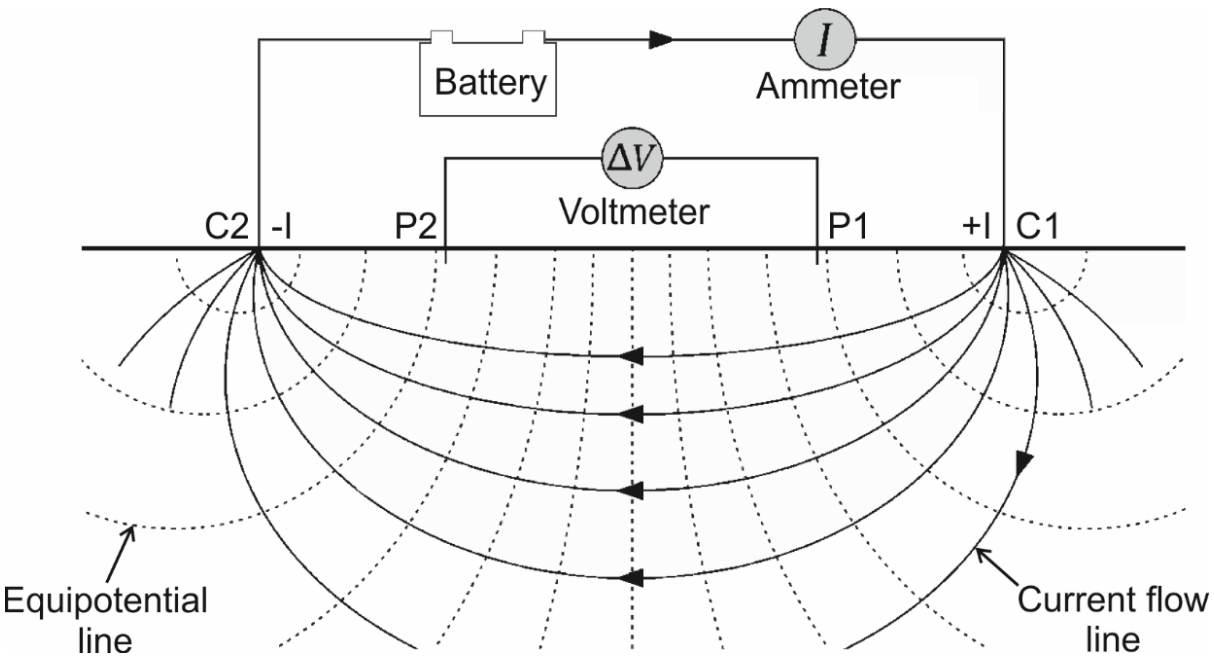

Figure 1.5: Current flow lines and equipotential lines arising from current injection in to the subsurface during an electrical resistivity survey. Modified from Binley and Slater (2020).

1.3.2 Principles of SR surveying

The aim of SR surveying is to produce velocity models of primary (also known as pressure waves, or P-waves) and secondary (also known as shear waves or S-waves) waves. When a stress is applied to the ground,

corresponding strain propagates from the source in the form of elastic waves. P-waves propagate this stress via particle compression and dilation in the direction of propagation. Hence, the volume of the material must change to propagate this elastic wave energy. In contrast, S-waves propagate stress via shear deformation orientated perpendicularly to the direction of propagation, and no volumetric change is required to propagate the wave. In either case, seismic waves lose energy through geometric spreading (i.e., loss of energy density due to an expanding wavefront), energy partitioning at boundaries, energy absorption and scattering. The latter two effects are frequency dependent.

In a homogenous medium with no boundaries, a wavefront radiates away from the source in a straight line. According to Huygen's principle, all points on a propagating wavefront are themselves sources of elastic energy from which waves propagate (Baker and Copson, 2003). When seismic waves encounter boundaries between layers with different velocities, some wave energy will be reflected toward the surface, and some wave energy may refract into the underlying layer depending on the angle of incidence of the wave. Whether a wave refracts, and the subsequent angle of refraction, is determined by Snell's Law (Mavko et al., 2020), which in terms of velocity is given as

$$\frac{\sin(\theta_1)}{V_1} = \frac{\sin(\theta_2)}{V_2} \qquad \text{Equation 1.2}$$

where θ_1 is the angle of incidence, V_1 is the velocity of the incident wave, θ_2 is the angle of refraction, and V_2 is the velocity of the refracted wave. Waves propagating from a single source will arrive at a boundary with different angles of incidence. However, SR exploits the waves that arrive at a boundary at a 'critical angle', that is, the angle at which refracted waves travel perpendicularly to the boundary, returning wave energy to the surface in the process. The path these waves travel along is known as the critically refracted ray path. This energy is collectively called the head wave, and is the wave that takes the least time to travel from source back to the surface (Figure 1.6). Waves arriving at a boundary with a super-critical angle will reflect toward the surface, whereas waves that arrive at the boundary with a sub-critical angle with refract in to the lower layer but with angles shallower than that of the boundary. However, these sub-critical rays may strike deeper boundaries at a different critical angle, consequently refracting head waves back to the surface. As shown by Snell's Law, accurate velocities cannot be recovered where the underlying layer is faster than the overlying layer, as the wave is refracted away from the boundary. This phenomena is known as a velocity inversion (Whiteley and Greenhalgh, 1979). Similarly, refracted waves may not arise at boundaries between layers with similar velocities, resulting in a hidden layer. The presence of velocity inversions and hidden layers are the main subsurface conditions that inhibit successful SR surveys.

P- and S-wave energy is recorded by deploying linear arrays of geophones along the ground surface. A controlled seismic source, typically a sledgehammer and plate, is used for shallow (i.e., top 30 m) engineering applications. A trigger system, activated when the hammer strikes the plate, results in a digital seismograph recording seismic signals from the geophone array at a pre-defined recording length and sampling frequency. The recorded file is known as a shot gather. The first energy recorded by the geophones is typically the critically refracted head wave, although direct waves can also be recorded at small source-geophone offsets, or if layers have similar velocities. The number of shot locations and their spacing depends on the required spatial detail required in the final model; to map broad structures in simple settings (e.g., identifying depth to bedrock in horizontally bedded units with

high seismic velocity contrast) only a few shots may be required to model the subsurface. In complex environments, with significant lateral or vertical heterogeneity, closer spaced shots are often required. Shots are typically repeated, and the shot gathers combined in a process called stacking. As the zero-time for each shot gather is the same (i.e. the point of hammer impact), the repeated seismic signals are easier to identify against transient background noise, improving the signal-to-noise ratio. Stacking can not only overcome issues with background noise at small source-geophone offsets, but can improve the identification of seismic wave energy at large source-geophone offsets even in quieter environments.

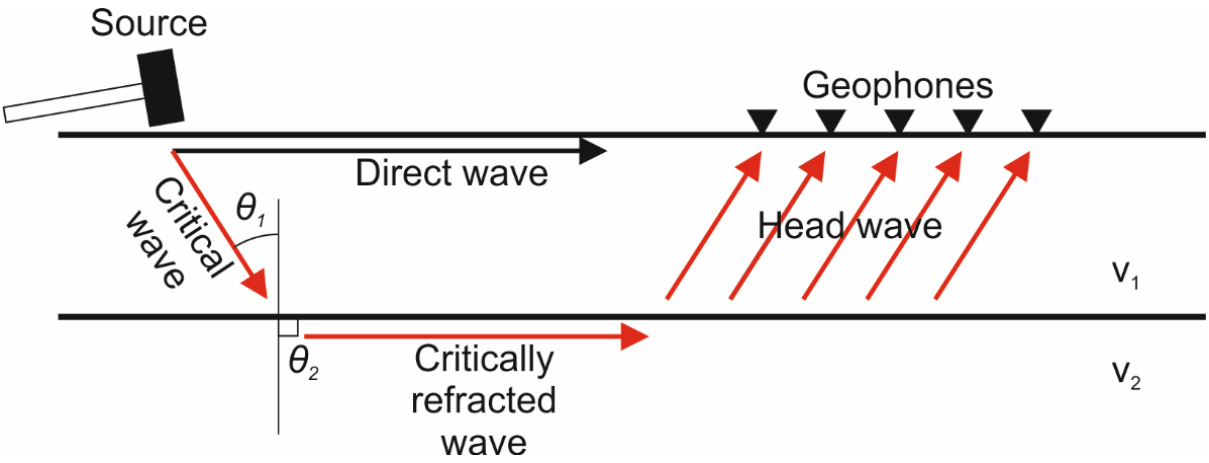

Figure 1.6: Seismic wave propagation at t = 0+n, showing the parameters of Snell's Law (Equation 1.2) and the refracted head wave overtaking the slower direct wave.

Seismic velocity models are created by identifying the first arrival of the critically refracted head wave (also known as a first break) in the shot gather. For each shot gather location, the travel-time of the wave and distance from source are recorded, and can be plotted as so-called travel-time curves. In simple geologic environments, these travel-time curves can be used to calculate the depth to a layer using either the Conventional Reciprocal Method (also known as the Plus Minus Method) (Hagedoorn, 1959) or Generalised Reciprocal Method (Palmer, 1981). Other means of processing include Term-Time Inversion (Scheidegger and Willmore, 1957) and with the use of genetic algorithms (Boschetti et al., 1996, Sambridge and Drijkoningen, 1992). However, the most recently developed and now most common form of processing for seismic refraction data is using a tomographic inversion approach using ray tracing or wave front tracking (also known as Wavepath Eikonal Traveltime inversion) (White, 1989, Rücker et al., 2017). Although many different tomographic inversion algorithms have been developed for seismic refraction processing, their performance has been shown to be comparable regardless of the specific algorithm used (Zelt et al., 2013).

1.3.3 Sources of error and uncertainty in ER and SR surveys

As with many areas of geoscience (Beven and Westerberg, 2011), there exist several sources of potential error and uncertainty within the stages of geophysical data acquisition, processing and interpretation. If these sources of

error and uncertainty are not firstly identified and secondly eliminated, minimised, or incorporated, they can significantly impact the validity of results and subsequent interpretations (Fournier et al., 2013). The concepts of error and uncertainty are closely related; 'error' is a calculation or estimation of the difference between a measurement and its true value (Pérez-Díaz et al., 2020). Error comprises elements of the trueness and accuracy of a measurement, and is a function of the degree of natural randomness in a process (Palmer, 2012). On the other hand, uncertainty relates to the quality and amount of knowledge available in relation to the amount and quality of knowledge required to make a decision; recognition of uncertainty is acknowledgement of the (known and unknown) limitations of data.

There are many potential sources of error within ER and SR surveying, both random and systematic (McCollum, 1952, Morelli and LaBrecque, 1996) (Table 1.2). Random errors can be minimised or removed through data averaging or filtering , however, systematic errors cannot be addressed in this way (La Brecque et al., 2007). Instead, systematic errors need to be understood and qualitatively or quantitatively accounted for in data processing and interpretation, or preferably avoided entirely through correct survey design and practice (Oldenborger et al., 2005). In simple terms, random errors affect the precision of a measurement, whereas systematic errors affect accuracy (Figure 1.7).

In addition to the many potential sources of errors found in geophysics, geophysical data are highly uncertain in contrast to other geoscientific investigations. Uncertainties in geophysical models arise from the ill-posed nature of geophysical problems and the indirect sensitivities of measurements to engineering properties. For a modelled solution to be 'well-posed', a solution for the model must exist, the solution should be unique and the behaviour of the model should depend entirely on the physical components of the system (Hadamard, 1902). Geophysical models do not fulfil these criteria, and instead are considered ill-posed, and an inverse problem, i.e., where observations are used to determine the causal effects (O'Sullivan, 1986, Kabanikhin, 2008).

In addition to the non-uniqueness of a modelled solution, geophysical measurements do not have unique sensitivities. Measured values can increase or decrease due to several factors that may all be in different states in the subsurface. For example, resistivity measurements are sensitive to both clay-content and saturation, with increases in either causing corresponding decreases in measured resistivity. How a causative effect is determined from the observation of a reduction in modelled resistivity will depend on the availability of additional information in order to reduce the uncertainty in the interpretation.

However, laboratory calibration of geophysical and geotechnical measurements can allow for quantitative estimates of geotechnical or hydrological properties (Binley et al., 2015). These can then be used directly as input into slope stability models (Gance et al., 2015). The use of multiple geophysical approaches can help to ameliorate the uncertainty associated with the many and different sensitivities that various geophysical methods have to ground conditions. However, a multi-method approach alone cannot replace the need for integrating geophysical models with geotechnical data for detailed investigations (Pazzi et al., 2019).

Table 1.2: Sources of random and systematic error in electrical resistivity and seismic refraction surveying

Type of error	Source of error	Present in ER?	Present in SR?	Error minimisation approach
Random	Malfunction in instrument / damage to cables / uncalibrated instrumentation	x	x	Equipment testing prior to use and regular equipment maintenance
	Inaccurate recording of sensor positions	x	x	Accurate recording of *x*, *y* and *z* positions using suitable survey equipment (e.g., total station, RTK GNSS)
	Poor signal-to-noise caused by weak signal or strong environmental noise	x	x	Measurement stacking, isolation of sensors from environmental noise source
	Differing interpretation of results between operators	x	x	Use of objective and / or automated interpretative aids
	Electrode polarisation caused by accumulation of charge at electrode / water interface	x		Repeat acquisition of survey in either i) normal configuration to observe drift of measurements, or ii) in reciprocal configuration to observe difference
	Noisy readings due to high contact resistance	x		Ensure acceptable contact resistances and test prior to survey
	Insufficient current injection to penetrate subsurface	x		Use larger power source
	Timing issues (e.g., Recording trigger ≠ 0 seconds)		x	Use trigger pre-record to identify correct 0 second time
	Incorrect identification of first arrivals		x	Judicious use of filtering to remove environmental noise
Systematic	Ground conditions unsuitable for surveying (e.g., very high resistivity material, low-velocity buried zones)	x	x	Use of multiple geophysical approaches with complementing sensitivities
	Including data with high errors in inversion	x	x	Filtering of data outliers
	Not capturing error distribution to guide data weighting in inversion	x	x	Creation of statistical error model for use in inversion
	Unsuitable parameters used for inversion	x	x	Appropriate sensitivity testing, forward modelling and use of error and fit assessment (i.e., root-mean-square error and chi-square test)
	Non-uniqueness of inversion solution	x	x	Comparison of inverted models with other available sources of geological information (e.g., maps, boreholes, samples etc.) for validation

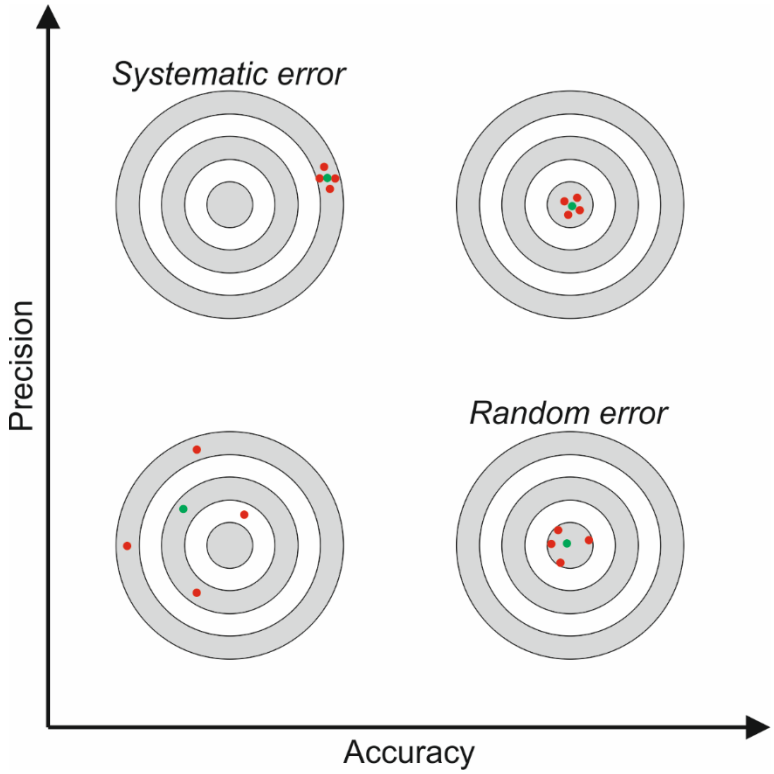

Figure 1.7: Precision and accuracy, and their relationship to random and systemic errors. Red dots represent measured data, and green dots are averages of the measurements. Random (i.e., accurate and imprecise) errors can be averaged to produce a reading close to the true value, while systematic (i.e., precise and inaccurate) cannot be averaged to produce a more accurate result.

Therefore, in geophysical datasets, uncertainty can both be dependent on, and independent of, random and systematic errors; errors can introduce additional uncertainties to a model, but data with low errors can also be highly uncertain. Strategies that can eliminate, minimise, or incorporate sources of error combined with tools to assist in reducing the uncertainties of data interpretation are necessary for the further uptake of geophysical monitoring approaches in to LoLEWS. Therefore, this thesis will look to address i) the handling of systematic and random errors associated with novel geophysical methodologies for landslide monitoring, and ii) utilising tools that can reduce uncertainty in the interpretation of geophysical datasets.

1.3.4 Geophysical inversion and random errors

Because of the ill-posed nature of geophysical problems, inversion of data is necessary to arrive at realistic models of geophysical properties. Inversion is the process of estimating a forward response to fit observed data (Ronczka et al., 2017). There are numerous inversion algorithms for ER (Doyoro et al., 2022, Loke and Barker, 1996, Saneiyan et al., 2018) and SR data (Guedes et al., 2022, Sheehan et al., 2005, Zelt et al., 2013). This work uses pyGIMLi, a library of geophysical modelling and inversion tools to process ER and SR data (Rücker et al., 2017). The main advantages in using this software are i) the same inversion frameworks are used to process both ER and SR data, ii) it is open-source and Python based, allowing for modification of the code to suit different applications and iii)

the software is designed to operate with other open-source data pre-processing (Geuzaine and Remacle, 2009) and post-processing visualisation (Ahrens et al., 2005) modules.

The default inversion framework in pyGIMLi is based on the generalised Gauss-Newton method, which can accept any forward operator, making it suitable for a range of applications. Therefore, the inversion problem can be stated as minimisation of an objective function comprising data misfit and model constraints, given by

$$\| W_d(\mathcal{F}(m) - d) \|_2^2 + \lambda \| W_m(m - m_0) \|_2^2 \rightarrow min \qquad \text{Equation 1.3}$$

where W_d is the data weighting matrix including the inverse errors, $\mathcal{F}$ is the forward operator mapping a discrete parameter (m) and W_m is the model constraint matrix. The weight of the regularisation term is determined by the dimensionless value of λ, which can include various smoothness and damping approaches (Rücker et al., 2017). Measurement errors determine the amount of damping imposed by an inversion algorithm, and affect the point at which convergence is reached (Tso et al., 2017). Even small variations in error measurements can influence the resulting inverted model, with underestimated errors tending to lead to over-fitting of the model solution, and overestimated errors resulting in under-fitting (Figure 1.8).

Therefore, it is necessary to quantify errors to include them in the inversion process. Measurement errors are most commonly determined by exploiting the concept of reciprocity, in which if the positions of a source and receiver are exchanged, the measurement made at the receiver should remain the same (Parasnis, 1988). The difference between a measurement and its reciprocal is given by

$$|e| = 100 \cdot \left(\frac{|m_n - m_r|}{m_n + m_r}\right) \qquad \text{Equation 1.4}$$

where m_n is the measurement recorded with a source at position A, and receiver at position B, and m_r is the measurement recorded with a source at position B and a receiver at position A. In ER surveys, reciprocal datasets are acquired by switching the position of the injection and potential electrodes (e.g., Barker, 1991, Delay et al., 2011). By repeating an entire set of ER measurements, reciprocal errors can be calculated for every reading in a dataset. Historically, exploiting reciprocity in SR measurements was the primary means of calculating wave travel-times; in order for a measurement to be used in wave travel-time calculations, a corresponding reciprocal measurement was required (Hagedoorn, 1959, Palmer, 1981). However, with the advent of tomographic inversion methods, which generally calculate the shortest path through the subsurface (Moser, 1991), reciprocal measurements were no longer required to calculate seismic velocities. One major advantage of implementing tomographic processing in SR is the ability to use greater numbers of geophones with dense source-receiver spacings, without the need to require reciprocal measurements for every shot location (White, 1989).

In ER studies, measurement errors are typically included in the inversion through the use of an error model linking error to transfer resistance (Binley et al., 1995, Mwakanyamale et al., 2012). This model can then be used to predict the errors for individual measurements and inform the data weighting in the inversion. Using a model of error is preferable over using directly observed errors, which may not be as statistically robust given they are often derived from only two measurement points (Tso et al., 2017). Although reciprocal measurements are obtained during SR data acquisition, the use of reciprocal measurements to create error models for inversion is

not typically used. Instead, estimates of errors tend to be quantified using statistical means (e.g., Dangeard et al., 2018, Uhlemann et al., 2016a). This thesis will explore the use of error models to improve the results of SR inversions.

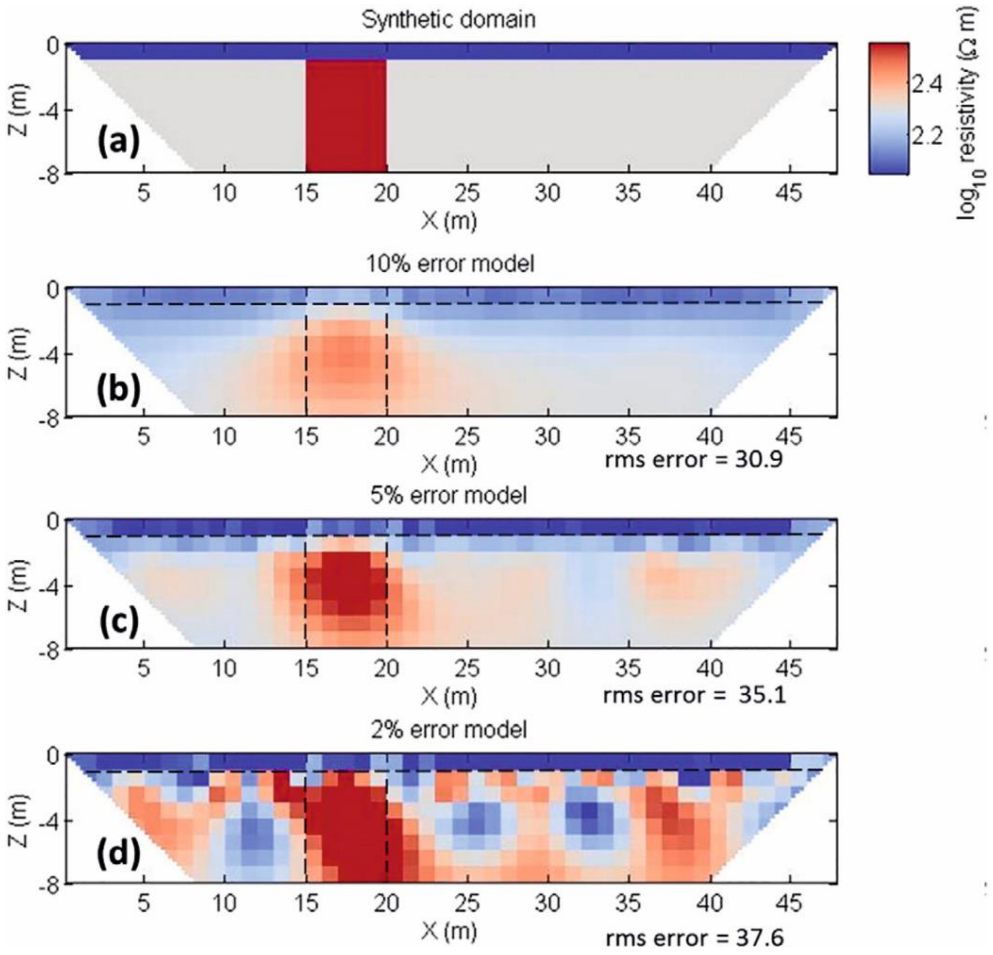

Figure 1.8: Demonstration of error impact using (a) synthetic ER data which are contaminated with 5% Gaussian noise, and inverted using a (b) 10% linear error model, (c) 5% linear error model and (d) 2% linear error model. Reproduced from Tso et al. (2017).

1.4 Landslide risk in the UK and the Hollin Hill Landslide Observatory

The UK experiences comparatively low loss of life due to landslide hazards compared to the global distribution of landslide risk (Froude and Petley, 2018, Kirschbaum et al., 2010, Petley, 2012). Although fatalities due to landslides do occur (Haines, 2021, Pennington et al., 2012), the number of landslides impacting critical infrastructure (such as rail and highway networks) and coastal communities is far greater (Gibson et al., 2013, Hobbs et al., 2020, Winter et al., 2016). As the primary trigger of landslides in the UK is due to ground saturation, they are typically considered as part of multi-hazard events associated with heavy rainfall and flood events (Argyroudis et al., 2020, Gill and Malamud, 2014).

The British Geological Survey has operated a network of landslide observatories to support research to understand the triggers and mechanisms of slope failure in the UK (Pennington et al., 2009). The HHLO site is a

testbed for novel landslide subsurface characterisation and monitoring technology. Research at the HHLO focuses on developing high spatial resolution geophysical systems and approaches, supported by geotechnical and geodetic observations, for improving understanding of landslide processes and providing early warning of slope failure. The complex morphology of the landslide system in Lias mudrocks, combined with the triggering of failures in periods of high antecedent rainfall (Figure 1.9) leads to saturated ground conditions. The site is analogous to many slow-moving, clay-rich landslides across the UK (e.g., Boon et al., 2015, Hobbs et al., 2012), Europe (e.g., Fiolleau et al., 2020, Malet et al., 2002, Jaboyedoff et al., 2009, Jongmans et al., 2009, Supper et al., 2014, Walter et al., 2011) and North America (e.g., Coe et al., 2003, Crawford and Bryson, 2018, Huntley et al., 2020).

The advances in high spatial resolution geophysical characterisation and monitoring developed at the HHLO form part of early warning strategies at other landslides where human life is at risk (Watlet et al., 2019). However, research has focused on enhancing early warning capability for economically high-value elements at risk of damage from natural landslides (Holmes et al., 2020, Huntley et al., 2019) and monitoring degradation within infrastructure assets that may be at risk of failure (Gunn et al., 2018).

At the HHLO, ER and SR high spatial resolution geophysical surveys ranging from reconnaissance to detailed studies, and including standalone surveys and permanent monitoring installations, have guided the evolving understanding of this complex active landslide. An initial walkover of the site, comprising a basic interpretation of the landslide geomorphology present at the surface, was undertaken by Jenkins et al. (2005), who first hypothesised that the subsurface movements of water could be causing the complex rotational and translational failures observed on the surface of the site.

The first comprehensive subsurface geological model was later derived from a series of 2D and 3D ER and self-potential (SP) surveys described by Chambers et al. (2011) (Figure 1.10). The contrast between the clay-rich, saturated and failure-prone Whitby Mudstone Formation (WMF) and underlying clay-deficient, porous and drained Staithes Sandstone Formation (SSF) was initially identified from four 2D ER and SP profiles surveyed at broadly equidistant separations across the slope of the landslide. A more detailed 3D ER and SP survey focused on providing higher resolution models across an area of surface geomorphological features including rotated blocks, translational failure and flow lobe formations. The subsurface geometries of these features were delineated at greater resolution in these focused 3D surveys. Supplementary geotechnical observations, acquired from auger holes, boreholes and subsequent sample acquisitions, were also made within the area of this 3D ER and SP surveys, permitting correlation of the inverted ER values with the underlying geology. From these data, a volumetric 3D geophysical-geotechnical model covering an area of the slope approximately 200 m x 280 m (approximately 5.6 x 10^6 m^2) to an average depth of 30 m across the site was constructed.

A more detailed interpretation of the initial ER results was undertaken by Merritt et al. (2013), demonstrating the added value that introducing conventional remote sensing, geotechnical and monitoring observations can contribute to landslide model development (see also Gunn et al., 2013). In addition, an SR survey was undertaken at the HHLO by Uhlemann et al. (2016a) in order to map the geomechanical properties of the landslide in three-dimensions, in terms of seismic velocities and derived elastic moduli. The refraction of seismic waves occurs at the interfaces of lithological units with contrasting densities and elastic moduli, and the seismic surveys

undertaken at the HHLO were primarily used to better delineate the contact between the WMF and SSF, a feature that is an important consideration when elaborating data using petrophysical relationships.

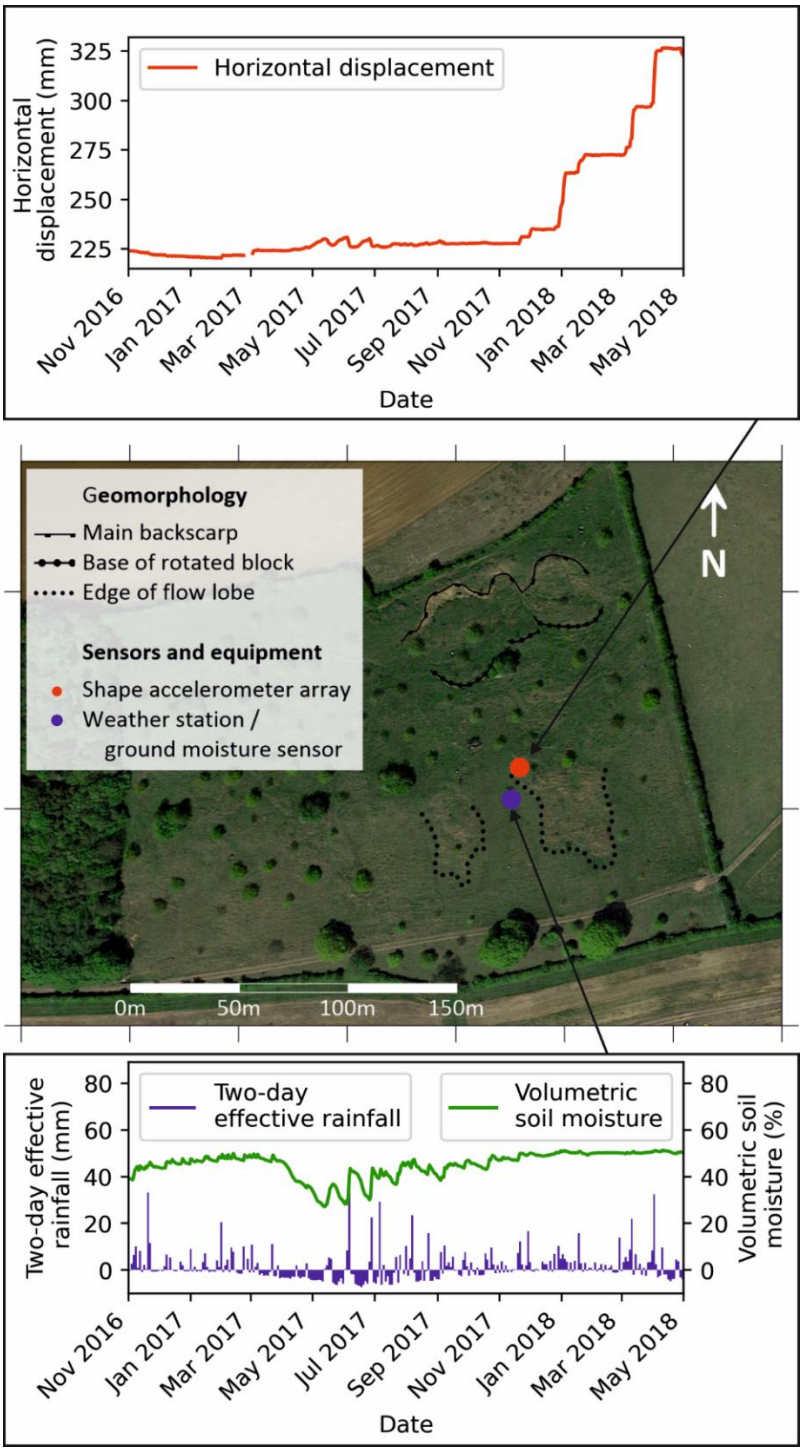

Figure 1.9: Map of the Hollin Hill Landslide Observatory showing the major geomorphological landforms (middle), showing the locations of a Shape Accelerometer Array (SAA) deformation sensor and weather station. The SAA deformation data (top) and effective rainfall and ground moisture data (bottom) collected over 18 months from the site show that slope displacements are more closely linked to increased ground saturation caused by long-term antecedent rainfall, rather than isolated, extreme rainfall events in periods of lower ground saturation. Map data: Google.

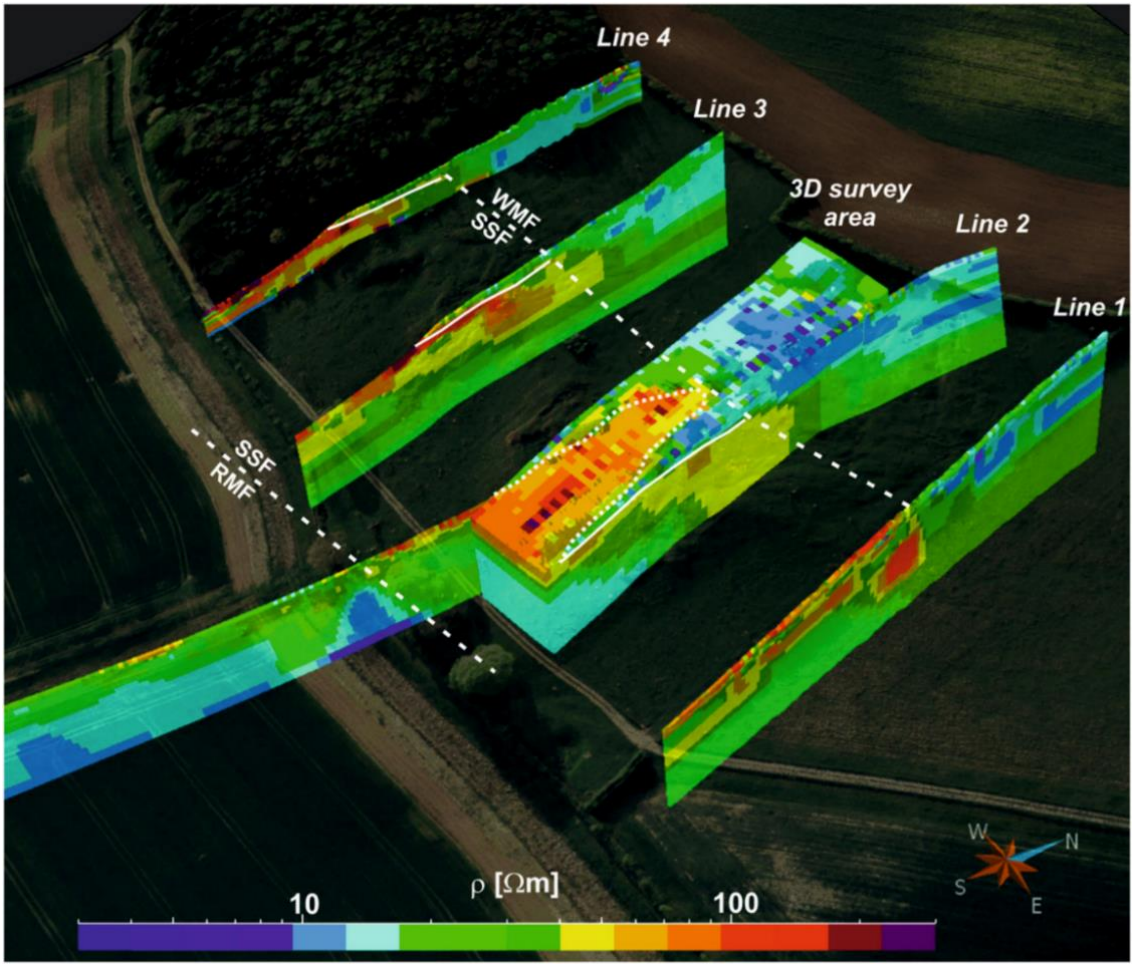

Figure 1.10: Initial 2D and 3D ER survey of Hollin Hill, showing the major lithological units identified by contrasts in resistivity. Reproduced from Chambers et al. (2011).

Petrophysics is the study of the physical characteristics of a soil or rock, including porosity, permeability, pore size distribution, capillary pressure and moisture content (Archie, 1950). Petrophysical relationships aim to predict the physical properties of soils and rock from geophysical inputs. Archie's Law (Archie, 1942) is one of the earliest examples of such a relationship, in which DC resistivity is used to predict saturation (S) by

$$S = \left(\frac{\rho}{\rho_s}\right)^{\frac{1}{n}} \qquad \text{Equation 1.5}$$

where ρ is resistivity, ρ_s is resistivity at 100% saturation, and n is an empirical saturation exponent. Modified versions of Archie's Law can include additional variables to account for the effects of cementation and use on granular, unconsolidated material (Telford et al., 1990). However, Archie's Law cannot be applied to materials where more than one conducting phase is present, such as when considering electrolytic conduction through

both pore fluids and the Electrical Diffuse Layer surrounding clay mineral. For this reason, the Waxman-Smits equation has been used to predict moisture content from resistivity at the HHLO.

The original Waxman-Smits equation (Waxman and Smits, 1968) describes resistivity as a function of relative saturation. However, a modified version of the Waxman-Smits equation can express resistivity in terms of gravimetric moisture content, given as

$$\rho = \frac{F}{S^n}\left(\frac{1}{\rho_w} + \frac{BQ_v}{S}\right)^{-1} \qquad \text{Equation 1.6}$$

where F is the formation factor, ρ_w is the pre fluid resistivity, B is the average mobility of the ions and Q_v the cation concentration per unit pore volume of the Electrical Diffuse Layer (Chambers et al., 2014, Merritt et al., 2016).

Merritt et al. (2016) first applied the modified Waxman-Smits model (Equation 1.6) to resistivity measurements from the HHLO. Uhlemann et al. (2017) then applied these petrophysical relationships to geophysical model translation, producing 4D soil moisture content volumes from time-lapse ER images acquired from a permanent ER monitoring system deployed at the HHLO. This approach identified vulnerable zones of the complex landslide, which were more likely to move due to increased moisture content. It also captured the seasonal scale variability of moisture dynamics, including the identification of subsurface moisture migration during periods when the landslide surface was dry. Furthermore, Uhlemann et al. (2017) used the modified Waxman-Smits model to establish that displacements at the HHLO occur more frequently when gravimetric moisture content exceeds 48%.

Within the context of past research undertaken at the HHLO, this thesis aims to develop the application of SR to monitoring landslide processes, moving toward bringing SR in line with current ER capabilities at the site. Additionally, this thesis will explore means of integrating ER and SR data to improve understanding of how these individual geophysical datasets can characterise and monitor the subsurface structures and process of the HHLO.

1.5 Research questions and thesis structure

The work of this thesis advances the application of high spatial resolution ER and SR methods to characterise and monitor landslides, with a view to their incorporation in to LoLEWS. This work uses ER and SR field data acquired at the Hollin Hill Landslide Observatory (HHLO). This research builds upon a significant body of research at the HHLO in to the development of geophysical monitoring systems, in particular using ER approaches. SR approaches are currently underdeveloped compared to ER, mostly due to unique and currently unaddressed challenges surrounding repeated data acquisition in dynamic environments, and identifying appropriate time-lapse inversion strategies. When developing any novel methodology, the bespoke errors and uncertainties associated with the approach must be considered, which forms a significant part of this research.

Hence, the integration of SR methods with the increasingly well-established ER monitoring systems used to study landslides can provide further lines of evidence in understanding landslide structure and processes, whilst also reducing uncertainty in ER interpretation. The combined use of these approaches can provide inputs to the

various components of LoLEWS, providing geoscientific knowledge to guide design, high-resolution spatiotemporal monitoring of landslide processes, and evidence of critical subsurface conditions that may indicate impending slope failure.

The questions considered in this thesis are:

- What role do different geophysical methods play in the current state-of-the-art of geophysical monitoring applied to landslides triggered by increases in saturation?
- Can SR methods be developed to monitor landslide processes, with a view to being integrated with long-term LoLEWS?
- Can integration of multiple methods improve understanding of landslide settings and processes for early reconnaissance and the design of LoLEWS?
- What contribution can the use of integrated high spatial resolution geophysical imaging capabilities (i.e., ER and SR) make to the implementation of LoLEWS?

To answer these questions, the structure of this thesis is as follows (see graphical summary, Figure 1.11). Firstly, Chapter 2 comprises an extended literature review exploring the current state-of-the-art of geophysical monitoring of moisture-induced landslides. The chapter builds on the work of Jongmans and Garambois (2007), who conducted a major review into the applications of geophysics to investigate the subsurface properties of landslides. This chapter aims to compile and evaluate recent case studies from the last decade, and in doing so, lays out the different types of geophysical methods used for landslide monitoring, assesses their strengths, challenges and considers the future of geophysical monitoring for landslides.

In Chapter 3, errors arising from a novel geophysical monitoring approach are considered. The results of an SR monitoring campaign at the HHLO comprising of 16 repeated SR (P- and S-wave) surveys over the course of 33-months between October 2016 and August 2019 are presented. This is the first documented use of SR for a multi-year landslide monitoring campaign. This chapter aims to address the challenges of acquiring repeated stand-alone surveys in a dynamic environment, specifically considering the potential random errors introduced by changes in landslide surface topography between surveys, and their impact on seismic velocity models. A novel pseudo-time-lapse inversion code is developed to provide temporal constraint when inverting a time-series of stand-alone survey data. Analysis of the results of the monitoring campaign focus on the temporal variations observed in the active landslide layer at the HHLO, demonstrating the relationship between seismic velocities and changing moisture content over time.

Chapter 4 addresses reducing the interpretative uncertainty using the results of an integrated ER and SR survey at the HHLO for the purposes of characterising the landslide system. The aim of the survey was to emulate a reconnaissance approach to landslide investigation, and as such, no prior information about the landslide, except for that which could be inferred from a geological map and on site observations, were incorporated in to the processing of the data. Firstly, the spatial discrepancies between the positioning of the two surveys was minimised by constructing a joint subsurface mesh using sensor positions interpolated on to a UAV-derived DEM of the site. After individual inversion of the datasets, a machine learning approach, using a Gaussian Mixture

Model (GMM), was used to classify different areas of the landslide based on their relative geophysical properties. The resulting subsurface model was compared to and showed strong agreement with, the current conceptual model of the HHLO produced from several years of geophysical, geotechnical and geodetic observations. This approach demonstrates the applicability of using multiple-method geophysical surveys to provide subsurface information for the design stage of LoLEWS (Chapter 5).

Chapter 5 firstly synthesises the results of Chapters 3 and 4 within the context of reducing errors and uncertainty in geophysical inputs used for characterising and monitoring landslide hazards. Secondly, Chapter 5 assess the contribution that geophysical imaging can make to LoLEWS, including in the design, monitoring, forecasting and education phases. A conceptual framework for implementing geophysical characterisation and monitoring approaches for LoLEWS is presented. This chapter aims to serve as a synthesis of the major themes explored in the thesis, within the context of development of geophysical approaches for LoLEWS. Finally, Chapter 6 provides a brief conclusion to the thesis, summarising the major findings, how they interrelate, and the direction of research required to build on this work in the future.

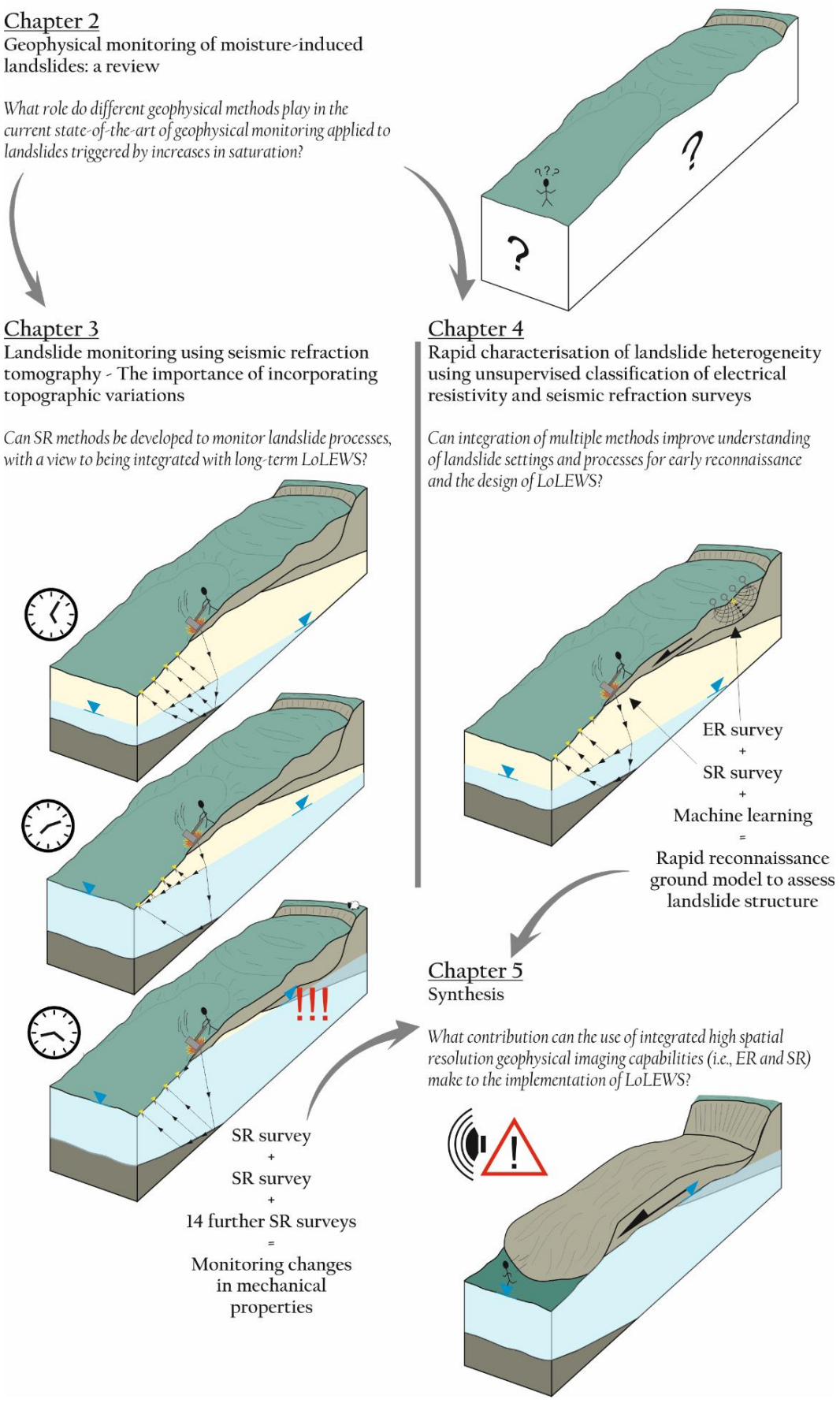

Figure 1.11: A graphical summary of the content of this thesis, showing the research questions addressed by each chapter.

2 Geophysical monitoring of moisture-induced landslides: a review

J. Whiteley, J. Chambers, S. Uhlemann, P. Wilkinson & J. M. Kendall (2019). Geophysical monitoring of moisture-induced landslides: A review. Reviews of Geophysics, 57, 106 – 145. https://doi.org/10.1029/2018RG000603.

Declaration and author contribution

The content of this chapter was published in *Reviews of Geophysics* in April 2019. Minor amendments have been made to the content to better integrate the work with the overall thesis. The summary, synthesis and comparison of previously published studies was conducted by J. Whiteley. The manuscript was written by J. Whiteley with the guidance of all co-authors, and supervision was provided by J. Chambers and J. M. Kendall.

Contributor Roles Taxonomy (CRediT) statement

Conceptualisation: *J. Whiteley*

Investigation: *J. Whiteley*

Visualisation: *J. Whiteley, S. Uhlemann*

Writing – original draft: *J. Whiteley*

Writing – review & editing: *J. Whiteley, S. Uhlemann, P. Wilkinson, J. Chambers, J. M. Kendall*

Supervision: *J. M. Kendall, J. Chambers*

Abstract

Geophysical monitoring of landslides can provide insights into spatial and temporal variations of subsurface properties associated with slope failure. Recent improvements in equipment, data analysis, and field operations have led to a significant increase in the use of such techniques in monitoring. Geophysical methods complement intrusive approaches, which sample only a very small proportion of the subsurface, and walk-over or remotely sensed data, which principally provide information only at the ground surface. In particular, recent studies show that advances in geophysical instrumentation, data processing, modelling, and interpretation in the context of landslide monitoring are significantly improving the characterization of hillslope hydrology and soil and rock hydrology and strength and their dynamics over time. This review appraises the state of the art of geophysical monitoring, as applied to moisture-induced landslides. Here the focus is on technical and practical uses of time-lapse methods in geophysics applied to monitoring moisture-induced landslide. The case studies identified in this review show that several geophysical techniques are currently used in the monitoring of subsurface landslide processes. These geophysical contributions to monitoring and predicting the evolution of landslide processes are currently under-realised. Hence, the further integration of multiple-parametric and geotechnically coupled geophysical monitoring systems has considerable potential. The complementary nature of certain methods to map the distribution of subsurface moisture and elastic moduli will greatly increase the predictive and monitoring capacity of early warning systems in moisture-induced landslide settings.

2.1 Introduction

The destabilisation and subsequent mass-movement of soil and rock on slopes occurs across the globe, leading to loss of life and damage to property and infrastructure (Froude and Petley, 2018, Petley, 2012). Investigation of landslides can determine their key characteristics, including (but not limited to) soil and rock properties, the landslide geomorphology, types of movement and velocity rates. Detailed knowledge of these characteristics can inform the modelling of the sensitivity of landslide masses to external triggers (Arnone et al., 2011, Jibson, 1993), which contribute to reducing risk posed by these globally occurring hazards.

The worldwide distribution of landslides is not uniform, with landslides occurring primarily where the requisite topographic, climatic and environmental conditions are prevalent. Figure 2.1 shows the distribution of rainfall-induced landslides (i.e., those caused by increased hydrological infiltration) recorded in the Global Landslide Catalog (GLC) between 2007 and 2016 (Kirschbaum et al., 2010, Kirschbaum et al., 2015). An obvious pattern is the greater occurrence of landslides in areas of greater topographic variation compared to areas of relatively low relief.

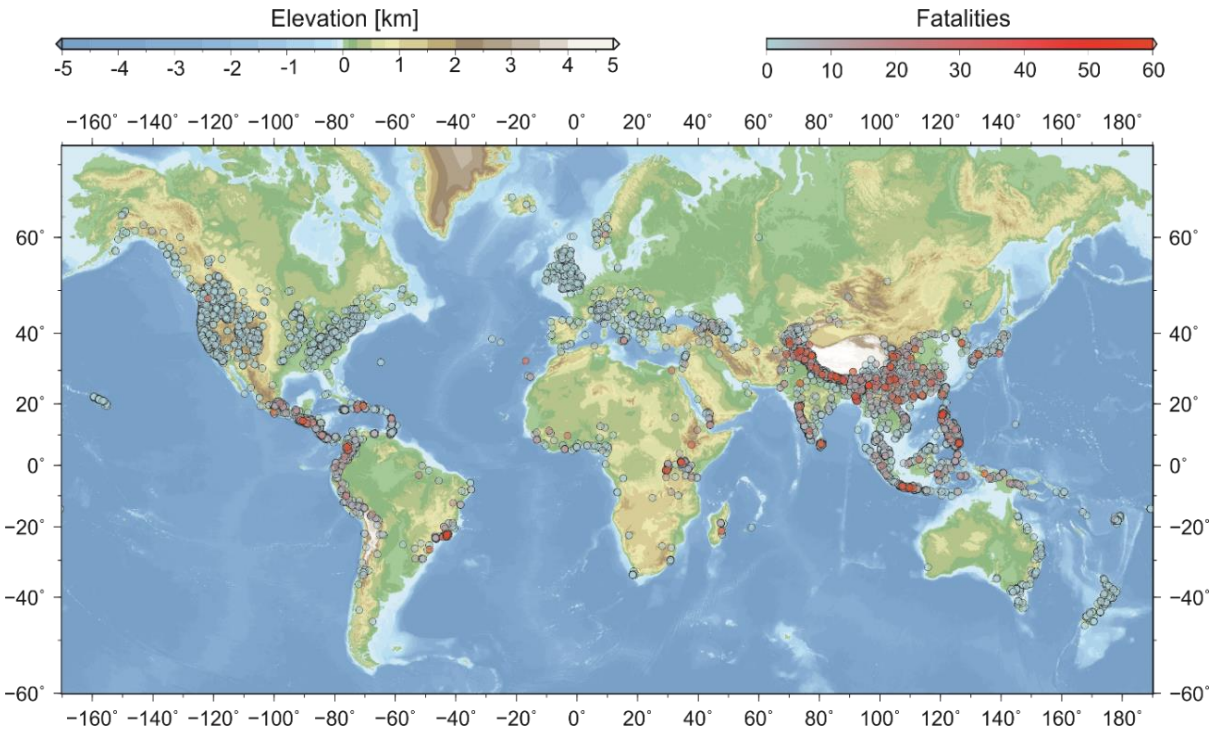

Figure 2.1: Global occurrences of landslides recorded in the Global Landslide Catalog between 2007 and 2016 (Kirschbaum et al., 2010, Kirschbaum et al., 2015), including associated fatalities. Reproduced from Uhlemann (2018).

High-incidence, high-fatality areas tend to be found in less developed regions (e.g., South East Asia, Central and South America) and high-incidence, low-fatality areas are generally located in more developed countries (e.g., North America, Europe). However, the GLC does not capture the whole picture of landslide distribution and impact across the globe (Kirschbaum et al., 2015). In the United Kingdom, there is a well-established and

maintained recording system for landslide events, operated by the British Geological Survey (Pennington et al., 2015). The United States Geological Survey has a national landslide mitigation strategy which recommends the mapping and assessment of landslide hazards (Spiker and Gori, 2003).. These landslide recording programs tend to capture the occurrence of both fatal and non-fatal landslide events at many scales. However, in many other countries, particularly developing nations, such recording systems are not established, and the landslide events recorded tend to be those that have a large enough impact on life, society or the economy to be reported in the media. Although fatalities are fewer in more economically developed countries, there are still issues of completeness in reporting landslides even in Europe (Haque et al., 2016). The incidence of landslide events across the globe can therefore be taken as a lower boundary of actual landslide occurrence, and loss of life and infrastructure from landslides can be greatly underestimated in such circumstances (Petley, 2012). Landslides are often considered a secondary hazard, forming part of the problem of cascading hazards (Fan et al., 2021, Pescaroli and Alexander, 2015), as they are triggered by catastrophic events such as storms, floods, volcanic eruptions and earthquakes (Gill and Malamud, 2014). This cascading effect was highlighted in Papua New Guinea in February 2018, with numerous landslides triggered by a large earthquake blocking many valleys. This valley blocking poses a continuing flood risk as water builds up behind these unstable structures with increased seasonal rainfall.

The term '*moisture-induced landslides*' (MIL) is used in this review to refer to landslides triggered by increased water content in the subsurface. Geological materials, including soils and rocks, make up the '*subsurface*', with the ground surface separating this area from the atmosphere above. Elevations in subsurface moisture content can be caused by extended periods of increased infiltration, or by increased volumes of water entering the system via other routes e.g., groundwater throughflow. Most infiltration in landslide settings comes from increased precipitation or snow-melt, and due to the complex role of evapotranspiration, the amount of rainfall or snow-melt that reaches the subsurface can vary throughout the climatic cycle. The amount of moisture that does reach the subsurface is known as '*effective infiltration*'. Therefore, the term MIL recognises the multiple sources of moisture that affect landslides, the importance of the concept of effective infiltration, and its subsequent effect on the instability of materials in response to moisture-infiltration.

The advances in hardware and software for geophysical monitoring reflect those made in remote sensor technology, mainly in the ability to deploy increasingly low-cost and low-power sensors to capture information from the subsurface with a minimal delay in data acquisition and transmission (Ramesh, 2014). The main benefit arising from these developments has been the increase in monitoring durations achieved by the installation of permanent sensors (Ramesh and Rangan, 2014). However, geophysical monitoring approaches have the added benefit of providing increasingly high-resolution spatial information.

This review appraises the state-of-the-art of the application of geophysical methods to monitoring moisture-induced landslides. Geophysical monitoring provides information on fundamental subsurface slope process, and is relevant to those studying landslides and their behaviour. However, this information can also be vital to those looking to mitigate landslide hazards, and in particular, can provide information on precursory failure conditions in unstable slopes. Therefore, the content of this review is also of interest to Landslide Early Warning Systems (LEWS) operators looking to incorporate spatial and temporal subsurface data into their monitoring systems. It

is most suited to LEWS operating at the slope-scale, also known as Local Landslide Early Warning Systems (LoLEWS) (Pecoraro et al., 2019).

In this review, '*geophysical methods*' specifically refers to surface deployed techniques to investigate features in the shallow subsurface. The term '*monitoring*' is used to indicate a time-lapse approach to investigate changes between two or more geophysical datasets acquired at the same location at different times. Recent literature shows two main methods being employed for the monitoring of landslides: geoelectrical and seismic. The relevance of geophysical monitoring to landslides is addressed by first identifying landslide characteristics and the application of geophysical methods. A review of case studies of geophysical monitoring of landslides is then undertaken in light of the methods currently in use. Finally, recommendations for the use of geophysical methods in the monitoring of landslides will be revisited in the context of LoLEWS.

2.2 Landslide settings and processes: definitions

The most longstanding and recognised classification of landslides is that of Cruden and Varnes (1996). This classification system has been updated in recent years to reflect modern standards of material properties (Hungr et al., 2014). Other well-established and regularly used systems exist for other specific landslide types (e.g., Fell, 1994, Leroueil et al., 1996, Skempton and Hutchinson, 1969). The updated Cruden and Varnes (1996) system by Hungr et al. (2014) comprehensively outlines the types of movement, the geological materials and velocities of material movement that describe the majority of landslide occurrences across the globe.

For this review, it is useful to distinguish between the spatial definition of a landslide setting, and the temporal description of the evolving processes of movement:

(i) The '*landslide setting*' is the spatial definition of a geographical area that may be prone to, or have experienced, the downslope mass-movement of geological material (e.g., Jongmans et al., 2009). Characteristics of the landslide setting would include the geological materials (rock, boulders, debris, sand, clay, silt, mud, peat, ice) as well as the geomorphology of the unstable slope (Guzzetti et al., 1999, Hungr et al., 2014).

(ii) '*Landslide processes*' indicate the onset and subsequent processes of movement of unstable geological material in time (e.g., Hutchinson and Bhandari, 1971). These include the changes in the subsurface conditions of landslides preceding observable failure, such as elevations in pore water pressure that may induce future movement in landslides. These processes may be difficult to measure, and often can only be inferred by observing changes in a property (e.g., ground moisture) over time. Factors relating to landslide processes would include the types of movement (flows, topples, slides, spreads and deformations), velocities of movement (<16mm/year to >5m/s) (Hungr et al., 2014) and the hydrogeological and geomechanical processes acting upon the landslide materials.

Identification of the affected area is typically undertaken by walk-over surveys, studying of aerial photographs, or via other remote sensing methods such as satellite imagery (Carrara et al., 1992, Carrara et al., 2003, Guzzetti et al., 2012). Landslide investigations using geotechnical means typically involve identification of the three-

dimensional subsurface structure of the landslide, the definition of the hydrogeological regime, and the detection of movement in the landslide mass (McCann and Forster, 1990). This has traditionally been undertaken with intrusive investigation methods, such as the use of trial pits and boreholes to recover samples and identify changes in materials and their properties within the body of a landslide (Angeli et al., 2000, Uhlemann et al., 2016b). These approaches allow for a great amount of detailed information to be gathered at discrete locations. However, due to the heterogeneous subsurface conditions of landslide settings and the dynamic response of landslide processes to external influences, they are not always adequate in providing a wider view of the landslide system, both spatially and temporally.

2.3 Landslide geophysics: an overview

Investigations of subsurface landslide features are necessary to provide the input for forward modelling and subsequent predictions of potential failure events, for example, estimating the run out length, the mobilised volume or the velocity of a potential failure event (Malet et al., 2005, Rosso et al., 2006). In general, geophysical techniques identify spatial variations of a physical parameter of the subsurface, from which inferences on a range of processes and properties can be made (Everett, 2013, Kearey et al., 2001, Parsekian et al., 2015). When applied to landslide investigation, geophysical techniques are able to target characteristics and features of landslide settings that are manifested by physical property contrasts in the subsurface (McCann and Forster, 1990), including:

- The physical extent of the landslide, comprising critical features such as the subterranean slip surface and water table
- Variations in lithological and soil units
- Variations in distribution and movement of moisture throughout the landslide body
- Variations in the geomechanical strength of the landslide body

2.3.1 The landslide setting and geophysical investigation

The features of a typical landslide system that can be identified and assessed using geophysical methods are shown in Figure 2.2. These features are typified by the existence of a physical discontinuity (e.g., slip surface, lithological contact) or a contrast in material properties (e.g., degree of saturation, clay-content) being present in the subsurface. Table 2.1 summarises the main landslide features identified in Figure 2.2, and lists the targeted discontinuity or property contrast, and the applicable geophysical techniques for identifying these features.

2.3.2 Landslide processes, soil mechanics and geophysical investigation

The major parameters influencing slope stability are summarised in Figure 2.3. This summarises the classical understanding of slope failure through the principles of soil mechanics (Terzaghi, 1943, Terzaghi et al., 1996) indicating the key geotechnical parameters acting upon unstable slopes. The figure is a simplified model of a slope, making many assumptions, such as the length of the slope, but indicates the main property to consider

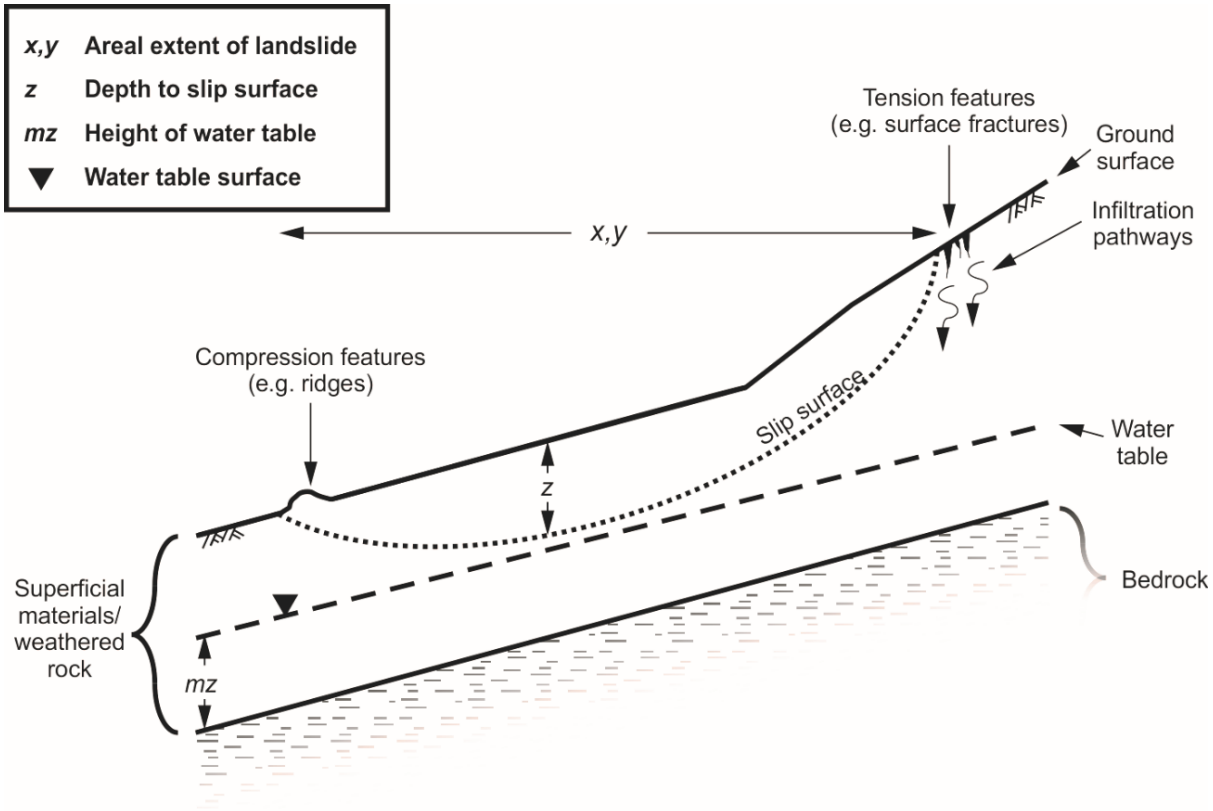

Figure 2.2: Schematic of a landslide system, showing the major landslide setting features that can be investigated and assessed using geophysical methods.

when estimating slope stability. The Mohr-Coulomb failure criteria (Terzaghi, 1943) determines the shear strength (τ_f) of the material at a given point at the slip surface interface, and is given by

$$\tau_f = c + (\sigma - u)\tan\phi'_{cv} \quad , \qquad \text{Equation 2.1}$$

where c is cohesion (i.e., the shear strength when the normal stress is equal to zero), σ is total normal stress, u is pore water pressure, and ϕ'_{cv} is the angle of shear resistance at a critical state. The total normal stress (σ) is given by

$$\sigma = \{m\gamma + m\gamma_{sat}\}z\cos^2\beta \quad , \qquad \text{Equation 2.2}$$

where m is height, γ is the unsaturated unit weight (i.e., total weight per unit volume) of material, γ_{sat} is the saturated unit weight of material, z is depth to slip surface, and β is slope angle. Shear stress (τ) is given by

$$\tau = \{m\gamma + m\gamma_{sat}\}z\sin\beta\cos\beta \quad . \qquad \text{Equation 2.3}$$

The pore water pressure (u) at the slip surface is calculated by

$$u = mz\gamma_w\cos^2\beta \quad . \qquad \text{Equation 2.4}$$

Table 2.1: Summary of the landslide features able to be identified, assessed and investigated using geophysical methods.

Feature of the landslide setting	Discontinuity or property contrast	Applicable geophysical methods	Example
Landslide extents (*x,y,z*)	Slip surface (subsurface and surficial extent) caused by or indicated by changes in density, water content etc. of material	Electrical resistivity, seismic reflection, seismic refraction, surface wave methods, ground penetrating radar	Chambers et al. (2011)
Subsurface material type and structure	Material density	Microgravity	Sastry and Mondal (2013)
	Relative degree of saturation	Electrical resistivity, electromagnetics	Springman et al. (2013)
	Relative clay-content	Electrical resistivity, electromagnetics	Göktürkler et al. (2008)
	Material velocity (as a function of density)	seismic reflection, seismic refraction, surface wave methods	Renalier et al. (2010a)
Water table	Height of water table	Electrical resistivity, electromagnetics, seismic refraction	Le Roux et al. (2011)
	Relative flow direction	Self-potential	Perrone et al. (2004)
Tension features (e.g., surface fractures)	Saturation contrasts (e.g., preferential infiltration pathways)	Electrical resistivity, electromagnetics, ground penetrating radar, self-potential	Bièvre et al. (2012)
Compression features (e.g., ridges)	Variations in material composition	Electrical resistivity, electromagnetics, ground penetrating radar	Schrott and Sass (2008)

In order for slope failure to occur, the restraining forces, in this case shear strength (τ_f) must be overcome by disturbing forces (τ). This can be expressed in terms of a factor of safety (FoS), given by

$$FoS = \frac{\tau_f}{\tau} \quad . \qquad \text{Equation 2.5}$$

When FoS ‹1 slope failure will occur, with FoS ›1 indicating stable slope conditions. FoS ‹1 can be reached by increasing τ, for example, by greater loading on the slope, or by reduction in τ_f for example, by increasing u (Equation 2.1). Not highlighted in these equations is the critical role that negative pore water pressures, or soil suction (or matric suction) can play in the stabilisation of landslide bodies (Toll et al., 2011). Materials with larger void spaces, such as sands and gravels, will have smaller capillary zones (the area of saturation above the water table caused by soil suction) than cohesive materials with smaller void spaces such as clays and silts (Craig, 2004). In some slopes, soil suctions may be the main restraining force preventing failure (Hen-Jones et al., 2017). In these settings, understanding of subsurface moisture dynamics relating to increased infiltration are critical for predicting future slope failures.

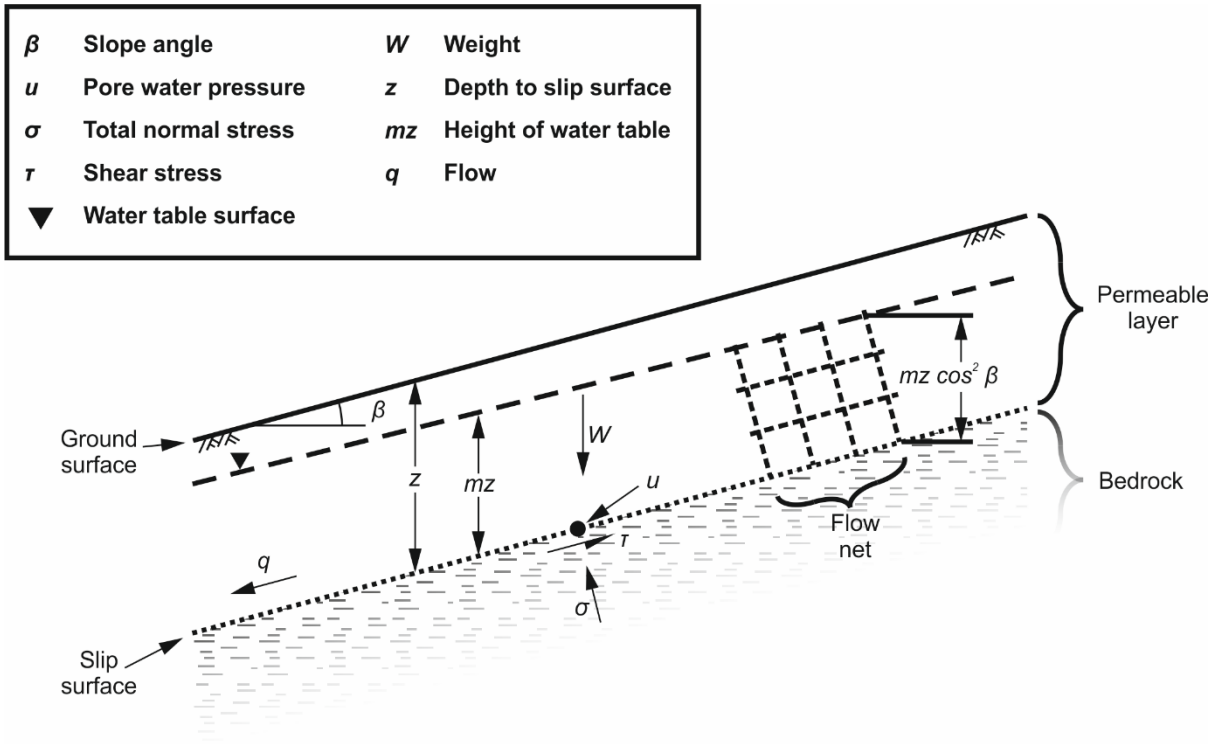

Figure 2.3: Schematic of an infinite slope model showing the main landslide processes showing the main components of a classical soil mechanics approach to slope failure (Terzaghi, 1943), adapted from Craig (2004).

In a geophysical survey, the result may determine the presence or extents of a landslide property (e.g., the water table). This time-static geophysical dataset gives information on the state of one (or more) property in the system at that particular time, but not how that property will change in response to some external influence (e.g., precipitation). With the addition of a second geophysical dataset at some point in the future, it may be possible to determine a change in that property (e.g. increase in water table height). The implicit assumption is that in order for a property change to have occurred, a process must have taken place in the time between the two surveys (e.g., infiltration). By looking at the differences between the data at each end of the time period, reasonable inferences can be made about the process that must have occurred to give rise to a change in the system.

Therefore, geophysical methods used in isolation are not able to definitively quantify the contributions that changes in these properties make to the overall stability of a slope, but the incorporation of environmental data (e.g., rainfall data) and the use of geotechnically-coupled surveys can provide empirical relationships that allow for such contributions to be assessed. Table 2.2 shows the parameters of landslide processes to which various geophysical methods are sensitive.

The figures presented in this section are simplified versions of landslide systems, meant to illustrate the features on landslide settings and processes that can be investigated in some way using geophysical methods. Field conditions are likely to present more heterogeneous conditions than those represented here. However, the identification of such heterogeneous conditions is itself an advantage of using geophysical methods to investigate landslide, with the spatial coverage of geophysical methods being one of the main benefits of the techniques (Everett, 2013, Kearey et al., 2001).

Table 2.2: Parameters of landslide processes that can be investigated using geophysical methods.

Slope stability property	Investigable feature	Applicable geophysical methods	Example
Normal stress (σ) $\sigma = \{m\gamma + m\gamma_{sat}\}z\cos^2\beta$	Depth to slip surface (z)	Electrical resistivity, seismic reflection, seismic refraction, surface wave methods, ground penetrating radar	Renalier et al. (2010a),
	Relative proportions of dry (or partially saturated) material ($(1-m)\gamma$)	Electrical resistivity, seismic reflection, seismic refraction, ground penetrating radar	Grandjean et al. (2010)
	Relative proportions of saturated material ($m\gamma_{sat}$)		
Pore water pressure (u) $u = mz\gamma_w \cos^2\beta$	Height of water table (mz)	Electrical resistivity, seismic reflection, seismic refraction, ground penetrating radar	Sastry and Mondal (2013), Grelle and Guadagno (2009)
Cohesion (c)	Presence of clay in subsurface material	Electrical resistivity, ground penetrating radar	Göktürkler et al. (2008)
Shear strength (τ_f) $\tau_f = c + (\sigma - u)\tan\phi'_{cv}$	Estimates of angle of shear resistance at critical state (φ'_{cv}) can be made using back analysis from estimating σ and u	Seismic refraction, surface wave methods	Al-Saigh and Al-Dabbagh (2010)

2.3.3 Applications of geophysical methods to landslide investigation

For a geophysical methodology to be effective as a monitoring tool, several criteria must be fulfilled:

- The subsurface property or process (e.g., moisture content) being measured or monitored must be detectable by the chosen method.
- The acquisition rate of data must be sufficiently high (with respect to changes in the monitored process) so as to be able to collect datasets that sample physical property changes at an appropriate rate.
- The measuring equipment must be able to be relocated accurately for series of discrete fieldwork campaigns, or the position of geophysical sensors must be accurately located if a semi-permanent installation is established.
- The data must ideally be able to be empirically linked to subsurface conditions to reflect the changes that occur in the physical properties of the subsurface over time.

In recent years, the application of geophysical methods to the characterisation of landslide settings has become increasingly common. Hack (2000) outlined the physics underpinning geophysical surveys for slope stability analyses, and Jongmans and Garambois (2007) provided a review of published landslide investigations using geophysical methods since the mid-1990s.

Both of these reviews highlight three important developments in landslide geophysics: the integration of multiple methods, the acquisition of multi-dimension data (including time-lapse approaches) and the quantification of geophysical results with geotechnical data. The integration of multiple geophysical methods for landslide investigations has become more common in recent years, allowing for better evaluation of internal structure to be made by overcoming the limitations of single-technique approaches (Schrott and Sass, 2008). However, multiple-method approaches to landslide monitoring using geophysical methods are still relatively scarce (Jongmans and Garambois, 2007).

The spatial dimensions across which geophysical data can be acquired have increased over time. One-dimensional (1D) 'sounding' type data provides information on the subsurface beneath a single location on the ground surface (e.g., Bièvre et al., 2012, Merritt et al., 2018). These vertical profiles of information can be interpolated to form pseudo two-dimensional (e.g., Harba and Pilecki, 2017) and pseudo three-dimensional data sets of subsurface properties (e.g., Renalier et al., 2010b).

True two-dimensional (2D) survey techniques allow data to be collected spatially across the ground surface (also referred to as 'geophysical mapping') (e.g., Colangelo et al., 2006), or as a subsurface profile or cross-section (e.g., Uhlemann et al., 2016a). The latter of these techniques can be interpolated to produce pseudo-three-dimensional volumes of data. True three-dimensional (3D) surveys involve the simultaneous acquisition of volumes of data (e.g., Chambers et al., 2011). All of these dimensions of data acquisition produce a static map of the distribution of physical properties within a landslide body, and prove invaluable for the characterisation of landslide settings. However, in order to work toward the prediction of landslide failure, an investigation method that takes into account the temporal variation within the landslide system should be used.

Geophysical techniques that include the addition of a time-series to the acquired data are sometimes referred to as '*time-lapse*', or '4D' datasets (e.g., Uhlemann et al., 2017). As '4D' specifically refers to a 3D dataset with multiple time-steps, the term 'time-lapse' will be used in this review to refer to datasets of any dimension (1D, 2D and 3D) which include multiple time-steps. Time-lapse geophysical monitoring of landslides is an area that has grown rapidly in the last decade or so (Jongmans and Garambois, 2007).

In order for the application of geophysical techniques to the monitoring of MIL over time to be successful, the frequency of dataset acquisition must be proportional to the timescale over which changes occur in the subsurface properties of the landslide. Geophysical monitoring therefore lends itself to the monitoring of slowly-deforming slopes. These slopes are typically comprised of highly-weathered rocks or soils and other superficial materials (such as tills, alluvium and other recently reworked materials). Failure in these landslide environments can be both 'brittle' (i.e., failure occurs along discreet shear-surfaces) or 'ductile' (i.e., the deformation processes are slow, such as slope creep). Landslides triggered by increased infiltration of water are of particular interest to geophysicists, as the formation and progression of precursory failure conditions can be detected using geophysical data, processing and interpretation (Baroň and Supper, 2013). For this reason, fast-failing and fast-

moving landslides that do not typically exhibit gradual changes in subsurface properties prior to failure are not considered in this thesis. These landslide types are typically fast-failing rockfalls and rock topples, fast-moving debris flows, and fast-failing and fast-moving rock avalanches (Hungr et al., 2014). In some instances, these types of failure may also be present in a MIL setting (e.g., Helmstetter and Garambois, 2010, Lacroix and Helmstetter, 2011) It is important to note, however, that geophysical monitoring systems do exist for these types of failure (Fiorucci et al., 2016, Lotti et al., 2015, Partsinevelos et al., 2016) and that many of the geophysical methods described here are similar in their application to these failure types. The case studies presented in this review therefore have a focus on the monitoring of landslides in settings comprising of soft-rock and superficial materials.

MIL are typically shallow, translational and/or rotational style landslides, with failure frequently occurring in soils and weathered bedrock layers. An exception to this are deep-seated gravitational slope deformation failures, which are characterised by very slow deformations of very large rock masses (Jomard et al., 2010, Lebourg et al., 2005). These have been included in this review as the progression of failure is slow enough to be robustly monitored using geophysical approaches, and periods of increased movement are linked to increases in precipitation (Helmstetter and Garambois, 2010, Lacroix and Helmstetter, 2011, Palis et al., 2017a). The study of landslides and their evolving processes is a highly interdisciplinary area of research. As such, the application of monitoring MIL has important implications for geologists, geomorphologists, geotechnical engineers and infrastructure stakeholders, especially as the impact of climate change is having a dramatic effect on the incidence of slope failures due to changing weather patterns (Gariano and Guzzetti, 2016).

2.4 Geophysical monitoring of landslides: methods and case studies

A list of publications in scientific journals and books since 2006 that utilize geophysical monitoring applied to landslides is shown in Appendix A. In total, 38 journal articles or book chapters are identified as using or describing geophysical monitoring approaches in landslide systems. Of these 38 publications, two are project updates that do not contain data, and 36 describe specific case studies. Some of the individual monitoring campaigns are described in more than one publication, and where possible this is indicated, leaving a total of 34 publications. Within these 34 publications, 54 monitoring campaigns at 27 separate landslides are identified from nine countries.

The geophysical monitoring methods identified and their corresponding abbreviations for this paper are shown in Figure 2.4. Further descriptions of these methods are found in the relevant sections detailing the case studies. Two broad types of geophysical methods are identified from this list: geoelectrical and seismic methods. In addition, two modes of acquisition are identified in both types; 'active' modes, in which the recorded geophysical signal is artificially generated, and 'passive' modes, in which the signal recorded is generated naturally.

In geoelectrical methods one active type, electrical resistivity (ER), and one passive type, self-potential (SP) monitoring, are identified. Typically 2D electrical resistivity (ER) profiles are acquired as part of the study, with similar instrumentation, acquisition parameters, processing routines and inversion methods applied across the case studies. Some examples where geoelectrical datasets are manipulated in bespoke ways do exist, for example,

the use of apparent resistivity (Palis et al., 2017b), transfer resistance data (Merritt et al., 2018) and 3D ER arrays (Uhlemann et al., 2017). The use of SP methods is also noted, although in a much reduced capacity to ER (Colangelo et al., 2006). In total, 20 time-lapse ER monitoring surveys are identified in the literature: Bièvre et al. (2012), Crawford and Bryson (2018), Friedel et al. (2006), Gance et al. (2016), Grandjean et al. (2009), Jomard et al. (2007), Lebourg et al. (2010), Lehmann et al. (2013), Lucas et al. (2017), Luongo et al. (2012), Merritt et al. (2018), Palis et al. (2017a), Palis et al. (2017b), Supper et al. (2014), Travelletti et al. (2012), Uhlemann et al. (2017), Xu et al. (2016). One time-lapse SP monitoring survey is identified, by Colangelo et al. (2006).

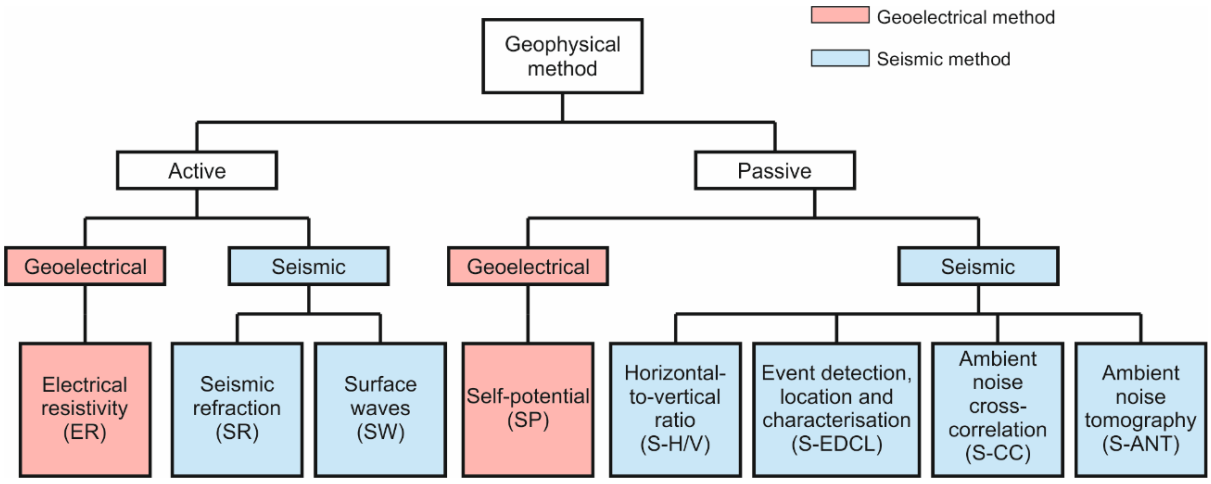

Figure 2.4: The geophysical methods identified in the 31 case studies, shown by mode of acquisition and method. The acronyms for each method are shown in the lower boxes.

In seismic methods, the active types of surveying include seismic refraction (SR) and analysis of surface waves (SW), and the passive types include seismic event detection, characterization and location (S-EDCL), seismic cross-correlation (S-CC), seismic horizontal-to-vertical ratio (S-H/V) and seismic ambient noise tomography (S-ANT). One study by Grandjean et al. (2009) used SR monitoring, and a study by Bièvre et al. (2012) utilised SW monitoring methods. In total, 31 case studies are identified as using passive seismic methods: Amitrano et al. (2007), Brückl and Mertl (2006), Brückl et al. (2013), Gomberg et al. (2011), Harba and Pilecki (2017), Imposa et al. (2017), Mainsant et al. (2012), Palis et al. (2017a), Provost et al. (2017), Renalier et al. (2010a), Tonnellier et al. (2013), Walter and Joswig (2008), Walter et al. (2009), Walter et al. (2011), Walter et al. (2012), Walter et al. (2013).

Some geophysical methods are absent from the literature surrounding landslide monitoring, for example, no studies in which ground penetrating radar has been used as a long-term monitoring tool are identified, although it has been used to provide detailed qualitative characterisation of landslide settings (Hruska and Hubatka, 2000).

Before presenting the details of individual methods and case studies, it is helpful to consider the different conditions under which the geophysical monitoring campaigns listed in Appendix A were acquired. The most

important aspects of these conditions to consider are the duration of monitoring, the modes of acquisition and the frequency at which data were acquired during the campaign.

2.4.1 Duration of geophysical monitoring data acquisition

The durations of geophysical monitoring are divided in to four approaches:

- *Controlled tests*: Typically artificial infiltration-type experiments in which an unstable slope was exposed to an increase in saturation by introducing simulated rainfall over a set period of time and subsurface conditions monitored throughout. Although the field instrumentation remained static between acquisitions, the field setups were not typically designed for long-term monitoring, and were assumed to have been accompanied by field crew for the duration of the experiment. The shortest and longest controlled experiments were both described by Lehmann et al. (2013), at 15 hours in one test and three days in another. All controlled experiment case studies showed a high-frequency of dataset acquisitions, typically every few hours. Six controlled tests were described in five publications: Grandjean et al. (2009), Jomard et al. (2007), Lehmann et al. (2013), Travelletti et al. (2012), Colangelo et al. (2006).
- *Transient measurements*: Typically involved the deployment of instruments for the duration of a single dataset acquisition, after which the instrumentation was removed from the field before being deployed again in the same location after a period of time. Monitoring periods varied greatly, with the shortest recorded as 62 days (Lucas et al., 2017) and the longest as 1589 days (Imposa et al., 2017). In both of these studies, six datasets were acquired over the monitoring period, highlighting the variability in acquisition frequency that can accompany a transient measurement approach.
- *Short-term installations*: Utilise equipment installed and left in the field, but for shorter periods than semi-permanent installations. Consequentially, the length of these monitoring campaigns fall between controlled tests and semi-permanent installations. Unlike controlled tests, environmental conditions are not artificially altered (e.g., by artificial rainfall) and instead natural variations in environment and subsurface response are monitored. However, equipment tends to be deployed for periods of less than 100 days, and so surveys cannot typically monitor seasonal or annual scale variations subsurface conditions, although the monitoring period may coincide with periods of increased rainfall. Often, the full cycle of a monitoring campaign may involve several short term installations at the same landslide (e.g., Brückl and Mertl, 2006), although in some studies, the exact position can vary between these repeated surveys (e.g., Walter et al., 2011). The shortest period of monitoring using short-term installations was for one day, although this day comprised one survey of a sequence described by Brückl and Mertl (2006). The longest period of monitoring achieved with a short-term installation was by Lebourg et al. (2010) at 90 days.
- *Semi-permanent installations*: Installations are left in the field to acquire data according to a predetermined (or sometimes remotely programmable) schedule. Unlike transient measurements, the time period between acquisitions was often regular. Semi-permanent installations allow for a high-frequency data acquisition (typically one or more datasets acquired per day) over long monitoring periods (typically months to years). The shortest monitoring period studied with a semi-permanent installation was 146

days in a study by Luongo et al. (2012). Most studies operating at annual-scale time periods, and often at an acquisition rate of more than one dataset per day. In Supper et al. (2014), two examples are given where datasets were recorded every 4 hours for 239 days and 275 days at two separate sites. These monitoring systems also tend to include the ability for data to be retrieved remotely from the equipment, often by utilizing telemetry and storage of data on a remote server.

2.4.2 Acquisition mode of geophysical monitoring data

Figure 2.5 shows the relationship between different geophysical methods, and how they are suited to different types of geophysical monitoring. Geophysical methods acquiring active mode data lend themselves to acquiring higher resolution spatial data, due to the tendency toward acquiring time-discreet datasets. Geophysical methods acquiring passive mode data tend to higher resolution temporal data, as they acquire temporally continuous datasets. Some geophysical methods, however, are able to produce high-resolution spatial data from passive acquisition modes.

2.4.3 Geophysical data acquisition frequency

Figure 2.6 shows a chart plotting the duration of each monitoring campaign against the number of datasets acquired in each monitoring campaign. There is some difficulty equating the number of datasets acquired in a monitoring period between different types of geophysical methods. The ER, SP, SR, SW, S-ANT and some S-H/V methods acquire time-discreet sets of data. This is because the entirety of a dataset is made up of a multitude of unique data points, the position and number of which determine the spatial resolution of the survey method. These methods therefore tend to have high spatial resolution and coverage (see Figure 2.5). It is the number of electrodes (in ER and SP surveys), geophones (in SR and SW surveys) or seismic sensors (in S-ANT and S-H/V surveys) that define the spatial resolution and coverage; the more measuring points to the system, the higher the resolution and/or the larger the spatial coverage of the monitoring system. However, the temporal resolution is limited to the amount of time it takes to acquire the full complement of unique readings in a whole dataset. In ER systems, for example, it can take several hours for a full dataset to be acquired.

In contrast, S-EDCL, S-CC and some S-H/V methods acquire data from continually recording seismometers. In these cases, data are acquired for the entirety of the monitoring period, with the exception of any periods of maintenance or failure. These methods therefore have high temporal resolution (see Figure 2.5), however, similarly to discreet dataset acquisition systems, the spatial resolution is still dependent on the number of measuring components. For some applications (e.g., S-CC and S-H/V), data are divided into daily records, but in some methods (e.g., S-EDCL) only the time of the event recorded is required. The number of datasets acquired in a monitoring period by seismometers is therefore technically one dataset per field campaign, although this can be completely arbitrary in some processing methods. In some approaches, such as in S-ANT, the distinction between continuously acquired and time-discreet data is blurred further, as the data processing typically deals with discrete time-steps extracted from the continuous dataset.

Therefore, in Figure 2.6, for time-discreet dataset acquisition systems (ER, SP, SR, SW, S-ANT and some S-H/V methods), the number of datasets acquired across the entire monitoring period are plotted. For monitoring campaigns that utilise continually recording seismometers (S-EDCL, S-CC and some S-H/V methods), the number of seismometers, rather than the number of datasets acquired, has been plotted. For seismometer entries, this therefore gives an indication of the spatial resolution of the survey, rather than the temporal resolution, which can be assumed to be total for the monitoring period.

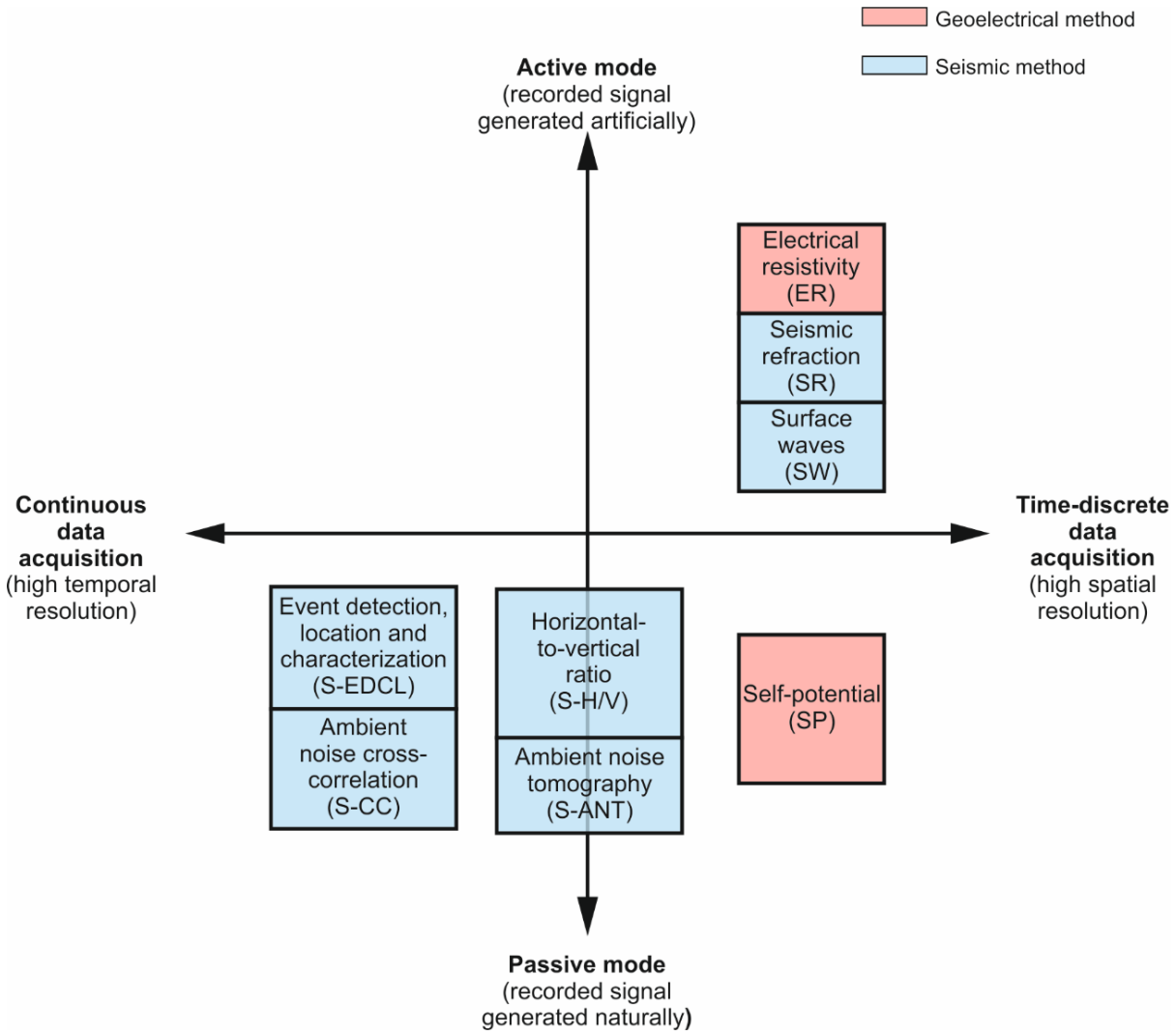

Figure 2.5: Relationship between the geophysical methods outlined in Appendix A in terms of their acquisition mode (active or passive) and temporal resolution (continual or time-discreet) demonstrating the trade-offs which must be considered when choosing a method for monitoring of MIL.

With regards to the spatial resolution and coverage of surveys, an ER system for example, may have a single unit (with a single data logger, single power source, single telemetric communication system) controlling an entire electrode array consisting of several tens of electrodes, across a profile of hundreds of metres. Conversely, a single seismometer, or localized array of seismometers, is typically operated by a single logger with a single power

source and the coverage of data acquisition is dependent on the events detected at that location. To expand the spatial resolution, a second seismometer with a separate logger and power source must be added. In contrast, expanding the spatial coverage of an ER monitoring system may be as simple as adding extra electrodes in to the system.

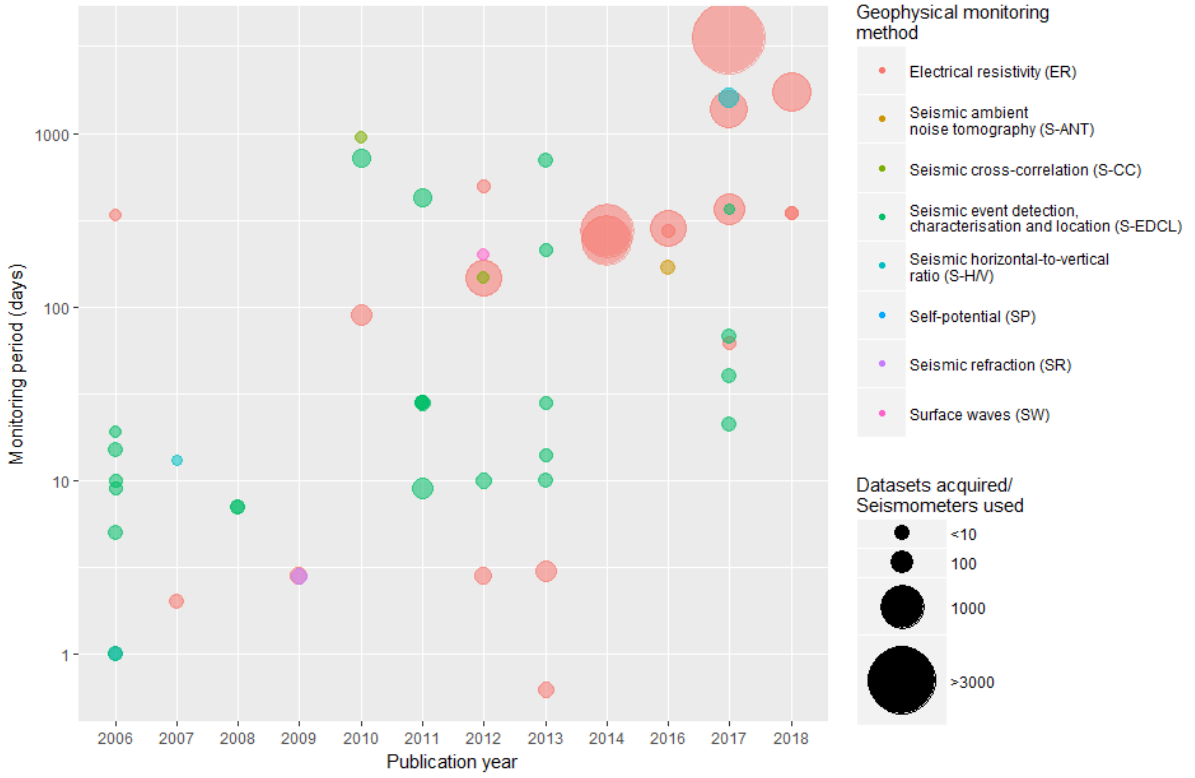

Figure 2.6: Plot showing the year of publication for case studies against the number of days in the monitoring period for each case study. The relative area of each data point is proportional to the number of datasets acquired. Data collected from seismic monitoring networks are considered to have collected one dataset per sensor for the entire monitoring period.

Figure 2.6 illustrates several interesting developments in the field of geophysical monitoring of MIL in the last decade or so. Firstly, that the number of published studies is increasing in time, suggesting increases in the application of geophysics to landslide monitoring, or in some cases, the recent maturation of long-term studies. Secondly, there is a notable increase in ER case studies from 2012, and a sharp increase in both the monitoring period lengths and amount of data collected by these studies. This suggests greater developments in the field of monitoring landslides using ER methods, compared to seismic methods, which show much more restrained increases. This trend is curious, as passive seismic instrumentation has been at a far more advanced state of development for long-term monitoring for much longer than ER methods.

2.4.4 Geoelectrical monitoring case studies

Moisture dynamics can vary greatly over time, although lithological composition tends to remain relatively constant, particularly in a pre-failure condition. Geoelectrical monitoring can therefore be used for the determination of moisture dynamics and hydrogeological processes within MIL bodies over time.

2.4.4.1 Electrical Resistivity (ER)

Electrical resistivity (ER) is a common technique routinely applied to the investigation of landslides (Jongmans and Garambois, 2007). The method can be applied in 1D, 2D and 3D investigations (Loke et al., 2013), although 2D and 3D investigations of landslides are more common in recent times. ER is measured by injecting a DC current into the ground between two electrodes, and measuring the potential difference between a separate pair of electrodes (Kearey et al., 2001). By deploying linear arrays of electrodes, measurements can be made using different combinations of electrodes in order to build a 2D image of the subsurface resistivity. Similarly, 3D datasets can be acquired using multiple parallel (and orthogonal) profiles or grids of electrodes.

In a typical 2D linear array, the number of unique measurements made is proportional to the number of electrodes deployed at the ground surface. The position of a single resistivity measurement is a function of the distance between the electrodes used, and their position on the ground surface. In most near-surface geophysical applications, the raw data recorded by ER meters ('apparent resistivity') is processed using a tomographic inversion. The process of tomographic inversion produces a ground model based on the data recorded and a set of assumptions made from physical laws (e.g., current flow through subsurface equipotential surfaces) and earth observations (e.g., subsurface models obeying geological principles). Crucially, the process provides information between the measurement points of an array based on the surrounding data. Inversions can be done in 2D and 3D, and with the addition of time-lapse sequences in which the time-series between dataset acquisitions is treated as a variable in the inversion process. However, a common approach is to undertake separate inversions of data at individual time-step, and create difference models (e.g., percentage changes or difference ratios) between the results. This approach, whilst less computationally expensive, can omit or exaggerate important features that may be highlighted by a true time-lapse inversion.

The result of any inversion is typically an image showing the distribution of resistivity in the subsurface. The full process from acquisition to inversion is often referred to interchangeably as electrical resistivity tomography (ER) or electrical resistivity imaging (ERI). This thesis uses the abbreviation ER to refer to these terms. Tomographic inversion can be computationally expensive, and for this reason, ER data is occasionally not inverted to produce images of the subsurface. Alternative uses of ER data include assessing the raw measurements, or apparent resistivity, visually and statistically to detect changes in the subsurface over time. Another use of non-inverted data is to look at transfer resistances between electrodes in an array. These measurements do not divulge information on spatial variations in the resistivity data, but are still sensitive to changes in moisture content over time. The advantage of these approaches is the rapidity of assessments that can be made with minimal manual interpretation and computing resources.

In the case study publications identified in Appendix A, 17 of the surveys used time-lapse ER methods; five were under controlled test conditions, four utilised transient measurements, and eight described semi-permanent installations of electrode arrays. In most of the studies, the stated aim of the time-lapse ER surveys were to identify properties pertaining to water movement or distribution within the landslide setting. These studies were all undertaken in 2D, with the exception of one time-lapse ER survey that was undertaken in 3D (Uhlemann et al., 2017).

In one controlled test case study by Travelletti et al. (2012), simulated rainfall was applied to a 100m^2 area of the accumulation zone in the Laval landslide, South French Alps. A 47m long profile comprising 48 electrodes spaced 1m apart collected electrical resistivity data over a 67-hour period of artificial rainfall of 11 mm h^{-1}. The experiment started under unsaturated conditions (at approximately 27% saturation) and aimed to determine the time at which steady-state flow was reached in the landslide body. By comparison with piezometer data, this was determined to have occurred 21 hours after the onset of artificial rainfall. The results of the time-lapse ER survey are shown in Figure 2.7. A total of 32 data acquisitions were made during the experiment, resulting in an acquisition frequency of approximately 2 hours. The results of the time-lapse survey were able to map the evolution of saturation within the slope, as well as determine the bedrock geometry of the area under investigation. The authors recommended increased acquisition rates during the experiment to better monitor wetting processes, and the incorporation of 3D arrays to improve the quantitative analysis of the data, primarily due to the suspected 3D effects that are likely to have occurred during the experiment, but that are not captured by the 2D inversion approach of the data.

The study by Travelletti et al. (2012) showed a relatively high frequency of data acquisition over a short period of time, and in this regard is similar to other artificial rainfall experiments which utilised time-lapse ER methods (Grandjean et al., 2009, Jomard et al., 2007, Lehmann et al., 2013). The timescales and acquisition rates of these studies are in contrast to longer term studies that utilise transient measurements and semi-permanent installations. In one study by Bièvre et al. (2012) transient time-lapse ER measurements were used to determine the role of fissuring on water infiltration over a 498 day period, by acquiring 4 time-lapse ER datasets in the unstable clay slopes of the Avignonet landslide in the Trièves area of the French Alps, France. Although the campaign lasted over a year, resistivity datasets were acquired at 0 days, 29 days, 236 days and 498 days, showing an irregular acquisition schedule. Despite the relatively low-frequency and irregularity of acquisition, the time-lapse approach suggests that the observed evolution of fissuring shows variations in resistivity that are related to the water storage capacity of the fissures. Higher-frequency dataset acquisition would benefit the monitoring of the evolution of fissure-aided infiltration.

The use of semi-permanent 3D arrays and regular acquisition schedules are able to overcome the issues of irregular acquisition rates and 3D effects in 2D surveys, and pseudo-3D surveys interpolated from 2D datasets. These 3D effects occur where a feature that may not be directly located beneath the ER profile influences the data. Such a study was described by Uhlemann et al. (2017), in which a semi-permanent time-lapse monitoring system was used to collect 3D ER data approximately every 2 days at the Hollin Hill landslide in North Yorkshire, United Kingdom. The study involved several other novel aspects beyond the incorporation of 3D data acquisition. First, inversion models were able to account for movement experienced by the electrodes in the sliding mass (Wilkinson et al., 2016), which can introduce significant errors in the data if not accounted for. Additionally, the

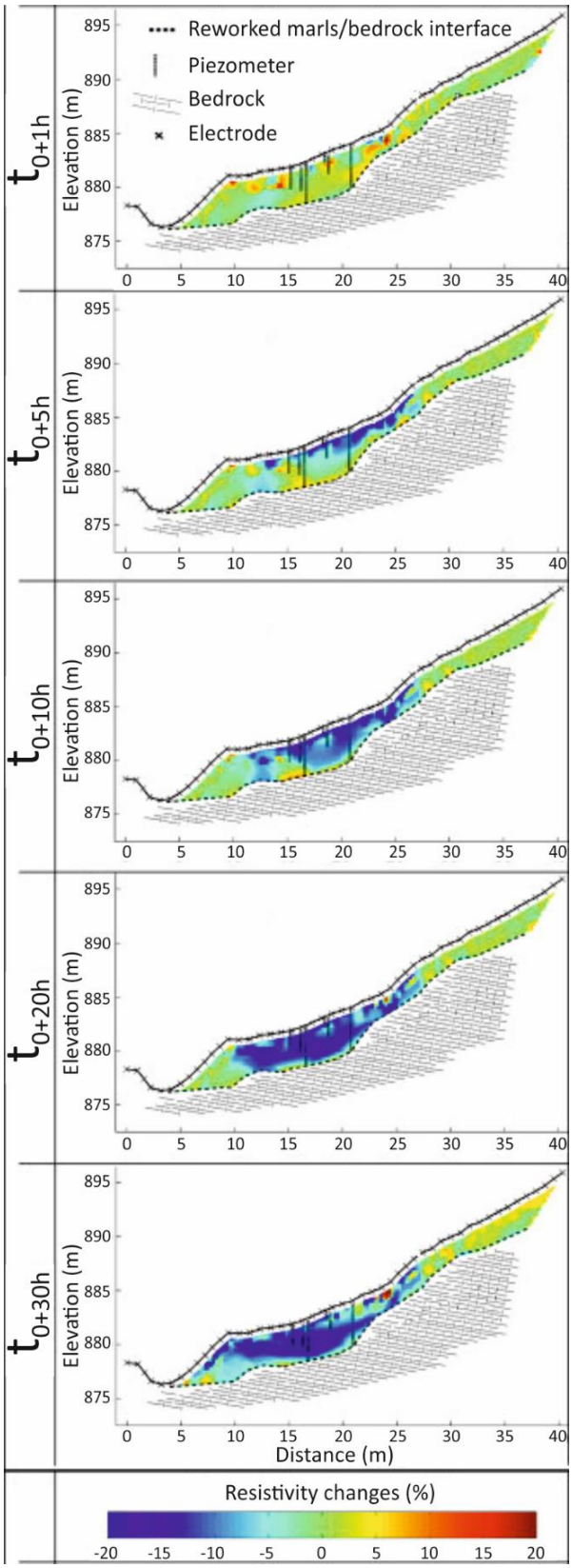

Figure 2.7: The results of a controlled test time-lapse ER survey by Travelletti et al. (2012) under artificial rainfall conditions (see text). The inverted ER images showing a decrease in resistivity in response to the increased saturation of the subsurface. Modified from Travelletti et al. (2012).

resistivity data were converted to gravimetric moisture content (GMC) by fitting of a Waxman-Smits model (Waxman and Smits, 1968) to laboratory experiments of wetting and drying of samples obtained from the site (Merritt et al., 2016). This allowed the production of volumetric images of GMC data, showing the hydrogeological variation in the landslide body both before and after a slope failure in December 2012 (Figure 2.8).

Other long-term time-lapse ER studies have utilised data in other novel ways in order to capture subsurface moisture variations within landslides over time. Studies utilizing non-inverted ER data as an indicator of hydrological variation have been made by several authors. These studies were able to detect features such as water table variations (Palis et al., 2017b), links between hydrological patterns and changes in apparent resistivity (Lebourg et al., 2010, Palis et al., 2017a) and relationships between resistance data and subsurface moisture dynamics (Merritt et al., 2018). In each of these studies, the data required significantly less processing than if tomographic inversion of the data had taken place.

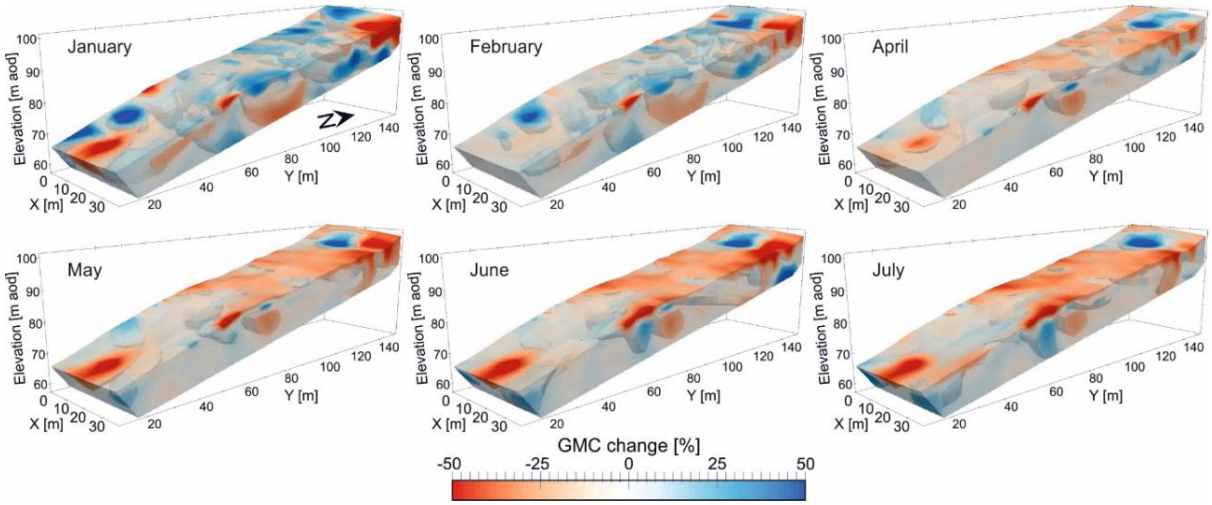

Figure 2.8: Volumetric images of gravimetric moisture content (GMC) derived from a 3D time-lapse ER system (Uhlemann et al., 2017) showing the progressive drainage of a landslide after significant movement in December 2012. Volumetric images shown here are from the later part of a monitoring campaign spanning over three years, and show the changes in GMC relative to a baseline model acquired at the beginning of the monitoring period in March 2010. Modified from Uhlemann et al. (2017).

After conducting time-lapse surveys to confirm the application of ER to the Vence landslide in south-eastern France, Lebourg et al. (2010) used apparent resistivity correlations compared to rainfall and ground water levels to conduct multi-dimensional statistical analysis and determine pre- and post-rainfall states of the landslide over a 90 day monitoring period. The simultaneous presentation of individual apparent resistivity measurements alongside rainfall events over a 275 day monitoring period at a landslide at Ampflwang-Hausruck, Austria, by Supper et al. (2014) allowed for rapid observations of the response of measurements to rainfall events to be made without the need for time-lapse inversions. However, it is worth noting that Supper et al. (2014) still produced time-lapse inversions for detailed determinations of movement events and relationships with precipitation. At

the La Clapière landslide in the Alpes Maritimes, France, Palis et al. (2017a) compared the median apparent resistivity value from a semi-permanent ER system to a cumulative rainfall index, and observed both short-term decreases in resistivity associated with acute rainfall events, as well as longer seasonal variability linked to solar radiation. Apparent resistivity data from a 9.5 year monitoring period was statistically analysed using cluster analysis in a study by Palis et al. (2017b). The results of the study allowed the determination of distinct hydrogeological units within the landslide without the need to make assumptions about the local geology, identifying areas of the landslide that react differently to water infiltration. However, the authors ultimately recommend further work to establish petrophysical relationships between the resistivity and moisture content, similar to the approaches undertaken by Uhlemann et al. (2017). Merritt et al. (2018) utilised resistance measurements to conduct rapid observations of moisture dynamics at the Hollin Hill landslide in North Yorkshire, UK. The resistance data were derived from the same ER system used in the study by Uhlemann et al. (2017). As resistance data can be analysed before the process of inversion, the study proved to be a rapid means of assessing the near-surface of the Hollin Hill landslide to identify areas of potential preferential infiltration. This type of approach can prove useful for the determining areas of a landslide in which more computationally expensive investigations should be undertaken.

2.4.4.2 Self-Potential (SP)

Self-potential (SP) techniques measure the presence of naturally occurring charges in the earth surface, primarily streaming potentials and electrochemical potentials, although thermokinetic potentials and cultural activity may also be recorded (Colangelo et al., 2006). As such, SP is defined as a passive geophysical method. Potentials between pairs of electrodes are measured to create areal maps of variation in self-potentials. In the context of landslides, this is normally to determine areas of subsurface flow within the subsurface material. As with electrical resistivity, semi-permanent arrays of electrodes can be installed to facilitate high-frequency long-term monitoring campaigns. Tomographic inversion of 2D and 3D surveys can be undertaken to ascertain information in cross-section and volumes (Ozaki et al., 2014).

Only one study used SP monitoring of landslides (Colangelo et al., 2006) in which temporal fluctuations of SP signals were monitored over a 24 hour period during a period of precipitation. A linear array of electrodes were deployed, and the data were inverted (to produce a tomographic inversion cross-section) to show the dynamics of subsurface flow during the rainfall event. The study describes in a qualitative manner the variation in flow, instead of moisture content as normally targeted by ER surveys. As the SP method does not give any information in itself on geological characterisation, the interpretations were made with the knowledge acquired from previous SP mapping and ER investigations of the landslide setting.

2.4.5 Active seismic methods

Active seismic methods provide information about the elastic properties of the media through which seismic waves travel. This reveals geomechanical properties of subsurface materials and can indicate changes in the

subsurface stress conditions associated with movement, as well as providing information on the porosity of materials, and in turn fluid flow characteristics.

Seismic refraction (SR) and surface wave methods (SW) use field deployments of surface geophones linked to a seismograph to record properties of artificially generated seismic waves. In SR, the arrival times of compressional waves (P-waves) and shear waves (S-waves) are recorded. P- and S-waves are typically generated using an impact source (e.g., a sledgehammer). P-waves are generated by a vertical impact to a plate resting on the ground surface, and recorded using geophones sensitive to movement in the vertical direction. S-waves are generated by a horizontal impact to a plate coupled to the ground, and the resultant waves recorded by geophones sensitive to motion in the horizontal plane. The arrival times ('first-breaks') on each geophone give information about the refracted pathway taken by the wave between the source and geophone. This information can then be inverted to give a model of the P-wave or S-wave distribution in the subsurface, which can then be interpreted in terms of variations in elastic properties of the subsurface.

SW methods record surface waves (primarily Rayleigh waves, although Love waves can also be analysed), which are typically much slower and of greater amplitude than refracted P-waves and S-waves. Analysing the frequency content of these waves can be used to produce dispersion-curves, which show phase velocity as a function of frequency. By analysing the fundamental mode energy in these images, a surface-wave velocity inversion is used to produce a 1D model of S-wave velocity as a function of depth. Lateral measurements of surface-wave velocity profiles can then be collated to produce 2D sections of interpolated S-wave velocity throughout the ground. Calculating S-wave velocity from surface waves is often preferred by investigators, as the field setup for acquiring surface waves is effectively the same as that of a P-wave SR survey, removing the need to repeat S-wave SR surveys to obtain S-wave velocities (Bergamo et al., 2016, Pasquet et al., 2015).

Two case studies utilised active seismic monitoring methods in landslide settings. Of these, one used SR surveys (Grandjean et al., 2009) and one utilised SW methods (Bièvre et al., 2012). Both studies achieved the stated aims of the experiments, but show relatively poor potential for obtaining long-term datasets at frequent intervals; indeed no examples of semi-permanent installations of active source SR or SW applied to landslides are apparent in the literature. This is likely due to the relative complexity of remotely generating the necessary seismic sources, although analogous borehole systems do exist (Daley et al., 2007).

2.4.5.1 Seismic Refraction (SR)

In the study of Grandjean et al. (2009), the main focus of the time-lapse P-wave SR surveys were to determine fissure density during a simulated rainfall experiment on a landslide in the Laval catchment in Alpes-de-Haute Provence, France. The P-wave survey was undertaken using a 48-channel seismic system, using 40Hz geophones and a hammer source. The aim of the survey was to integrate the SR datasets with simultaneously collected ER datasets using a fuzzy logic approach. Direct analysis of the P-wave SR suggested that low P-wave velocities in the near-surface were due to increased fissure density. However, in contrast with the ER survey, P-wave SR showed very little change with increasing saturation over the course of the experiment, which underscores the usefulness of integrated use of SR and ER surveys.

2.4.5.2 Analysis of Surface Waves (SW)

Bièvre et al. (2012) used the variations in SW dispersion (Rayleigh waves) to assess the state of fissuring in the clay-rich slopes of the Avignonet landslide in the Trièves area of the French Alps, France. Surface waves were acquired using 24 4.5Hz geophones, and a hammer source. Analysis of the surface waves using amplitudes and spectral ratios were undertaken for two different acquisition dates, one in January and the other in July, in order to determine relative differences between the states of fissuring on each occasion. The authors determined that the fissures remained open at these different times, with some possible minor variation in the depth of the fissures.

2.4.6 Passive seismic methods

In order to obtain continuous seismic data over longer monitoring periods, it is necessary to look to methods more typically adopted by the seismological monitoring community for the assessment of large scale natural hazards such as volcanoes and earthquakes (Daskalakis et al., 2016). In recent years, the application of passive seismic monitoring techniques have increasingly been applied to engineering issues (Öz, 2015), with notable advances in the field of ambient noise measurements and the application of spectral analyses to passive measurements (Park and Miller, 2008, Planès et al., 2016). Early work by Suriñach et al. (2005) identified changes in the frequency content of seismic records at avalanche and landslide sites that were associated with initiation of mass movement.

Although the treatment and processing of passive seismic data varies depending on the intended use, the principal style of acquisition is essentially the same. A seismic recording instrument is left for a period of time to record signals that may be generated by movement within the landslide body, or signals that are generated by known or unknown, endogenous and exogenous sources. The instruments used can be geophones (typically for shorter recording periods), broadband seismometers, or other adapted sensors (e.g., accelerometers). Properly maintained and adequately powered semi-permanent installations of seismic sensors are able to record continuous datasets for very long time scales. For example, the monitoring period in a study by Renalier et al. (2010a) exceeded 2.5 years. Some studies employ sensor deployments for much shorter periods of time (i.e., <100 days) (e.g., Amitrano et al., 2007), in what have been described here as short-term installations. These deployments are generally short due to equipment availability or the lack of in-field power sources to maintain long monitoring periods. Single sensor deployments can be used, for example to detect movements within an area (e.g., Amitrano et al., 2007), or multiple sensor deployments can be used for more detailed interpretations (e.g., Brückl et al., 2013).

The case studies reveal a range of data analysis methods using passive seismic approaches. To simplify the description of approaches, the use of passive seismic methods is split into four categories: seismic horizontal-to-vertical ratio measurements (S-H/V), event detection, characterisation and location (S-EDCL), seismic ambient noise cross-correlation (S-CC), seismic ambient noise tomography (S-ANT).

2.4.6.1 Seismic H/V ratio (S-H/V)

The S-H/V technique involves recording ambient noise and analysing the Fourier amplitude spectra ratio between the horizontal and vertical components of the seismometer, known as the horizontal-to-vertical ratio (Chatelain, 2004, Nakamura, 1989). The resulting S-H/V spectral ratio curves can be used to determine relative seismic impedance in the subsurface, and can therefore identify changes in layer thicknesses or the presence of other features, such as slip planes.

S-H/V methods have been used in two studies to monitor landslides (see Appendix A), but with two very different approaches. In Amitrano et al. (2007), S-H/V measurements were made from a short-term installation of a single broadband seismometer located at the Super-Sauze landslide in France. The calculated cumulative RMS of the S-H/V ratio for several frequency bands showed a correlation with periods of increased rainfall, indicating changes in the mechanical properties of sliding material during periods of acceleration.

Imposa et al. (2017) utilised a transient measurement approach, using a sensor specifically designed for the acquisition of S-H/V readings. These readings were acquired at the same stations in two separate surveys separated by five years. For transient S-H/V measurements, recording durations between 2 and 24 minutes are typically used (Acerra et al., 2002). The individual S-H/V spectral ratios that are produced per sensor location were processed and interpolated to produce cross-sections of seismic impedance, showing changes in the location of the potential slip surface post-failure.

2.4.6.2 Seismic event detection, characterisation and location (S-EDCL)

S-EDCL utilises the more traditional aspects of seismology commonly applied in earthquake and volcano monitoring. The approach is to detect events and classify them based on the source provenance and generation. This approach involves direct interpretation of the signals recorded by semi-permanent seismic sensors, either by identifying and classifying seismic events associated with movement in the landslide mass (i.e., 'slidequakes' (Gomberg et al., 1995)) or by precursory activity that may be linked to impending movement (a phenomenon observed in rockfalls and other brittle landslides (e.g., Bell, 2018, Poli, 2017)), or a response to recent increased infiltration (e.g., Palis et al., 2017a). A single seismic sensor installation is capable of achieving this type of monitoring (e.g., Amitrano et al., 2007), however, a network of seismometers is required to locate detected events (e.g., Walter et al., 2011). It is worth mentioning here that S-EDCL methods are also the only approaches used in the near real-time detection and characterisation of landslides at the regional scale (e.g., Kao et al., 2012, Manconi et al., 2016), and are commonly used in studies relating to rockfalls and other fast-failing landslides.

An example of event detection and characterisation is described in Provost et al. (2017). In this study, the authors proposed an automatic classification system, in order to identify and separate seismic events recorded at the Super-Sauze landslide in France based on their source and provenance. Sources included signals from rockfalls and 'slidequake' events within the landslide, and earthquakes and ambient noise events originating from outside the landslide setting. Example seismic signals are shown in Figure 2.9.

Brückl et al. (2013) undertook seismic monitoring of the Gradenbach landslide in Austria. They were able to locate events recorded using six seismometers installed at the site, and noted increases in seismic activity up to 1.5 months before the manifestations of slope deformations that coincided with snowmelt. Palis et al. (2017a) also noted increased seismic activity as a result of increased precipitation at the La Clapière landslide, France, aiding in the establishment of rainfall threshold values for slope movement at the site.

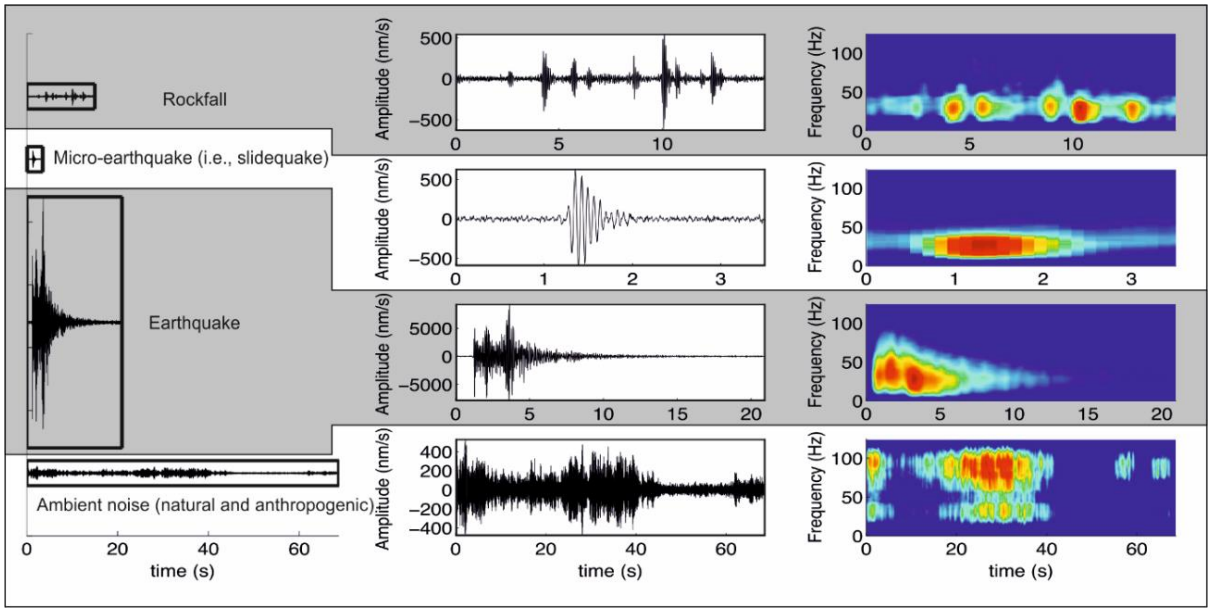

Figure 2.9: Example of seismic event detection and classification at the Super-Sauze landslide. The types of seismic events include endogenous (rockfall and slidequake) and exogenous (earthquake and ambient noise) events. Modified from Provost et al. (2017).

The studies by Gomberg et al. (2011) at the Slumgullion landslide in the US, Walter et al. (2011) at the Heumoes landslide in Austria, and Walter et al. (2012) at the Super-Sauze landslide in France are all summarised in a study by Walter et al. (2013). The authors related increases in seismic activity to brittle failure (i.e., fracture generation) of the landslide material, but also noted periods of movement that were not associated with increases in seismic activity. These aseismic movement events were related to periods of viscous creep, rather than brittle failure events. Location of the seismic sources of these events showed very different areas of seismic activity, and a strong association with the profile of the slip surface, the type of materials present, and the style of failure. Figure 2.10 shows the slidequake events located at the Heumoes landslide using S-EDCL methods (Walter et al., 2013).

2.4.6.3 Seismic ambient noise cross-correlation (S-CC)

Cross-correlating signals from a pair of seismic sensors recording the same random ambient noise can be used to generate the impulse signature (Green's function) of wave propagation between sensors (Wapenaar et al., 2010). Many sources of natural and anthropogenic noise can be utilised (for example, oceanic noise, vehicle traffic noise) if the source can be averaged over time to simulate a random ambient source. These cross-correlation functions

(CCFs) can be used to monitor variations in surface-wave velocity over time, indicating changes in the stress field of subsurface materials (Lecocq et al., 2014).

Two of the case studies (Appendix A) utilise cross-correlation methods to determine variations in geological material strength over time within moving landslides (Mainsant et al., 2012, Renalier et al., 2010b). Renalier et al. (2010a) observed increases in seismic wave arrival times between two semi-permanent seismometers over a 32-month monitoring period at the Avignonet landslide in the Trièves area of the French Alps, France. The differential in arrival times equated to an almost 0.2% decrease in velocity over time, with relative differences in ground motion between the seismometers only able to account for an equivalent of a 0.06% change in seismic wave arrival times. The authors concluded that the increase in arrival times corresponded to an increase in "damage" (i.e. fissuring and destruction of soil fabrics) to the material of the landslide. This area of damaged material was characterised by a stand-alone S-wave SR survey, in which the velocity of the damaged material was shown to be two to three times less than the surrounding undamaged area.

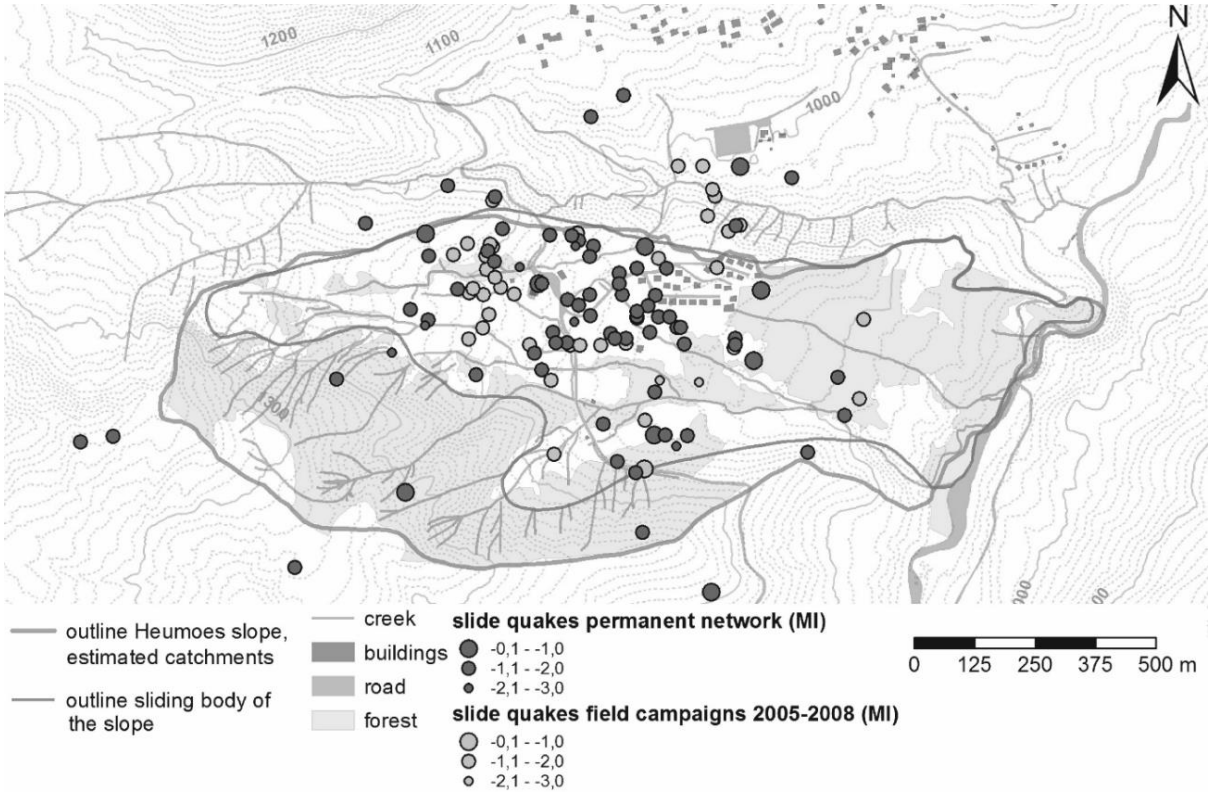

Figure 2.10: Locations and magnitudes of slidequake (i.e., seismic activity generated by slope movement) events detected at the Heumoes landslide, Austria by several seismic networks. Events are identified by different size and colour dots on the map. The seismic networks include one semi-permanent installation (see "permanent network") and several short-term deployments (see "field campaigns 2005 – 2008"). From Walter et al. (2013).

A study by Mainsant et al. (2012) over a shorter period of 146 days at the Pont Bourquin landslide in Switzerland was able to detect variation in surface-wave velocities a few days before significant slope failure on the 19th August (Figure 2.11). A drop of 2% in surface-wave velocity occurred over a period of 20 days after heavy rainfall, with

the surface-wave velocity dropping a further 5% in the 7 days preceding a significant failure at the landslide. The study highlights the applicability of long-term seismic monitoring to determining variations in subsurface material strength, and the potential landslide predictive capacity of seismic monitoring.

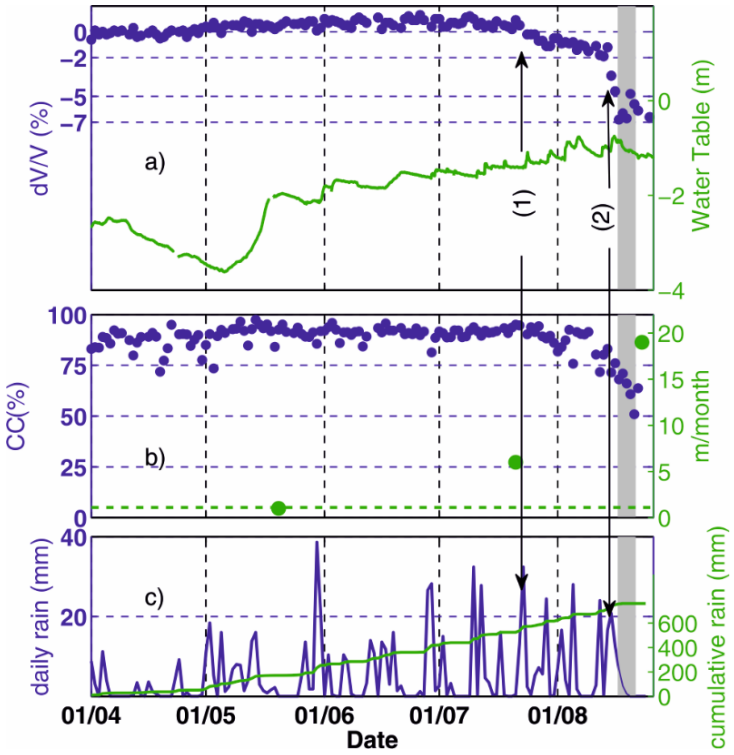

Figure 2.11: (a) The results from calculating changes in relative surface-wave velocity over time via cross-correlation of ambient noise seismic records by Mainsant et al. (2012). Decreases in velocity by 2% develop over 20 days (1), before a total decrease of 7% is observed (2) in the 7 days preceding a significant failure (shaded grey area). (b) The cross-correlation coefficient and (c) the daily and cumulative rainfall.

2.4.6.4 Seismic ambient noise tomography (S-ANT)

A frequency-time analysis of the outputs from cross-correlations can allow for the generation of dispersion curves (Bensen et al., 2007), which can in turn be inverted for the S-wave velocity of the near-surface (e.g., Stork et al., 2018). Interpolation of the inverted dispersion curves between sensor pairs allows for the production of images similar to those seen in previous active seismic and geoelectrical techniques. Linear deployments of sensors allow the acquisition of data in 2D profiles, and studies have been able to image landslide bodies in 3D using non-linear arrays, although these have not incorporated a time-lapse element yet (Renalier et al., 2010b).

Only one case study produced these cross-section images by acquiring transient measurements on separate dates acquired from an array of 12 seismometers. In the study by Harba and Pilecki (2017) ambient noise data were acquired for 60 minute periods at two profiles using 12 seismometers. Measurements were made at the profiles at three separate dates over seven months. The study took place at the Just-Tegborze landslide in Nowy Sacz, southern Poland. The first acquisitions were made during a dry period in January 2015, the second acquisitions

in March 2015 after the spring thaw, and finally during a very wet period in July 2015. One-dimensional inversions of dispersion curves were performed on the cross-correlated signals between sensor pairs, and the subsequent interpolated 2D cross-sections showed variations in the shear-wave velocity distribution throughout the landslide mass between acquisition dates (Figure 2.12). The authors attribute the decreasing shear-wave velocity in the mid-section of the landslide to the increasing moisture content of the landslide associated with spring thaws and increased rainfall.

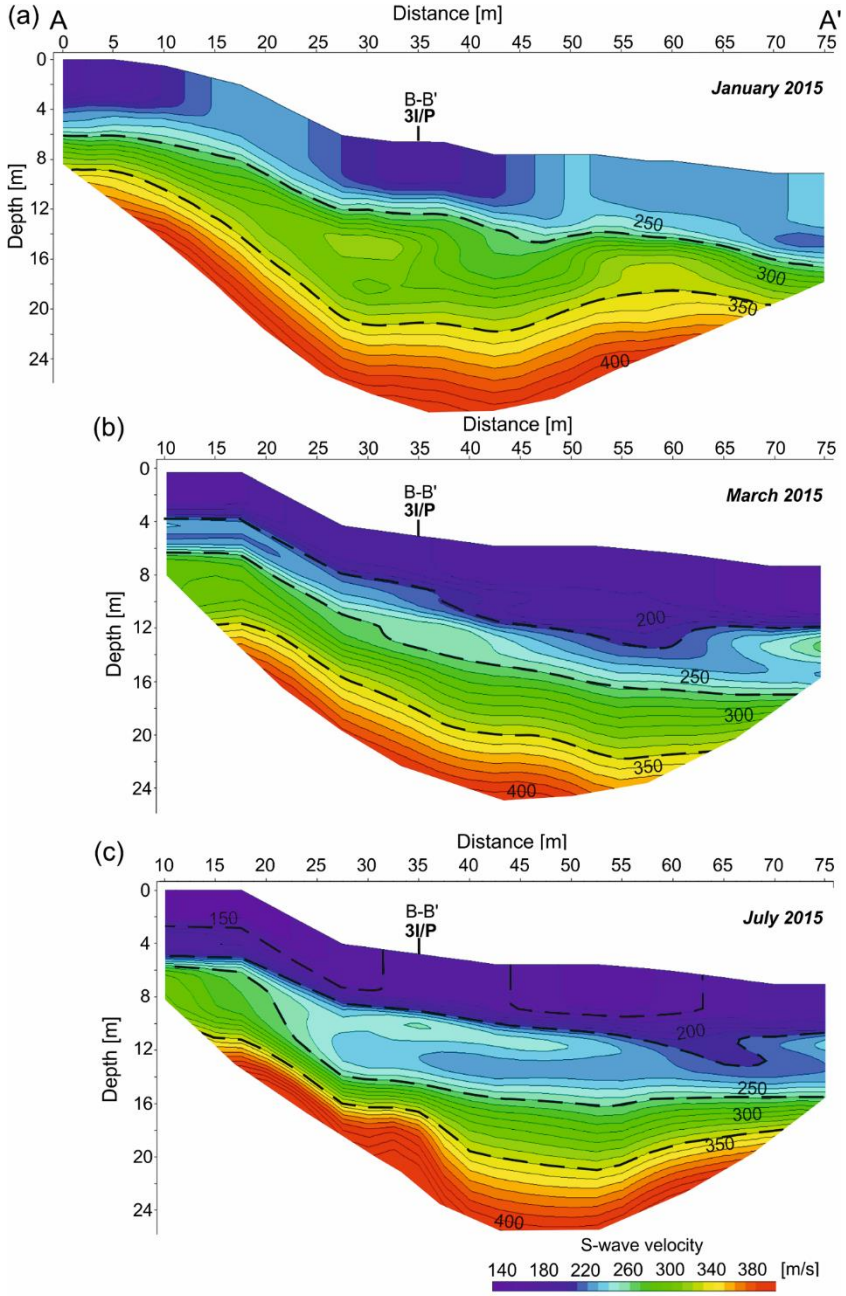

Figure 2.12: The results of ambient noise tomography (ANT) undertaken on a series of transient measurements acquired from seismometers by Harba and Pilecki (2017). Ground moisture is increasing from January to July, likely causing the observed in decrease shear-wave velocity in the landslide body.

2.4.7 Integrated surveys

The preceding section has focused on the individual methods utilised for the geophysical monitoring of landslides. One major limitation of geophysical investigations is the non-uniqueness of results obtained from surveys. The process of data inversion reduces this inherent ambiguity by providing spatial distributions of geophysical parameters. However, inversion of geophysical data is in itself a non-unique problem, as usually an infinite number of subsurface models can explain the data equally well and constraints need to be introduced to obtain the most likely subsurface distribution of the sought parameter. Although this non-uniqueness of both raw and inverted data can be addressed, one major limitation remains that an individual method is normally only sensitive to one physical property in the subsurface, the distributions of which may be variable in both time and space, and the occurrence of which may depend on several transient factors.

2.4.7.1 Multi-parametric geophysical monitoring

Multiple methods can reduce the uncertainty in the assumptions made about the ground condition by comparing the interpretations of each. Further quantitative analysis can be made by the use of joint inversions that incorporate physically constrained factors when creating models of the ground condition. This approach is referred to here as '*multi-parametric geophysical monitoring*'.

Relatively few examples are present in Appendix A in which more than one geophysical method has been utilised in a monitoring campaign. Multi-parametric geophysical monitoring campaigns (i.e., utilizing more than one acquisition method) have been used in three of the studies identified in Appendix A, with all using ER and SR methods (Bièvre et al., 2012, Grandjean et al., 2009, Palis et al., 2017a). Typically, multi-parametric geophysical monitoring is successful where the sensitivities of the methods are unique (i.e., each geophysical method is sensitive to a different subsurface property) and complementary (i.e., each subsurface property plays a role in the stability of a slope). It is for this reason that the combination of ER (sensitive to hydrological properties) and SR (sensitive to mechanical properties) is prevalent.

In the study by Grandjean et al. (2009), ER and SR surveys were carried out on co-located survey profiles across the Laval landslide in Draix, south French Alps. The results of the two independent surveys were fused using a fuzzy logical approach, utilizing probabilistic methods to test the validity of expert hydrological meta-hypotheses across the area of the monitored subsurface. The data were fused using three 'meta-hypotheses', which are probabilistic functions that link the measured geophysical value to the probability of a particular condition in the ground. These meta-hypotheses are, i) the probability of the ground being fissured is 1 if V_P < 300m/s, and 0 if V_P > 1500 m/s, ii) the probability of the ground being saturated is 1 if resistivity < 10 Ωm, and 0 if resistivity > 100 Ωm, and iii) the probability of the ground having high porosity is 0 if the slowness difference (defined as $1/Vs - 1/V_P$) < 0.00055 s/m^{-1}, and 1 if slowness difference > 0.0022 s/m^{-1}. All probability functions are linear between the respective values indicating probability of 0 and 1. These meta-hypotheses are informed by empirical geotechnical observations obtained from separate geotechnical information.

This approach allowed for the independent results of each method to be combined during a controlled rainfall experiment, resulting in the quantification of the development of expected phenomena (e.g., presence of fissures, development of saturated zones and areas of high porosity). This study is the most in-depth attempt to fuse data in such a way that the output of the study is more robust than the typical cross-sections of property distributions normally found in geophysical surveys. The probabilistic approach of the study also pays significant attention to the reliability, or conversely the uncertainty, of the data, another area that can be overlooked in the application of geophysical methods.

In the studies by Bièvre et al. (2012) and Palis et al. (2017a), the geophysical datasets are not interpreted in such a joined quantitative manner, but instead all contribute to the overall qualitative interpretation of the landslide processes at play in the individual studies. For example, Bièvre et al. (2012) exploited the sensitivity of electrical resistivity methods to the presence of water infiltrating fissures, and the effect of attenuation on surface-waves caused by the presence of fissures to determine extents of fissuring in the near-surface of the clay-rich Avignonet landslide. The different properties assessed by the two techniques were able to qualitatively confirm the hypothesis that fissuring played an important role in the infiltration of water at the landslide, despite the independent acquisition and processing of the datasets. Similarly Palis et al. (2017a) were able to link changes in the annual climatic cycle to variations in seismic monitoring responses and electrical resistivity values, allowing for a better understanding of the response of the landslide processes to external influences such as increased rainfall.

2.4.7.2 Environmentally-coupled monitoring

Incorporation of environmental data (e.g., rainfall data, displacement rates) allows for the temporal variations in geophysical monitoring data to be classified as being due to causative property changes in the landslide (e.g., increased saturation preceding failure) or resultant property changes (e.g., seismic responses generated by movement of the landslide). Incorporation of these external data sources is referred to in this review as '*environmentally-coupled geophysical monitoring*'. The importance of monitoring environmental fluctuations has been noted by several authors. Luongo et al. (2012) stated the importance of a weather monitoring station at the location of a prototype semi-permanent ER system, and similar local weather data was collected in other studies (Uhlemann et al., 2017). Particularly with ER, external environmental variations, most notably thermal variations, have a strong influence on the data, and thermal effects need to be corrected (Lucas et al., 2017).

The displacement of landslides does, however, present a problem for ongoing monitoring using geophysical methods. As mentioned previously, the success of monitoring campaigns depends on being able to spatially locate the datum at which measurements are being taken. In some types of geophysical monitoring approach, for example when using single-seismometer monitoring for event detection, the detailed location of the seismometer and its movement over time may not be of consequence to the aim of the monitoring (Amitrano et al., 2007). However, in some other methods, such as semi-permanent installations of ER arrays, movements in electrodes can have profound effects on the data quality, creating artefacts in the data if unaccounted for. This is typically overcome by periodic measurement of the movement of electrodes. These positional measurements need to be taken at a frequency at which movement can be captured. Recent advances in geophysical inversion have been

able to recover electrode movements over time, and therefore incorporate the movements in to the processing of ER data to prevent the introduction of data artefacts by electrode movements (Boyle et al., 2017, Loke et al., 2017, Wilkinson et al., 2010, Wilkinson et al., 2015). This has been an important step in developing the autonomy of semi-permanent installations, and has greatly improved the data quality available from such campaigns (Uhlemann et al., 2017).

Establishing thresholds for landslide movement from geophysical data coupled with environmental data is a critical component of understanding subsurface process evolution. Palis et al. (2017a) were able to establish a rainfall threshold of 3.5 ±1 mm day^{-1} above which the seismic sensors at the La Clapière recorded increased endogenous events associated with movement. Palis et al. (2017a) also showed that long-term analysis of rainfall with ER and S-EDCL methods allowed for the variable kinematics of the landslide to be established, with the authors noting delayed responses in displacement rates associated with the intensities, durations and repeat intervals of rainfall events. In many cases however, the determination of thresholds from rainfall alone coupled to geophysical responses, is unlikely to be successful unless the infiltration rate is well understood, as the subsurface moisture dynamics that can vary greatly depending on lithology, precipitation, temperature etc. are not captured by such a simplified relationship. This is particularly apparent where effective rainfall (i.e., the amount of water that arrives at ground level, which is not inhibited by evapotranspiration) or effective infiltration (i.e., the amount of water reaching the subsurface, which is not inhibited by evapotranspiration and surface runoff) is not taken into account. A further approach can therefore be to couple geophysical responses to monitoring measurements made from the subsurface, via the use of geotechnical monitoring methods.

2.4.7.3 Geotechnically-coupled monitoring

Even with the incorporation of multiple geophysical methods to landslide monitoring, the sensitivity of the geophysical method (or methods) is to the changes in the soil or rock property that is being monitored, rather than being a direct measurement of the property itself. For example, shear-wave velocity can be used to calculate shear-strength of the subsurface when other data (i.e. density data) are incorporated, but it is not a direct measurement of shear-strength. In order for geophysical measurements to be of use to end-users (who may not be geophysicists), the results need to be coupled to known parameters in the landslide environment. The relationship between geophysical measurements and the petrophysical properties of rocks and soils has most widely been applied in the hydrocarbon exploration industry (Barton, 2007). These coupling relationships are normally established by the careful selection and preparation of representative samples of subsurface material, upon which laboratory tests to determine the relationship between environmental influences (e.g., soil moisture), petrophysical properties (e.g., porosity, density), and a geophysical response (e.g., electrical resistance) can be established, as in the example of Merritt et al. (2016). A study by Carrière et al. (2018) into the rheological properties of soil samples from six clay-rich landslides across Europe recommended the application of geophysical methods for determining the properties of slide-to-flow dynamics. The main challenge to establishing reliable geophysical-petrophysical relationships is that of sample selection, and ensuring that samples collected and tested are representative of the conditions of subsurface materials, as landslides typically have highly heterogeneous subsurface conditions (van Westen et al., 2006).

Upon the establishment of such relationships, the ability to then compare the results of these geophysical-petrophysical relationships with data gathered from sensors installed in landslides is referred to here as '*geotechnically-coupled monitoring*'. Lehmann et al. (2013) determined the relationship between soil moisture as measured by time-domain reflectometer (TDR) sensors at the same time as ER measurements during two simulated rainfall tests. From this relationship, they were able to produce cross-sections of volumetric moisture content (VMC) and demonstrate the variations in VMC over time. In a study by Lucas et al. (2017) VMC was measured directly by several sensors on site, and the data used to derive a relationship between ER measurements and VMC, allowing for reliable spatial subsurface mapping of VMC. The authors noted the benefit of using ER for determining VMC values at a large spatial resolution, but noted the need for care in calibrating the ER measurements to determine VMC. In a similar study, Travelletti et al. (2012) were unable to establish a relationship between moisture content and ER data due to issues with non-uniqueness in the ER data, and scalability issues with using sparsely located moisture content measurements derived from point-sensors. This issue of inherent heterogeneity and extrapolation of data from a sparse network of direct measurement sensor remains a challenge for geotechnically-coupled geophysical monitoring.

Uhlemann et al. (2017) established a relationship between ER values and laboratory determined values of gravimetric moisture content (GMC) from samples collected at the landslide site rather than using measurements derived from sensors during the geophysical monitoring period, although retrospective comparison between the ER-derived GMC and sensor-measured GMC was in good agreement. The authors were then able to establish a failure threshold based on GMC, rather than rainfall, a measurement that better reflects the complex interactions between rainfall and subsurface moisture. In particular, estimated values of subsurface moisture content have implications for soil suction, which can be one of the most important stabilising forces in landslides (Toll et al., 2011).

The complexities of establishing such relationships in practice are identified by Hen-Jones et al. (2017), who identified that such geotechnically-coupled relationships often display hysteretic behaviour in relation to seasonal variations, adding a temporal heterogeneity to the already present spatial heterogeneity present in landslide settings. An additional consideration is that, in a similar way that geophysical responses can be caused by a multitude of factors, geotechnical property variations can have a variety of causes. For example, the reduction of shear-strength in soils due to loss of suction in wetting and drying cycles, and soil fabric deterioration across successive seasonal cycles (Hen-Jones et al., 2017).

2.5 Discussion

2.5.1 Strengths in geophysical monitoring of moisture-induced landslides

There are three areas in which geophysical monitoring of landslides is particularly successful. These are:

- Providing high-resolution spatial information on landslide features (i.e., discrete spatial features).
- Providing high-resolution temporal information on the evolution of landslide processes (i.e. analysing how a subsurface property has changed over time and inferring the causal process).
- Calibrating and coupling data with other sources of environmental and geotechnical information.

The first area, the provision of high-resolution spatial information on landslide setting features, is an extension of the aforementioned benefits of geophysical methods in earlier sections (Jongmans and Garambois, 2007, McCann and Forster, 1990). The same advances in technology that have allowed for the establishment of permanent monitoring installations have also allowed for greater measurement accuracy and resolution (Loke et al., 2013). The application of geophysical methods to image the subsurface between direct measurement locations is well established (Parsekian et al., 2015), and typically is where the use of near-surface geophysical methods lends most benefit to ground investigations. This can allow identification of features including the slip surface (Harba and Pilecki, 2017), analysis of the volumetric extent of disturbed materials (Uhlemann et al., 2017), and identification of deformation features and preferential infiltration pathways (Bièvre et al., 2012). Images, produced by tomographic inversion of data, can be assessed by comparative image analysis (e.g., Friedel et al., 2006), or through difference analysis compared to an initial image (e.g., Lucas et al., 2017). Direct measurements from these sources is near essential in the accurate interpretation of geophysical images, highlighting the complementarity between well-sited direct measurements (the placing of which can be optimised by geophysical methods) and geophysical images of the subsurface. The geophysical images produced are further enhanced by the expansion from 2D to 3D data capture (Uhlemann et al., 2017) and relation to property distributions (Crawford and Bryson, 2018, Lehmann et al., 2013).

The second area of strength for monitoring relates to the progression of landslide processes. These processes include rapid moisture infiltration in response to acute rainfall (Travelletti et al., 2012), seasonal variations in subsurface moisture content (Uhlemann et al., 2017), short-term variations in ground saturation (Lehmann et al., 2013) and material strength (Mainsant et al., 2012) immediately preceding failure, measurements of flow in landslide bodies (Colangelo et al., 2006) and detection of landslide movement (Brückl et al., 2013). The temporal resolution of data that can be obtained from geophysical monitoring campaigns in many cases can match those of installed point sensors (i.e., daily or sub-daily measurements), whilst in many cases still producing subsurface images that cannot be obtained from such sensor networks (Supper et al., 2014).

The third area is the one in which most development is required, but perhaps the area in which the most stands to be gained for monitoring of landslides. Demonstrated data-coupling approaches include linking changes in geophysical measurements to rainfall (Palis et al., 2017a) and ground moisture (Uhlemann et al., 2017) thresholds preceding failure, establishing property relationships between volumetric moisture content and ER measurements (Lehmann et al., 2013, Lucas et al., 2017) and shear strength parameters and ER measurements (Crawford and Bryson, 2018). It is in this area that geophysical monitoring approaches can contribute most to LoLEWS, not only due to the spatial and temporal resolution of data, but by linking these data to other areas of landslide study that can be understood by the wide range of stakeholders involved in the establishment, maintenance and management of LoLEWS.

S-EDCL approaches are well represented in the literature, but currently deal primarily with a retrospective analysis of seismic signals generated by landslides failure. ER monitoring is particularly well suited to monitoring precursory infiltration and subsurface movements and distributions of water, which is a key driver in the destabilisation of landslides through the reduction of matric suctions in partially saturated conditions (Toll et al., 2011). In addition to this, the application of ER monitoring has seen large interest not only in the field of landslide investigation and monitoring (Perrone et al., 2014), but also in other areas of hydrogeophysical research

(Binley et al., 2015). This interest has driven technological advancements in the application of geoelectrical monitoring of landslides, something which is likely reflected in the increasing length of monitoring periods and frequency of dataset acquisition over time. A geotechnically-coupled approach is important in informing the predictive capacity of geoelectrical monitoring systems. When integrated with transmission of data from site to stakeholders via telemetry, it can allow for near-real time monitoring of conditions as they move toward critical hydrogeological failure states.

In summary, the success of ER methods to monitoring of landslides is due to the longevity of the monitoring periods that can be achieved (e.g., Palis et al., 2017b), the resolution at which datasets can be acquired (e.g., Supper et al., 2014), the use of semi-permanent installations of geophysical monitoring infrastructure coupled with environmental and geotechnical sensor networks (e.g., Uhlemann et al., 2017), the ability for the results to be related to subsurface properties pertinent to landslide processes (e.g., Crawford and Bryson, 2018, Lucas et al., 2017) and in some cases the ability to yield critical subsurface information with minimal post-acquisition processing (e.g., Lebourg et al., 2010, Merritt et al., 2018).

2.5.2 Challenges to geophysical monitoring of moisture-induced landslides

Of the methods assessed in this review, ER monitoring has the greatest potential for monitoring subsurface material properties that may lead to slope failure. This is despite limitations surrounding power supplies to instruments, the practical considerations of deploying an electrode array in topographically difficult terrain and the limitation of high-resolution spatial information to the near-surface. With regards to semi-permanent ER monitoring, these issues have mostly been addressed as many of the semi-permanent ER systems in this review have been developed specifically for landslide monitoring, whilst other approaches have adapted existing equipment and methodologies. Further technological developments are still required in these approaches to optimize their application to landslide monitoring.

Active seismic methods (SR,SW) require the use of impulsive sources for generating seismic waves on site, limiting their use to transient measurements rather than semi-permanent installations (e.g., Grandjean et al., 2009, Renalier et al., 2010a) as no remote impulse generators exist for this application in surface deployed arrays (Daley et al., 2007). Other methods, such as SP, seem to be less used due to potential ambiguities in data interpretation, and the heavy reliance in determining subsurface conditions, such as lithology, from other sources. However, the single example of SP monitoring by Colangelo et al. (2006) demonstrates the value of SP approaches, particularly when included as part of a wider geophysical, environmental and geotechnical landslide monitoring campaign (Perrone et al., 2004). The passive approach provided by SP monitoring should lend itself to integration into new and existing geophysical monitoring observatories, as the infrastructure required is significantly less than that required for the establishment of ER monitoring systems.

Whilst passive seismic methods are widely used to retrospectively analyse the patterns of seismicity associated with landslide movements, their use to monitor the evolution of subsurface conditions preceding failure is underutilized. This can be considered a missed opportunity, particularly given their ability to monitor at higher temporal resolutions than active geophysical methods, and image to greater depths (where such imaging

capabilities can be employed, such as using S-ANT). This is despite the field of passive seismic monitoring being both highly developed and widely applied in monitoring both macroseismic (e.g., Öz, 2015) and microseismic (e.g., Chambers et al., 2010) events in a wide range of applications, including hydraulic fracture stimulation, geothermal systems, waste storage (e.g., CO_2) and mining. Seismic monitoring is also not uncommon in landslide monitoring, most commonly for detection and analysis of rockfall failure events (e.g., Hibert et al., 2017, Manconi et al., 2016, Partsinevelos et al., 2016). Similar approaches have been undertaken in some of the case studies identified in this review, such as event classification (Palis et al., 2017a) and event location (Brückl et al., 2013).

A significant challenge common to most geophysical monitoring applications remains the large volumes of data that can be acquired and the time requirements to quality assess, process and interpret these data. Currently, most data is still assessed and processed manually, although significant strides in acquisition methods, automated filtering, inversion methods have increased productivity in these areas (Loke et al., 2013). Challenges such as the accounting for movements in electrodes in active landslides (Wilkinson et al., 2010, Wilkinson et al., 2015) have been overcome, although similar challenges remain in the areas of automated image and pattern analysis (Chambers et al., 2015, Ward et al., 2016), the development of which would significantly reduce the requirement for manual processing of monitoring data. While robust hardware for geophysical monitoring seems to have reached good operational standards in recent years, developments in the associated software capabilities are still required to optimise the monitoring process.

2.5.3 Future look and opportunities

Currently, the only other methodology that is able to deliver robust monitoring capabilities and soil and rock property identification in a similar manner to semi-permanent ER monitoring systems are long-term passive seismic monitoring campaigns. A particularly novel but promising approach to passive monitoring is the use of ambient noise monitoring at landslide sites, with studies by Harba and Pilecki (2017), Mainsant et al. (2012) and Renalier et al. (2010a) demonstrating particularly interesting results. The predictive capacity of using cross-correlations of ambient noise is made clear in the study by Mainsant et al. (2012), where relative velocities in surface-waves are seen decreasing days before slope failure. Critically, this failure did not seem to be linked to obvious changes in the rainfall regime, suggesting that a long-term retrospective establishment of threshold values from rainfall data would not have worked in this landslide setting. The production of subsurface images of S-wave velocity from ambient noise recordings by Harba and Pilecki (2017) also shows that passive monitoring methods can determine subsurface properties and produce images at similar spatial resolutions to transient SR and SW surveys. However, improvements to the methodology described in Harba and Pilecki (2017) could improve the robustness of the results. Ambient noise sources ideally need to be both stable in time and non-directional, although the former can be overcome by averaging over increased measurement times (e.g., Mainsant et al., 2012). In the case study by Harba and Pilecki (2017), the acquisition of 60 minute datasets derived from traffic noise may not be sufficient to reliably reconstruct the Green's function of an ambient noise field. Accurate reconstruction of the Green's function is crucial due to the accuracy of the imaging capability. The deployment of permanent arrays, from which longer ambient noise records could be extracted, would greatly improve the reliability of the results. Despite this, the case study by Harba and Pilecki (2017) is one of the only attempts to

create subsurface images from ambient noise for the purpose of monitoring landslides. As such, it represents an important step in providing increased temporal and spatial subsurface geophysical models of landslides, and demonstrates the capacity for employing such approaches in future studies.

Crucially, unlike transient SR and SW surveys, subsurface images produced from ambient noise have the potential to be produced at a similar acquisition frequency to long-term semi-permanent ER monitoring systems. Recent developments in technology, particularly around linear Distributed Acoustic Sensing (DAS) monitoring show the potential for these new senor types to replicate the resolution of traditional transient SW surveys, but at much higher data acquisition frequencies (Dou et al., 2017). Developments in this field, potentially into 3D surveys, will be particularly relevant to the monitoring of landslides. Renalier et al. (2010b) demonstrate the application of these ambient noise applications using a network of seismometers to create a 3D image of a landslide body, but without a time-series element to the data. Similarly, while some non-monitoring studies have analysed seismic data and inferred property distributions from active seismic measurements (Uhlemann et al., 2016a), this has not been applied to time-lapse seismic studies, actively or passively acquired, and represents a significant gap in the field.

Therefore, there appears to be three areas in which seismic monitoring can be improved for the application of monitoring landslides: by utilizing ambient datasets acquired by dense seismometer networks or DAS arrays over longer periods of time, by attempting to link changes observed in these datasets to subsurface properties, and by producing high-resolution spatial images of the subsurface from passive data. In the past, a barrier to improving resolution of ambient noise surveys has been the cost associated with broadband seismometers typically used for very sensitive planetary-scale measurements. However, recent studies in other areas show the successful deployment of low-cost, low-energy consumption geophone based networks for the monitoring of glaciers (Martinez et al., 2017), infrastructure (Olivier et al., 2017, Salvermoser et al., 2015) and landslides (Deekshit et al., 2016). Similar moves toward lower-power, lower-cost systems in ER monitoring are also apparent (Chambers et al., 2016), which will increase the availability and application of geophysical monitoring in the field.

The simultaneous acquisition of continuous passive seismic and ER data would open up opportunities for the further development of integrated quantitative processing and inversion, further increasing the usefulness of geophysical monitoring data. The near-real time element of some monitoring systems could therefore be used for near-time modelling and decision making on high-risk slopes endangering critical social or economic infrastructure, or risk to human life.

2.5.4 The contribution of geophysical methods to LoLEWS

The compilation of catalogues of landslide events are often the first step to constructing landslide inventory maps. These maps inform the designation of zones based on their level of risk to landslide events (Fell et al., 2008, van Westen et al., 2006). Implementation of appropriate land use planning and subsequent enforcement of this planning is arguably the most effective tool for mitigating future risk from landslide events, and can be practiced at different scales (Cascini, 2008). However, in some situations, the presence of risk from landslides may exist in the absence of appropriate risk zonation maps, or may become apparent in the later development of land.

Changing environmental conditions can also induce new landslide events, or reactivate dormant landslide activity (Gariano and Guzzetti, 2016). In these instances, different courses of action must be taken to mitigate the risk from future landslide events.

In cases where the elements at risk of a landslide hazard cannot be relocated, or are of high socioeconomic value (Manconi and Giordan, 2015) or where structural mitigation measures would be too resource intensive, undesirable or ineffective, the implementation of LoLEWS may be the preferred option for risk mitigation (Intrieri et al., 2012). The concept of an early warning system applied to natural hazards can be defined as "*...monitoring devices designed to avoid or to mitigate the impact posed by a threat*" (Medina-Cetina and Nadim, 2008). LoLEWS for landslide monitoring require a detailed understanding of the triggers and mechanisms in order to be effective (e.g., Manconi and Giordan, 2016). Successful LoLEWS must include a detailed understanding of the character of the landslide, the processes acting on the slope, and the response of the slope to external influences, such as increased infiltration (SafeLand, 2012). The main components of a generic LEWS are shown in Figure 2.13.

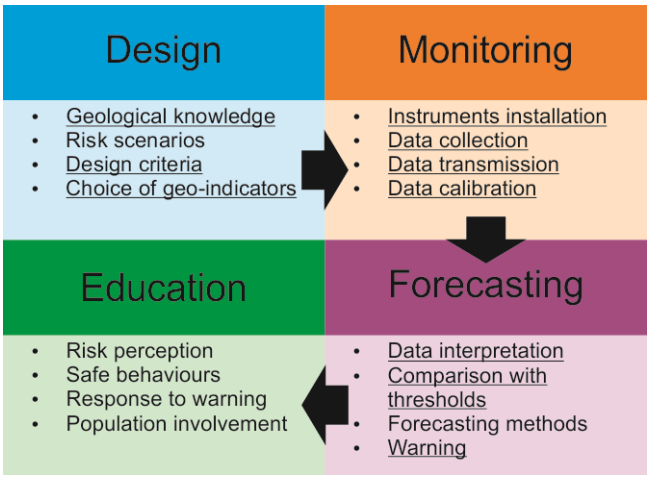

Figure 2.13: Four main activities of Landslide Early Warning Systems reproduced from Intrieri et al. (2013). Sections underlined show the areas in which geophysical investigations and/or geophysical monitoring can be used to assist in LEWS.

Typically, LoLEWS are established by acquiring and monitoring changes in both environmental (i.e., rainfall, temperature, soil moisture content, pore water pressure) and kinematic (i.e., slope movement) data (Uhlemann et al., 2016b). Commonly, these data are acquired through geomorphological mapping, geodetic surveys and borehole measurements (e.g., inclinometers) are used in monitoring campaigns. Data can also be acquired from sensors measuring piezometric head, tilt and soil suction. More recently, wireless sensor networks comprising sensors with low-power requirements and large data-storage or telemetric capabilities have been deployed in landslide settings to acquire direct measurement data with higher spatial and temporal resolution (Ramesh, 2014). Despite these advances, logistical and economic constraints remain barriers to optimum data acquisition for the establishment of effective LoLEWS. Currently, geophysical investigations and monitoring methods are not widely used in LoLEWS.

Table 2.3 shows the contribution that geophysical monitoring approaches can make to the four stages of establishing LoLEWS, as defined by Intrieri et al. (2013) and shown in Figure 2.13. Entries highlighted green are those areas in which capability has been demonstrably developed. Orange entries indicate those areas in which challenges still exist but where the requisite technology may have been applied to other areas of geophysical monitoring outside of landslide studies, for example, in the automatic detection of geophysical responses, and installation of high-resolution monitoring arrays. Entries in red indicate areas in which significant development is still required before operational deployment to a field setting, the most significant one of which being the ability to issue reliable warnings based on the integration of environmental, geotechnical and geophysical data.

2.6 Conclusions

The use of geophysical monitoring systems to assess the evolution of subsurface property distributions and changes over time have been reviewed. The benefit of long-term geophysical monitoring campaigns in assessing the evolution of MIL is demonstrable. A significant advantage of the use of geophysical monitoring systems is their complementarity with existing monitoring systems. Many areas of landslide monitoring are highly developed, with innovative advances in technology progressing a wide range of applications. Developments in UAV technology (Walter et al., 2009), interferometric synthetic-aperture radar (InSAR) (Hilley et al., 2004) and other remote sensing capabilities (Kirschbaum et al., 2015) have increased the temporal and spatial resolution at which surface deformations can be monitored. Geophysical data can enhance the deformation data captured by these technologies by providing an understanding of the subsurface processes driving them, something that is not achievable at such high temporal and spatial resolutions with other monitoring methods. Sensor technology has also advanced, with installations of tiltmeters, inclinometers and piezometers being enhanced with the addition of shape acceleration arrays, acoustic-emission waveguide sensors and tensiometers (Uhlemann et al., 2016b). Geophysical methods are able to interpolate between the locations of these direct measurements, extending by proxy the spatial coverage of these sensor types.

Key advances in the field of geophysical monitoring in the last decade include:

- Telemetric capabilities in geoelectrical and seismic monitoring methods, increasing the length of monitoring periods and allowing near-real time data acquisition.
- Coupling of geophysical data to geotechnical properties, particularly in the field of ER.
- The potential for integration of passive seismic and ER methods to decrease uncertainty in single-method geophysical monitoring campaigns.

A key area for future development is the implementation of multi-parametric monitoring with geotechnically-coupled approaches. This can be achieved through better calibration of geophysical measurements with geotechnical data, and the establishment of threshold values for failure based on these outputs.

Recent advances in incorporating slope displacements in the data processing phase of geophysical monitoring campaigns has greatly reduced the presence of artefacts in the resultant subsurface images (Wilkinson et al., 2010, Wilkinson et al., 2015), as well as advances in the inversion of time-lapse data (Loke et al., 2013) and automated image analysis (Chambers et al., 2015, Ward et al., 2016). The establishment of site-specific

geotechnical-geophysical relationships to obtain the subsurface spatial distribution of geotechnical properties, and the ability to monitor changes in these properties over time, is valuable to a wide range of end-users and stake holders (Crawford and Bryson, 2018, Merritt et al., 2016, Uhlemann et al., 2017). The developments highlighted in this review underscore the potential for the combined use of geophysical monitoring methods with existing remote sensing, earth observation and direct measurement monitoring approaches to improve the current capacity for high-resolution LoLEWS (Intrieri et al., 2013, Intrieri et al., 2012).

Table 2.3: The contributions that geophysical monitoring approaches can make to LoLEWS in the context proposed by Intrieri et al. (2013) in Figure 2.13. Those contributions highlighted red indicate areas in which the most development is still required, those in orange are where research is currently being undertaken but not yet applied to the monitoring of MIL, and green identifies those areas in which geophysical monitoring can already contribute the LoLEWS on MIL.

LoLEWS Activity (after Intrieri et al., 2013)		Contribution by geoelectrical monitoring methods	Contribution by passive seismic monitoring methods
Monitoring	Instruments installation	Installation of semi-permanent 2D monitoring arrays	Installation of seismometer(s)
		Installation of semi-permanent 3D monitoring arrays	Installation of dense networks of low-cost, low-power seismic sensors or DAS arrays
	Data collection	Regular, short-time scale (≤1 day) data acquisition	Continual data recording
		Large data storage or telemetric capabilities	
	Data transmission	Telemetric capability can send data to central observatory	
	Data elaboration	Integration of data with environmental, geotechnical and kinematic data collected simultaneously from locally installed sensors	
Forecasting	Data interpretation	Automatic image analysis and change detection of hydrogeological process through time-lapse imaging	Automatic seismic event detection
		Automated geotechnical-coupled and environmentally coupled monitoring	Automated event classification
			Automated event location
	Comparison with thresholds	Establishment of relevant subsurface hydrogeological thresholds preceding movement (e.g., moisture content, shear strength)	
	Forecast methods	Monitoring of subsurface conditions toward hydrogeological failure threshold	Monitoring of subsurface conditions toward geomechanical failure threshold
	Warning	High-resolution spatial and temporal geophysical monitoring, calibrated with and linked to environmental, geotechnical and kinematic data to provide multi-level warnings based on monitoring of several physical subsurface parameters	

Acknowledgements

The authors would like to thank Fabio Florindo (Editor in Chief, Reviews of Geophysics) and six anonymous reviewers for their insightful comments and helpful suggestions. This work was funded by a NERC GW4+ UK Doctoral Training Partnership Studentship (Grant NE/L002434/1) and in part by the BGS University Funding Initiative (S337), which are gratefully acknowledged. Jonathan Chambers and Paul Wilkinson publish with the permission of the Executive Director, British Geological Survey (UKRI-NERC). No new data were produced in the formation of this review, and all data used are cited in the reference list.

3 Landslide monitoring using seismic refraction tomography – the importance of incorporating topographic variation

J. Whiteley, J. Chambers, S. Uhlemann, J. Boyd, M. Cimpoiasu, J. Holmes, C. Inauen, A. Watlet, L. Hawley-Sibbett, C. Sujitapan, R. Swift & J. M. Kendall (2020). Landslide monitoring using seismic refraction tomography – The importance of incorporating topographic variations, Engineering Geology, 268, 105525. https://doi.org/10.1016/j.enggeo.2020.105525.

Declaration and author contribution

The content of this chapter was published in *Engineering Geology* in April 2020. Minor amendments have been made to the content to better integrate the work with the overall thesis. The 16 surveys were designed and supervised by J. Whiteley, as were the field logistics. Between October 2016 and August 2019 many people attended site to help acquire data, however, J. Boyd, M. Cimpoiasu, J. Holmes, C. Inauen, A. Watlet, L. Hawley-Sibbett, C. Sujitapan, R. Swift and S. Uhlemann were present for the majority of the visits and are included as co-authors in recognition of their physical and conceptual contributions to the fieldwork. The quality assurance and quality control, processing, analysis, visualisation and interpretation of the data were undertaken by J. Whiteley. S. Uhlemann compiled the inversion code, which was modified and used by J. Whiteley. J. Whiteley composed the original draft for publication, which was reviewed by all authors. The work was supervised by J. M. Kendall and J. Chambers.

Contributor Roles Taxonomy (CRediT) statement

Conceptualisation: *J. Whiteley*

Investigation: *J. Whiteley, J. Boyd, M. Cimpoiasu, J. Holmes, C. Inauen, A. Watlet, L. Hawley-Sibbett, C. Sujitapan, R. Swift, S. Uhlemann*

Methodology: *J. Whiteley*

Formal analysis: *J. Whiteley, S. Uhlemann*

Software: *S. Uhlemann*

Visualisation: *J. Whiteley*

Writing – original draft: *J. Whiteley*

Writing – review and editing: *J. Whiteley, J. Boyd, M. Cimpoiasu, J. Holmes, C. Inauen, A. Watlet, L. Hawley-Sibbett, C. Sujitapan, R. Swift, S. Uhlemann, J. Chambers, J. M. Kendall*

Supervision: *J. M. Kendall and J. Chambers*

Abstract

Seismic refraction tomography provides images of the elastic properties of subsurface materials in landslide settings. Seismic velocities are sensitive to changes in moisture content, which is a triggering factor in the initiation of many landslides. However, the application of the method to long-term monitoring of landslides is rarely used, given the challenges in undertaking repeat surveys and in handling and minimizing the errors arising from processing time-lapse surveys. This work presents a simple method and workflow for producing a reliable time-series of inverted seismic velocity models. This method is tested using data acquired during a recent, novel, long-term seismic refraction monitoring campaign at an active landslide in the UK. Potential sources of error include those arising from inaccurate and inconsistent determination of first-arrival times, inaccurate receiver positioning, and selection of inappropriate inversion starting models. At the site, a comparative analysis of variations in seismic velocity to real-world variations in topography over time shows that topographic error alone can account for changes in seismic velocity of greater than ±10% in a significant proportion (23%) of the data acquired. The seismic velocity variations arising from real material property changes at the near-surface of the landslide, linked to other sources of environmental data, are demonstrated to be of a similar magnitude. Over the monitoring period subtle variations in the bulk seismic velocity of the sliding layer are observed that are demonstrably related to variations in moisture content. This highlights the need to incorporate accurate topographic information for each time-step in the monitoring time-series. The goal of the proposed workflow is to minimize the sources of potential errors, and to preserve the changes observed by real variations in the subsurface. Following the workflow produces spatially comparable, time-lapse velocity cross-sections formulated from disparate, discretely-acquired datasets. These practical steps aim to aid the use of the seismic refraction tomography method for the long-term monitoring of landslides prone to hydrological destabilization.

3.1 Introduction

The implementation of robust and appropriate monitoring strategies is critical for the ongoing assessment of potentially destabilising processes in landslide systems (Angeli et al., 2000). Near-surface geophysical methods are increasingly used to monitor the subsurface conditions of landslides susceptible to hydrological destabilization (Perrone et al., 2014, Whiteley et al., 2019), most commonly by active-source DC electrical resistivity (ER) (e.g., Lucas et al., 2017, Uhlemann et al., 2017) and passive-source seismic monitoring (e.g., Walter et al., 2012). ER can provide information on the moisture dynamics of an unstable slope, and passive-source seismic can provide information on the kinematics of failure events. One major advantage of active-source geophysical methods, such as ER, is their ability to produce spatially high-resolution, time-lapse tomographic images of the subsurface. However, the majority of seismic landslide monitoring campaigns utilise passive-source methods, which provide superior temporal resolution, but are limited in their spatial resolution due to practical limitations on the number of sensors in an array.

Seismic refraction (SR), an active-source seismic tomography method, can characterize the spatial heterogeneities in elastic properties of materials in landslide systems (e.g., Uhlemann et al., 2016a). SR determines the travel-time of artificially generated seismic waves, to build up a series of travel-times for waves propagating through the subsurface. These travel-times are inverted to produce subsurface models of seismic velocity. The two types of body waves used in SR, P-waves and S-waves, propagate through subsurface media at different speeds depending on lithological and physical properties. The P-wave velocity, V_p is given by

$$V_p = \sqrt{\frac{K+\frac{4}{3}G}{D}} \quad , \qquad \text{Equation 3.1}$$

in which K is the bulk modulus (a measure of a material's resistance to uniform compression), G is the shear modulus (a measure of a material's resistance to shear strain) and D is material density. The S-wave velocity, V_s, is given by

$$V_s = \sqrt{\frac{G}{D}} \quad . \qquad \text{Equation 3.2}$$

In solid rock, the relationship between seismic velocity and saturation has been empirically demonstrated, and is relatively well understood. Considering a fully saturated rock, as liquid (with a higher K; Equation 3.1) in pore spaces initially become replaced by gas, V_p decreases rapidly and V_s decreases with increased saturation due to changes in bulk density and shear modulus (Equation 3.2) (Wyllie et al., 1956). These seismic attributes and their relationship to the petrophysical properties of rock can be used to determine the effects of saturation on seismic velocity (e.g., Biot, 1956, Gassmann, 1951).

In soils, the effect of variations in saturation on seismic velocity is less well-understood. Existing evidence indicates that both the distribution of moisture throughout the soil structure, as well as the influence that capillary forces have on effective pressure, influence V_p at small scales (Romero-Ruiz et al., 2018). Experiments in artificial, well-mixed, homogenous soils, have demonstrated that V_p decreases with increasing saturation (Lu and Sabatier, 2009) and similar results have been obtained from laboratory measurements on undisturbed samples of

Loess soils (Flammer et al., 2001). These decreases in V_p are dominated by changes in the matric potential of the soil (related to capillary forces). The effects of capillary forces are likely to be very different between artificial and natural soils, with the former having no internal structure or little consolidation, both of which reduce the influence of capillary forces.

Despite this lack of understanding on the precise mechanism by which seismic velocities are influenced by moisture content in soils, seismic attributes are still routinely used in larger scale field studies to assess characteristics of near-surface sediments. The ratio between V_p and V_s (V_p/V_s) can be used to assess lithology, strength and quality, structure and saturation of near-surface sediments for geotechnical investigations (Bhowmick, 2017). Seismic surveys to obtain in-situ V_p, V_s and V_p/V_s have been used to image physical properties, including ground saturation, in the field (Dashwood et al., 2019, Pasquet et al., 2016b), and have been used to monitor shallow saturation processes in the laboratory (Pasquet et al., 2016a). Poisson's ratio, a property closely related to V_p/V_s ratio which measures lateral strain to axial strain, has been shown to relate to porosity in near-surface sediments, and can be used to determine areas of localised saturation (Uhlemann et al., 2016a, Uyanık, 2011).

The use of SR as a tool for long-term landslide monitoring is almost absent from the literature. Examples of active-source seismic landslide monitoring campaigns focus on the characterization of surface fissures (see Bièvre et al., 2012, Grandjean et al., 2009) rather than the monitoring of moisture-induced elastic property variations. The dearth of studies using SR as a long-term monitoring tool for landslides is likely due to the complexity of managing and minimizing the several sources of error in the individual surveys (i.e., time-steps) that comprise a monitoring time-series. In this study, a methodology to acquire, process and invert a long-term SR time-lapse dataset collected from an active landslide is presented. The use of SR in a monitoring campaign at an active landslide site has not previously been implemented. The methodology is applied to time-lapse SR monitoring at a site of active slope failure in North Yorkshire in the UK. This study aims to develop a practical approach for active-source time-lapse seismic surveying of vulnerable slopes, and to demonstrate the applicability of high spatial resolution subsurface monitoring using SR. The approach taken is summarised in a workflow, from which a practical walkthrough of how the time-lapse SR data were acquired, processed and inverted using a novel two-stage inversion procedure is presented. The importance of incorporating the topography of the landslide surface from every survey (i.e., for each time-step) in a monitoring campaign is highlighted. Summary results from the SR monitoring campaign are presented and discussed, and support the use of SR to monitor moisture dynamics at active landslide sites. The approach and results of this study should be of interest to researchers studying the evolution of subsurface processes acting to destabilise landslide systems (Jaboyedoff et al., 2019), and to those using geophysical methods in landslide early-warning systems (Intrieri et al., 2012) and monitoring environmental changes.

3.2 Seismic refraction tomography monitoring at the Hollin Hill Landslide Observatory

The Hollin Hill Landslide Observatory (HHLO) in North Yorkshire, UK (Chambers et al., 2011, Merritt et al., 2013), is operated by the British Geological Survey. The landslide comprises an interbedded series of Lower and

Middle Jurassic sandstones and mudstones (Figure 3.1), namely the Whitby Mudstone Formation (WMF) and Staithes Sandstone Formation (SSF).

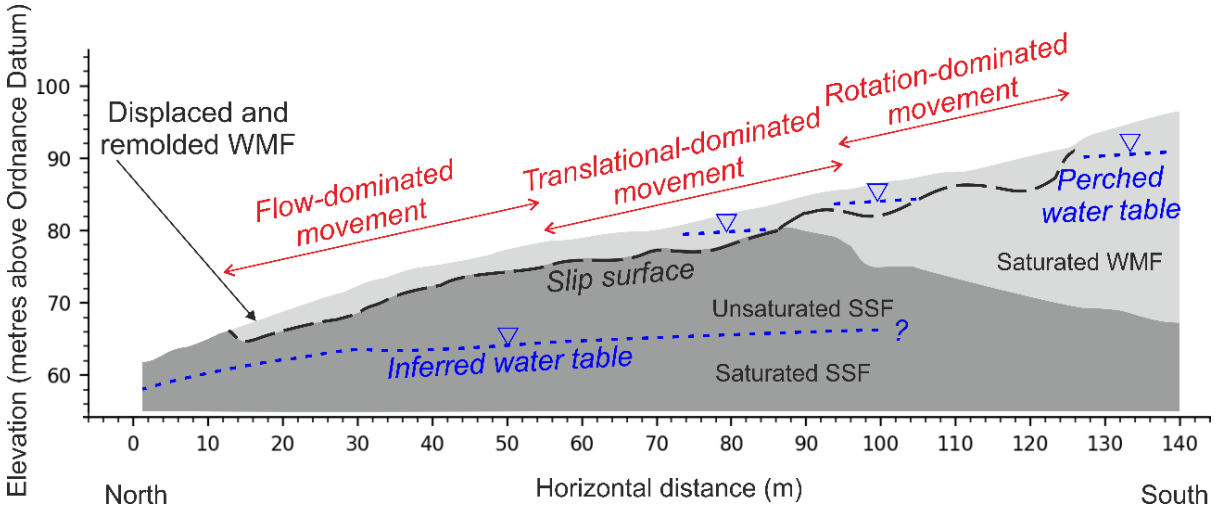

Figure 3.1: A simplified conceptual model of the HHLO (modified from Uhlemann et al., 2016a), indicating movement domains, slip-surface, indicative positon of water tables, and main lithological units comprising the Whitby Mudstone Formation (WMF) and Staithes Sandstone Formation (SSF).

The moisture content of the WMF controls displacement occurrence at the site. The WMF is of low permeability and drains slowly into the underlying SSF. Hence, during periods of increased precipitation, moisture content within the WMF increases quickly (creating localized perched groundwater tables), and decreases slowly during periods of lower precipitation. Slope failure is most likely during these periods of intense and prolonged rainfall.

Seasonal variations in moisture content, linked to regional groundwater levels and local infiltration of rainwater, decrease restraining soil-suction forces (potentially producing destabilising positive pore-water pressures) initiating movement at the slip-surface mid-slope. This translational displacement propagates uphill as support for overlying material is removed, culminating in the development and widening of rotational backscarps in the saturated WMF at the top of the slope. Downslope, mobilised material is reworked to form flow lobes at the base of the landslide, where movement is eventually arrested through drainage to underlying deposits of well-sorted, aeolian quaternary sands deposited at the top of the SSF. Aerial imagery from 2007, 2017 and 2018 shows the development of geomorphological landslide features at the HHLO (Figure 3.2). The main backscarp at the top of the slope first initiated in 2016, and increases in size (in both the cross- and down-slope direction) between the 2017 and 2018 aerial imagery. The base of this rotated block remains relatively static over the period shown in Figure 3.2, but the base of the flow lobe at the bottom of the landslide can be seen to extend downslope over time. Similarly, the increase in downward extent of the convex break of slope of the flow lobes indicates increased material accumulation in this zone over time.

SR monitoring at the HHLO aims to identify changes in the elastic properties of the underlying lithological units. These variations in elastic properties are primarily driven by variations in slope moisture dynamics. Between

October 2016 and August 2019, 16 SR surveys were acquired, resulting in the production of 16 V_p and 16 V_s cross-sections spanning a period of 1001 days, close to 33-months. The length of time of the monitoring period allowed data to be collected over two distinct annual climatic cycles, ensuring data were acquired at different subsurface moisture contents, and during multiple wetting and drying phases of the landslide system, capturing temporal heterogeneity in hydrological condition. Data were acquired at an average return interval of 9 weeks, which was deemed practicable given the characteristics of the landslide system and long-term monitoring period. A shorter return interval would have been desirable, but this was prevented by the logistical and financial cost of mobilisation, equipment availability and deployment, and acquisition and processing time associated with each survey; surveys typically involved two to three days of fieldwork, followed by several days of data processing.

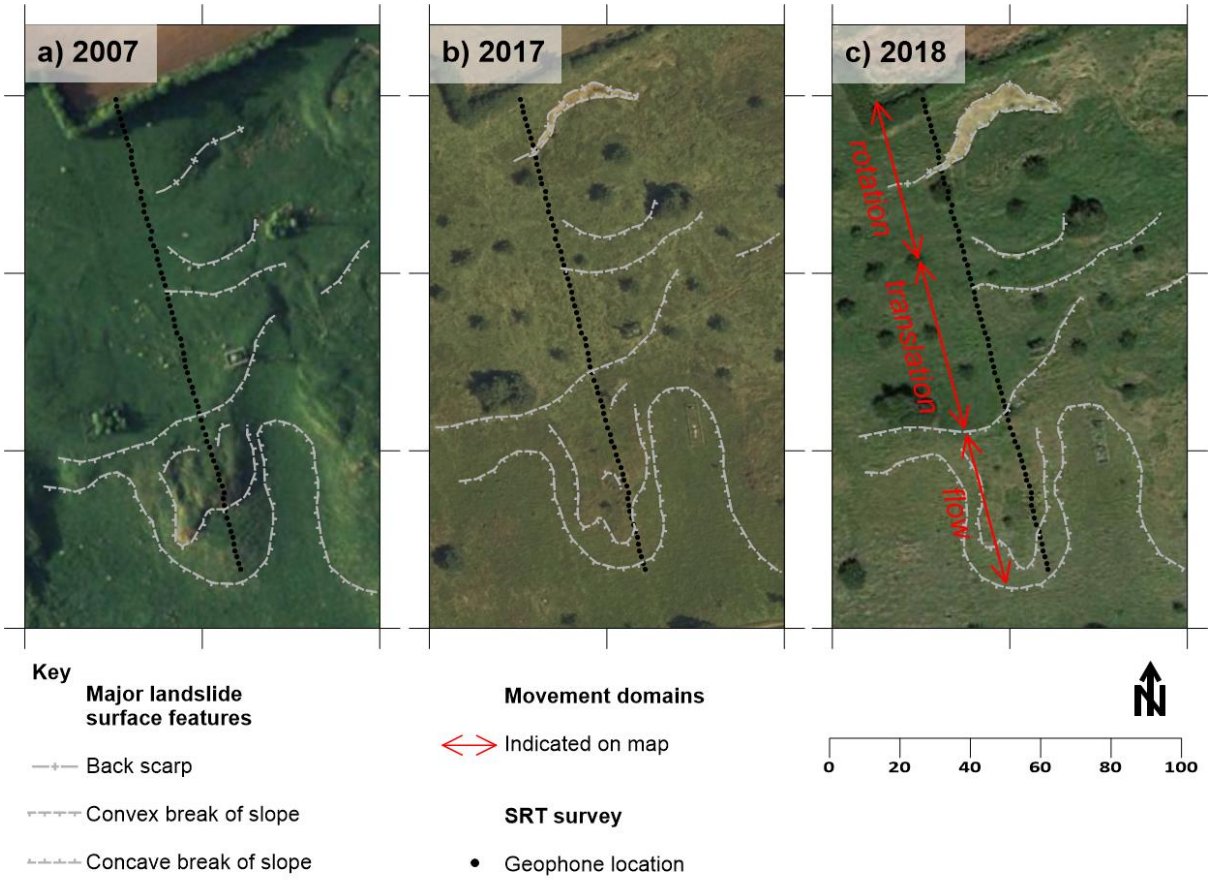

Figure 3.2: Aerial photographs from the HHLO. a) Image from 2007 showing the main features of the landslide, including backscarps at top of slope (north), and flow-lobes at base of slope (south). Map data: Google, Infoterra Ltd and Bluesky. b) Image from 2017 showing development of new backscarp after movement in 2016. Map data: Digimap. c) Continued backscarp development shows landslide extension, and propagation of the backscarp to the west. Map data: Google. Black dots are the indicative locations of receivers used in the SR surveys, with the first receiver location (northern most dot) located outside of the active landslide area, acting as a static reference point against which the receiver arrays are deployed. The location of this receiver is marked by a ground peg installed at the site.

The SR surveys were acquired along the same profile location over the duration of the monitoring campaign. The profile comprised of 2 m spaced geophones (i.e., receivers), positioned from the crest of the landslide to the toe (Figure 3.2). The location of the survey profile was chosen based on previous geophysical surveys that have been undertaken at the site (see Uhlemann et al., 2016a) and position of geotechnical sensors (see Merritt et al., 2013). For both the P- and S-wave surveys, a 48-channel ABEM Terraloc Mk6 was used to acquire seismic refraction data. To acquire contiguous data from the entire spread length (142 m total length, comprising 72 receiver locations), two separate 48 receiver (94 m long) profiles with a 46 m overlap between the surveys were acquired. Receivers used in both deployments were not moved between spread acquisitions, and repeat shots were undertaken so that the overlapping spreads could be processed as a single profile of data.

Vertical geophones with a dominant frequency of 8 Hz were used as receivers for the P-wave survey, and a 4 kg sledgehammer and horizontal steel plate were used as a source. At each shot location, data were recorded for 1 second, in order to acquire both refracted P-wave arrivals and surface wave data (these latter data are not described in this study). Shot records were stacked in the field, and the number of stacked shot records varied between surveys based on environmental conditions, such as wind speed and rain; a minimum of two stacks per location were acquired in optimal conditions (i.e., low or no wind and rain), and up to six stacks per location were acquired in poorer conditions. Data were stacked automatically in the field, and assessed for any timing discrepancies by visual assessment at the time of acquisition. If any timing issues were detected, the data were re-acquired. A pre-record of 10 ms was used to check that no data were recorded before the 0 ms time. The system 0 ms time is triggered by closing a circuit connected to the seismograph, which was achieved by the use of a trigger switch unit attached to the stem of the sledgehammer, which closes upon impact. Tests with this unit showed the triggering to be consistent across surveys. No additional errors were ascribed to the stacking procedure or triggering system.

For the S-wave survey, horizontal geophones with a dominant frequency of 14 Hz were used as the receivers, and a prism with ~45° inclined face was used to generate S-waves in opposing polarisations, perpendicular to the orientation of the receiver profile (Uhlemann et al., 2016a). Data were recorded for 0.5 seconds, and same-polarisation shot records were stacked, with a minimum of two stacked per receiver location saved in optimal survey conditions, and up to a maximum of six shot records per location saved in poor survey conditions.

In both surveys, geophones were deployed every 2 m and buried to a depth of ~10 cm below ground level in an attempt to isolate the receivers from aerial environmental noise, and to provide better coupling with the subsurface. Shots were acquired at every other receiver location (i.e., every 4 m) for the whole of the receiver spread, starting at the first receiver at the crest of the slope. It was not possible to acquire off-end shots at the top of the profile (i.e., before the first geophone) due to access restrictions. For the P-wave surveys, off-end shots at the end of the of the spread were acquired at 4m intervals beyond the penultimate receiver at the toe of the slope to a maximum off-end distance of 22 m beyond the last receiver (i.e., 164m from the first receiver). For the S-wave surveys, off-end shots were acquired at 10 m intervals to a distance of 20 m beyond the last receiver (i.e., 162 m from the first receiver). For both surveys, the same shot locations were used throughout the entire monitoring campaign, ensuring consistent spatial coverage between surveys.

3.3 Overcoming challenges in long-term SR monitoring of landslides

In this study, several sources of error in SR surveys need to be accounted for during data acquisition, and in the subsequent data processing and inversion stages. Some of these sources of error are unique to landslide monitoring. The goal during processing is to minimize transient changes in time-lapse data that may arise from differences in survey set-up and processing of data between surveys, and to preserve changes arising from genuine variations in the properties of landslide materials. As velocity is the ratio of distance and time, the determination of accurate velocities relies on accurate positioning (i.e., determining true distances) and correct picking (i.e., identifying correct travel-times) of data. The major sources of potential error in SR acquisition and processing are identified in Table 3.1, along with their solutions presented in this study and stage at which the error should be considered. A workflow to produce a robust seismic velocity time-series, taking into consideration the potential sources of error identified in Table 3.1 is shown in Figure 3.3. In this study, the 1001-day monitoring period is considered as a 'time-series' of SR data, with the 16 individual surveys comprising 'time-steps' within this time-series. The following sections describe how the stages of the workflow are used to address the potential errors listed in Table 3.1 that occur within individual time-steps, and across the time-series as a whole.

Table 3.1: Potential sources of error arising from the acquisition, processing and inversion of time-lapse SR data.

Potential source of error:	Addressed by use of:	Addressed during:
Inconsistent repositioning of receivers to same locations between surveys	Permanent reference points in the field for repeatable receiver deployment	Data acquisition
Failure to capture accurate 3D locations of receivers deployments, and subsequent differences in positions between surveys	RTK-GNSS systems to obtain accurate 3D receiver positions	Data acquisition
Inconsistent data coverage within surveys and across the time-series	Repeatable field procedures to boost data coverage; common travel-time maxima across time-series to give consistent data coverage	Data acquisition/ data processing
Inconsistent picking of first arrivals	Reciprocal error analysis to identify data for re-processing	Data processing
Not accounting for changes in surface topography between surveys	Unique inversion for each survey (i.e., time-step) derived from individual RTK-GNSS acquired topography	Data inversion
Not incorporating errors in to the inversion	Error model derived from reciprocal error analysis	Data processing/ data inversion
Using inappropriate constraints for initial data inversion	Tests to determine best starting parameters for first stage inversion	Data inversion
Using inappropriate constraints to regularize data over time	Selecting 'best' data from first stage inversion to use as a 'reference model' for second stage of inversion	Data inversion

3.3.1 Assessing first arrival quality

Identifying consistent, repeatable first arrivals in SR data is a recognised challenge with no universally accepted solution. Attempts include using automatic picking algorithms (e.g., Khalaf et al., 2018) and using statistical approaches (e.g., Dangeard et al., 2018) to minimize absolute and relative errors introduced by operators picking time-lapse SR data. In this study, reciprocal errors between inverse source-receiver configurations are used to identify 'bad' picks that display an unacceptable differential in reciprocal travel-time. Reciprocal measurements require receiver locations to be used as both receiver and source location during the course of the survey. Therefore, reciprocal analysis is undertaken on ~50% of the entire data for any given survey, and is used as a representative sample of the entire survey dataset i.e., a reciprocal error subset.

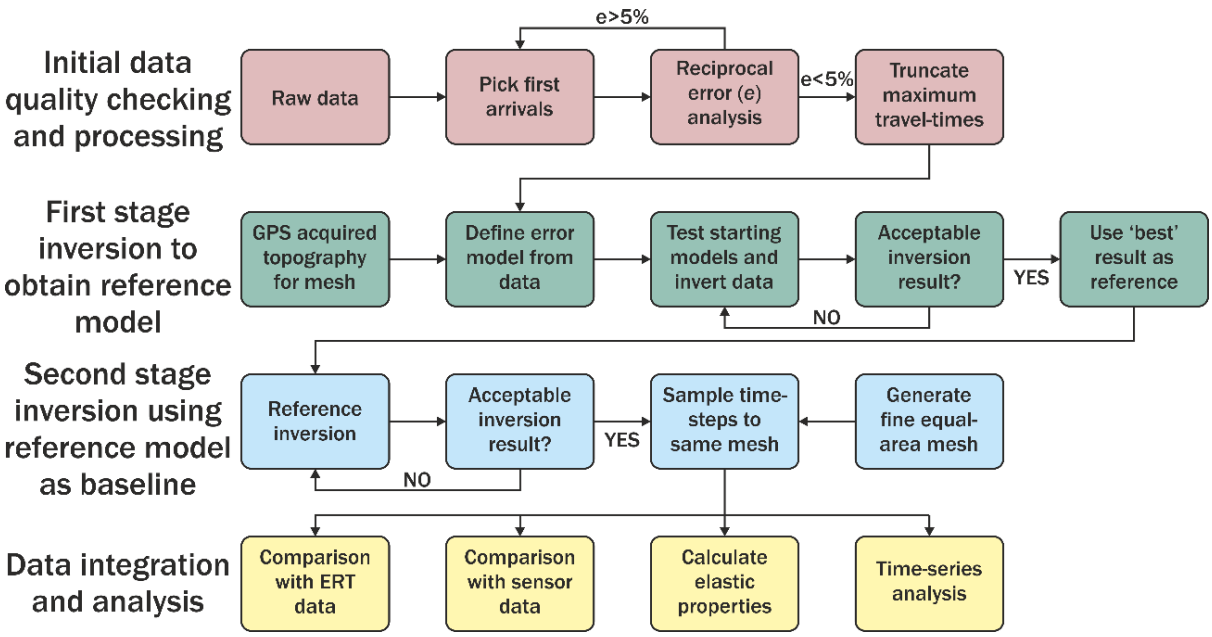

Figure 3.3: Proposed workflow for processing SR surveys (i.e., time-steps) to produce a reliable time-series of time-lapse SR data. SR data are first processed using reciprocal data analysis for quality control. Individual SR survey data are initially inverted to determine the best time-step, from which the resulting model us then used as a 'reference model' for all the time-steps in the time-series. Time-lapse SR images are then created using unique topography acquired at each survey, in order to determine velocity changes in the subsurface between surveys.

The error (e) in a reciprocal measurement (defined as the mean travel-time of the two measurements) is defined as

$$|e| = 100 \cdot \left(\frac{|t_n - t_r|}{t_n + t_r}\right) \quad , \qquad \text{Equation 3.3}$$

in which t_n is the travel-time between a source at position A, and receiver at position B, and t_r is the travel-time between a source at position B and a receiver at position A. Reciprocal measurements cannot always be acquired when intra-survey (i.e., within the same time-step) data coverage is inconsistent. Factors leading to poor data coverage include low signal-to-noise-ratio at greater source-receiver offsets and interference from noise sources,

such as wind, rain and amplification of these noise sources through nearby trees (Figure 3.4a). Large reciprocal errors occur in travel-times with greater source-receiver offsets, and therefore the use of reciprocal measurements as a data quality indicator favours data acquired from the very near-surface (i.e., shots with smaller source-receiver offsets). Across all of the reciprocal error subsets from each time-step in this study, 12.5% of the V_p data

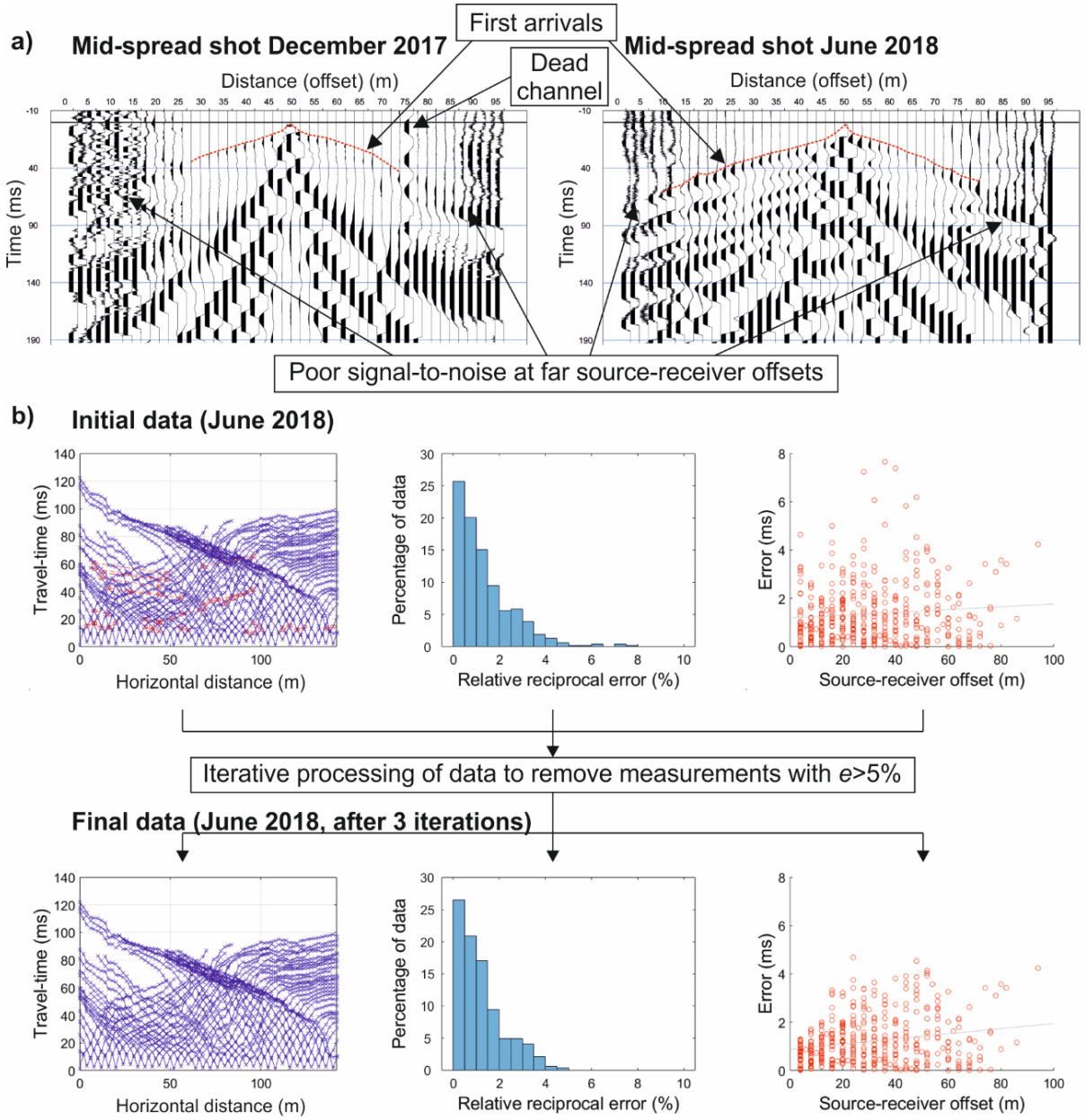

Figure 3.4: a) Examples of V_p shot records from the same position at the HHLO from December 2017 (left panel) and June 2018 (right panel). Poor signal-to-noise at larger source-receiver offsets prohibits the identification of first arrivals, and prevents acquiring reciprocal pairs for every measurement in the survey. b) The process of identifying reciprocal errors within a subset of the refraction survey data with e>5% from V_p data from June 2017. Top left panel shows all first-arrival data (displayed as travel-time curves) with pairs of measurements of e>5% circled in red. Top centre panel shows the distribution of relative reciprocal errors within the reciprocal error data subset, and the top right panel shows the distributions of absolute reciprocal errors from this data subset as a function of source-receiver offset, indicating that shots with further offsets have higher errors. The corresponding panels below show the effect of iteratively identifying and re-picking data with e>5%, in order to reduce errors across the dataset.

and 14.1% of the V_s data are not analyzed due to lack of reciprocal measurements. Remaining reciprocal-pairs of measurements showing a discrepancy e>5% are re-examined and re-picked (Figure 3.4b). Shot records adjacent to a reciprocal-pair with e>5% are also considered during this procedure. The data are then re-analyzed, and any further measurements with e>5% are re-picked. This iterative process continues until all measurements in the dataset have e<5%.

A further issue arising from implementing a time-lapse approach is achieving consistent inter-survey (i.e., between time-steps) data coverage over time. Consistent coverage cannot always be achieved due to variations in noise sources and environmental factors between surveys. For example, surveys undertaken in periods of increased ground moisture show lower signal-to-noise compared to surveys undertaken in drier conditions, and subsequently individual surveys show a significant variation in maximum-recorded travel-times. Without normalization of these maximum travel-times, comparison of the inverted sections to determine an appropriate reference model is challenging, primarily due to differences in maximum travel-times inducing significant variations in the maximum depths of coverage in the inverted models.

To overcome this, the distribution of all travel-times from across the monitoring period is plotted, and a travel-time value that preserves the majority of the data is chosen as a cut-off. In this case, the chosen cut-off travel-times are 86 ms and 178 ms for the V_p and V_s data, respectively. Data with travel-times over this cut-off are discarded, creating consistency in coverage between time-steps, but reducing the total number of data points. Across all of the time-steps of this study, 1.5% of the V_p data and 17.1% of the V_s data are discarded, giving a common maximum travel-time between surveys. The V_s surveys tend to have better signal-to-noise ratios, which results in a higher number of reliable first arrivals being recorded, however, this ultimately means that more data are discarded in order to match the relatively poorer coverage achieved in the V_p surveys.

3.3.2 Using accurate topography

Repositioning of receivers to repeatable x, y and z positions on the landslide surface is crucial to ensure that seismic ray paths are sampling comparable domains of the subsurface over time. The positioning error in x and y can be minimized by deploying receivers relative to permanent markers located outside of the active area of the landslide, and recording absolute x and y positions for receiver locations. Furthermore, the slope surface (z) will change between surveys. This effect cannot be removed by accurate positioning, and therefore needs to be incorporated into the data processing. Variations in z, as well as small unavoidable discrepancies in x and y positions can be captured using accurate geodetic surveying methods.

In this study, receivers are deployed every 2 m, with the first receiver located outside of the active landslide area (i.e., above the backscarp) and deployed at the same absolute position for each survey. A permanent ground peg marks the location of this first receiver, and a tape measure draped across the ground surface is used to deploy the remainder of the survey profile relative to this location. A Real-Time Kinetic Global Navigation Satellite System (RTK-GNSS) is used to capture the absolute positions in x, y and z of all receivers with a precision <0.05

m. With accurate positional data for each survey, the 'line-of-sight' distance (d) between one receiver location with coordinates (x_i, y_i, z_i) and another with coordinates ($x_{i-1}, y_{i-1}, z_{i-1}$) can be expressed as

$$d_i = \sum_1^i \sqrt{(x_i - x_{i-1})^2 + (y_i - y_{i-1})^2 + (z_i - z_{i-1})^2} \quad . \qquad \text{Equation 3.4}$$

Topographic features between these receiver locations (i.e., those features smaller than the receiver spacing) are not captured in the data.

For accurate 2D seismic travel-time inversion, accurate elevations and surface distances of the receivers are required, as the fundamental problem to be solved is one of distance and time. It is common in SR surveys for the elevations (z_i) of sensors to be recorded accurately, but for the inter-receiver spacing to be assumed to be a "fixed" nominal surface distance. This is particularly common in surveys on flat or uniformly dipping surfaces, where accurate inter-receiver spacing are easier to measure and control. However, in environments where topography can vary sharply within the receiver array, such as landslides, this approach can lead to errors in the positioning of receivers, which in turn introduces errors in to the generation of subsurface meshes for inversion, ultimately influencing the resulting inverted travel-times. Figure 3.5 shows the discrepancies that can arise from assuming a "fixed" nominal spacing (e.g., assuming receivers are deployed every 2 m, without accounting for the changes in distance that topography will create) with variable z_i measurements (red points) against using the true x_i, y_i and z_i positions to generate line-of-sight distances using Equation 3.4 in this study (green points). Using a "fixed" nominal spacing for time-lapse monitoring ignores lateral variations in receiver spacing, and results in an overestimation of array length. Therefore, the line-of-sight distances and the elevation of the receivers is used in the inversion process. Acquiring topographic information at every survey (i.e., time-step) allows for accurate inversion of travel-times.

At the HHLO, the SR profile is orientated to match the maximum slope profile, which is broadly parallel to the north-south orientation, and therefore the main direction of recorded wave propagation for the SR survey was also in a north-south direction. Given the alignment of the *y* coordinate orientation with the direction of wave propagation, greater variations in the *y* coordinate of the receiver position (i.e., north-south orientation, parallel to slope) introduce larger errors to the results of the seismic survey if not accounted for. Variations in *x* coordinates (i.e., east-west orientation, perpendicular to slope) have a smaller effect on measurement accuracy, as they are perpendicular to the wave propagation direction. Between each survey, the mean variation in receiver repositioning is 0.03 m in the *x* coordinate (1.5% of receiver spacing), and 0.01 m in the *y* coordinate (0.5% of receiver spacing), which is below the nominal accuracy of the equipment used for data acquisition. Across the entire monitoring period, receiver positions vary by an average of 0.41 m in the *x* coordinate (20.5% of receiver spacing) and 0.15 m in the *y* coordinate (7.5% of receiver spacing). The increased accuracy of deployment in the *y* coordinate is due to the use of a tape measure deployed in the same orientation. Some active areas of the landslide experience much greater variations in topographic change due to slope displacements (Figure 3.5).

3.3.3 Defining appropriate inversion parameters

In this study, 2D inversion of the seismic data is undertaken using the open-source Python based software *pyGIMLi* (Rücker et al., 2017). This software allows the inclusion of an error model fitted to the distribution of reciprocal errors across the entire time-lapse dataset. A linear error model was fitted to a plot of reciprocal errors and average travel times, and the parameters of this model included in the *pyGIMLi* inversion. A mesh-generation module in *pyGIMLi* produces unique meshes for each time-step inversion, derived from the RTK-GNSS measurements (see section 3.2). The production of unique meshes for each time-step increases the accuracy of the model for each time-step, but presents issues for later time-series analysis; in an ideal monitoring campaign, the inversion meshes for each of the survey time-steps would be identical, allowing for comparison of inverted velocity models on a cell-by-cell basis. However, given the overriding importance of capturing the differences in receiver positions and topography between time-steps, the use of unique meshes is necessary, and this issue is addressed after the data inversion stage.

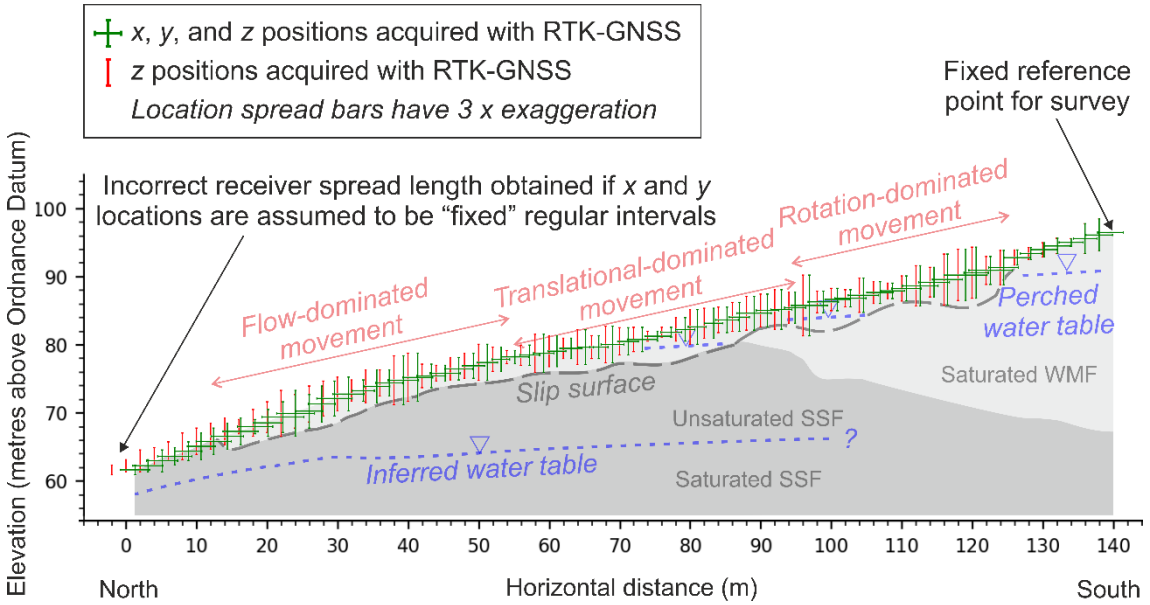

Figure 3.5: The positions of receivers used in the SR surveys at HHLO superimposed on to the site conceptual model, and their variation over the monitoring period; the bars indicate the spread of locations over the time-series (with 3 x exaggeration applied). The green points are surveyed positions using an RTK-GNSS system, where Equation 3.4 has been used to generate true line-of-sight receiver distances. The red points show how errors in positioning can arise if a "fixed" nominal receiver spacing is assumed, resulting in lateral errors in receiver positions, and over-estimation of slope length, which can result in inaccurate inverted seismic velocities.

For this study, a two-stage 'reference model' inversion approach is used to constrain the inversion and minimize differences between time-steps (Figure 3.3). In the first stage, stand-alone inversions of all of the individual time-steps are undertaken, with the aim of identifying the single time-step with the 'best' inverted model in terms of data fit. For this first-stage, it is necessary to define a generic velocity gradient model (i.e., velocity increasing with depth) as the starting model for the inversion process. In the first instance, test the effects of changing

different parameters of the starting velocity gradient model are tested by changing these parameters and performing repeat inversions. The parameters tested include the velocity bounds of the starting gradient model (i.e., velocity at the surface and base of the model) and the maximum depth of the starting model. From this process, a range of inverted models are obtained, and assess which starting velocity gradient model parameters provide good results both in terms of data-fit (by considering RMS and χ^2 values) but by also giving consideration to the subsurface based on the site conceptual model (Figure 3.1). There is a risk that the inversion process will introduce artefacts to improve data-fitting, and so qualitative comparison of results with *a priori* site information is as equally important at this stage as considering quantitative metrics of data-fitting. For this study, several sources of previous intrusive and geophysical data are used to validate the inverted velocity model (see Chambers et al., 2011, Merritt et al., 2013, Uhlemann et al., 2016a, Uhlemann et al., 2017). Stand-alone inversions of each time-step are performed using the parameters for the starting velocity gradient model shown in Table 3.2.

RMS and χ^2values are calculated for each inverted time-step model. The 'best-fit' model is assessed by looking at the divergence of χ^2 from a 'perfect-fit' model, in which $\chi^2 = 1$. The model with the lowest absolute divergence (i.e., closest to $\chi^2 = 1$) is designated as the 'reference model' for the second inversion stage. As no modelling error is included in the inversion, inversions do not typically converge at $\chi^2 = 1$. Details of the values of χ^2 and divergence from χ^2 for each inversion are shown in Table 3.2. From here, a single model is identified as having the 'best' fit and is taken forward to the second stage; all other resulting inverted models computed up to this stage are discarded.

Table 3.2: The optimal parameters for the staring velocity gradient model used in the first-stage inversion. These were obtained by changing their values and observing their effects on the inverted model output in terms of both data fit and comparison with the site conceptual model. Parameter values resulting in the 'best-fit- model were then used to invert all of the time steps, in order to identify the 'best-fit' model used for the second-stage of inversion.

Inversion settings							
Inversion parameter	**Depth of mesh**	**Minimum velocity at surface**	**Maximum velocity at base**	**Smoothing factor (lambda)**	**Maximum travel time**	**Absolute data error**	**Relative data error**
P-wave inversion input value	40 m	300 m/s	3000 m/s	25	86 ms	0.0242 ms	0.02 %
S-wave inversion input value	40 m	100	1500	25	178 ms	0.0194 ms	0.006 %

In the second stage of the inversion process, the inversion of the entire data set is then repeated, but this time using the 'reference model' (i.e., the 'best' fit model) from stage one as the starting model (Table 3.3). Using this

method provides all of the time-steps with a realistic and common starting model that is appropriately constrained and represents the local subsurface seismic properties. Within this second stage of the inversion, a nearest-neighbour lookup function allows the starting model to be sampled from the 'reference model' mesh to the inversion mesh, overcoming issues of topographic variance encountered by using different topography for mesh generation at each time-step. The result is a time-series of inverted seismic velocity models, all inverted using a common, real-world derived starting model.

Table 3.3: The results of the two-stage inversion process for both the V_p and V_s surveys. In stage one, a velocity gradient model with the parameters in Table 3.2 is used to perform stand-alone inversions of each time-step. The 'best' result (highlighted green) is then assessed by looking at divergence from a perfect model fit (i.e., a normalised $\chi 2$ ¬value, or '$\chi 2$ divergence'). The 'best' model is then used as a 'reference model' for the second stage inversion. The 'reference model' is used for the inversion of each time-step in the second stage inversion, providing a real-world, common starting model for the time-series.

P-wave inversions																
First stage inversion	**Starting model**	Velocity gradient model (see Table 3.2 for values)														
	Time-step	**0**	**1**	**2**	**3**	**4**	**5**	**6**	**7**	**8**	**9**	**10**	**11**	**12**	**13**	**14**	**15**
	χ^2	0.982	1.495	1.952	1.345	1.478	1.138	1.434	1.358	1.848	1.573	1.288	1.316	1.258	0.982	1.157	0.992
	RMS	2.970	3.788	4.971	4.310	4.143	4.412	4.721	5.244	5.713	5.431	4.010	3.965	3.727	3.404	4.157	3.492
	χ^2 divergence	0.018	0.495	0.952	0.345	0.478	0.138	0.434	0.358	0.848	0.573	0.288	0.316	0.258	0.018	0.157	0.008
Second stage inversion	**Starting model**	Reference model derived from results of first stage inversion (i.e., time-step 15)														
	Time-step	**0**	**1**	**2**	**3**	**4**	**5**	**6**	**7**	**8**	**9**	**10**	**11**	**12**	**13**	**14**	**15**
	χ^2	0.984	1.516	1.904	1.486	1.593	1.440	1.733	1.445	2.238	1.893	1.442	1.351	1.357	1.161	1.330	0.927
	RMS	3.157	3.935	4.860	4.466	4.069	5.044	4.729	5.202	5.693	5.515	4.314	3.966	4.050	3.987	4.148	3.385
	χ^2 divergence	0.016	0.516	0.904	0.486	0.593	0.440	0.733	0.445	1.238	0.893	0.442	0.351	0.357	0.161	0.330	0.073
S-wave inversions																
First stage inversion	**Starting model**	Velocity gradient model (see Table 3.2 for values)														
	Time-step	**0**	**1**	**2**	**3**	**4**	**5**	**6**	**7**	**8**	**9**	**10**	**11**	**12**	**13**	**14**	**15**

	χ^2	1.117	1.416	2.061	1.959	2.654	1.991	2.499	1.563	1.771	3.822	1.614	2.873	2.517	1.910	2.179	2.100
	RMS	1.206	1.415	1.764	1.678	2.001	1.685	1.910	1.491	1.704	1.974	1.716	2.068	1.933	1.629	1.770	1.750
	$\chi 2$ divergence	0.117	0.416	1.061	0.959	1.654	0.991	1.499	0.563	0.771	2.822	0.614	1.873	1.517	0.910	1.179	1.100
Second stage inversion	Starting model	Reference model derived from results of first stage inversion (i.e., time-step 0)															
	Time-step	0	1	2	3	4	5	6	7	8	9	10	11	12	13	14	15
	$\chi 2$	0.990	1.520	2.082	1.988	2.629	1.912	2.243	1.713	1.681	1.728	1.812	2.861	2.533	1.913	2.047	2.039
	RMS	1.124	1.479	1.657	1.745	2.018	1.532	1.820	1.731	1.724	1.716	2.349	2.106	2.074	1.612	1.889	1.675
	$\chi 2$ divergence	0.010	0.520	1.082	0.988	1.629	0.912	1.243	0.713	0.681	0.728	0.812	1.861	1.533	0.913	1.047	1.039

As a result of incorporating unique topography for each time-step, each time-step uses a different mesh structure. To allow for consistent analysis of inverted velocity models between time-steps, the models are re-sampled and interpolated to a regular, refined, triangular mesh (constructed using the same *pyGIMLi* module), effectively creating a spatially-identical time-series on a consistent mesh (Figure 3.7a). A mesh generated with the most recent topography in the monitoring campaign is used, to better reflect an up to date state of the system. One consequence of this approach is that some cells from earlier surveys, in which the surface positions may now have slipped downslope, are not sampled to the resampling mesh. To mitigate against this effect, a refined cell size that is smaller than the original cells is used for the inversion, purposefully oversampling the inverted data in order to discretize the subsurface, and capture variations in the very near-surface. This enables a range of analyses of the time-lapse dataset (Figure 3.3).

3.4 Topographic induced variations in seismic velocity

This work places an emphasis the importance of accurately capturing the intra-survey topography by using 2D line-of-sight distances from 3D GNSS surveys, and using topography data acquired for each individual survey in the monitoring campaign. This short section serves to demonstrate how failing to accurately capture variations in topography can have a significant impact on final inverted V_p and V_s measurements.

To demonstrate the effect of temporal topographic variation on seismic velocity, the first 14 V_p datasets (D_0:D_{13}) and accompanying topographic surveys (T_0:T_{13}) are processed according to the workflow in Figure 3.3. A P-wave travel-time dataset from midway through the monitoring campaign, January 2018 (D_8), is processed and inverted using the surveyed topography (T_8) to produce a 'true' time-step dataset (TTS_8) comprising 2128 subsurface V_p

model points. The same seismic dataset (D_8) is then processed using the remaining topographic data in the time-series (T_0:T_7, T_9;T_{13}), resulting in 13 SR time- steps with 'false' topography (FTS_0:FTS_7, FTS_9:FTS_{13}). The variations present in these 'false' time-steps represent the effect that real-world variations in topography across the monitoring period have on seismic velocity. By normalising all of the time-step data to TTS_8, the results from January 2018 become a baseline against which variations in seismic velocity arising from subtle, but realistic changes in landslide topography are assessed. The result of this analysis is shown in Figure 3.6. They indicate that topographic variations can have a large impact on the resulting V_p, with 23% of the total data showing velocities greater than ±10% of the true maximum recorded velocity. This has significant implications when trying to identify variations arising from genuine subsurface elastic property changes caused by environmental factors, as these variations can be very subtle.

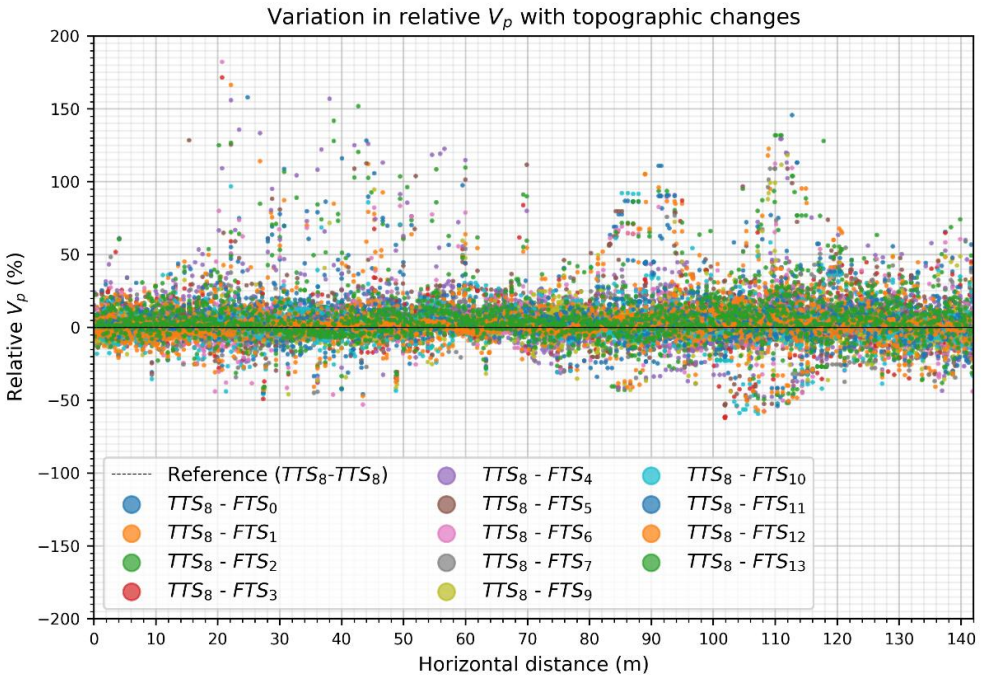

Figure 3.6: Relative changes in V_p caused by subtle, real-world changes in topography. The solid black line at y=0 represents a normalised baseline (TTS_8-TTS_8). The same seismic dataset (D_8) has been processed using the other time-step topographic data; any variations in V_p are therefore a product of these subtle topographic changes between surveys.

3.5 Data analysis and results

One approach to analysing time-series SR data is to look at how the seismic attributes of discrete seismic units respond to changing environmental conditions. The prevalent subsurface lithological discontinuities (i.e., those that are stable in time) are highlighted by plotting the mean values of the individual cells across the 33-month monitoring period (Figure 3.7). These plots are displayed using the most recent topography in the time-series. The individual cross-sections highlight significant subsurface features, including changes in lithology at depth,

and different domains of movement in the near surface. Plots showing the standard deviation of these mean values (Figure 3.7) indicate the areas of the landslide that show greatest velocity variation across the monitoring period.

Here the sliding layer at the HHLO (extending from the surface to 2 – 4 m depth) is considered which is identified by the low V_p and V_s at the surface of the cross-sections. This extends from beneath the break in slope at the bottom of the back scarp (~15 m horizontal distance), to the base of the flow lobes (125 m horizontal distance). At the HHLO, this surface sliding layer is monitored by several subsurface and surface environmental sensors, recording rainfall and changes in moisture content, allowing direct comparison with inverted cross sections. By selecting grid cells within this layer, it is possible to calculate the change in velocity over time. In

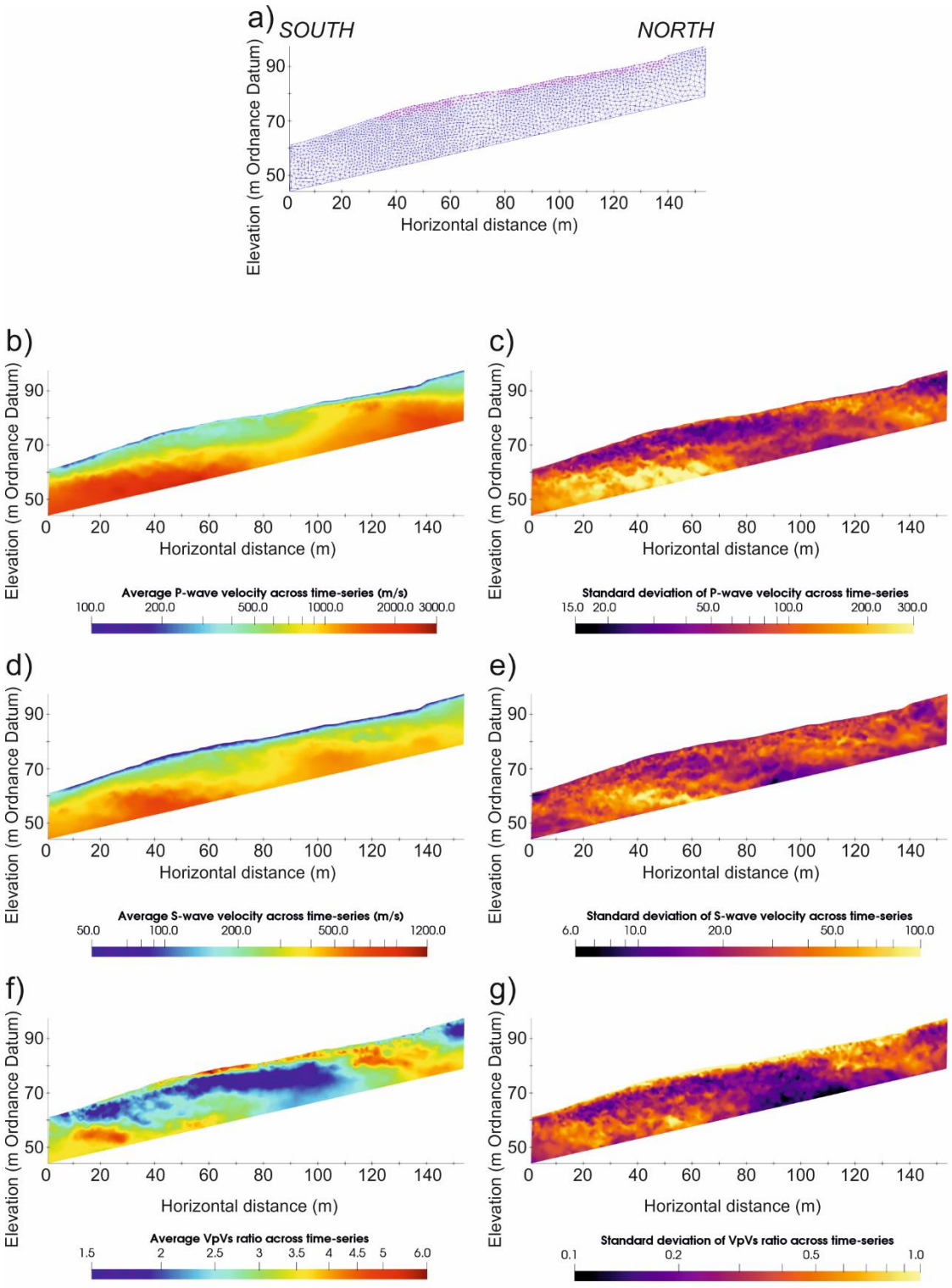

Figure 3.7: a) The regular mesh used to sample all of the individual time-steps to create spatially comparable datasets for the time-series. The cells highlighted purple in the surface sliding have been used for the analysis in Figure 3.8. b) The mean V_p and c) standard deviation of the V_p over the 33-month monitoring period. d) The mean V_s and e) standard deviation of the V_s over the 33-month monitoring period. f) The mean V_p/V_s and g) standard deviation of V_p/V_s over the 33-month monitoring period.

this case, the surface layer comprises model cells from both the V_p and V_s time-series datasets (Figure 3.7b and Figure 3.7d), the positions of which are fixed using a common mesh.

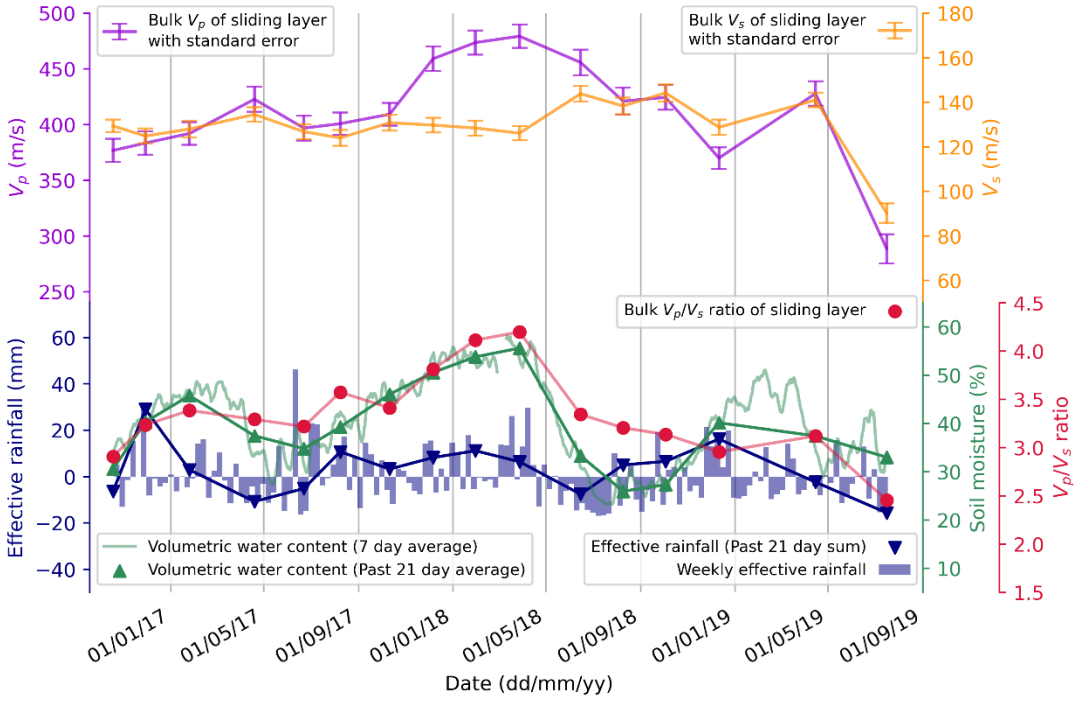

Figure 3.8: The top panel shows variation in bulk V_p and V_s readings from the sliding layer at the HHLO (see Figure 3.7 for location of this layer). The V_p/V_s s ratio, derived from the bulk V_p and V_s readings is shown. In the bottom panel, weekly effective rainfall, showing periods of net infiltration/evapotranspiration at the HHLO, and soil moisture from a surface sensor measuring to <0.1m bgl. The variation in V_p broadly follows the increases and decreases in moisture content, while V_s shows little variation. The derived V_p/V_s s ratio shows greatest sensitivity to the moisture content of the surface sliding layer at HHLO.

Figure 3.8 shows the time-series V_p and V_s inverted values extracted from this surface layer, alongside calculated effective rainfall, soil moisture data from a cosmic-ray sensor measuring shallow (~0.1 m bgl) moisture content across the site. V_p increases and decreases in relation to soil moisture, but with a slight time lag. The lag effect is caused by the difference of the sampling depth of the moisture sensor (<0.1 m bgl) and the depth of the V_p readings (2 – 4 m bgl); the moisture content of the HHLO near-surface changes more quickly in relation to net infiltration and evapotranspiration rates (shown by the hourly soil moisture, faint green line) than the top 2 – 4 m of the landslide, which will be less subject to evapotranspiration processes at depth. It is also worth noting that inverted velocities will be smoothed values from the true velocities, due to the spatial and temporal smoothness constraints used.

Furthermore, the calculated V_p/V_s ratio (Figure 3.7f), which is an indicator of material saturation (Uyanık, 2011), better reflects changes in moisture content in Figure 3.8. Crucially, the minimum V_p (350 m/s) in the time-series is 24% less than the maximum V_p (462 m/s). Given that topographic effects alone can cause variations in V_p >±10%

(Figure 3.6), the changes in seismic velocity over time could easily be masked if the data are not processed correctly. This demonstrates the necessity for including accurate topography in long-term SR monitoring campaigns in landslide settings.

3.6 Conclusions

SR is rarely used for the long-term assessment of landslides prone to hydrological destabilization, but has great potential for high-resolution spatial monitoring. This is particularly the case in slopes with high spatial heterogeneity in which monitoring data obtained from sparse point observations is insufficient to capture the complexity of the landslide system. Landslide monitoring campaigns using SR can determine seismic attributes of slipped materials, which provides information on elastic property changes due to temporal variations in moisture content. However, failing to give due attention to the possible sources of error in SR surveys can lead to artefacts in the time-lapse data, which can easily mask changes arising from genuine variations in the elastic properties of landslide materials, including the underlying rock. In this study, a workflow for addressing the errors associated with producing a reliable time-series of inverted seismic velocity models is presented, and have shown how velocities in the near-surface soil layers are sensitive to variations in moisture content.

Standard approaches to quality assessment and processing of SR data aid in minimizing individual survey data error. The use of emerging methods to increase picking accuracy, such as automatic detection algorithms, machine learning and statistical approaches will also decrease data errors introduced in to the creation of time-lapse data from standalone surveys. In this study, data from each survey were processed using reciprocal error analysis to ensure ϵ<5% of travel-time for all datasets. However, in the case of producing time-lapse data from these individual datasets, the importance of using detailed, unique topography data for processing each time-step is emphasised. This crucial step could easily be overlooked by inaccurate assumptions regarding field setup, receiver spacing landslide surface movement between surveys, even by experienced SR operators.

For the data considered here, changes in topography lead to >±10% variations in apparent seismic velocities in 23% of the data for the unconsolidated near-surface. The data exhibits a 24% difference between the fastest and slowest V_p observed in this layer, caused by variations in elastic properties induced by changes in moisture content, underscoring the need to properly account for topography effects. To avoid the errors associated with changes in topography, accurate source-receiver positions are important when processing SR monitoring data. Several other steps, including the repositioning of receivers in the field, the use of data quality indicators (such as travel-time reciprocity) and robust reference models for inversion further reduces these errors. If these potential sources of error are managed correctly, SR presents a useful tool for the identification of heterogeneous subsurface conditions and their changing properties over time in active landslide settings.

Acknowledgements

The authors would like to acknowledge Florian Wagner for advice on the *pyGIMLi* API. The authors would also like to acknowledge members, students and visiting scholars of the BGS' Geophysical Tomography team for their

input and support. The authors would like to thank Josie Gibson, Frances Standen and James Standen for their continued support of monitoring activities at Hollin Hill. This work was funded by a NERC GW4+ UK Doctoral Training Partnership Studentship (Grant NE/L002434/1) and in part by the BGS University Funding Initiative (S337), which are gratefully acknowledged. Jim Whiteley, Jonathan Chambers, Jimmy Boyd, Mihai Cimpoiasu, Jessica Holmes, Cornelia Inauen, Arnaud Watlet, Luke Hawley-Sibbett and Russell Swift publish with the permission of the Executive Director, British Geological Survey (UKRI-NERC).

4 Rapid characterisation of landslide heterogeneity using unsupervised classification of electrical resistivity and seismic refraction surveys

J. Whiteley, A. Watlet, S. Uhlemann, P. Wilkinson, J. Boyd, C. Jordan, J. M. Kendall & J. Chambers (2021c). Rapid characterisation of landslide heterogeneity using unsupervised classification of electrical resistivity and seismic refraction surveys. Engineering Geology, 290, 106189. https://doi.org/10.1016/j.enggeo.2021.106189.

Declaration and author contribution

The content of this chapter was published in *Engineering Geology* in May 2021. Minor amendments have been made to the content to better integrate the work with the overall thesis. The fieldwork to collect the data for this work was planned and overseen by J. Whiteley. The seismic and resistivity surveys were acquired by J. Whiteley, A. Watlet and J. Boyd., and the quality assurance and quality control, processing, analysis, visualisation and interpretation of the geophysical data were undertaken by J. Whiteley. C. Jordan acquired and processed the UAV-acquired topography data. S. Uhlemann and P. Wilkinson advised on inversion parameters for the seismic and resistivity surveys, and provided feedback on results. The machine learning elements of the work were undertaken by J. Whiteley after discussions with A. Watlet. J. Whiteley composed the original draft for publication, which was reviewed by all authors. The work was supervised by J. M. Kendall and J. Chambers.

Contributor Roles Taxonomy (CRediT) statement

Conceptualisation: *J. Whiteley*

Investigation: *J. Whiteley, A. Watlet, S. Uhlemann, J. Boyd, C. Jordan*

Formal analysis: *J. Whiteley, A. Watlet, S. Uhlemann, P. Wilkinson*

Methodology: *J. Whiteley*

Visualisation: *J. Whiteley*

Writing – original draft: *J. Whiteley*

Writing – review and editing: *J. Whiteley, A. Watlet, S. Uhlemann, P. Wilkinson, J. Boyd, C. Jordan, J. M. Kendall, J. Chambers*

Supervision: *J. M. Kendall, J. Chambers*

Abstract

The characterisation of the subsurface of a landslide is a critical step in developing ground models that inform planned mitigation measures, remediation works or future early-warning of instability. When a landslide failure may be imminent, the time pressures on producing such models may be great. Geoelectrical and seismic geophysical surveys are able to rapidly acquire volumetric data across large areas of the subsurface at the slope-scale. However, analysis of the individual model derived from each survey is typically undertaken in isolation, and a robust, accurate interpretation is highly dependent on the experience and skills of the operator. A machine learning process for constructing a rapid reconnaissance ground model is demonstrated, by integrating several sources of geophysical data in to a single ground model in a rapid and objective manner. Firstly, topographic data are acquired by a UAV survey to co-locate three geophysical surveys of the Hollin Hill Landslide Observatory in the UK. The data are inverted using a joint 2D mesh, resulting in a set of co-located models of resistivity, P-wave velocity and S-wave velocity. Secondly, the relationships and trends present between the variables for each point in the mesh (resistivity, P-wave velocity, S-wave velocity, depth) are analysed to identify correlations. Thirdly, a Gaussian Mixture Model (GMM), a form of unsupervised machine learning, is used to classify the geophysical data into clusters with similar ranges and trends in measurements. The resulting model created from probabilistically assigning each subsurface point to a cluster characterises the heterogeneity of landslide materials based on their geophysical properties, identifying the major subsurface discontinuities at the site. Finally, the results of the clustering are compared to intrusive borehole data, which show good agreement with the spatial variations in lithology. This work highlights the applicability of integrated geophysical surveys coupled with simple unsupervised machine learning for producing rapid reconnaissance ground models in time-critical situations with minimal prior knowledge about the subsurface.

4.1 Introduction

Growing populations and concomitant land use change are increasing the exposure of people and infrastructure to landslide hazards (Froude and Petley, 2018). Characterising the subsurface of a landslide is the first step toward understanding the future causes of instability and mechanisms of failure, which in turn forms the basis of assessing and mitigating risk through monitoring, modelling, and early-warning (Pecoraro et al., 2019, Intrieri et al., 2013). Geophysical measurements play an increasingly important role in characterising and monitoring landslide systems at the slope-scale (i.e., covering the entire area of a landslide, in contrast to regional-scale studies) due to their greater spatial coverage and acquisition rates compared to detailed intrusive observations (see reviews by Hack, 2000, Jongmans and Garambois, 2007, Schrott and Sass, 2008, Van Dam, 2012, Perrone et al., 2014, Pazzi et al., 2019, Whiteley et al., 2019). As such, geophysical surveys are well suited for rapid reconnaissance activities and are able to provide significant volumes of subsurface data at the slope-scale, which can inform initial ground model development in the absence of further intrusive information.

Of the wide range of geophysical methods used in landslide investigations, geoelectrical and seismic methods are the most common (Baroň and Supper, 2013, Jaboyedoff et al., 2019, Whiteley et al., 2019). In particular, electrical resistivity (ER) tomography and seismic refraction (SR) tomography are two complementary methods that are able to produce high spatial resolution models of the subsurface, and are sensitive to different hydro-mechanical properties of the rocks and soil that make up the landslide material. Generally, in landslide investigation (and in other types of ground engineering investigations), interpretation of geophysical measurements relies on a qualitative, heuristic approach based on visual analysis of an inverted model. In rapid reconnaissance surveys where only a single geophysical method is used, there can be high uncertainties when determining the source of spatial variation in the observed measurements. For example, resistivity decreases in areas of higher moisture content, but also in materials with increased clay content. Identifying the underlying cause of ER anomalies can be difficult without a priori information or more detailed follow-up information, thereby significantly affecting the reliability and speed of the interpretation.

Landslide systems move toward critical failure when the restraining forces that give materials shear strength (τ_f) are overcome by destabilising forces that act to reduce shear strength. Therefore, understanding the landslide system in terms of the state of τ_f is crucial for understanding risk of failure. Equation 2.1 defines τ_f in terms of a simple infinite slope model, where c is cohesion, σ is total normal stress, u is pore water pressure, and ϕ'_{cv} is the angle of shear resistance at a critical state. ER measurements are sensitive to variations in moisture content, porosity and clay content, whilst seismic methods are sensitive to elastic properties controlled by material strength, density, porosity and saturation, particularly the distinction between saturated and partially saturated ground in the case of P-wave velocity (Whiteley et al., 2020b). In a rapid reconnaissance setting, it may not be possible to quantify absolute values for the parameters of τ_f from geophysical measurements; such an approach requires the determination of petrophysical relationships in a laboratory setting. Examples of this approach include relationships between resistivity and moisture content (Merritt et al., 2016, Uhlemann et al., 2017), resistivity and soil suction (Holmes et al., 2020), and shear-wave velocity and shear strength (L'Heureux and Long, 2017, Oh et al., 2017, Trafford and Long, 2020). However, relative states of the parameters of τ_f can be estimated from geophysical models. For example, ER measurements can provide information on the moisture and

clay content of materials in order to distinguish lithological formations (e.g., Chambers et al., 2011), which can provide indirect information on the likely state of u and c respectively (e.g., Merritt et al., 2013). SR measurements can provide information on elastic moduli, which relate to the relative state of σ in the landslide system (e.g., Uhlemann et al., 2016).

To improve the interpretation of geophysical data, exploit the different sensitivities of different methods and to move toward repeatable and more objective ground model development, multi-method geophysical surveys combined with increasingly automated data integration and processing approaches are needed. Data from an integrated near-surface geophysical survey are used to provide insights into soil and rock properties and to map subsurface heterogeneity in terms of the major subsurface discontinuities at an active landslide in North Yorkshire, UK. A rapid reconnaissance ground model using unsupervised machine learning techniques applied to ER and P- and S-wave seismic refraction (SR) tomography data is produced. Here, the term 'rapid' is used to refer not just to the speed of data acquisition and processing, but to how rapid this approach is when compared to the time taken to achieve the same coverage, detail and reduced uncertainty in interpretation obtained from other previous studies of the landslide (see studies by Chambers et al., 2011, Gunn et al., 2013, Merritt et al., 2013, Uhlemann et al., 2016a).

Integrated surveys combining these data sources are abundant in the literature (e.g., Merritt et al., 2013, Francioni et al., 2019, Kannaujiya et al., 2019, Cody et al., 2020). In this approach, the surface of the landslide is mapped using high-resolution imagery acquired by unmanned aerial vehicle (UAV). The UAV topographic data are then used in the construction of a joint 2D mesh incorporating topographic points from both surveys, allowing individual inversion of the near-surface ER and SR data on a joint mesh. To produce a more objective ground model requiring minimal user interpretation, a simple unsupervised clustering algorithm is applied to the modelled geophysical data cross-plotted against each other to identify areas of similar and contiguous properties. This approach requires minimal a priori information about the subsurface. Finally, the results of this approach are validated by comparison with pre-existing ground models of the site and geotechnical observations acquired from a borehole.

4.2 Site description

Landslide hazards are common in the UK, although they generally pose a low risk to human life (Gibson et al., 2013). They are most often triggered by periods of intense or prolonged rainfall, and their locations are strongly linked to the underlying geology. The rocks of the Lias Group are responsible for several types of geohazards across the UK, including cambering, valley bulging and landsliding, outcropping in a broad zone extending from the south-west to north-east coasts, along with other smaller outlying outcrops (Figure 4.1a). In particular, weak clay-bearing horizons within the Whitby Mudstone Formation (WMF) in the Lower Jurassic Upper Lias Group experience some of the highest densities of landslides in the UK at approximately 42 landslide per 100 km^2 of outcrop recorded in the National Landslide Database (Hobbs et al., 2012, Pennington et al., 2015). To study the processes that destabilise the formations of the Lias Group, the British Geological Survey established the Hollin Hill Landslide Observatory (HHLO) over a decade ago. The HHLO, located in North Yorkshire, UK, is a complex,

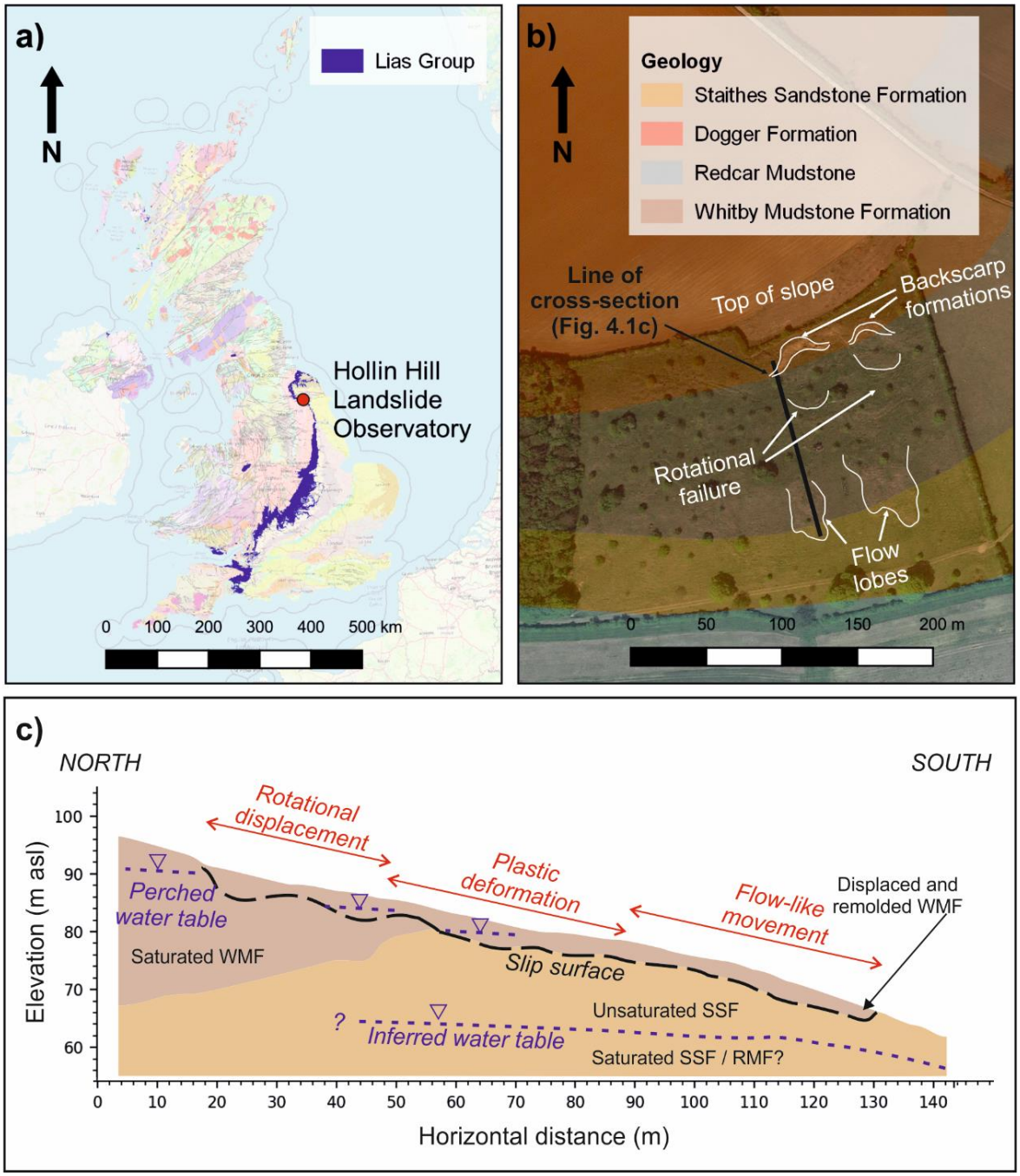

Figure 4.1: a) Location of the Hollin Hill Landslide Observatory and its situation within the Lias Group outcrop of the UK. Map data: British Geological Survey, Open Street Map. b) Satellite image of the site, with the major surface geomorphological features labelled and publicly available geological information shown. Map data: Google. c) Geological cross-section derived from several studies conducted at the site (see text for references). Modified from Uhlemann et al., 2016; Whiteley et al., 2020.

slow moving earth slide-flow, situated in the Lias Group mudrocks. It serves as a test bed for novel geophysical, geodetic and geotechnical landslide characterisation and monitoring technologies (Chambers et al., 2011).

Developments in ER optimisation (Loke et al., 2010, Uhlemann et al., 2015, Wilkinson et al., 2012), electrode displacement monitoring (Boyle et al., 2017, Loke et al., 2017, Wilkinson et al., 2010, Wilkinson et al., 2016), geophysical-geotechnical petrophysical relationships (Merritt et al., 2016) and landslide monitoring using geophysics (Merritt et al., 2018, Uhlemann et al., 2017, Whiteley et al., 2020b, Whiteley et al., 2021a) have all taken place at the HHLO. The following site description is summarised from these works.

The HHLO is located on a south facing ~12° slope on the north eastern edge of the Sherriff Hutton Carr embayment, formed by the draining of Lake Mowthorpe after the Devensian glaciation (Figure 4.1b, see also Figure 1.9). The site comprises agricultural land used for seasonal grazing and associated agroforestry. The slope comprises a series of interbedded shallow marine Lias Group mudstones and sandstone, comprising (from the base of the slope in ascending order) the Redcar Mudstone Formation (RMF), Staithes Sandstone Formation (SSF) and Whitby Mudstone Formation (WMF) (Figure 4.1b). The escarpment is capped by the Dogger Formation (DF), a limestone and sandstone unit forming the base of the Ravenscar Group, which also acts as a minor aquifer in the area. These units are conformably deposited, and gently dipping to the north at an angle of 1 - 2°. A thin layer (<0.3 m) of topsoil is present across the site, beneath which the underlying rocks are highly weathered and present at residual strengths, often showing properties similar to soil (Merritt et al., 2013). A working conceptual model of the site (Figure 4.1c) has been developed as a result of several studies which have used combinations of geophysical, geotechnical and geodetic investigations to investigate the subsurface structure of the landslide (see studies by Chambers et al., 2011, Gunn et al., 2013, Merritt et al., 2013, Uhlemann et al., 2016a).

The main landslide processes occur in the highly weathered near-surface zone of the WMF. The WMF is up to 25 m thick and comprises grey to dark grey mudstone and siltstone showing bands of calcareous and sideritic concretions with high to very high plasticity. From 1013 tests, the WMF has a median liquid limit of 53% GMC and median plastic limit of 24% GMC, giving a plasticity index of 29% (Hobbs et al., 2012). Uhlemann et al. (2017) noted that GMC of greater than 48% can cause the clay-rich WMF to approach or exceed the liquid limit, causing mid-slope plastic deformation and translational movement of weathered WMF downslope. Material at the base of this translational zone accumulates at a break of slope indicating the surface outcrop of the underlying SSF. The SSF formation is approximately 20 m thick, although the contact between the SSF and underlying RMF is not well defined. The SSF comprises ferruginous, micaceous siltstone, with fine-grained sandstones and thin mudstone layers. The SSF is a comparatively porous sandstone unit that permits drainage of the overlying mobilised WMF, arresting the movement of the plastically deformed material from the mid-slope. The RMF is present at the site, underlying the SSF, although the exact boundary is uncertain due to the location of a persistent water table at a similar horizon, as evidenced by spring lines further down the slope. WMF material accumulated at the surface of the SSF is subject to sub-aerial weathering processes, including seasonal temperature cycling, inducing shrinkage and subsequent cracking. Water ingress into these shrinkage cracks can induce mud flows, further transporting disturbed WMF material downslope and leading to the formation of flow lobes. Above the mid-slope zone of plastically deforming WMF, support for overlying WMF material is removed, and rotational slumps form, creating large (3 – 4 m vertical displacement) backscarps close to the contact between the WMF and overlying DF. In a similar manner to the disturbed WMF material accumulated on the

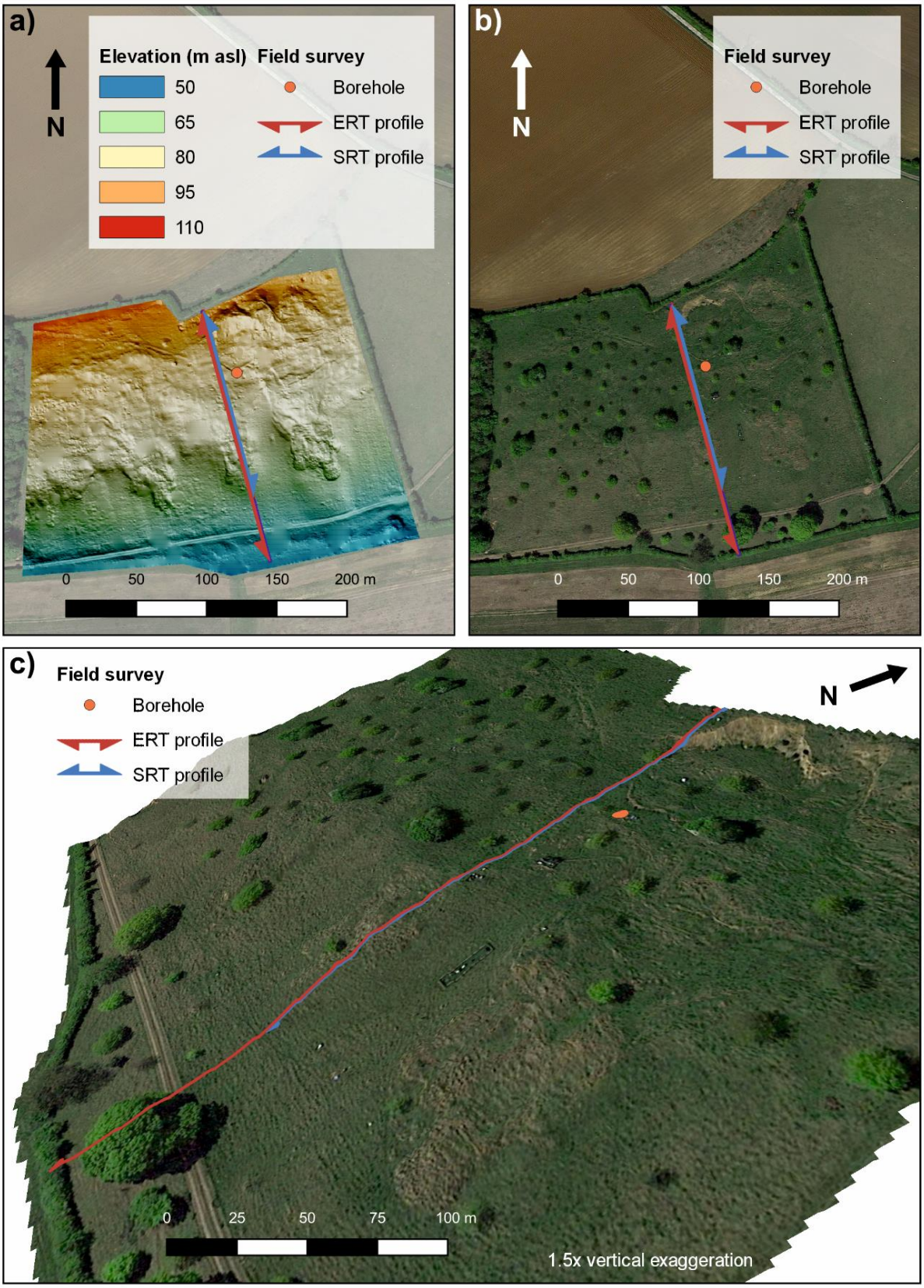

Figure 4.2: a) The DTM produced from the UAV survey of the Hollin Hill Landslide Observatory, undertaken at the same time as the geophysical surveys. Map data: Google. b) The UAV DTM combined with satellite imagery. Map data: Google. c) An oblique view of the DTM and satellite imagery showing the main geomorphological features of the Hollin Hill landslide. Map data: Google.

Table 4.1: Comparative parameters of the different surveys undertaken at the Hollin Hill Landslide Observatory in July 2019.

	UAV survey	Electrical resistivity (ER) survey	Seismic refraction (SR) survey (P-wave)	Seismic refraction (SR) survey (S-wave)	Borehole drilling
Type	Remote sensing	Surface geophysical			Intrusive geotechnical
Equipment	DJI Inspire 1 Raw	AGI SuperSting	Geometrics Geode, vertical geophones	Geometrics Geode, horizontal geophones	Dando Terrier 2002
Data target	Surface	Subsurface			
Data acquired	Surface imagery	Electrical resistivity	P-wave travel time	S-wave travel time	Soil / rock cores
Measurement sensitivity	Topographic variation	Lithology and saturation		Lithology and stiffness	Lithology
Processed information	Orthographic imagery / topography model (DEM/DTM)	Inverted resistivity model	Inverted velocity model		Geotechnical log / core scan
Dimension	3D (surface)	2D (cross-section)	2D (cross-section)		1D (log)
Depth of penetration	N/A	~15 m	~25 m		9 m (maximum in BH1902)
Personnel required	1	2	3		2
Measurement resolution	0.1 m	0.4 m	<0.5 m		Near-continuous
Area covered	150 m x 275 m surface area	180 m profile	142 m profile		~0.1 m x 17 m core (from two boreholes)
Acquisition time	<2 hours	2 - 3 hours	3 - 4 hours		2 - 3 days
Processing time	3 hours	1 – 2 hours	2 – 3 hours		1 day

SSF lower down the slope, the WMF material upslope that is disturbed by rotational failure also forms shrinkage cracks, providing pathways for future water ingress into the landslide system.

4.3 Survey activities

The remotely sensed UAV photogrammetry, near-surface geophysical and geotechnical data were obtained over four days in July 2019 (Figure 4.2), with the seismic and ER survey acquired on two consecutive days. Due to equipment and personnel restrictions, it was not possible to acquire all of the geophysical data in a single day. Table 4.1 shows the attributes of the various surveys, comparing resolution, acquisition rates and dimensions of each survey type. The individual activities for each survey are described in the following sections.

For the ER survey, electrodes were deployed at 2 m intervals from the top of the landslide, and 96 electrodes were deployed to give a nominal survey profile length of 190 m. A dipole-dipole array with $a = 4$ and $n = 8$ (where a is the maximum separation between current electrodes and n is the ratio of distance between the first current and potential electrodes to current dipole spacing), was used to acquire measurements, and reciprocal measurements were acquired for each reading.

For the SR surveys, hammer shots were acquired from the first geophone (0 m) of the survey profile at 4 m intervals along a series of geophones deployed at 2 m intervals (i.e., hammer shots at every other geophone). A flat horizontal plate source was used for the P-wave survey, and an inclined source with an angled face >45° to horizontal was used to generate horizontally polarised S-waves. A total of 72 geophone locations were measured (comprising two overlapping 48 geophone spreads acquired separately), giving a nominal survey length of 142 m.

4.4 Data processing

4.4.1 UAV data acquisition and processing

A UAV survey was conducted using a DJI Inspire 1 Raw rotary drone, equipped with a Zenmuse X5S 16 megapixel camera. In total, 210 vertical airphotos were acquired with 70% forward and sideways overlaps at an altitude of 90 m. Seven ground control points were georeferenced using RTK-GPS. Structure from motion processing was undertaken using Pix4Dmapper to produce a point cloud (11.9 million points, with an average density of 207 points per m^3), digital elevation model (DEM) with a horizontal resolution of 0.1 m, and orthophotograph. The raised vegetation (scrub and trees) was automatically removed from the DEM using the automatic digital terrain model (DTM) generator in Pix4D.

4.4.2 Topographic pre-processing and joint 2D mesh generation

The first electrode and geophone in the survey arrays were positioned at the top of the slope adjacent to a permanent marker peg. The remainder of the electrodes and geophones were deployed downslope at 2 m intervals relative to this position using a tape measure. However, the surveys were not conducted simultaneously, and the

tape measure was inadvertently moved between deployments for each survey. Consequently, later analysis of the RTK-GPS measurements of the electrode and geophone positions shows some positional discrepancies between the positions of the geophones and electrodes, meaning that these locations are not truly 'co-located' (Figure 4.3).

Using the same subsurface mesh to invert multiple-methods allows for interpretation of the model in the same spatial dimensions and at comparable resolution. If the same mesh can be used, then every cell in that mesh will have a value of P- and S-wave velocity and resistivity, allowing for easier statistical comparison of the values using approaches such as cross-plotting. Although it is possible to invert ER data acquired in 2D using a 3D inversion scheme, the seismic first-arrivals are inverted using a 2D inversion, and so aligning data positions is necessary to emulate spatial co-location of the data. A 2D mesh is constructed from 3D positions, firstly by translating points from British National Grid coordinates (as acquired from the RTK-GPS survey) to a local coordinate system, where the *x* position is perpendicular to the profile orientation, and the *y* position is parallel to the profile orientation. There are discrepancies in the positions of the electrodes (red dots) and geophones (blue dots) as deployed in the field (Figure 4.3a). To be able to create a joint mesh, the local *x* position between each electrode and geophone (black triangle) are interpolated, averaging the difference between the true electrode and geophone location. At each of these interpolated sensor positions, a new elevation (*z*) is extracted from the DEM at that position. The elevation of the interpolated positions shows little variation relative to the true elevation of the electrodes and geophones as deployed in the field (Figure 4.3b). During this process, the position of the electrodes and geophones in the *y* orientation (i.e., along the survey line) are preserved. It is worth noting that although this procedure was implemented to correct discrepancies from the field that could have been avoided, nonetheless this approach to minimising the differences between closely positioned datasets can prove useful for future surveys where unavoidable spatial discrepancies exist e.g., when comparing repeated measurements from monitoring campaigns.

After pre-processing, a joint 2D mesh is created on which both ER and SR data are inverted, acknowledging that small errors are introduced into both datasets by this process. However, the introduction of small errors associated with using an interpolated position is more favourable than preserving the original positions of one dataset at the expense of introducing significantly larger errors to the other; in other words, averaging the error across all data is preferable to prioritising one dataset over the other. Despite this, the interpolated positions used to create the 2D mesh all have deviations in the *x* direction of less than 0.3 m, which is 15% or less than the 2 m electrode and geophone spacing used (Figure 4.3a). This level of error is not unusual when collecting geophysical data in a steeply dipping, rough terrain environment with an undulating surface (Wilkinson et al., 2010). The variation in elevation by extracting a new z position from the DEM is shown to be very low, with a maximum variation of ‹0.08 m (Figure 4.3b), although the majority of points show a much lower difference than this. he joint mesh is created using the mesh generation module in pyGIMLi (Rücker et al., 2017). The result is a joint 2D mesh with a large number of small cells in the near-surface, due to the very small electrode and geophone separations (i.e., distance in the *y* orientation) found at some locations. Only the surface nodes corresponding to the electrode or geophone locations for the appropriate data type inverted are used by PyGIMLi as sensor locations for the inversion, with the remainder providing inter-sensor topographic refinement.

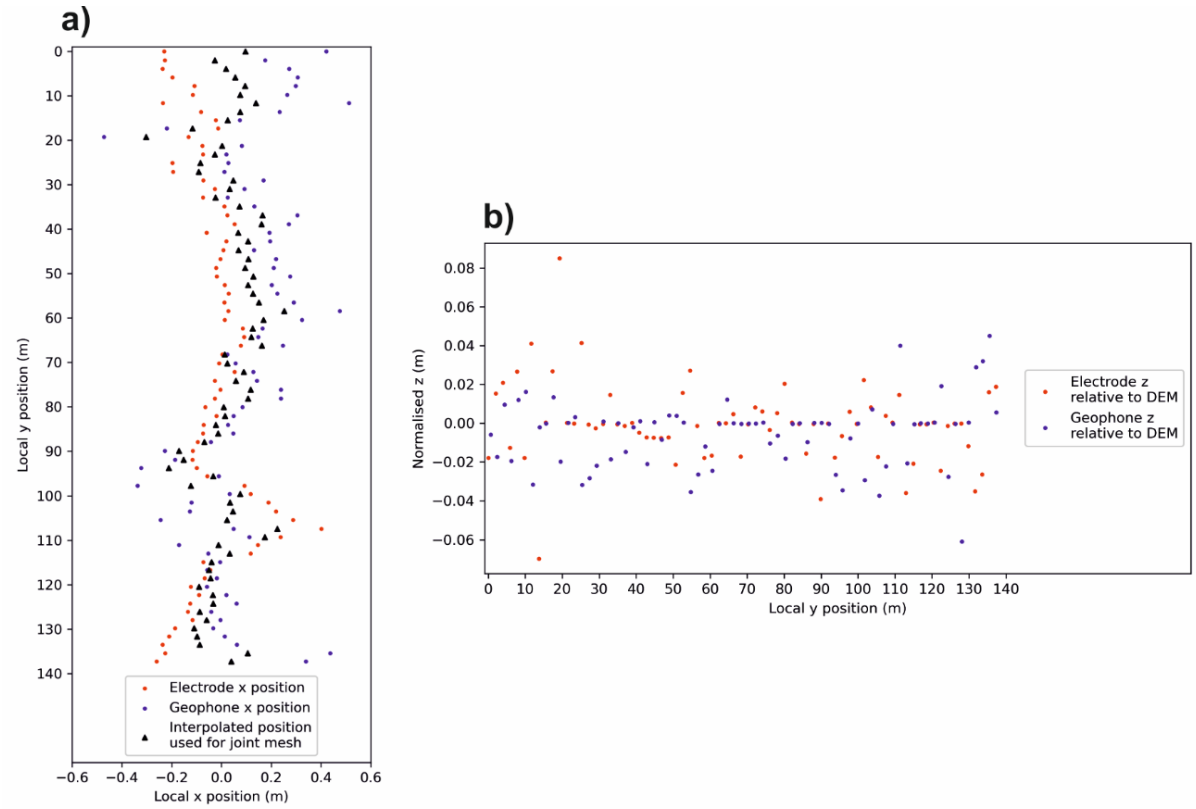

Figure 4.3: a) The positions of the electrodes and geophones translated to a local coordinate system, where x *is perpendicular and* y *is parallel to the survey profile orientation. The black triangles indicate the interpolated* x *positions used to create the 2D mesh. b) From the interpolated positions, a new* z *value is extracted from the DEM. Comparison between the extracted DEM elevation and the true elevation of the electrodes and geophones shows very little variation across the survey profile.*

4.4.3 ER inversion

The raw ER data are filtered to remove measurements with reciprocal errors >20 %. The reciprocal error (e) of a measurement is given in Equation 1.4, in which m_n is the measurement recorded with a source at position A, and receiver at position B, and m_r is the measurement recorded with a source at position B and a receiver at position A. A reciprocal error model is produced by binning the reciprocal error and resistance (r) data in logarithmically increasing bin sizes and fitting a line to the distribution of these bins (Mwakanyamale et al., 2012). An error model with R^2 = 0.973 (a+rb where a = 0.0036, b = 0.0003, Figure 4.4d) is fitted to the six bins of reciprocal and resistance data. This shows a significant improvement over using unbinned data, which has a fit with R^2 = 0.387 (a+rb where a = 0.00434, b = 0.00036, Figure 4.4a). The data are filtered again to remove reciprocal errors >10 %, and invert the ER data using the ER manager module of PyGIMLi with the joint 2D mesh constructed from the UAV topography. The resulting inverted model converges at χ^2 = 1.23 and relative root-mean-square error (RRMSE) of 3.82% after five iterations. The initial threshold for creating the error model (20%) is higher than the inversion threshold (10%) so that a wider range of error data are better characterised (e.g., identification of long-tail and non-Gaussian distributions).

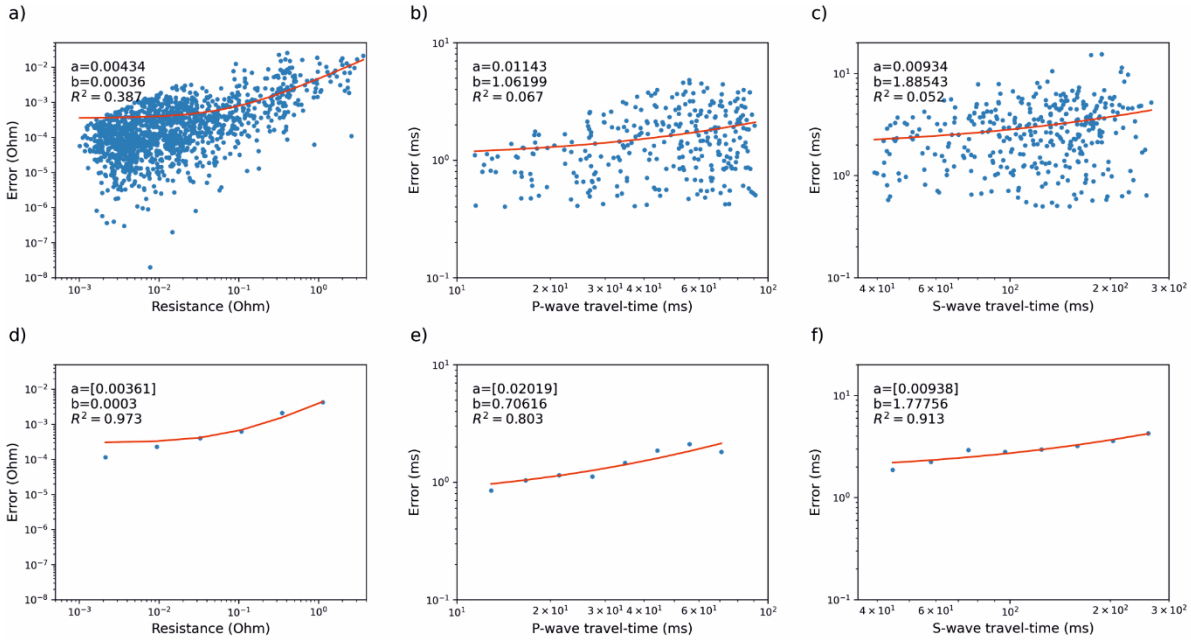

Figure 4.4: Error models using non-binned errors from a) the ER, b) P-wave, and c) S-wave surveys, and using binned errors from the d) ER, e) P-wave and f) S-wave surveys.

4.4.4 SR inversion

The first-arrivals of the P- and S-wave datasets are picked, and the dataset analysed to estimate random errors. Unlike ER, reciprocal data are only available for a subset of each SR dataset, as hammer shots were not undertaken at every geophone; consequently, for the first-arrivals detected by geophones where no hammer shots were undertaken, there is no means of directly assessing the quality of the data, other than following basic seismic refraction principles (Leung, 2003). Similarly, where environmental conditions (e.g., wind, rain) are different between the recording of the forward and reverse shots of a single reciprocal measurement, then the signal-to-noise ratio may be worse at one location, preventing identification of a clear first-arrival to the same offset of that measured from the reciprocal shot location. As such, reciprocal measurements are not always available for all picked first-arrivals even at shot locations where reciprocal data are available. For the P-wave dataset, only 373 of the 2124 picked first-arrivals (17.5%) have reciprocal measurements. In the S-wave dataset, 393 of the 1751 picked first-arrivals (22.4%) have reciprocal measurements. Reliable inversion of the data relies on the creation of an error model from the available reciprocal data, and so the SR data are filtered on modelled errors, unlike the pre-filtering of reciprocal errors undertaken on the ER data before the creation of an error model.

Error models for the P- and S-wave SR datasets are created using the same procedure; for all reciprocal measurements, the reciprocal errors and travel-time (t) of the datasets are divided into logarithmically increasing bin sizes. An error model with an R^2 value of 0.76 ($a+tb$, where a = 0.014, b = 0.827, Figure 4.4b) is fitted to the P-wave data, and with an R^2 value of 0.91 ($a+tb$, where a = 0.0094, b = 1.778, Figure 4.4c) to the S-wave data. This shows a significant improvement in fit above using unbinned errors, where the fit for the P-wave data is R^2 = 0.067

($a+rb$ where a = 0.01143, b = 1.06199, Figure 4.4e) and for the S-wave data is R^2 = 0.052 ($a+rb$ where a = 0.00934, b = 1.88453, Figure 4.4f). Points with modelled error of >5 % are removed, resulting in the removal of 8.7% of the P-wave data and 5.1% of the S-wave data. The P- and S-wave data are inverted using the SR manager module in pyGIMLi on the joint 2D mesh constructed from UAV topography. The P-wave model converges with a χ^2 of 1.6 and RRMSE error of 2.38% after nine iterations. The S-wave model converges with a χ^2 of 1.14 and an RRMSE error of 2.27% after 11 iterations.

4.4.5 Unsupervised learning for ground model development

In order to produce an objective ground model that provides a robust interrogation of the modelled data with minimal a priori information or operator interpretation, an unsupervised learning algorithm is used to group areas of similar geophysical properties in the landslide subsurface. Unsupervised learning algorithms are a basic form of machine learning, which are more commonly used at the regional scale in landslide studies for the identification of slopes at risk of future failure across large geographical areas based on pre-conditioning factors (Merghadi et al., 2020). In near-surface geophysics, they are increasingly used for identifying data patterns in processing (Sun and Zhang, 2020, Xia et al., 2018), predicting petrophysical relationships between geophysical measurements and material states (Ihamouten et al., 2016, Moghadas and Badorreck, 2019), identifying time-lapse variations in monitoring scenarios (Audebert et al., 2014, Delforge et al., 2021, Xu et al., 2017) and identifying zones of common geophysical properties for characterising the subsurface (Doetsch et al., 2010, Ward et al., 2014). One form of unsupervised learning is clustering, in which the aim is to separate data in to groups with similar groups of characteristics (i.e., clusters) (Dinov, 2018, Rodriguez et al., 2019).

For this exercise in rapid reconnaissance, a balance is required between a user-friendly algorithm (i.e., an algorithm with minimal hyperparameters to tune) and one that can appropriately identify trends and relationships in the geophysical data. An assumption in this approach is that the ER and SR measurements made within contiguous subsurface units of similar subsurface properties will display relationships unique to specific hydrogeological conditions. As no training data are available, an unsupervised clustering method is used which can assign data points as belonging to one of n numbers of clusters within an unsorted dataset that contains overlapping relationships between potential clusters.

One such approach is the Gaussian Mixture Model (GMM), a probabilistic unsupervised learning algorithm that classifies data in to clusters. The GMM is an extension of the k-means algorithm, one of the most common and easiest to use unsupervised learning algorithms (Raykov et al., 2016). There are three stages to implementing k-means clustering. The first is initialisation, in which a number of centroids (k) are seeded at random within a dataset. Next, all data points are classed as 'belonging' to one of these centroids based on the Euclidean distance from the centroids. Finally, the mean of the clusters are calculated, and the centroids moved to these positions (Dinov, 2018). The process is re-run, until the algorithm converges on a local optimum (i.e., when the locations of the centroids do not change).

A major drawback in the use of k-means clustering is that using Euclidean distance to calculate cluster assignment results in concentric (i.e., isotropic) clusters. If the spread of data is anisotropic (i.e., not equal in all

directions) or there is overlap between data points of separate clusters, k-means can fail to identify correct cluster assignments, even if the correct cluster assignments are clear to the human eye (Figure 4.5). A GMM differs from k-means in two main ways; i) clusters in a GMM are defined by their means and variance which are modelled as Gaussian distributions, and ii) a GMM assigns data to a cluster probabilistically (Jung et al., 2014). Therefore, a GMM is better suited to overcoming these limitations of the k-means approach.

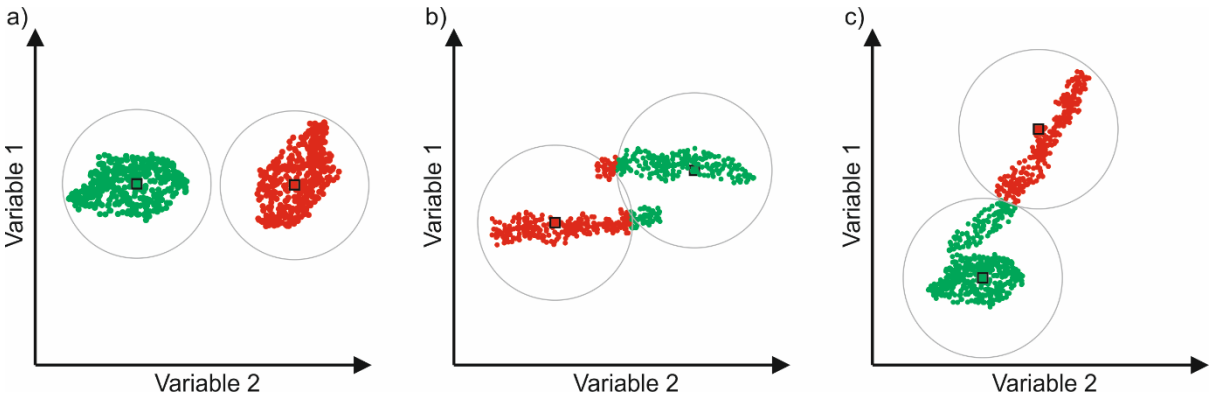

Figure 4.5: Schematic showing a) a good candidate dataset for k-means clustering comprising separate, isotropic clusters, and a poor candidate dataset for k-means clustering due to b) anisotropic clusters and c) cluster overlap between an isotropic and anisotropic cluster. Data are assigned to one of two clusters (red and green) based on the Euclidean distances shown by grey lines, with the cluster centroids shown by squares.

A GMM implements the Expectation-Maximization (EM) algorithm. EM is an iterative process that initially uses random components in the data and then switches between calculating the probability of a data point being generated by the Gaussian components of the model (i.e., expectation), and then maximizing the likelihood of the data given the classification (i.e., maximization). The result is a dataset that produces a series of classification labels identifying data points as belonging to one of a specified number of modelled Gaussian probability distributions present in the dataset. The dimensions of the modelled Gaussian probability distributions can be determined by assessing the variance (i.e., the spread of numbers away from the mean of the group) and covariance (i.e., the direction of the relationship between two variables). In a GMM, the covariance is expressed in a matrix, and determines the size and orientation of the modelled Gaussian distributions used in the clustering process (Pedregosa et al., 2011). The covariance types typically used in GMM clustering (Figure 4.6) are:

- Spherical: Produces modelled Gaussian distributions that have the same shape with isotropic variances in all directions (i.e., spherical shape).
- Diagonal: Produces modelled Gaussian distributions with different shapes, but that are orientated along coordinate axes.
- Tied: Produces modelled Gaussian distributions that have the same shape, but with anisotropic variances in any direction
- Full: Produces Gaussian distributions that can have any shape with no constraint on variance.

Using a full covariance matrix allows the Gaussian distributions to model data that contain strong but heterogeneous correlations between variables. The diagonal and tied covariance matrices assume strong but homogenous correlations between variables, and the spherical covariance matrix assumes no correlation between variables.

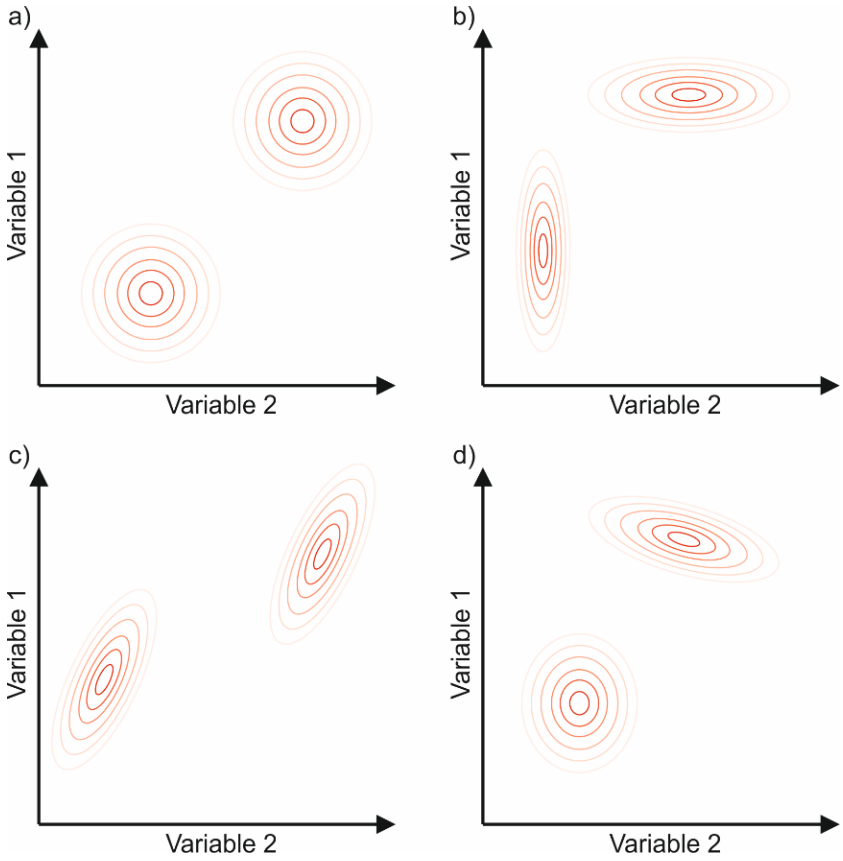

Figure 4.6: The types of Gaussian distributions produced from using different covariance matrices including a) spherical, b) diagonal, c) tied and d) full. Darker red contours indicate higher probability.

A GMM is used as i) it is unsupervised (i.e., requires no training data), ii) it assigns each point in the dataset to one of a specified number of clusters in a probabilistic manner, identifying potential areas of uncertainty (Doetsch et al., 2010), iii) it allows a range of covariance types in the data, allowing for identification of anisotropic, convex clusters in the parameter space (Delforge et al., 2021), and iv) it is easily implemented using the scikit-learn package, a collection of machine learning tools for predictive data analysis that is part of the Python based SciPy library (Pedregosa et al., 2011).

Four geophysical variables are available for passing to the GMM algorithm, three geophysical variables (resistivity, P-wave velocity (V_p) and S-wave velocity (V_s)) and one spatial variable (depth in z from the ground surface). Two combinations of inputs to the GMM are considered; one using only the three geophysical inputs (i.e., a GMM without depth constraint) and one using the four inputs combining the geophysical and depth inputs (i.e., a GMM with depth constraint). An important hyperparameter to tune in a GMM is the number of

expected clusters in the data. Given that only basic a priori information are assumed for the site, similar to that which might be obtained from a simple desk study, the number of expected clusters are determined using statistical analysis of the model inputs to the GMM and comparing this result with the a priori information available from a geological map.

Firstly, the optimal number of clusters is assessed by considering the Bayesian Information Criterion (BIC) for a range of number of clusters (Schwarz, 1978). The BIC is a general statistical means of scoring a range of candidate models to identify the model with the highest probability of fitting the data (Neath and Cavanaugh, 2012). In the context of a GMM, the objective of considering the BIC is to identify the minimum number of clusters that can describe the heterogeneity of the model (Delforge et al., 2021). Bayesian statistics are used to calculate the conditional probability of an event (i.e., the posterior probability) based on information that may be relevant to the occurrence of the event (i.e., prior probability and likelihood) (McNamara et al., 2006). The BIC as proposed by Schwarz (1978) assumes that one model is a 'true' model that fits the data. According to Bayes' theorem, the degree to which one model (M_i) fits the data over another model (M_j) is given by the ratio of the posterior odds to the prior odds as

$$\frac{\frac{\Pr(M_i|y)}{\Pr(M_j|y)}}{\frac{\Pr(M_i)}{\Pr(M_j)}} \qquad \text{Equation 4.1}$$

where $\Pr(M_i)$ is the prior probability and $\Pr(M_i|y)$ the probability density of the data given M_i, and $\Pr(M_j)$ is the prior probability and $\Pr(M_j|y)$ the probability density of the data given M_j (Dziak et al., 2020). If the prior probabilities for each model are equal, this can be simplified to the 'Bayes factor' of two models (B_{ij}) as

$$B_{ij} = \frac{Pr(y|M_i)}{Pr(y|M_j)} \quad . \qquad \text{Equation 4.2}$$

Schwarz (1978) demonstrated that for many models the Bayes factor can be approximated by $\exp(-\frac{1}{2}BIC_i + \frac{1}{2}BIC_j)$ where

$$BIC = -2\ell + ln\, n\, p \quad , \qquad \text{Equation 4.3}$$

where ℓ is the log-likelihood of the entire dataset within the model, $ln\, n$ is a function of the sample size n, and p is the number of parameters within a model (Dziak et al., 2020). Therefore, according to Equation 4.3, the lowest BIC value, or threshold at which increasing the number of clusters does not change the gradient between BIC values, can be considered the optimum number of clusters to use in the GMM algorithm.

In the case of the GMM without depth constraint, the absolute BIC values decrease significantly above two clusters, and continue to decrease marginally with increasing cluster numbers, showing no obvious absolute BIC minima. However, the BIC gradient becomes asymptotic to 0 at four clusters, indicating that the gain in increasing the number of clusters is marginal above this value. Conversely, in the GMM with depth constraint, a sharp decrease in the BIC is observed at four clusters, above which the BIC increases again. Although the BIC marginally decreases again at seven clusters, given the objective of considering the BIC is to minimise the number of clusters to describe the data, four is identified as the optimal number of clusters for both models.

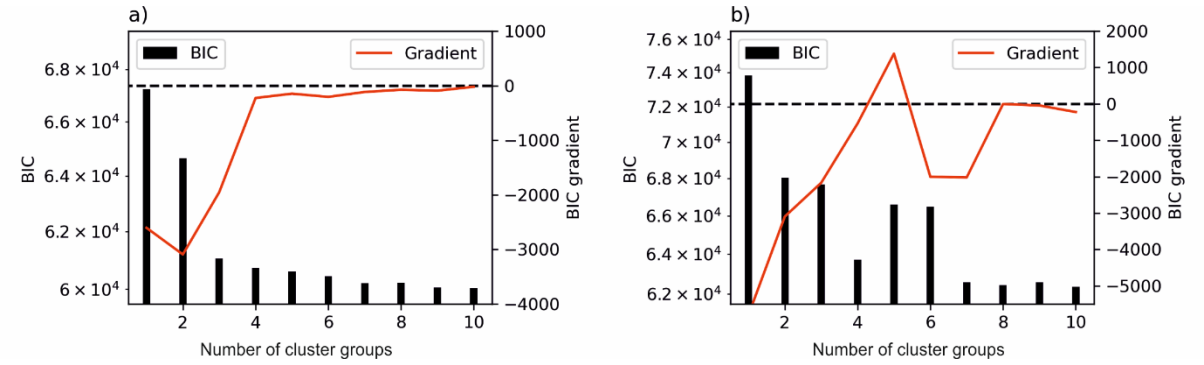

Figure 4.7: The Bayesian Information Criterion (BIC) and gradient of the BIC for a range of a number of clusters for a) inputs without depth constraint including resistivity, P- and S-wave velocity and b) inputs with depth constraint including resistivity, P- and S-wave velocity and depth. The lowest number of clusters above which adding additional clusters does not change the BIC or gradient of the BIC indicates the optimal number to use, in each case four clusters.

Secondly, the use of four clusters is confirmed by considering basic a priori information about the site from maps and on site observations. The publicly available geological map of the site (Fox-Strangways and Howell, 1983) shows four stratigraphic units beneath the slope; the Dogger Formation (DF), Whitby Mudstone Formation (WMF), Staithes Sandstone Formation (SSF), Redcar Mudstone Formation (RMF) (Figure 4.1b). Within these four units, two distinct lithologies are present; mudstone (WMF and RMF) and sandstone (DF and SSF). The satellite images (Figure 4.2b and Figure 4.2c) show surface materials (derived from these parent lithological units) that are in the process of being reworked by creeping landslide processes, for example, as reworked WMF material forming the flow lobes at the site. Areas of very little deformation are observed, where the surface materials are assumed to be stable. Therefore, the a priori information confirms the use of four clusters in either GMM model, representing i) sandstones, ii) mudstones, iii) actively deforming (disturbed) surface material likely derived from the displaced WMF, and iv) relict (undisturbed) surface material likely derived from the SSF. In addition to deciding the number of clusters, some additional hyperparameters require tuning. For each cluster in both GMM models, the covariance type is set to full to allow for the identification of anisotropic clusters with different variances and Gaussian distributions. In addition, a random state is passed to the algorithm to allow for reproducibility between separate runs of the algorithm.

4.5 Results

4.5.1 Individual model results

The inverted geophysical models are shown in Figure 4.8. Figure 4.8a, b and c show the data inverted using the individual meshes derived from the RTK-GPS positions of electrodes and geophones in the field. Figure 4.8d, e and f show the results of inverting the data using the joint mesh. The methods have varying depths of penetration, with the P-wave model reaching deeper parts of the landslide, and the ER model imaging shallower areas. The inverted ER model shows a small zone of intermediate (20 – 50 Ωm) resistivity at the top of the slope, above a

large unit of low resistivity (<20 Ωm) extending from the base of the section to the surface is identified at 20 – 60 m horizontal distance. Downslope of this, the low resistivity layer is present as a shallow surface layer, extending to ~130 m horizontal distance along the profile. A zone of increased resistivity underlies this surface layer, containing some thin layers of high resistivity (>100 Ωm), which are identified at the surface from 120 – 170 m horizontal distance. At the base of the slope, an area of intermediate resistivity values underlie this higher resistivity area between 110 – 180 m horizontal distance, which also shows localised zones of lower resistivity.

The P-wave model shows uniformly low velocity surface layer of 300 – 500 m/s, thickest in the central part of the slope (60 – 100 m horizontal distance) and thinning toward the surface both from 0 – 60 m horizontal distance and from 100 – 150 m horizontal distance. Units of increased velocity are present at depths of >15 m bgl at the top of the slope (between 10 and 50 m horizontal distance) and shallowing from ~20 m bgl to ~10 m bgl between 80 and 150 m horizontal distance. This latter high velocity unit at the base of the slope has the highest P-wave velocities, in excess of 2000 m/s, while the former high velocity unit toward the top of the slope has reduced P-wave velocities in the range of 1000 – 1500 m/s. P-wave velocity should be sensitive to changes in bulk modulus, and will increase significantly as materials move from a highly- to fully-saturated state. However, it is not clear from the P-wave velocity alone whether this lower unit represents a change in lithology, or is a water table.

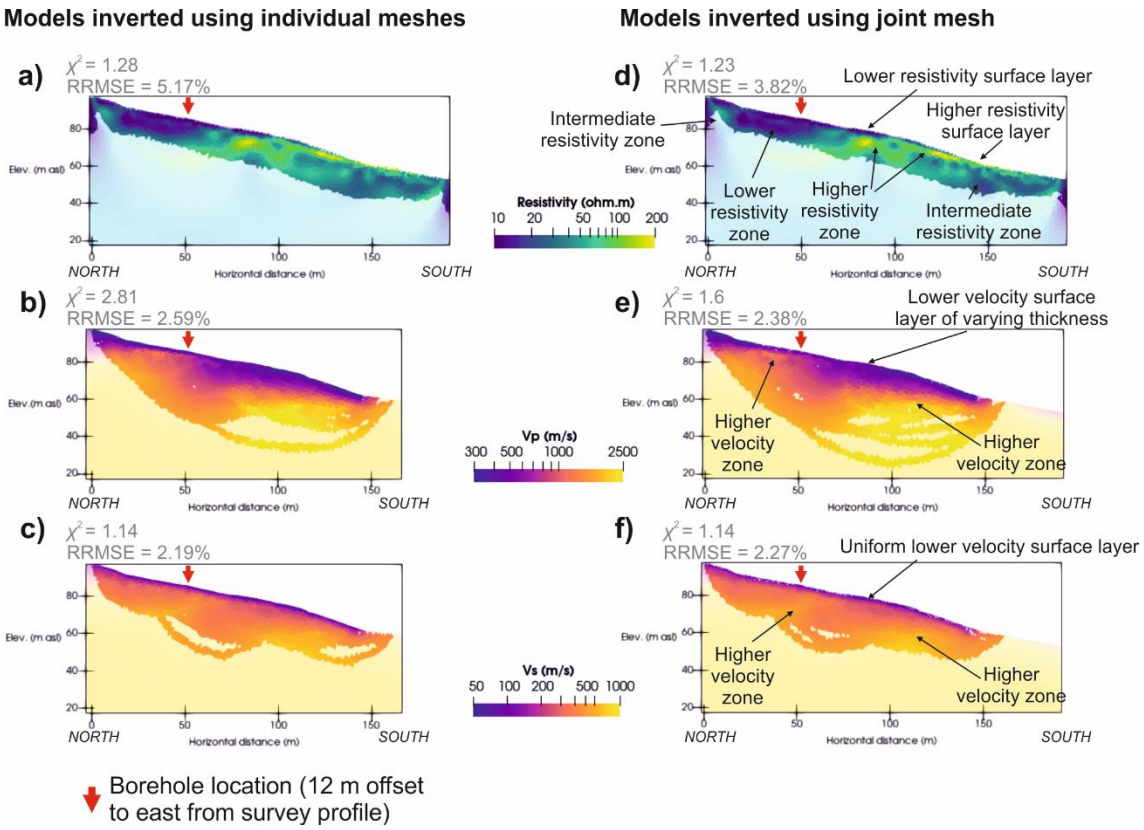

Figure 4.8: The inverted geophysical models from the Hollin Hill Landslide Observatory. a) Resistivity model, b) p-wave model and c) S-wave model inverted using individual meshes derived from original survey geometry. d) Resistivity model, e) P-wave model and f) S-wave model inverted using a joint mesh created with interpolated sensor positions. Models of each method are presented on the same colour scale, with the more transparent areas showing where there is low data coverage in the model.

The S-wave model shows a smaller range of velocities, with a very uniform low velocity layer of 50 – 100 m/s from the surface to about 2 m bgl across the slope. An increased velocity boundary is identified between 30 – 70 m horizontal distance, rising from ~20 m bgl to the near-surface across this area. Similarly, a broadly horizontal increase in S-wave velocity is identified from 90 – 150 m horizontal distance, at ~60 m elevation asl. S-wave velocity is sensitive to variations in shear modulus, generally decreasing with increasing saturation, but with no rapid rise at the highly- to fully-saturated state (as with P-waves velocity).

4.5.2 Geophysical model relationships

After inversion of the individual geophysical datasets on the joint 2D mesh, a model is extracted with co-located resistivity, P-wave and S-wave velocity values. The points are extracted from the centre of cells that have overlapping coverage from all of the geophysical surveys, limiting the data to a shallow layer approximately 20 m thick (the maximum depth extent of the ER survey) and extending from 0 - 144 m horizontal distance along the survey profile (the maximum horizontal extent of the SR survey). The co-located model comprises 1937 data points with values of resistivity and P- and S-wave velocity (Figure 4.9). In each of the individual models, these points have full coverage by each method in each survey; reducing this threshold has the potential to produce a co-located model with a greater number of points, at the cost of increasing the uncertainty associated with the non-uniqueness of inverted measurements in the model.

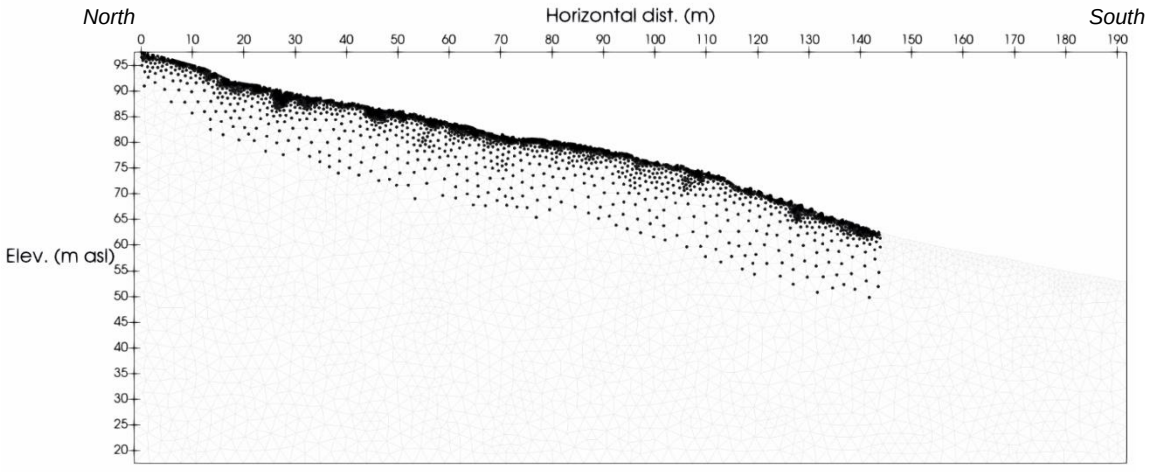

Figure 4.9: The 1937 data points (black dots) that have a co-located measurements of V_p, V_s and resistivity, and their position on the joint 2D mesh created from the separate topography of the ER and SR surveys (grey background).

Cross-plots and simple statistics of the different data variables (resistivity, P-wave and S-wave velocity, and depth below ground level) are used to explore potential relationships in the co-located models. Combining these approaches, a 'cross-plot correlation matrix' is produced, in which each variable in the co-located model is plotted

against each other, shows the different relationships present in the data (Figure 4.10). A Spearman rank correlation test, measuring the statistical dependence between two variables described by a monotonic function, provides a simple means of identifying positive or negative correlations in multi-variate data. In the cross-plot correlation matrix, the background of each plot is coloured according to the Spearman rank correlation coefficient (r_s), with dark red indicating strong positive correlations in the data, and dark blue indicating strong negative correlations. The Spearman rank correlation is a non-parametric means of evaluating the degree of linear association (i.e., correlation) between two variables, calculated by

$$r_s = 1 - \frac{6\sum d_i^2}{n(n^2-1)} \qquad \text{Equation 4.4}$$

where d_i is the difference between ranks for each x_i, x_y pair, and n is the number of data pairs (Gauthier, 2001). Data with perfect positive correlation have r_s = 1, and data with a perfect negative correlation have r_s = -1.

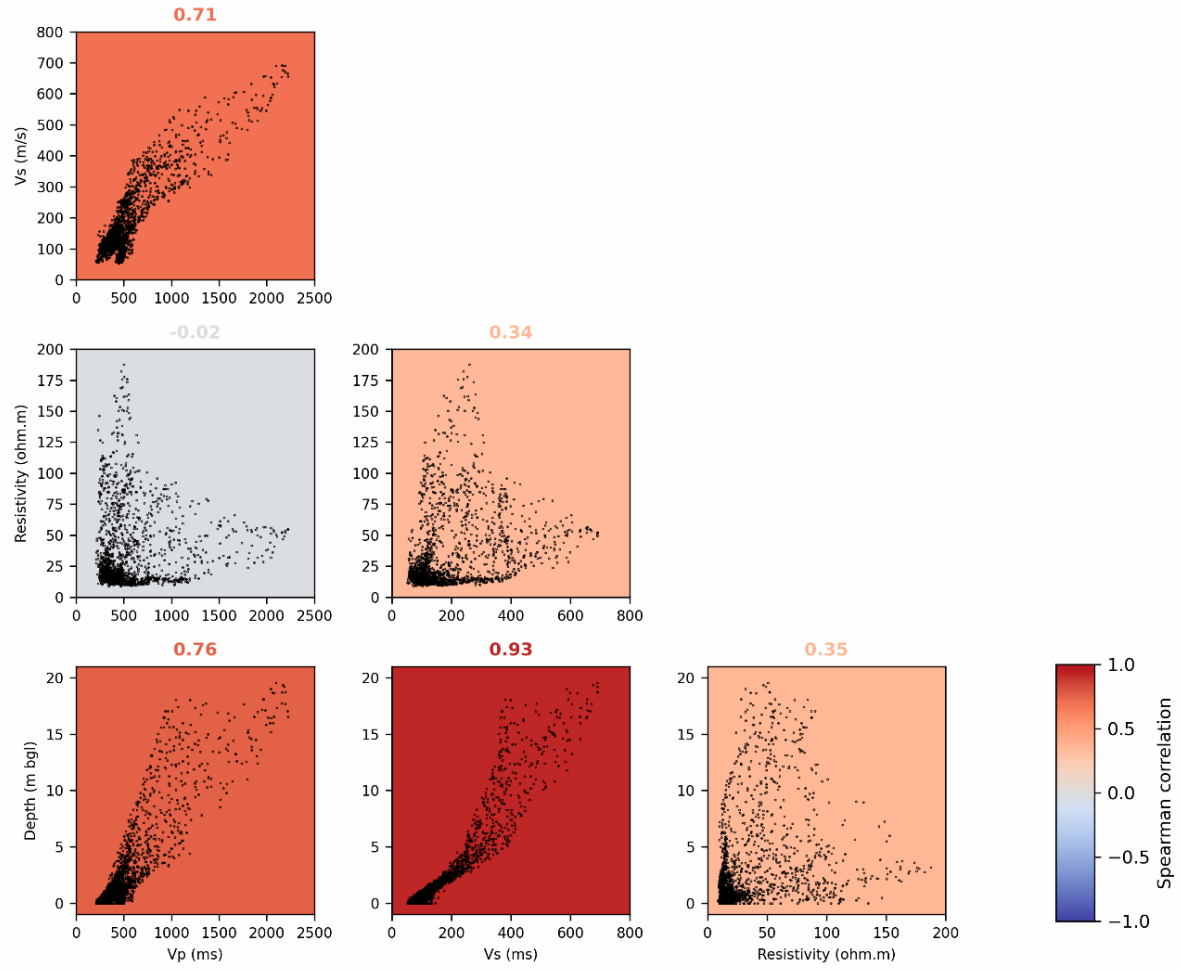

Figure 4.10: A cross-plot correlation matrix, plotting each variable from the co-located model (resistivity, P-wave velocity, S-wave velocity, and depth below ground level). The shading behind each panel corresponds to the Spearman rank correlation, printed above each panel, measuring statistical correlation between the variables.

For some cross-plots in the correlation matrix, r_s is expectedly high. S-wave velocity is sensitive to increases in stiffness, which is increased by compaction, and therefore a very strong positive approximately linear correlation between S-wave velocity and depth (r_s = 0.93) is identified. S-wave velocity is a function of soil density, void ratio and effective stress (L'Heureux and Long, 2017), all of which are expected to increase with burial depth, leading to the strong correlation shown in Figure 4.10. Similarly, P-wave velocity increases with bulk modulus and density, which is increased with compaction, and therefore has a strong approximately linear correlation with depth (r_s = 0.76). Additionally, moisture variations within soil will induce significant changes in the P-wave velocity (Ilori et al., 2013), which points toward the greater spread of higher P-wave velocities with greater depth when comparted to the S-wave velocity (which remains comparatively unaffected by moisture variation). Due to the effect of compaction on both seismic velocities, the correlation between P-wave and S-wave velocity is also strongly positive and approximately linear (r_s = 0.71). The approximately linear nature of the relationships between seismic velocity and depth indicate a simple relationship in which increasing depth results in increased seismic velocities; this is expected as greater compaction is experienced with the increasing volumes of material overlying deeper points.

However, some variable pairs show r_s closer to 0, even though the human eye can see patterns in the data that suggest non-random relationships. For example, resistivity and P-wave velocity (r_s = -0.02) show no statistically significant correlation. This is not unexpected given the primary sensitivity of P-wave velocity to density and bulk modulus, and resistivity to moisture content and clay-content (Mreyen et al., 2021). However, overlapping non-linear relationships between certain sets of P-wave and resistivity variables are observed. This also appears to be true for the very weakly positively correlated resistivity and S-wave velocity (r_s = 0.34) and resistivity and depth (r_s = 0.35) variables. In an attempt to separate and classify these sub-relationships within the geophysical data, the unsupervised GMM algorithm is applied to the co-located model to objectively determine classifications of data based on these relationships.

4.5.3 Clustered ground model results

Two GMM outputs are assessed for producing ground models of the subsurface; one without depth constraint, in which resistivity, P- and S-wave velocity are passed to the algorithm, and another including depth constraint. The resulting classifications of the model values identify clusters of points with similar trends and ranges of measurements (Figure 4.11a and Figure 4.11c), rather than classifications based on generic reference values. Cluster 1 (blue) is characterised by lower resistivity, lower P-wave velocities and lower S-wave velocities, while cluster 2 (green) shows lower to medium resistivity values, with medium to higher P- and S-wave velocity ranges. Cluster 3 (orange) is characterised by lower to higher resistivity, lower to medium P-wave velocity and medium to higher S-wave velocities, while cluster 4 (brown) show lower to higher resistivity with low P- and S-wave velocities (see Table 4.2 for summary).

When the clusters are plotted back to their locations in the landslide subsurface, the groups form highly contiguous regions (Figure 4.11), with clusters 3 and 4 each forming two separated units at depth, likely to indicate separate lithological units, and clusters 1 and 2 forming adjacent surface regions, indicating different

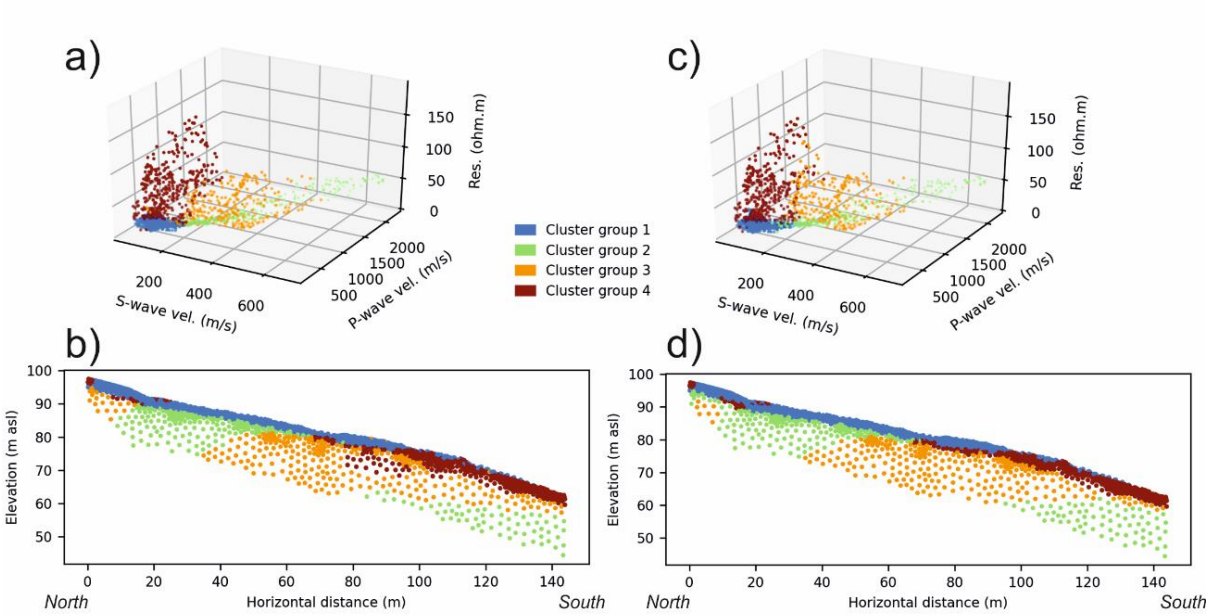

Figure 4.11: The results of the two GMM models; a) the data distribution and b) cluster ground model for the GMM with no depth constraint, and c) data distribution and d) cluster ground model for the GMM with depth constraint.

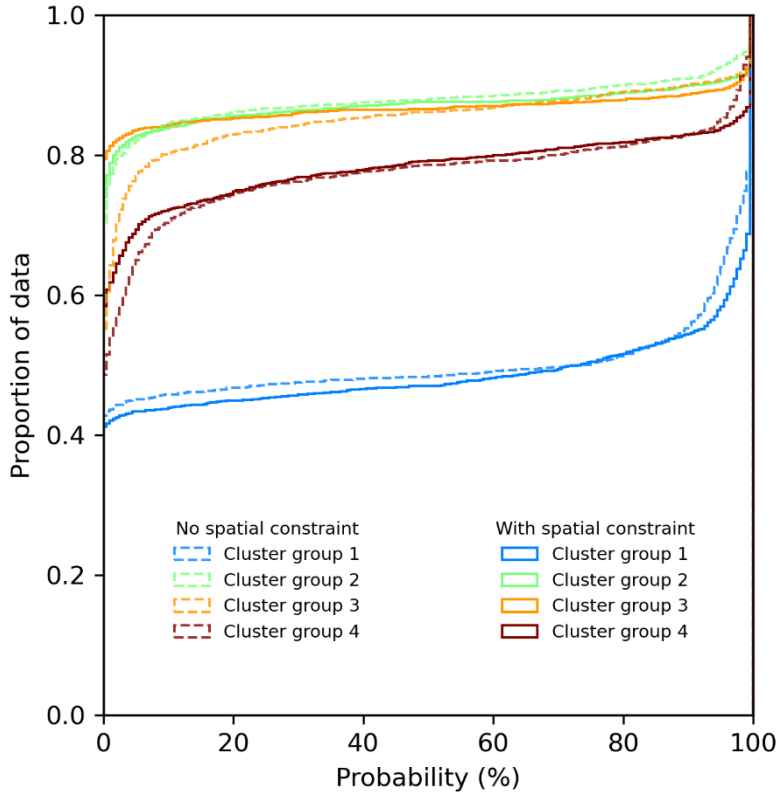

Figure 4.12: The probability of each variable in the two GMM models being assigned the correct cluster. Using depth constraint reduces uncertainty in clusters 3 and 4, at the cost of introducing marginally higher uncertainties in to the assignment of cluster 1.

Table 4.2: The properties of the cluster assignments output from the GMM.

	Resistivity (Ωm)	P-wave velocity (m/s)	S-wave velocity (m/s)	Depth (m bgl)	Interpreted lithology
Cluster 1	9 – 34 Ωm; mean = 15 Ωm	222 – 715 m/s; mean = 422 m/s	52 – 213 m/s; mean = 115 m/s	0 – 3 m	Slipped surface material (derived from Whitby Mudstone Formation)
Cluster 2	10 – 78 Ωm, mean = 27 Ωm	366 – 2220 m/s; mean = 1142 m/s	174 – 691 m/s; mean = 367 m/s	2 – 20 m	Whitby Mudstone Formation (upper slope) / Redcar Mudstone Formation (lower slope)
Cluster 3	14 – 153 Ωm; mean = 58 Ωm	432 – 1367 m/s; mean = 751 m/s	221 – 548m/s; mean = 349 m/s	3 – 18 m	Dogger Formation (upper slope) / Staithes Sandstone Formation (unsaturated, lower slope)
Cluster 4	11 – 188 Ωm; mean = 67 Ωm	206 – 676 m/s; mean = 378	56 – 323 m/s; mean = 152 m/s	0 – 5 m	Stable surface material (derived from Staithes Sandstone Formation)

states of surficial materials. The two GMM models show a similar pattern of cluster distribution; the main regions described above are present in both models, but with some areas of cluster 3 assigned to cluster 4 in the lower slope in the GMM model with no depth constraint. As the GMM algorithm assigns clusters based on probability, the probability of assignment for each point in a cluster can be used to assess the result of the model output (Figure 4.12) Using depth constraint in the GMM increases the probability of clusters 3 and 4 being assigned to the correct cluster, while the probabilities of cluster 2 remain broadly the same. There is a marginal reduction in the probability of cluster 1 being correctly assigned, but this reduction is much less than the gains made in clusters 3 and 4. Consequently, the GMM using depth constraint can be considered the more reliable of the two GMM outputs. A cross-plot correlation matrix showing the relationships between the various geophysical data variables with the cluster assignments shows the different properties of the clusters (Figure 4.13). The clusters within the cross-plot correlation matrix highlight the relationships between the different geophysical properties of the various rocks and soils present at the site, and these distributions can be used for determining potential lithology based on the ranges of values present.

4.6 Discussion

Acquiring multi-method, co-located geophysical measurements can reduce uncertainty in ground model development, as different geophysical techniques are sensitive to different properties of the subsurface. Although increasing the number of geophysical techniques can reduce uncertainty, nonetheless, a qualitative, heuristic form of comparative interpretation can be open to operator bias (Niccoli, 2014), and requires both prior knowledge of the subsurface and of the sensitivity of the geophysical method to other similar subsurface

conditions to produce a robust interpretation. In some instances, ranges of reference values may be used to aid the interpretation of geophysical data (e.g., Bichler et al., 2004). With this approach, large assumptions are made regarding the validity of measurements acquired in one setting and used to interpret geophysical models acquired from another. Additionally, the typical ranges that are presented by such reference values are usually very large and tend to overlap between material types, therefore still relying on the judgement of an operator to use effectively. Over-confidence in interpretation may produce a detailed ground model with many (unknown or undisclosed) uncertainties, whilst under-confidence in interpretation may result in a conservative ground model that does not capture the heterogeneity of the subsurface. In either case, the resulting ground model does not reflect the true heterogeneity of the subsurface and may fail to map major subsurface discontinuities. Furthermore, the process of arriving at the final ground model is unlikely to be repeatable between operators.

Therefore, rapid geophysical investigation and processing methods that can produce robust and objective results for informing ground model development are needed. Using co-located models shows that there exist relationships between geophysical variables that are more complex than can be described by simple statistics that consider the dataset as a whole. A GMM is able to identify overlapping relationships and trends in the co-located dataset, and classify data according to these distributions. The resulting ground model, created by plotting the cluster assignments to their spatial location, has identified the major subsurface discontinuities present in the subsurface identified in prior ground models of the HHLO produced from joint geotechnical and geophysical studies.

In previous studies of the HHLO, arbitrary values of geophysical measurements have been used to identify the boundary between lithological units. Chambers et al. (2011) used a resistivity value of 30 Ωm to distinguish between the clay-rich WMF and clay-deficient SSF at the site, based on visual inspection of inverted ER models. Uhlemann et al. (2016a) used rapidly increasing seismic velocity gradients to locate potential lithological boundaries between the WMF and SSF. This boundary was then later used in the processing of 3D ER surveys from the site, and was used as a boundary within the inversion process and to determine different zones of the subsurface for applying petrophysical relationships by Uhlemann et al. (2017). Similarly in the study by Whiteley et al. (2020b) considering time-lapse SR models from the HHLO, an arbitrary value from the *Vp/Vs* model (*Vp/Vs* >5) based on the judgement of the operator was used to identify the sliding layer at the HHLO. In all of these previous studies, different persons considering the inverted models may have produced different opinions or interpretations of the location of these discontinuities. That is not to say that these results are necessarily incorrect or inaccurate; the cross-section in Figure 4.1c is the result of these many studies, including information from other intrusive (Gunn et al., 2013) and remote-sensing observations (Merritt et al., 2013), and consequently uncertainties in interpretation are reduced with each additional data source incorporated. The discontinuities from this ground model have been transposed to the rapid reconnaissance ground model for comparison (Figure 4.14). The approach presented in this study provides a means of identifying these discontinuities by interrogating the relationships present in the parameter space (see Figure 4.13), rather than based on judgement alone or by incorporation of many different geophysical, geotechnical and geodetic datasets. Crucially, this approach will yield repeatable results independent of the skill and experience of the operator.

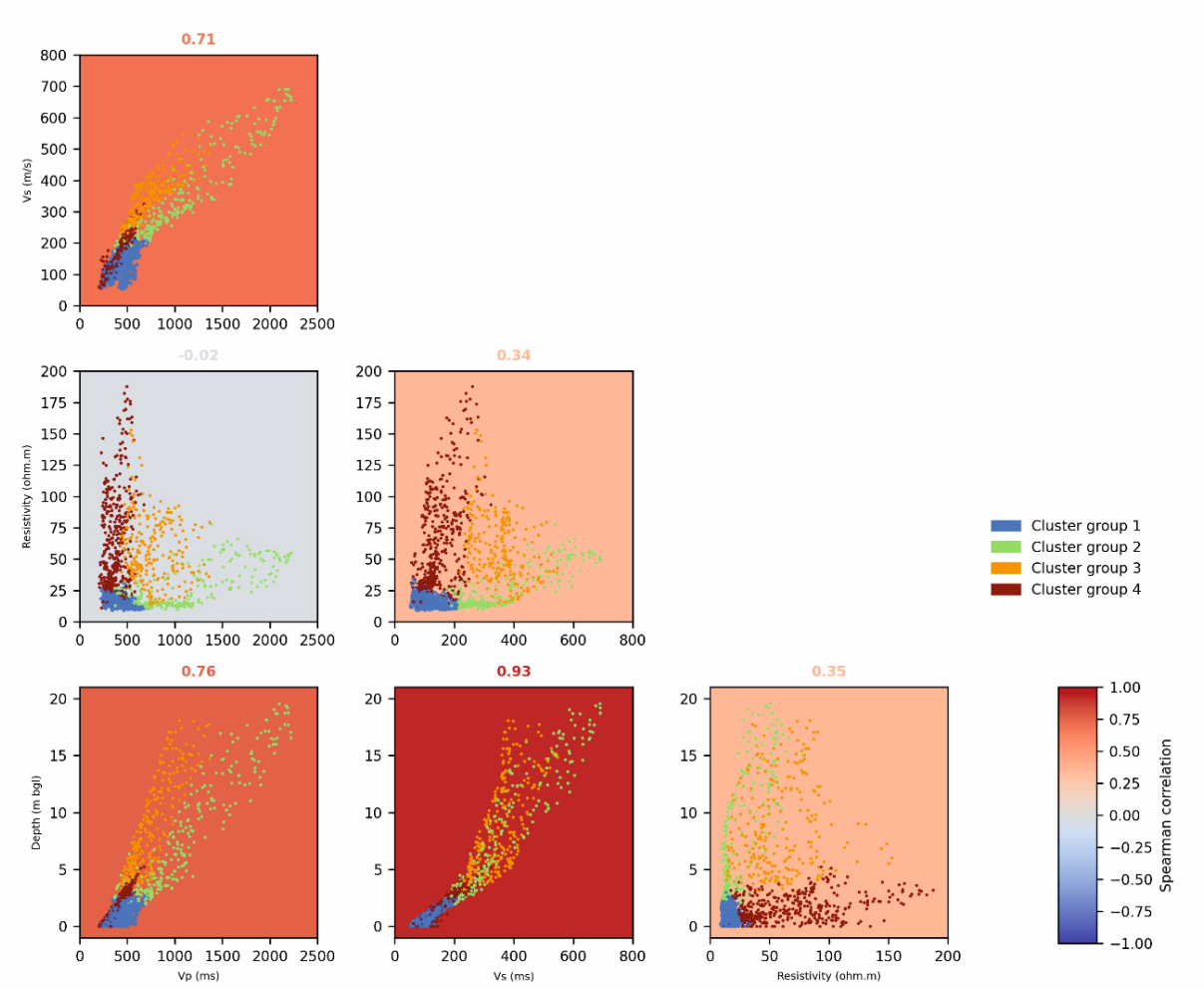

Figure 4.13: A cross-plot correlation matrix of the inverted geophysical data, showing the cluster assignments from the GMM using depth constraint.

The geophysical properties of each cluster are summarised in Table 4.2, and these geophysical properties characterise the materials of the landslide. The surface layers, cluster 1 and 4, which are located toward the mid to upper slope and lower slope respectively, share broadly similar seismic velocities (low to medium velocities) but have different resistivity ranges. The low seismic properties of both these groups indicate disturbed and unconsolidated material in this surface layer, consistent with other seismic investigations conducted by Uhlemann et al. (2016a) and Whiteley et al. (2020b). In cluster 1, which extends to ~2 m bgl from 0 m to 90 m horizontal distance before thinning out at the surface by 120 m horizontal distance, the low range of resistivity (‹25 Ωm) points to a high clay content in the surface layer (high levels of saturation in this surface layer are unlikely due to the antecedent dry conditions that preceded the survey), similar to those observed by Chambers et al. (2011) and Uhlemann et al. (2017). The underlying Whitby Mudstone Formation (WMF) located in the upper slope has a high clay content and is the primary failing unit at the HHLO, and is also the parent unit for this disturbed surface layer identified by cluster 1. Cluster 4, underlying cluster 3 from 65 m horizontal distance and outcropping at the surface from 90 m, has a much higher range of resistivity (25 to ›100 Ωm). This indicates a material with lower clay content, likely derived from the relatively sand-rich Staithes Sandstone Formation

(SSF) underlying this part of the landslide. The small zone of cluster 4 identified at the top of the slope is likely associated with the presence of highly fissured ground associated with the backscarp and rotated block in this area, with the presence of cracks leading to low seismic velocities and higher resistivity values.

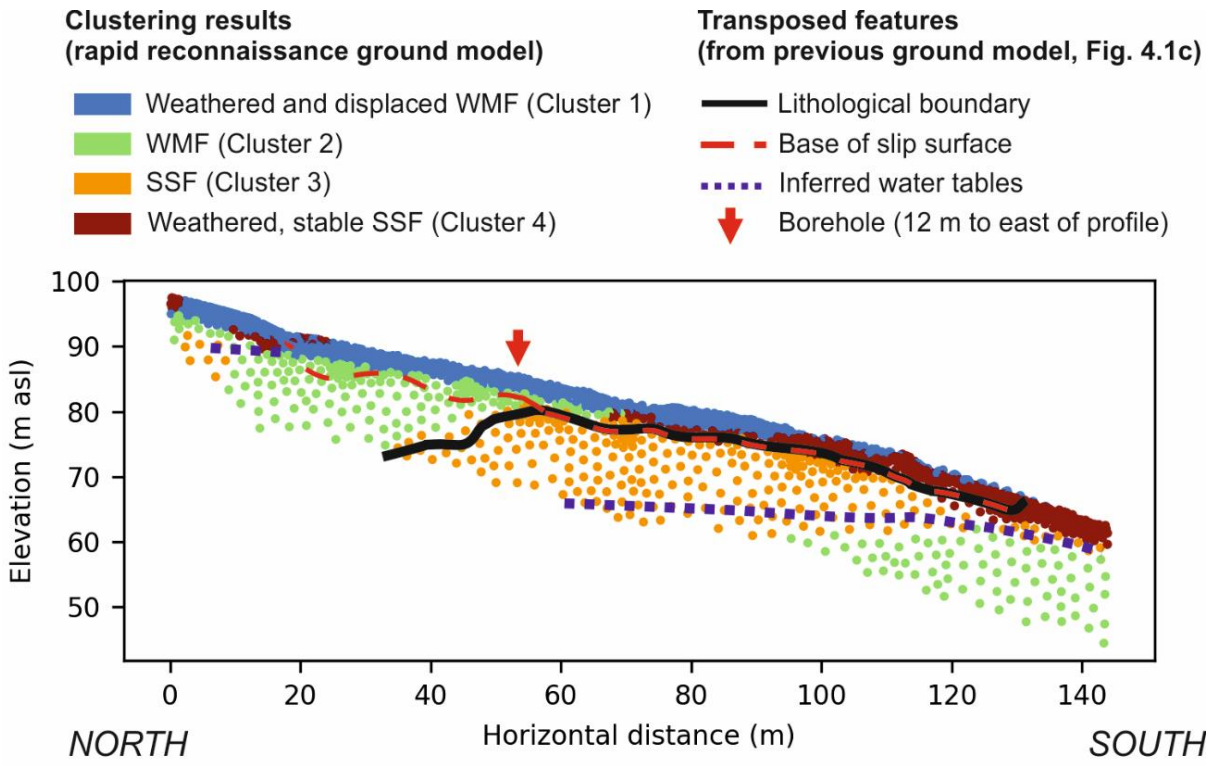

Figure 4.14: The rapid reconnaissance ground model, derived from the GMM approach described in this study, with the major boundaries from the working ground model of the Hollin Hill Landslide Observatory (Figure 4.1c) transposed to their referenced positions. The rapid reconnaissance ground model captures the broad scale heterogeneity of the landslide subsurface.

Beneath these surface layers, areas of cluster 3 (located in a small area at the top of the landslide slope from 0 – 10 m horizontal distance, and again from 45 m to the end of the survey line) and cluster 2 is intercalated in cluster 3. The seismic properties of each unit are broadly similar, showing medium to high P- and S-wave velocities, and indicating more consolidated deposits. The high range of resistivity of cluster 3 indicate a material with variable clay content and saturation regime, whereas the limited, low resistivity of cluster 2 indicates a clay-rich and saturated material. Therefore, the large zone of cluster 3 located below 2m bgl between 45 m and the end of the survey line is likely to be the SSF, which is a relatively porous and a sand-rich unit. The small area of cluster 3 located at the top of the landslide is likely a small section of DF, the sandstone and limestone unit capping the escarpment. The two zones of cluster 2 represent units of different materials but with similar properties. The upper area of cluster 2 is the WMF, as indicated by low resistivity and medium to high seismic velocities, and the lower area is most likely the RMF, a unit of clay-rich material situated within a location more prone to increased saturation at the base of the landslide, giving it similar properties to the clay-rich WMF in the upper slope.

The results of the GMM clustering can be compared with intrusive borehole data from the site, and acquired at the same time as the surveys (Figure 4.15). A borehole drilled at 52.85 m horizontal distance (and offset by 12 m to the east of the survey line) recovered a core including disturbed surface deposits, and underlying WMF and SSF materials to a depth of ~10 m bgl. The lithological transitions are identified by the changes in colour from the grey WMF to brown SSF, although the transition between these units is not well reflected by individual variations in the geophysical logs extracted from the borehole position. However, changes in the cluster profile reflect the changes from disturbed surface material (0 – 2 m bgl; cluster 1) to WMF (2 – 7.5 m bgl; cluster 2) and SSF (>7.5 m bgl; cluster 3), highlighting the use of the GMM in identifying subtle variations that may not be easily identified by individual visual inspection and comparison alone.

It is important to note that the machine learning approach presented in this study does not remove uncertainties associated with the non-uniqueness of inverted geophysical data. For this, data integration at the inversion stage is required, which requires a different and more technically demanding approach, such as the use of petrophysical joint-inversions (e.g., Mollaret et al., 2020, Wagner et al., 2019). Neither does the approach presented in this study advocate the omission of individual evaluation of inverted geophysical models; although skills and experience may vary between persons, this does not preclude expert analysis of inverted models as has been the approach taken for many decades with great success in the field of near-surface geophysics. Rather, this approach unifies the interpretation of three individually inverted geophysical models in to a single model, which is easier to understand, rapidly identifies major subsurface discontinuities, and is compiled in a more rapid and objective manner than individual comparison between models. Because of the level of detail regarding major subsurface features acquired in comparison to the many more detailed studies preceding this one, this single unified model is termed a 'rapid reconnaissance ground model'. Additionally, as the machine learning approach exploits inherent relationships within the co-located measurements, the rapid reconnaissance ground model contains lower interpretation uncertainties than that which may result from using, for example, comparison to generic reference values (e.g., Bichler et al., 2004).

4.7 Conclusions

Three sets of geophysical models are produced from electrical resistivity tomography and P- and S-wave seismic refraction tomography at a slow-moving clay-rich landslide. After data pre-processing to co-locate the surveys using topography acquired from a UAV, the geophysical data are inverted on a joint 2D mesh, producing co-located geophysical models. The variables of resistivity, P-wave velocity and S-wave velocity are cross-plotted (Figure 4.10) revealing complex trends and relationships in the data, indicating the presence of multiple contiguous geophysical zones in the subsurface.

Using an unsupervised GMM algorithm, points in the geophysical models are classified (resistivity, P-wave and S-wave velocity) as belonging to one of four clusters, with the number of groups being chosen based on statistical measurements of the data, alongside the expected lithological variations present at the site. The GMM algorithm identified four distinct areas of the landslide; a surface layer of low resistivity and low seismic velocity, thought to represent the failing Whitby Mudstone surface layer, and a second surface layer showing higher resistivity believed to be a sand-rich surface material derived from both the underlying Staithes Sandstone Formations.

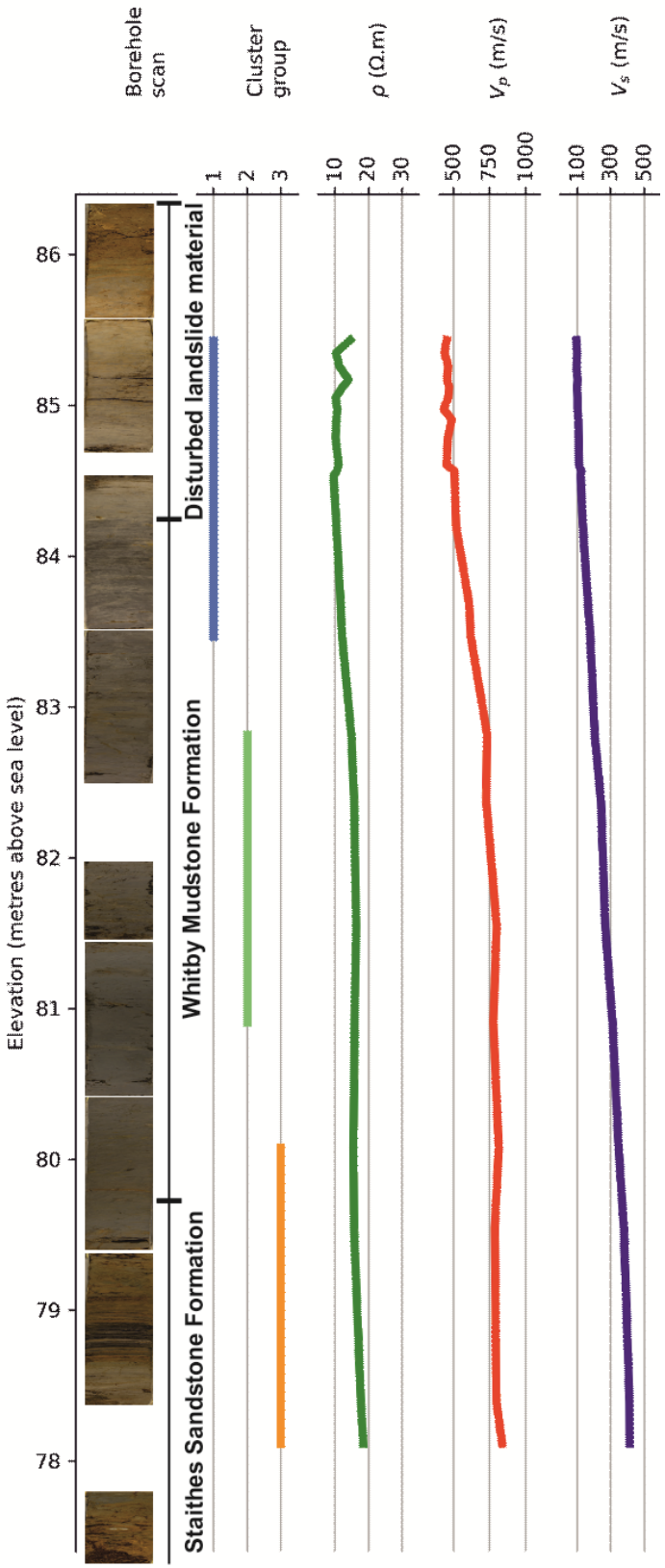

Figure 4.15: Comparison between the photographic borehole log (stretched horizontally for visibility), cluster assignments and geophysical profiles. The borehole is located approximately 12 m to the east of the geophysical survey profile.

Beneath these surface layers, the GMM algorithm identified four discrete domains comprising two clusters, indicating areas of mudstones and sandstones with similar geophysical properties in the landslide. The cluster of low resistivity and increased seismic velocities is interpreted as the underlying Whitby Mudstone formation in the mid to upper slope, and the Redcar Mudstone Formation at the bottom of the slope. Another cluster with a high resistivity range and slightly decreased seismic velocities is interpreted as the Dogger Formation at the very top of the slope, and the unsaturated Staithes Sandstone Formation in the mid-slope area.

The ground model produced by plotting these clusters back to their location within the landslide subsurface maps the major discontinuities identified in previous ground models of the HHLO constructed by qualitative and heuristic interpretations of geotechnical and geophysical data (e.g., Uhlemann et al., 2016a, Whiteley et al., 2020b). Additionally, when compared to a borehole log from near the geophysical survey line, the extracted geophysical and cluster logs show good agreement with the main lithological changes identified in the subsurface.

These types of ground models, acquired rapidly over large areas at the slope-scale using multi-geophysical survey approaches, and processed and interpreted using objective and automated methods, are a valuable tool in the rapid reconnaissance of landslide systems. Using unsupervised machine learning algorithms for these purposes is an emerging field in engineering geophysics, and one that shows much promise in overcoming the pitfalls associated with operator bias, overdependence on operator skill and interpretation, and conveying results objectively to other end users with clarity. This approach to producing rapid reconnaissance ground models gives broad stroke information about the subsurface with little prior knowledge, and can be crucial in disaster risk reduction scenarios and time-critical ground investigations, or for providing early stage design information for the establishment of slope-scale landslide early warning systems.

Acknowledgements

The authors would like to acknowledge Tiphanie Creusel, Chedtaporn Sujitapan and Russell Swift for their help with the field geophysical surveys, and Helen Smith and Steve Thorpe for operating the Dando drilling rig. The authors would also like to thank Josie Gibson, Frances Standen and James Standen for their continued support of monitoring activities at Hollin Hill. The NumPy, SciPy and pandas python libraries are used for data processing. The pyGIMLi python library is used for data inversion. Figures are produced using QGIS, the matplotlib python library and ParaView. This work was partly funded by a NERC GW4+ UK Doctoral Training Partnership Studentship (Grant NE/L002434/1) and the BGS University Funding Initiative (S337), and is presented as an output of the programme grant ACHILLES (programme grant number EP/R034575/1) funded by the UK Engineering and Physical Sciences Research Council (EPSRC). Jim Whiteley, Arnaud Watlet, Paul Wilkinson, Jimmy Boyd, Colm Jordan and Jonathan Chambers publish with the permission of the Executive Director, British Geological Survey (UKRI-NERC).

5 Synthesis

Whiteley, J. S., Watlet, A., Kendall, J. M. & Chambers, J. E. 2021b. Brief communication: The role of geophysical imaging in local landslide early warning systems. Nat. Hazards Earth Syst. Sci., 21, 3863-3871.

Declaration and author contribution

The latter part of this chapter, concerning geophysical imaging for local landslide early warning systems, is based on work that was published in *Natural Hazards and Earth System Sciences* in December 2021. Minor amendments have been made to the content to better integrate the work with the overall thesis. J. Whiteley was responsible for constructing the conceptual framework regarding the use of geophysical imaging for local landslides early warning systems, with input from A. Watlet. The original draft for publication was written by J. Whiteley. All authors were responsible for reviewing and editing. J. M. Kendall and J. Chambers were responsible for supervision.

Contributor Roles Taxonomy (CRediT) statement

Conceptualisation: J. Whiteley

Methodology: J. Whiteley, A. Watlet

Visualisation: J. Whiteley

Writing – original draft: J. Whiteley

Writing – review and editing: J. Whiteley, A. Watlet, J. Chambers, J. M. Kendall

Supervision: J. M. Kendall, J. Chambers

5.1 Introduction

This thesis concerns the characterisation and monitoring of moisture-induced landslides (i.e., landslides that are prone to destabilisation due to increased saturation). Geophysical investigation methods, both to map the subsurface of a landslide as well as monitor changes therein, have become increasingly widespread in recent years (Whiteley et al., 2019). Geophysical imaging methods produce models of the subsurface at the slope-scale, overcoming the shortcomings of diffuse data from point sensor networks and limited penetration of remote sensing methods. Hence, geophysical monitoring plays a demonstrably important role bridging the gaps in scale, resolution and coverage between these existing landslide monitoring methods for the purposes of delivering early warning of landslide failure.

Chapter 2 of this work identifies ER as an increasingly used method to monitor landslides. ER measurements are sensitive to variations in lithology (particularly the clay-content of soils and rock), porosity and moisture content (Merritt, 2014). In a monitoring context, where the lithology and porosity tend to remain the same over time, ER has proved an effective tool for imaging the movement of water through the ground in 3D, and has been used to monitor slopes at risk of moisture-induced failure (Holmes et al., 2020, Uhlemann et al., 2017). However, persistently identified shortcomings in the use of geophysics for slope monitoring include i) the impact that systematic and random errors can have on the reliability of results (Tso et al., 2017), and ii) the non-unique relationships between geophysical measurements and engineering properties of soils, giving rise to interpretative uncertainty (Fournier et al., 2013).

Despite the rise of ER as a monitoring tool for imaging the subsurface, no other geophysical imaging methods have been adapted for long-term monitoring, despite the obvious candidacy of some techniques, such as SR. Consequently, long-term geophysical monitoring studies tend to rely more heavily on data translation techniques, such as the use of petrophysical relationships, to reduce interpretative uncertainty (Holmes et al., 2022). There is therefore a demonstrable need to develop other geophysical monitoring methods for subsurface imaging to complement the advances in ER monitoring, and reduce interpretative uncertainty.

To address this need, this thesis firstly aims to develop SR as a monitoring tool to complement ER (Chapter 3). Adaptation of SR for monitoring requires consideration of novel errors and uncertainties that may arise from implementing a time-lapse SR approach. In addition to the consideration of errors and uncertainties, the sensitivity of the measurements to relevant properties of the landslide system must also be considered, and how these sensitivities complement those of the ER approach. Secondly, this thesis uses machine learning to integrate ER and SR data in a quantitative manner (Chapter 4). This approach has an emphasis on semi-automated data classification to identify geophysically similar zones within a landslide system that represent contiguous hydrogeological units.

This chapter (Chapter 5) synthesises the main findings of this thesis by identifying the interoperable concepts and results between developments in monitoring and integrated characterisation using geophysical imaging of landslides. Furthermore, this chapter considers the role of these developments within the broader context of local landslide early-warning systems (LoLEWS), and contextualises the nascent but critical role that geophysical monitoring systems play in these risk mitigations strategies.

5.2 The case for developing SR as a monitoring tool

The literature review presented in Chapter 2 identifies only two examples of landslide monitoring using active seismic methods. Of these, one uses SR (Grandjean et al., 2009), and the other uses surface waves (SW) analysis, which requires an almost identical methodological setup to SR investigations (Bièvre et al., 2012). Both studies demonstrate the suitability of seismic methods to monitor relevant properties of the landslide system. Bièvre et al. (2012) use SW measurements recorded approximately 5 months apart to investigate the role of fissuring in a clay-rich landslide. They determine from spectral ratios and amplitude analysis that the fissures were open at the time of both surveys, but that the depth of fissuring may vary between the two dates. Notably, ER monitoring identifies widespread moisture content increases associated with rainfall infiltration, but does not provide additional information on the role of fissuring. Similarly, Grandjean et al. (2009) use P-wave velocity to characterise the fissure density of a landslide subject to a simulated rainfall experiment. Reduced P-wave velocities in the surface of the landslide over the course of the experiment are associated with increases in fissuring. However, P-wave velocity does not increase with increased saturation in deeper zones of the landslide. Instead, this is detected by ER measurements, which are acquired throughout the experiment.

Both of these studies highlight the use of SR as a tool for monitoring mechanical properties of the ground, in both cases related to fissuring. Fissuring plays an important role in the hydrological – mechanical feedback of a landslide system, by creating preferential pathways for water infiltration (Krzeminska et al., 2012, Krzeminska et al., 2013, Rosone et al., 2018). Both of the studies by Grandjean et al. (2009) and Bièvre et al. (2012) note that SR is more sensitive to variations in seismic velocity caused by mechanical changes in the landslide material. In contrast, the ER measurements instead identify changes in ground moisture. These observations neatly summarise the necessity for multi-method approaches in landslide monitoring, and reiterate the importance of understanding both the hydrological and mechanical aspects of slope stability, both of which can be approximated from ER and SR measurements respectively. However, both of these studies are limited in scope when looking to understand the long-term mechanical behaviour of landslides, as both studies comprise short durations (from days to months), and employ a low number of repeated surveys.

The lack of use of SR monitoring identified in Chapter 2 cannot be assumed to point to the unsuitability of SR for understanding landslide properties. On the contrary, there are numerous examples of SR being used to provide highly relevant information on the subsurface structure and lithological properties of landslides (e.g., Imani et al., 2021, Mreyen et al., 2021, Perrone et al., 2021, Samyn et al., 2012, Tomás et al., 2018, Uhlemann et al., 2016a). In a recent review, Pazzi et al. (2019) note that SR is the third most used geophysical method to characterise landslides in both soil and rock environments; only microseismic (i.e., passive seismic) analysis, followed by ER investigations, are more prevalent. Furthermore, the number of studies identified using either of these three approaches are an order of magnitude larger than all other geophysical methods, suggesting that these methods are most successful in characterising landslides. A similar trend is observed in the review conducted in Chapter 2; passive seismic monitoring campaigns comprise 29 entries in Table A.1, followed by ER monitoring campaigns (20 entries). However, active seismic methods (SR and SW) have only two entries, which comprise the studies by Grandjean et al. (2009) and Bièvre et al. (2012) outlined above. Furthermore, almost all of the

passive seismic studies and nearly half of the ER monitoring campaigns were deployed for long-term monitoring purposes. The two active seismic studies comprised a controlled test lasting 2.5 of days (Grandjean et al., 2009), and a monitoring campaign of two surveys spaced 5 months apart (Bièvre et al., 2012), neither of which were designed to capture long-term variations in landslide properties. Therefore, it would seem that the limited number of case studies identified in Chapter 2 both i) using SR as a monitoring tool, and ii) in a long-term monitoring context, is driven by lack of development of SR as a monitoring tool rather than unsuitability of the approach to provide useful monitoring information.

5.3 Developing SR for characterisation and monitoring of the HHLO

5.3.1 Identifying and minimising errors in SR

The underuse of SR as a landslide monitoring tool is related to practical difficulties in obtaining reliable time-lapse measurements due to the unique sources of random error that need to be considered. These include previously known sources of random error associated with SR surveying (Dangeard et al., 2018, Khalaf et al., 2018), but also novel random errors specifically related to monitoring landslides which tend to have dynamic surfaces. These errors are identified and explored in Chapter 3. Table 3.1 details these potential sources of systematic and random errors, and identifies them as falling in to one of three stages of the SR monitoring approach: i) data acquisition, ii) data processing and iii) data inversion. The potential sources of error identified in Table 3.1 are unique to the use of SR as a monitoring tool. However, many are closely related to more general and previously known sources of errors when SR is used in a characterisation capacity (see Table 1.2). These include obtaining correct locations of receivers, appropriate survey design to achieve sufficient coverage, inconsistent picking of first arrivals, error modelling in the inversion process, and using appropriate constraints for data inversion.

Chapter 3 places a large emphasis on assessing and minimising random errors arising in the data acquisition stage. This is because the challenges faced in the data processing and data inversion stages of SR monitoring share similar challenges to non-landslide applications (Blazevic et al., 2020, Dangeard et al., 2021). The unique aspect of this thesis is the application of this approach to monitoring a dynamic landslide. In addition, random errors generated in the data acquisition stages are some of the most fundamental, and yet potentially overlooked, aspects of geophysical surveying (Maurer et al., 2010).

A major question addressed by implementing SR as a monitoring tool was; what role do the topographic changes of an active landslide surface have on the modelled velocities of the time-lapse models? To explore this, the data were inverted using a static inversion mesh (i.e., no topographic change included across the monitoring period). When compared to the time-series incorporating topographic changes, 23% of the data points in the time-series showed velocities with variations of more than ±10% of the true velocity (Figure 3.8). This is a significant finding, for two reasons: firstly, it demonstrates the impact that error can have in creating uncertainty; by assuming no topographic changes across the monitoring period, only 77% of the data can be considered 'reliable' if a ±10% error margin is accepted. Secondly, the variation of these measurements, which is greater than ±10% of the true velocity, is within the range of naturally varying bulk velocities of the sliding layer at the HHLO. The average bulk P-wave

velocity for the siding layer is 411 m/s across the 16 inverted time-steps; ten of these time-steps showed variation in P-wave velocity of less than ±10% of this average (Figure 3.8). By not incorporating the topographic movements from the landslide surface, it is likely that the true variation in velocity of the sliding layer could be smaller than the errors introduced.

In addition to identifying best practice (i.e., incorporating topographic variations across the time-series) to minimise errors introduced to the processing stage, two novel approaches to incorporating and reducing errors are developed in this thesis: i) using reciprocal SR measurements to estimate dataset error, and ii) using a two-stage inversion process to provide a reference model for time-lapse SR inversion. The first of these adopts the use of reciprocal measurements as a means of estimating the errors of measurements within a dataset for the inversion stage (Binley et al., 1995, Mwakanyamale et al., 2012). Estimating individual measurement errors plays a crucial role in data weighting during inversion (Tso et al., 2017). Although reciprocal measurements in SR are not typically available for every field measurement, even using the subset of measurements that have reciprocals can improve estimations of error. In the P-wave survey presented in Chapter 4, 17.4% of the total dataset had reciprocal measurements, and in the S-wave survey, this was 22.4%. The resulting error model developed from binning the SR reciprocal measurements and fitting an error model to these bins (Figure 4.4) shows significant improvement over using unbinned data for estimating the errors, or by assuming an arbitrary level of error in the data, as is often used in SR processing (Rücker et al., 2017). Using reciprocal measurements to estimate errors is also used for the entire SR time-series presented in Chapter 3.

The second approach developed in this thesis to reduce errors, this time specifically for time-lapse SR, is the novel methodology to constrain the inversion for time-lapse SR data (Figure 3.3) presented in Chapter 3. At the time of the study, there were no time-lapse SR inversion codes available, a further indication of the lack of development of SR as a monitoring tool. Hence, Chapter 3 develops a two-stage inversion approach, in which all of the time-steps are inverted individually, and the 'best' model, assessed using model error (i.e., RMS error) and closeness of fit (i.e., $\boldsymbol{\chi^2}$), This model is then used as the reference model against which the entire time-series could be inverted. This approach tended to reduce the model errors and improve the data fitting in the final inverted model (Table 3.3).

5.3.2 Investigating the structure and processes of the HHLO using SR

The resulting time-series of seismic velocities, and in particular the V_p/V_s ratio of the sliding layer at the HHLO, provide an important insight in to the behaviour of the clay-rich WMF. Although Uhlemann et al. (2017) identify a link between increases in moisture content and occurrences of failure at the HHLO, they infer, rather than observe, a change in the mechanical state of the WMF. In Chapter 3, a time-series of V_p/V_s ratio from the sliding layer at the HHLO is produced (Figure 3.8). The V_p/V_s ratio is a measurement of the ratio of longitudinal to transverse strain, and indicates the degree of deformation experienced by a material (Raharjo et al., 2016). This therefore provides evidence that the mechanical state of the WMF changes because of increased moisture content. Furthermore, this change is observed at the unit-scale, indicating that the entirety of the shallow outcrop of WMF at the HHLO may be at risk of moisture-induced strain-softening and failure.

In addition to contributing to the understanding of failure processes at the HHLO, the time-series SR results provide fresh insight in to the structure of the landslide. By considering the variation in standard deviation of V_p, V_s and the V_p/V_s ratio over the entire time-series (Figure 3.7), the distinct lithological units at the HHLO are identified more clearly than if a single survey is considered (Figure 4.8). In terms of reducing the uncertainty in characterising units using SR velocities, considering how the velocity of a unit changes over time may be a better identifier of the lithology and engineering properties than identifying the bulk velocity of a unit at a single point in time. However, this long-term approach is impractical when looking to map subsurface structures rapidly and objectively, and so for these applications, others means of reducing uncertainty are required.

5.3.3 Reducing interpretative uncertainty through multi-method integration

The methodology developed in Chapter 3 deals with reducing the uncertainty of SR monitoring results by addressing potential sources of error arising in data acquisition and data inversion. However, the resulting models still contain uncertainty related to the sensitivity of SR measurements to variations in the engineering properties of soils and rocks. Comparison with other data, such as rainfall and soil moisture, highlight the link between variations in the hydrological system and changes in seismic velocity (Figure 3.8). However, there remains uncertainty regarding how the spatial variations in seismic velocity relate to landslide structure, and the non-unique relationships between seismic velocities and material properties. Hence, Chapter 4 adopts the widely used practice of reducing interpretative uncertainty through the use of multiple geophysical methods (Pazzi et al., 2019). In particular, the study in Chapter 4 leverages the complementarity of SR and ER measurements to assess mechanical and hydrological properties respectively (e.g., Bièvre et al., 2012, Bièvre et al., 2021, Grandjean et al., 2009, Imani et al., 2021, Mreyen et al., 2021, Perrone et al., 2021).

However, Chapter 4 also aims at addressing a further source of uncertainty arising from interpretative bias. Bias in geophysical interpretation typically arises from the process of knowledge-driven (i.e., heuristic) modelling, which heavily relies on expert opinion (Burkin et al., 2019). For example interpreting the structures and discontinuities in seismic velocities to produce an interpretative model of geological structure and lithology relies on expert opinion (e.g., Uhlemann et al., 2016a). In the hands of a different operator, the resulting model may have different positions of boundaries, or identification of material types. These biases can be related to a number of factors, including operator assumptions of uncertainty and confidence (Rowbotham et al., 2010), how data are presented (Alcalde et al., 2017) and what previous information is available to inform the current interpretation (Mulargia, 2001). These biases ultimately affect the reproducibility of an interpretative model; in an ideal scenario, the same model would be produced independent of the operator. There is therefore a need to identify approaches that can aid in increasing the reproducibility of geophysical interpretation (Church et al., 2020).

Chapter 4 therefore looks to machine learning as a means of integrating SR and ER with reproducible results. The type of machine learning algorithm used, the Gaussian Mixture Model (GMM), is a probabilistic unsupervised algorithm, which classifies points in a dataset as belonging to one of a number of modelled Gaussian distributions in the dataset, known as clusters. The resulting 'rapid reconnaissance ground model' derived from applying the GMM to the SR and ER data (Figure 4.14) significantly reduces uncertainty in identifying boundaries between discontinuous units at the HHLO. This reduction in uncertainty arises from i) the

integration of the ER and SR data (Figure 4.11), and ii) the probabilistic information provided on cluster assignment which is itself a measure of uncertainty of the approach (Figure 4.12).

The rapid reconnaissance ground model highlights the same landslide structure as identified in the variation of standard deviation in velocity plots presented in Chapter 3 (Figure 3.7). In turn, both of these results are confirmed by conceptual models produced by past studies at the HHLO using geophysical and geotechnical data (Gunn et al., 2013, Uhlemann et al., 2016a). The rapid reconnaissance ground model is validated against past studies, comparison with long-term SR results (Figure 3.7) and available intrusive information from the survey (Figure 4.15). This indicates that a multi-method geophysical approach using machine learning to produce repeatable results provides rapid results with lower uncertainties than other single-method approaches used at the HHLO.

5.3.4 Future monitoring of landslide processes at the HHLO with SR

The focus on minimising errors in SR monitoring in Chapter 3, and the integration of data using reproducible interpretation methods in Chapter 4 lay the groundwork for deploying ER and SR as long-term monitoring tool at the HHLO. It is clear from the results of Chapter 3 that there is utility in using SR to monitor moisture-induced changes in the elastic properties of landslide materials. In the absence of complementary geophysical data, the bulk V_p/V_s ratio of the sliding layer at the HHLO shows close relationships with ground moisture, highlighting the influence of moisture dynamics on the mechanical properties of the WMF. The importance of understanding ground moisture for accurate prediction and warning of landslide failure cannot be understated. Pecoraro et al. (2019) identified that the most commonly monitored parameter in slope-scale landslide early warning systems is rainfall (20 instances), although when taken as a whole, separate indicators of deformation (including displacement, velocity, acoustic emission, cracking, acceleration and strains) are more common (38 instances). However, monitoring deformation and/or rainfall alone can be problematic. Landslides may have already moved toward a critical state of failure at the point deformation becomes measurable, significantly reducing lead times from warning to failure. Additionally, using rainfall as a monitoring parameter at the slope-scale is subject to the same assumptions and simplifications as when used at the regional-scale (Guzzetti et al., 2020), particularly when considering the role of infiltration. Subsequently, in an early warning context, false alarms from using rainfall thresholds alone are high (Marino et al., 2020).

Recently, measurements of ground moisture have been proposed as inputs for establishing intensity-duration thresholds based on physical properties of soils and rocks, rather than using duration of rainfall or a measure of antecedent or accumulated rainfall (Bogaard and Greco, 2018). In this approach, moisture measurements (or approximations thereof) are most commonly acquired using local sensors or remote sensing (Marino et al., 2020). However, networks of sensors provide diffuse measurements when considered across the scale of the landslide system, and satellite-derived measurements provide only very shallow, or low spatial resolution measurements of ground moisture. Neither approach alone provides the information required to consider the effects of ground moisture across different scales and coverage (Bogaard and Greco, 2016). ER monitoring, as identified in Chapter 2, provides as means of monitoring precursory ground moisture conditions without the spatial limitations of sensor networks or depth limitations of remote sensing. However, to understand fully how these changes in

moisture affect the mechanical behaviour of a soil or rock, SR should be considered as a complementary tool to understand the impact that hydrology has on mechanics.

The integration and interpretation approaches developed in Chapter 4 can be applied to time-series data (e.g., Delforge et al., 2021, Whiteley et al., 2020a). Implementation of a clustering approach, even on long-term single method data such as SR alone, would provide a means of assessing the probability of data point assignment to a given cluster (e.g., Figure 4.12). From here, it would be possible to assess in a more quantitative manner any improvement that introducing further geophysical methods could deliver. Given that considering the variation of standard deviation of velocities over time (Figure 3.7) provides higher certainty in subsurface structure than considering standalone survey results (Figure 4.8), implementing a time-series clustering approach should make structural contrasts more readily identifiable with lower uncertainty. This will allow for improved discretisation of the subsurface for assessing the time-varying bulk properties of individual units. For example, the identification of the sliding layer in Chapter 3 was derived from qualitatively assessing P- and S-wave velocities, and using best judgement regarding the threshold at which the material could be considered 'displaced', along with knowledge of the depth of the sliding layer form past studies (Uhlemann et al., 2016a). However, a more objective assessment of the thickness of the sliding layer are obtained from the machine learning approach used in Chapter 4 (Figure 4.15). Incorporating time-series data would make the identification of the sliding layer less uncertain given the variation of geophysical properties within this layer over time (Figure 3.8).

The GMM algorithm could be applied to time-lapse monitoring data, clustering all data in a time-series in the same manner described in Chapter 4. The hyperparameters of the algorithm, of which the most important is being the expected number of clusters, depends on spatial, rather than temporal, a priori information. For this reason, the clustering approach is useful for identifying the spatial extents of units at the HHLO. The location of the boundaries between these units are unlikely to change over time. This is due to the range of geophysical values for each cluster group being highly distinct (Table 4.2). Additionally, as identified in Chapter 3, variations in seismic velocity associated with ground moisture can be <±10%. Hence, points are unlikely to be re-assigned to different cluster groups because the expected range in temporal variations of the distinct groups is small compared to the absolute mean values of each unit (Table 4.2).

However, automatically classifying units through clustering provides a means of segmenting the landslide subsurface for time-lapse analysis of individual lithological units. Using a clustered cross-plot matrix (Figure 4.13), individual relationships can be identified within the units identified at the HHLO. Producing these plots for each time-step in a monitoring campaign would provide an understanding of how ground moisture is affecting both SR and ER measurements simultaneously and at the slope-scale. Given the sensitivity of ER and SR measurements to hydrological and mechanical properties respectively, it may even by possible to determine thresholds based on the geophysical measurements at which failure conditions of the landslide are reached.

However, a further step to integration of these data with LoLEWS would be the application of petrophysical relationships. Currently, relationships between resistivity and moisture content have been established for the HHLO (Merritt et al., 2016, Uhlemann et al., 2017) using Waxman-Smits modelling (Waxman and Smits, 1968). Exploring the use of laboratory measurements of seismic velocities and the shear strength of materials from the HHLO would provide an interesting avenue of future research stemming from this thesis.

5.4 The role of geophysical imaging in local landslide early warning systems

This part of the synthesis will consider the wider context of how the concepts discussed and developed in this work can contribute to providing practicable early warning of failure at the slope-scale. Focusing on the concepts of geophysical characterisation and monitoring of landslides, Figure 5.1 presents a conceptual framework that highlights the role that geophysical imaging (supported by field and laboratory measurements) can play in establishing LoLEWS for landslides triggered by increases in ground moisture conditions. This framework uses a modified version of that proposed by Intrieri et al. (2013) for establishing generic LEWS.

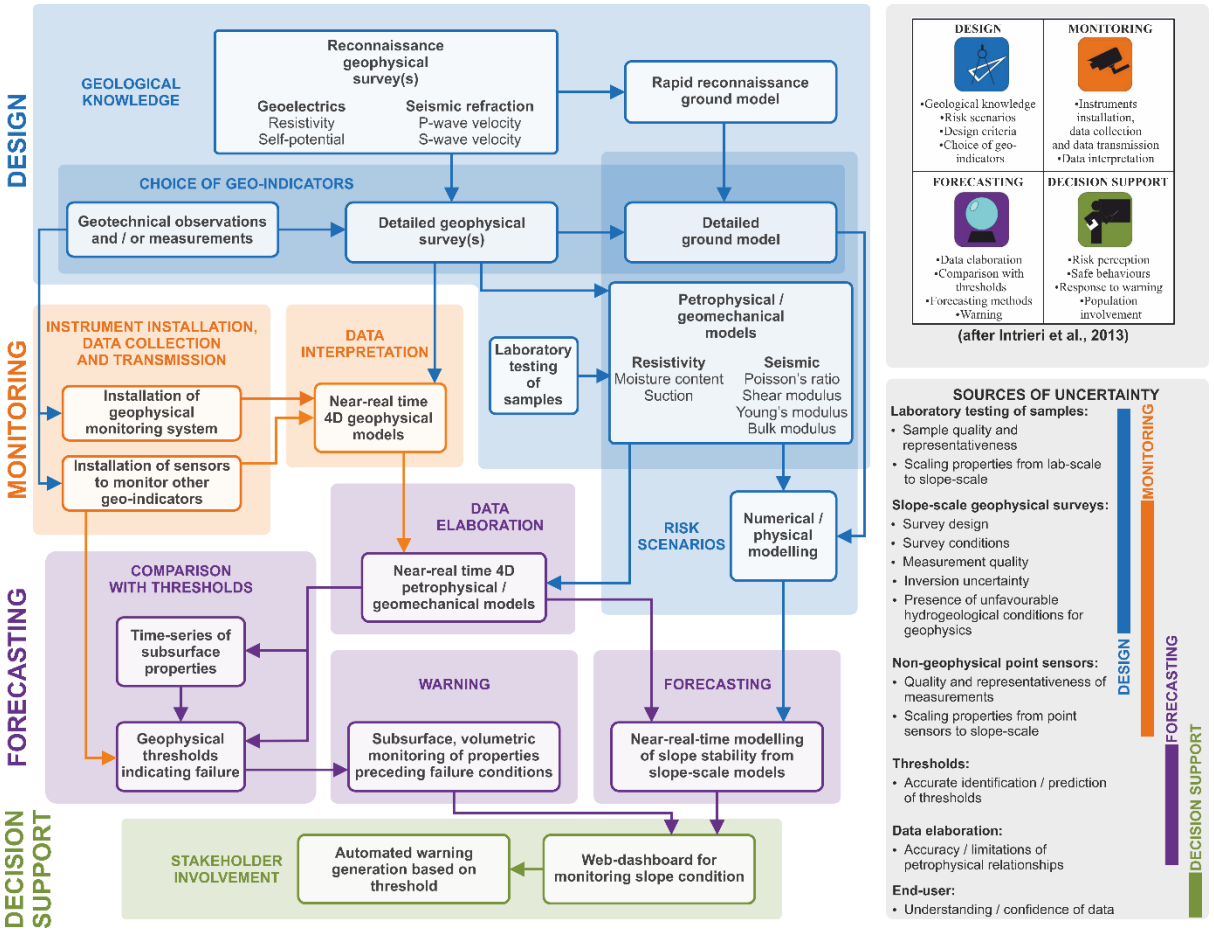

Figure 5.1: A conceptual framework highlighting the role that geophysics can play in the establishment and operation of local landslide early warning systems.

The following sections provide a brief description and summary of the major contributions that geophysical imaging can make to the components (and sub-components) of LoLEWS presented in Figure 5.1, which include design (geological knowledge, risk scenarios, design criteria, choice of geo-indicators), monitoring (instruments installation, data collection, data transmission, data interpretation), forecasting (data elaboration, comparison with thresholds, forecasting methods, warning) and decision support (risk perception, safe behaviours, response

to warning, stakeholder involvement) (Intrieri et al., 2013). The conceptual framework (Figure 5.1) also indicates some of the sources of uncertainty that may arise from the inclusion of geophysical data and geophysically supported geotechnical measurements in LoLEWS.

5.4.1 Geophysical imaging in LoLEWS

Geophysical imaging, particularly geoelectrical and seismic tomographic methods, can conceptually contribute to establishing LoLEWS, with particular benefits to the design and monitoring components due to their ability to characterise and monitor slopes at high spatial resolutions. However, the imaging and visualisations provided by geophysics (in comparison to single point measurements from sensors or from surface-only observations) and their ability to be calibrated with laboratory geotechnical measurements bring benefits to other components of slope monitoring activities downstream, including forecasting and decision support. In the conceptual framework (Figure 5.1), information from any downstream stage can be used to refine information gathered in upstream stages. For example, monitoring data may provide useful information to be incorporated in a detailed ground model of the landslide.

The framework also highlights the major sources of potential uncertainty that require consideration, including (i) laboratory testing of samples (e.g. quality of samples and how well samples reflect the heterogeneity of a geological formation) and issues scaling laboratory measurements to the slope scale; (ii) geophysical surveys, including the design of the survey (e.g. equipment used, data coverage and data resolution), the survey conditions (e.g. signal-to-noise ratio impacting measurement quality), uncertainties surrounding the inversion process (e.g. model sensitivity, non- uniqueness, fitting of geophysical models to measured data or the sensitivity of the inversion to regularisation constraints) and the presence of unfavourable conditions for geophysical surveying (e.g. buried low-velocity or high-conductivity zones inhibiting accurate seismic and geoelectrical measurements, respectively); (iii) the accuracy, precision and representativeness of non-geophysical point sensors used to supplement geophysical monitoring systems and issues surrounding scaling localised point-sensor measurements to the slope scale; (iv) the identification of geophysical thresholds at which critical slope conditions are reached; (v) the limitations, particularly in the ranges of co-sensitivity, of petrophysical relationships; and (vi) the confidence of end users to incorporate sources of geophysical data into decision making processes surrounding slope-scale early warning. In the following sections, the emerging opportunities for integrating geophysical imaging into LoLEWS are explored by summarising the contributions to the components in the framework (Figure 5.1).

5.4.2 Design

5.4.2.1 Geological knowledge

Characterising the geological setting and identifying precursory conditions to landslide failure is an important initial step in establishing LoLEWS (Intrieri et al., 2013). Geophysical imaging can help inform this stage by contributing to a spatially complete geoscientific understanding of the subsurface in terms of the geological

setting, hydrological regime and geomorphological indicators of slope displacement. Characterisation and monitoring using geophysical imaging have a demonstrably important role in establishing LoLEWS owing to high-resolution spatiotemporal subsurface data acquisition and the sensitivity of different methods to properties and processes that form and destabilise vulnerable slopes, respectively (Whiteley et al., 2019). Geophysical measurements can be made at a range of depths and resolutions depending on financial and temporal constraints and study scope. The resolution of geophysical measurements made at the ground surface decrease with depth. Reconnaissance surveys, where measurements are acquired rapidly and at large measurement separations, offer low-resolution data giving a broad overview of subsurface variations. Chapter 4 presents an example of a reconnaissance survey, the results of which may guide the design of more detailed follow-up geophysical surveys or may inform the design of additional intrusive investigations.

5.4.2.2 Risk scenarios

Geophysical data are well placed to offer slope-scale inputs for a range of qualitative (e.g. conceptual site model) and quantitative (e.g. analytical and numerical) modelling approaches. Quantitative analyses of slope failures using physical- or process-based approaches are often required to model modes of failure, estimate potential mobilised volumes, predict landslide runout length and determine slope factor of safety, all of which will have a large effect on a given risk scenario. To mathematically model the stability of a slope, van Asch et al. (2007a) identified five key features on which information is required:

- geometry (including topography), which can be obtained during geophysical survey deployment;
- geomorphology, identified by geophysical variations indicating the presence of structural variations (e.g. slip surface(s), emplaced slipped material, surface fissures);
- kinematics, such as landslide displacement rate and its controlling factors, which can be ascertained from geophysical monitoring;
- geotechnics, where additional data from laboratory testing and the determination of petrophysical relationships (i.e. the estimation of a property such as porosity, density or moisture content from a proxy geophysical measurement) can provide appropriately discretised slope-scale geotechnical models (e.g. Uhlemann et al., 2017); and
- geomechanics, which can be determined using outputs from the above step.

All of these types of models can be produced on discretised subsurface meshes (e.g., Figure 3.7), which can form inputs to the quantitative monitoring of landslides.

5.4.2.3 Choice of geo-indicators

Commonly in LoLEWS, information on the environmental factors influencing or indicating displacement (or "geoindicators") is gathered from the installation of surface or subsurface sensors installed in the landslide (e.g., Figure 3.8). Geophysical models can be calibrated to a particular site condition (i.e. through petrophysical relationships, joint inversion or comparison with thresholds), after which the local condition measured at a

sensor (or across a network of sensors) can be extrapolated and interpolated across a wide area at high-resolution. It is recommended that measurement of one or several of a range of geo-indicators is made using associated instrumentation (Intrieri et al., 2013). This includes the direct use of geophysical measurements (in particular, geoelectrical measurements) as a geo-indicator of potential failure. The use of appropriate data elaboration techniques, typically linking geophysical and geotechnical measurements through laboratory-based petrophysical relationship development, can convert other geophysical measurements to proxies for several other geo-indicators (e.g. seismic velocity to elastic moduli).

5.4.3 Monitoring

5.4.3.1 Instruments installation, data collection and data transmission

Geophysical monitoring applied to unstable slopes has advanced significantly in recent decades (Whiteley et al., 2019). ER monitoring is one of the most developed geophysical methods for integrating into LoLEWS; however, recent developments in seismic acquisition systems, such as the use of nodal arrays of seismic sensors or distributed acoustic sensing (DAS) systems are becoming increasingly prevalent. Chapter 3 presents an example of a long-term SR monitoring campaign to monitor landslide processes. Several bespoke resistivity imaging systems have been developed for long-term deployment to unstable slopes, including ALERT (Kuras et al., 2009), GEOMON (Supper et al., 2014) and PRIME (Holmes et al., 2020) amongst others. In order to be suitable for slope monitoring, these systems have overcome several challenges, including the provision of off-grid power, the ability to automatically acquire scheduled measurements and the inclusion of telemetry for near-real-time transmission of data. For example, the PRIME resistivity monitoring system includes all of these elements, lending itself to integration with new and existing LoLEWS. The low-cost modular and robust construction of monitoring systems such as PRIME, combined with their low power consumption and optimised acquisition and data telemetry schedules, makes them adaptable for installing in harsh environments and difficult terrain, for example, where access may only be possible on foot (see Holmes et al., 2020; Whiteley et al., 2019, and references therein).

5.4.3.2 Data interpretation

Geophysical models require some specialist knowledge to interpret and are often interpreted with a degree of uncertainty, but integrating multiple data streams (e.g. other geophysical methods, geotechnical observations and remotely sensed deformation data) increases the accuracy of the interpretation and reduces uncertainties (Whiteley et al., 2021c). An example of quantitative data integration using machine learning is presented in Chapter 4.

Error and uncertainty can be ameliorated further with the use of petrophysical relationships (Merritt et al., 2016, Uhlemann et al., 2017). With this elaboration of geophysical data, each cell within the geophysical model can emulate the function of a geotechnical sensor, giving localised information on subsurface properties and, in the case of geophysical monitoring data, time-series point information. As such, geophysical time-series data from individual model cells (emulating point-source sensors), collections of model cells with similar properties

(emulating geomorphological-scale features) or the entire model itself (considering the entire slope) can be incorporated with other sources of information collected at similar scales to identify thresholds at which failures may occur.

5.4.4 Forecasting

5.4.4.1 Data elaboration

A powerful approach to elaborating geophysical images is to link geophysical and geotechnical measurements in a quantitative manner with petrophysical relationships. Examples of this include Archie's equation (Archie, 1942) (Archie, 1942) to determine porosity and saturation in clay-free rocks and soils or the Waxman–Smits model for clay-rich material (Waxman and Smits, 1968) to translate resistivity measurements to gravimetric moisture content (Uhlemann et al., 2017). Other translations of resistivity include the use of relationships between the soil water potential, saturation and geoelectrical properties (Fredlund and Xing, 1994, Vanapalli et al., 1996) of a material to ultimately derive unsaturated shear strength from field resistivity measurements (Crawford and Bryson, 2018). Similar approaches can be applied to seismic data, where estimations of density either from field observations or through laboratory measurements can be combined with seismic velocity models to derive field-scale measurements of elastic moduli including bulk modulus, shear modulus, Young's modulus and Poisson's ratio (Uhlemann et al., 2016a). Alternatively, shear-strength and shear-wave velocity can be measured in the laboratory (e.g. using direct simple shear testing and bender element measurements) or in the field (e.g. using shear vanes and field seismic measurements) to derive a relationship between the two properties (Trafford and Long, 2020). Petrophysical joint inversion, where two geophysical datasets are inverted together to provide quantitative estimations of subsurface properties, is also possible when considering multiple co-located geophysical datasets, although this approach does not remove the need for non-geophysical observations to resolve some ambiguities arising in the resulting models (Wagner et al., 2019).

5.4.4.2 Comparison with thresholds and forecasting methods

Recently there has been a recognition that the use of subsurface data for establishing thresholds may improve LoLEWS due to the effects of surface runoff, evapotranspiration, preferential flow and heterogeneous soil properties. For example, remotely sensed near-surface ground moisture data may reduce the number of false alarms in LoLEWS compared to when only rainfall thresholds are used (Marino et al., 2020)Ma. Additionally, measurements of ground moisture content and/or deficit are increasingly being recognised by engineers as potential indicators of slope failure. Geophysical imaging, particularly when translated to geotechnical or geomechanical models through petrophysical relationships, provides the opportunity to incorporate data at a range of scales and positions within the subsurface of a slope, for example, from installed geotechnical sensors. Similarly, time-series geophysical monitoring data can provide inputs for machine learning algorithms used in the nowcasting and forecasting of potential landslide failures.

5.4.5 Decision support

Using geophysical results for conveying complex spatial and temporal information is apt due to the scales and dimensions of the results in relation to the scale of unstable slopes. Geophysical data can easily be incorporated into 3D visualisation environments, where it can be displayed and manipulated alongside other sources of data in the development of integrated ground models (Whiteley et al., 2021c). An example of this is presented in Chapter 4. Furthermore, providing differential time-lapse images or time series of sub-sections of modelled data can be an important step in translating the information from the technical to nontechnical domain and form part of the visual basis for identifying slope instabilities or issuing warnings.

5.4.6 The future of geophysics for LoLEWS

The continued integration of geophysical imaging approaches into LoLEWS will be driven by developments in four areas: (i) further research into the petrophysical relationships between geophysical and geotechnical properties (in particular seismic velocity–stress state relationships) with improved consideration of uncertainty propagation through LoLEWS and with a view to providing inputs to geophysical–geotechnical models of slope stability; (ii) the maturation of technologies that allow the acquisition of passively acquired seismic data from fibre optic cables and large-*n* sensor arrays that can be deployed at the same spatial resolution as resistivity-monitoring arrays; (iii) the continued development of increasingly robust, low-power and low-cost geophysical systems for deployment to vulnerable slopes; (iv) research into the automation of data processing, modelling and interpretation in order to streamline the ever increasing volumes of data being acquired from monitoring systems. In addition, the establishment of a network of geophysically supported LoLEWS within a catchment (or multi-catchment region) can also feed information into TeLEWS, improving early warning at the larger scale. In this case, individual LoLEWS would be analogous to a network of sensors deployed within a single slope, each reporting the condition of their local area to establish a broader picture of landslide susceptibility based on near-real-time, slope-scale data.

Identifying appropriate slopes and research collaborators for the deployment of geophysics-supported LoLEWS is partly an issue of outreach but one that is addressed through the establishment of interdisciplinary organisations such as the recently established LandAware: the international network on LEWS (Calvello et al., 2020). Additionally, the work undertaken at natural observatory sites, such as the Hollin Hill Landslide Observatory (HHLO), has established proof-of-concept geophysics-supported slope-scale early warning. This provides a blueprint for establishing similar monitoring approaches more rapidly at future sites, streamlining the application of geophysics for LoLEWS (Holmes et al., 2020). Additionally, resource availability may limit the investment into establishing all the aspects of geophysics for LoLEWS, in which case the HHLO case study provides a useful reference for which components may be suited to other sites with specific and unique requirements. It is clear that, as observed in currently operating LoLEWS, an interdisciplinary approach is necessary in order to understand, integrate and exploit the many data streams feeding into a monitoring system. Furthermore, research in the field of geophysical monitoring can benefit from developments in other areas of study, e.g. machine learning, equipment manufacturing, signal processing and smart sensor networks.

Acknowledgements

The authors would like to thank Paul Wilkinson from the British Geological Survey for his comments on this work. This work is part of the "Multi-observational data for linked modelling methodology development" activity of the NERC-funded Enhancing Resilience to Landslide Hazard project (NEE7680S). Jim Whiteley, Arnaud Watlet and Jonathan Chambers publish with the permission of the executive director of the British Geological Survey (UKRI-NERC). This research has been supported by UK Research and Innovation (grant nos. NE/L002434/1 and S337) and the Engineering and Physical Sciences Research Council (grant no. EP/R034575/1).

6 Conclusions and outlook

"To acquire competence in the field of earthwork engineering one must live with the soil. One must love it and observe its performance not only in the laboratory but also in the field, to become familiar with those of its manifold properties that are not disclosed by boring records."

K. Terzaghi (1957)

The backscarp of the Hollin Hill Landslide Observatory, North Yorkshire, UK as seen from the sky

6.1 Summary

In recent decades, geophysical surveying has become a mainstay technique for characterising landslides, and has more recently emerged as a tool for monitoring slope processes (Hack, 2000, Jongmans and Garambois, 2007, Perrone et al., 2014, Schrott and Sass, 2008, Whiteley et al., 2019). Geophysical techniques are well suited for this purpose as they can acquire subsurface data across an entire slope concurrently. Consequently, they overcome the shortcomings in other monitoring approaches, including the surface-only observations acquired from remote sensing (Bovenga et al., 2018, Wasowski and Bovenga, 2014), and the highly local subsurface information of geotechnical point measurements and observations (Uhlemann et al., 2016b). Geophysical approaches have potential for providing data for the design and implementation of LoLEWS for mitigating landslide risk. However, their use as a tool integrated in to early warning is currently under-realised.

For slope characterisation, multi-method geophysical surveys are often integrated with remote sensing and intrusive investigations. Using multiple methods provides increased sensitivity to different subsurface properties, and reduces uncertainties in the interpretation of data (Chávez-García et al., 2021, Cody et al., 2020, Francioni et al., 2019, Kannaujiya et al., 2019, Mreyen et al., 2021, Perrone et al., 2021). A qualitative interpretation of multi-method surveys, reliant on the skill and experience of the interpreter, is still the most common approach found in the literature, typically achieved by visually comparing individual geophysical models and incorporating the information in to a ground model. Quantitative approaches to data integration, such as machine learning or petrophysical- and other joint-inversion approaches, remain more technically demanding and therefore less common in practice (Delforge et al., 2021, Grandjean et al., 2009, Mollaret et al., 2020, Wagner et al., 2019).

The field of geoelectrical monitoring, in particular electrical resistivity (ER), has undergone major developments and innovations, driven by advances in instrumentation, automated measurement scheduling, data telemetry and the linking of geoelectrical properties to geotechnical measurements (Holmes et al., 2020, Holmes et al., 2022, Loke et al., 2013, Perrone et al., 2014). The development and uptake of ER for landslide characterisation and monitoring sets a clear template for how the high spatial (and more recently, high temporal) resolutions of geophysical data acquisition can monitor time-varying processes in highly heterogeneous environments. In particular, active-source seismic methods, specifically seismic refraction (SR) and surface-wave (SW) methods can emulate these developments in ER; both SR and ER measurements are acquired using similar sensor array configurations and produce models of the subsurface at comparable resolutions and dimensions. Additionally, the measurements made by each method complement each other in terms of their sensitivity to landslide stability parameters. In the soil mechanics theory of slope stability proposed by Terzaghi (1943), effective strength, which is equal to normal stress minus the effect of pore water pressure, is the main dynamic variable controlling slope stability over time (Equation 2.1). ER and SR measurements are sensitive to changes in these parameters, although they are unable to provide direct quantities. However, the use of petrophysical relationships to translate geophysical measurements to other geotechnical parameters, such as from resistivity to moisture content (Merritt et al., 2016, Uhlemann et al., 2017) and soil suction (Boyd et al., 2019), or from seismic velocity to shear strength (L'Heureux and Long, 2017, Trafford and Long, 2020), can aid in providing more useful assessments of slope stability from geophysical measurements. Hence, there is a clear scientific basis for developing SR as a monitoring tool for landslides.

Hence, this thesis adds to the knowledge surrounding geophysical characterisation and monitoring of landslides in three main ways:, i) by addressing the knowledge gap in the use of SR as a long-term monitoring tool for landslides by presenting a 33-month monitoring campaign comprising 16 repeat SR surveys, ii) by adding to the existing case studies integrating multiple geophysical methods through novel processing approaches, in this work by using a simple machine learning algorithm, to better understand the subsurface in a more rapid and objective manner and iii) summarising the contributions that these approaches make to the wider application of LoLEWS.

In Chapter 2 of this thesis, the state-of-the-art of geophysical monitoring of moisture-induced landslides is summarised. The prominence of ER in the field due to developments in instrumentation and data processing is evidenced, and the case for integrating other approaches, in particular active seismic methods, is made. This chapter highlights three main strengths of geophysical monitoring which are, i) the high spatial resolution of measurements, ii) the high temporal resolution of measurements, and iii) the opportunities for calibrating and coupling geophysical data with other sources of environmental and geotechnical information. Challenges to future developments in geophysical monitoring identified in this chapter include i) the lack of developments in instrumentation (outside of the use of ER) required to realise remote time-lapse acquisition using other geophysical imaging methods, ii) the tendency of passive seismic monitoring approaches, which also show huge potential for landslide monitoring, to focus on retrospective analysis of past landslide failures rather than considering signals that may indicate the precursory conditions to slope failure, and iii) continued challenges in automatically acquiring, telemetering, processing and interpreting ever increasing volumes of data acquired from remote monitoring systems. The chapter concludes by highlighting the potential role that geophysical monitoring can play in LoLEWS. In response to the findings of this chapter, the remainder of the thesis is dedicated to exploring the development of active-source SR as a monitoring approach, and integrating SR with ER as a tool for slope characterisation.

Chapter 3 presents the results of a 33-month monitoring campaign, over which 16 P- and S-wave SR surveys were acquired along the same profile at the HHLO. This chapter considers three main aspects of the field campaign, including i) the practical considerations in acquiring standalone, repeated surveys in a dynamic environment, ii) developing a means of reliably inverting a time-series of SR data in the absence of true time-lapse inversion software, and iii) using the resulting dataset to explore the effects of changing moisture content on the seismic velocity of the active sliding layer at the landslide site. Analysis of the seismic velocities shows that without accurate incorporation of the topography and geophone positions for each survey in the time-series, nearly a quarter of the modelled cell velocities in a given model can have velocity errors of ±10%. The final processed time-series of the bulk velocity of the active sliding layer at the HHLO shows variations in seismic velocity of a similar order, which may have been easily masked without considering the time-varying changes in topography. Additionally, the time-series V_p/V_s ratio of the sliding layer shows a strong relationship with the moisture content, demonstrating the potential for time-lapse SR methods to monitor moisture-induced variations in elastic properties. This latter finding further bolsters the case for continued research in to integrating SR and ER methods for landslide monitoring.

In Chapter 4, SR and ER surveys are employed in a reconnaissance-style investigation of the HHLO, designed to emulate an initial survey that might be undertaken at a site with no prior knowledge from other forms of field

investigation, other than consultation with a geological map and on-site observations. The study addresses i) issues of data co-location, by using a common subsurface mesh to separately invert the individual datasets to provide co-located subsurface models, and ii) a means of producing a subsurface ground model less reliant on user input and more on identifying data relationships. To achieve the latter, the seismic and geoelectrical data are classified using a Gaussian Mixture Model (GMM), a form of machine learning that determines clusters of data with similar properties based on the distribution of the data in the parameter space. The resulting 'rapid reconnaissance model', shows strong structural and lithological similarities to the working conceptual model developed through several geophysical, geotechnical, geodetic and geomorphological surveys, but with the former costing only a fraction of the time spent in the field and with less reliance on user skill and expertise for interpretation. In addition, the clustered data correspond to variations in a borehole drilled on site at the time of the geophysical survey. Hence, this integrated approach provides both a means of undertaking a rapid reconnaissance assessment of the subsurface and objectively discretising the subsurface in to zones of contiguous properties.

Finally, Chapter 5 synthesises the results of Chapters 3 and 4, within the context of the HHLO, and secondly by identifying the benefits that geophysical characterisation and monitoring can make to operating LoLEWS. This chapter highlights how high spatial resolution geophysics can provide relevant inputs to the four main activities of establishing a slope-scale early warning system, namely: design, monitoring, forecasting and education. A conceptual framework detailing the potential contributions of geophysics to LoLEWS is devised.

In summary, this thesis demonstrates the benefits of SR characterisation and monitoring capability in the investigation of landslides. The integrated approaches in characterisation and monitoring presented here address the need to measure the processes that destabilise heterogeneous slopes at the appropriate (i.e., entire slope) scale. Geophysical investigations of landslides can provide insights to the subsurface at unprecedented spatiotemporal resolutions, bridging gaps in the current approaches taken to characterising and monitoring the subsurface. The research within this thesis lays the foundation for the development of active seismic methods as a tool to understand, monitor and mitigate the risk of slope failure. Such integrated geophysical monitoring approaches have a wide field of applicability to a range of natural landslide settings in which slowly evolving subsurface dynamics are a trigger for slope failure. Furthermore, these approaches have applicability outside the field of landslide monitoring, particularly for engineered slopes such as cuttings and embankments.

6.2 Outlook

It is clear from the research presented here, and from the numerous case studies preceding it, that seismic methods play a key role in the characterisation of landslide systems, and are particularly effective when integrated as part of a multi-method geophysical investigation (Hussain et al., 2019, Imani et al., 2021, Mreyen et al., 2021, Perrone et al., 2021, Rusydy et al., 2021, Zakaria et al., 2021). However, the pace of development in the transfer of ER from a characterisation to a monitoring technique has not been seen in the field of SR in recent years. Technical barriers to this development, such as how to deal with incorporating time-varying topography in to the processing stages, and producing a reliable, appropriately temporally constrained inversion scheme, have been addressed in this thesis. Further overarching reasons for the lack of development are primarily logistical;

the source signal (i.e., current injection) required to measure resistivity can be easily generated by field-based equipment, and measurements made automatically across many configurations of electrodes within an array without the need for manual input. In order to achieve comparable high-resolution imaging from seismic surveying, an active seismic source is required, which still relies on the manual generation of signals (i.e., seismic waves), typically made by personnel using impact sources. The location of these sources must be manually moved throughout the geophone array to build the shot density required to produce a detailed subsurface image, and the number of shots at a single location stacked to enhance signal-to-noise ratio in poor environmental conditions, such as during periods of increased wind or rain.

The research in this thesis highlights that the goals of such field campaigns (i.e., seismic wave velocity monitoring) are well-suited to monitoring landslides, but that the current field methodologies are not. The strength in ER monitoring lies partly in the remotely operated systems that allow for data to be acquired and system health to be monitored without the need to visit the field. In Chapter 3, the seismic field campaign consists of 16 individual visits to the HHLO, typically with a team of 3 – 4 people who would acquire seismic data over the course of 2 – 3 days in the field. The permanent ER system at the HHLO can acquire the same volume of data in less than an hour. Similarly, in the processing phase, the relationships between seismic velocities and key indicators of strength, such as shear strength, are still not well understood, whilst in the field of ER, the petrophysical relationships used to translate geophysical to geotechnical data have broadened the applications of the monitoring results to non-geophysicists. This has facilitated a wider acceptance and uptake of the method outside of the geophysical research community. Therefore, further research and development is needed in two main areas to bring the capability of seismic monitoring in line with current ER monitoring capability, which are i) seismic velocity – geotechnical relationships, and ii) remote seismic imaging development.

6.2.1 Seismic velocity – geotechnical relationships

In order to progress seismic velocity monitoring for landslide assessment and early warning, further research in to the relationships between seismic velocity and the geotechnical properties of rocks and soil is required. In a similar manner to the translation of resistivity to moisture content, expressing seismic velocity in terms of a parameter related to the mechanical stability of a slope, such as shear strength (L'Heureux and Long, 2017, Oh et al., 2017, Trafford and Long, 2020) or other geomechanical properties (Carrière et al., 2018), is needed. Such approaches make the data generated by geophysical monitoring more accessible and useful to fields beyond that of geophysics; as highlighted in Chapter 5, geophysical monitoring is unlikely to find significant support from non-geophysicists without this crucial data elaboration step, and this approach can only be fostered through an interdisciplinary approach to slope-scale monitoring.

As with resistivity – moisture relationships, links between seismic and geotechnical properties will be site specific, but more useful for integration in to modelling and early warning activities than geophysical measurements alone. For example, co-located measurements of hydrological properties from resistivity and mechanical properties from seismics could provide unique cell values for mesh-based finite element modelling of slope stability, rather than extrapolating values from single-point laboratory sample analysis or on site geotechnical measurements. Time-lapse implementations of these approaches will be able to move modelling

approaches toward near-real-time analysis, reducing the time window from modelling to warning. Furthermore, producing co-located subsurface images of these geotechnical properties allows time-lapse implementation of the machine learning approaches (Delforge et al., 2021) explored in this thesis, which will aid in the automated analysis of time-lapse data for assessing changes in ground conditions preceding failure. However, in order for seismic measurements to be made at comparable spatiotemporal resolutions to ER, developments in field methodologies and equipment are first required.

6.2.2 Remote seismic imaging development

Advances in acquiring seismic data to image the subsurface will significantly boost the applicability of the approach to landslide monitoring, particularly when combined with ER monitoring. Passive seismics, which do not require an active-source, have been used extensively in the study of landslides, formerly as a tool for monitoring microseismic events (Brückl and Mertl, 2006, Brückl et al., 2013, Helmstetter and Garambois, 2010, Lacroix and Helmstetter, 2011, Palis et al., 2017a, Walter et al., 2013), where increases in their count often indicate the onset of slope displacement, and more recently using methods to analyse the properties of materials before failure (Fiolleau et al., 2020, Fiolleau et al., 2021, Mainsant et al., 2012). Typically financial cost precludes the density of sensors required to produce images at a comparable resolution to ER systems, which typically utilise arrays with metre-scale separation (Holmes et al., 2020, Uhlemann et al., 2017, Supper et al., 2014, Luongo et al., 2012, Gance et al., 2016). In near-surface geophysical surveying, the multi-channel analysis of surface waves (MASW) technique is used to image the subsurface using passive seismic signals, although these passive surveys are less common than their active-source equivalents (Craig et al., 2021). However, the passive MASW approach is still more commonly found in standalone surveys rather than in semi-permanent deployments as a monitoring tool, as geophone arrays and their controllers are rarely designed to be deployed to the field for long periods.

Despite the limitations imposed by equipment expense or a lack of design for long-term deployment, if the need for personnel to visit the field to generate seismic signals can be removed this will significantly reduce some of the logistical barriers to implementing SR and SW monitoring approaches. One solution is to utilise passive seismic (i.e., ambient noise) sources, which are increasingly used for investigating, monitoring and imaging the subsurface (Le Breton et al., 2021). However, long-term use of these approaches relies heavily on the presence, persistence and consistency of appropriate noise (Mainsant et al., 2012), with fluctuations in these parameters hampering monitoring capability. One alternative is to use permanently deployed seismic sources, which have the advantage of being specified in terms of their timing, duration and frequency-content when operating (Cheng et al., 2021, Ikeda et al., 2018). However, this adds expense and further considerations in terms of power consumption to the field deployment phase.

Regardless of whether the sources utilised for imaging are generated by passive sources or by remote-active sources, use of either approach will significantly increase the temporal resolutions at which seismic images can be generated from weeks, as seen in this thesis, to hours or even near-continuously (Hanafy et al., 2021). Such approaches have also been made possible by moves toward lowering the cost and power requirements of seismometers in recent years, making a high-density deployment of sensors feasible. In addition, a particularly promising emerging technology is that of distributed acoustic sensing (DAS) systems which utilise fibre optic

cable to record seismic signals (in addition to strain and temperature measurements in some systems). Such systems have the capability to measure passive seismic signals at comparable spatiotemporal resolutions to ER systems, consequently making them a highly relevant technology for landslide monitoring (Ajo-Franklin et al., 2019), and a potentially important tool for developing integrated geophysical monitoring systems in the future.

7 References

Acerra, C., Alguacil, G., Atakan, K., Azzara, R., Bard, P.-Y., Blarel, F., Borges, A., Cara, F., Teves-Costa, P., Duval, A.-M., Guillier, B., Grandison, M., Havskov, J., Ohrnberger, M., Rao, S., Theodoulidis, N., Tvedt, E., Utheim, T., Vidal, S. & Zacharopoulos, S. 2002. Site Effects Assessment Using Ambient Excitations. Institute of Solid Earth Physics, University of Bergen.

Agostini, A., Tofani, V., Nolesini, T., Gigli, G., Tanteri, L., Rosi, A., Cardellini, S. & Casagli, N. 2014. A new appraisal of the Ancona landslide based on geotechnical investigations and stability modelling. *Quarterly Journal of Engineering Geology and Hydrogeology*, 47, 29-43.

Ahrens, J., Geveci, B. & Law, C. 2005. ParaView: An End-User Tool for Large Data Visualization. *Visualization Handbook*.

Ajo-Franklin, J. B., Dou, S., Lindsey, N. J., Monga, I., Tracy, C., Robertson, M., Rodriguez Tribaldos, V., Ulrich, C., Freifeld, B., Daley, T. & Li, X. 2019. Distributed Acoustic Sensing Using Dark Fiber for Near-Surface Characterization and Broadband Seismic Event Detection. *Scientific Reports*, 9, 1328.

Al-Saigh, N. H. & Al-Dabbagh, T. H. 2010. Identification of landslide slip-surface and its shear strength: A new application for shallow seismic refraction method. *Journal of the Geological Society of India*, 76, 175-180.

Alcalde, J., Bond, C. E. & Randle, C. H. 2017. Framing bias: The effect of figure presentation on seismic interpretation. *Interpretation*, 5, T591-T605.

Amitrano, D., Gaffet, S., Malet, J.-P. & Maquaire, O. 2007. Understanding mudslides through micro-seismic monitoring: the Super-Sauze (South-East French Alps) case study. *Bulletin de la Societe Geologique de France*, 178, 149-157.

Angeli, M.-G., Pasuto, A. & Silvano, S. 2000. A critical review of landslide monitoring experiences. *Engineering Geology*, 55, 133-147.

Archie, G. E. 1942. The electrical resistivity log as an aid in determining some reservoir characteristics. *Transactions of the AIME*, 146, 54-62.

Archie, G. E. 1950. Introduction to Petrophysics of Reservoir Rocks. *AAPG Bulletin*, 34, 943-961.

Argyroudis, S. A., Mitoulis, S. A., Hofer, L., Zanini, M. A., Tubaldi, E. & Frangopol, D. M. 2020. Resilience assessment framework for critical infrastructure in a multi-hazard environment: Case study on transport assets. *Science of The Total Environment*, 714, 136854.

Arnone, E., Noto, L. V., Lepore, C. & Bras, R. L. 2011. Physically-based and distributed approach to analyze rainfall-triggered landslides at watershed scale. *Geomorphology*, 133, 121-131.

Audebert, M., Clément, R., Touze-Foltz, N., Günther, T., Moreau, S. & Duquennoi, C. 2014. Time-lapse ERT interpretation methodology for leachate injection monitoring based on multiple inversions and a clustering strategy (MICS). *Journal of Applied Geophysics*, 111, 320-333.

Baker, B. B. & Copson, E. T. 2003. *The mathematical theory of Huygens' principle*, American Mathematical Soc.

Barker, J. A. 1991. The reciprocity principle and an analytical solution for Darcian flow in a network. *Water Resources Research*, 27, 743-746.

Baroň, I. & Supper, R. 2013. Application and reliability of techniques for landslide site investigation, monitoring and early warning – outcomes from a questionnaire study. *Nat. Hazards Earth Syst. Sci.*, 13, 3157-3168.

Barton, N. 2007. *Rock Quality, Seismic Velocity, Attenuation and Anisotropy*, CRC Press.

Bell, A. F. 2018. Predictability of Landslide Timing From Quasi-Periodic Precursory Earthquakes. *Geophysical Research Letters*, 45, 1860-1869.

Bell, R., Thiebes, B., Glade, T., Vinogradov, R., Kuhlmann, H., Schauerte, W., Burghaus, S., Krummel, H., Janik, M. & Paulsen, H. 2008. The technical concept within the Integrative Landslide Early Warning System (ILEWS). *Landslides and Engineered Slopes. From the Past to the Future, Two Volumes + CD-ROM*. CRC Press.

Bensen, G. D., Ritzwoller, M. H., Barmin, M. P., Levshin, A. L., Lin, F., Moschetti, M. P., Shapiro, N. M. & Yang, Y. 2007. Processing seismic ambient noise data to obtain reliable broad-band surface wave dispersion measurements. *Geophysical Journal International*, 169, 1239-1260.

Bergamo, P., Dashwood, B., Uhlemann, S., Swift, R., Chambers, J. E., Gunn, D. A. & Donohue, S. 2016. Time-lapse monitoring of climate effects on earthworks using surface waves. *GEOPHYSICS*, 81, EN1-EN15.

Beven, K. & Westerberg, I. 2011. On red herrings and real herrings: disinformation and information in hydrological inference. *Hydrological Processes*, 25, 1676-1680.

Bhowmick, S. 2017. Role of Vp/Vs and Poisson's Ratio in the Assessment of Foundation(s) for Important Civil Structure(s). *Geotechnical and Geological Engineering*, 35, 527-534.

Bichler, A., Bobrowsky, P., Best, M., Douma, M., Hunter, J., Calvert, T. & Burns, R. 2004. Three-dimensional mapping of a landslide using a multi-geophysical approach: the Quesnel Forks landslide. *Landslides*, 1, 29-40.

Bièvre, G., Jongmans, D., Lebourg, T. & Carrière, S. 2021. Electrical resistivity monitoring of an earthslide with electrodes located outside the unstable zone (Pont-Bourquin landslide, Swiss Alps). *Near Surface Geophysics*, 19, 225-239.

Bièvre, G., Jongmans, D., Winiarski, T. & Zumbo, V. 2012. Application of geophysical measurements for assessing the role of fissures in water infiltration within a clay landslide (Trièves area, French Alps). *Hydrological Processes*, 26, 2128-2142.

Binley, A., Hubbard, S. S., Huisman, J. A., Revil, A., Robinson, D. A., Singha, K. & Slater, L. D. 2015. The emergence of hydrogeophysics for improved understanding of subsurface processes over multiple scales. *Water Resources Research*, 51, 3837-3866.

Binley, A., Ramirez, A. & Daily, W. Regularised image reconstruction of noisy electrical resistance tomography data. Proceedings of the 4th Workshop of the European Concerted Action on Process Tomography, Bergen, Norway, 1995. 6-8.

Binley, A. & Slater, L. 2020. *Resistivity and Induced Polarization: Theory and Applications to the Near-Surface Earth*, Cambridge, Cambridge University Press.

Biot, M. A. 1956. Theory of Propagation of Elastic Waves in a Fluid-Saturated Porous Solid. I. Low-Frequency Range. *The Journal of the Acoustical Society of America*, 28, 168-178.

Blazevic, L. A., Bodet, L., Pasquet, S., Linde, N., Jougnot, D. & Longuevergne, L. 2020. Time-Lapse Seismic and Electrical Monitoring of the Vadose Zone during a Controlled Infiltration Experiment at the Ploemeur Hydrological Observatory, France. *Water*, 12, 1230.

Bogaard, T. & Greco, R. 2018. Invited perspectives: Hydrological perspectives on precipitation intensity-duration thresholds for landslide initiation: proposing hydro-meteorological thresholds. *Nat. Hazards Earth Syst. Sci.*, 18, 31-39.

Bogaard, T. A. & Greco, R. 2016. Landslide hydrology: from hydrology to pore pressure. *WIREs Water*, 3, 439-459.

Boon, D. P., Chambers, J. E., Hobbs, P. R. N., Kirkham, M., Merritt, A. J., Dashwood, C., Pennington, C. & Wilby, P. R. 2015. A combined geomorphological and geophysical approach to characterising relict landslide hazard on the Jurassic Escarpments of Great Britain. *Geomorphology*, 248, 296-310.

Boschetti, F., Dentith, M. C. & List, R. D. 1996. Inversion of seismic refraction data using genetic algorithms. *GEOPHYSICS*, 61, 1715-1727.

Bovenga, F., Belmonte, A., Refice, A., Pasquariello, G., Nutricato, R., Nitti, D. O. & Chiaradia, M. T. 2018. Performance Analysis of Satellite Missions for Multi-Temporal SAR Interferometry. *Sensors (Basel, Switzerland)*, 18, 1359.

Boyd, J., Chambers, J., Wilkinson, P., Uhlemann, S., Merritt, A., Meldrum, P., Swift, R., Kirkham, M., Jones, L. & Binley, A. Linking Geoelectrical Monitoring to Shear Strength-A Tool for Improving Understanding of Slope Scale Stability. 25th European Meeting of Environmental and Engineering Geophysics, 2019. European Association of Geoscientists & Engineers, 1-5.

Boyle, A., Wilkinson, P. B., Chambers, J. E., Meldrum, P. I., Uhlemann, S. & Adler, A. 2017. Jointly reconstructing ground motion and resistivity [0.1em]for ERT-based slope stability monitoring. *Geophysical Journal International*, ggx453-ggx453.

Brückl, E., Brunner, F. K., Lang, E., Mertl, S., Müller, M. & Stary, U. 2013. The Gradenbach Observatory—monitoring deep-seated gravitational slope deformation by geodetic, hydrological, and seismological methods. *Landslides*, 10, 815-829.

Brückl, E. & Mertl, S. 2006. *Seismic Monitoring of Deep-Seated Mass Movements*.

Burkin, J. N., Lindsay, M. D., Occhipinti, S. A. & Holden, E. J. 2019. Incorporating conceptual and interpretation uncertainty to mineral prospectivity modelling. *Geoscience Frontiers*, 10, 1383-1396.

Calvello, M., Devoli, G., Freeborough, K., Gariano, S. L., Guzzetti, F., Kirschbaum, D., Nakaya, H., Robbins, J. & Stähli, M. 2020. LandAware: a new international network on Landslide Early Warning Systems. *Landslides*, 17, 2699-2702.

Carrara, A., Cardinali, M. & Guzzetti, F. 1992. Uncertainty in assessing landslide hazard and risk. *ITC Journal*, 1992-2, 172-183.

Carrara, A., Crosta, G. & Frattini, P. 2003. Geomorphological and historical data in assessing landslide hazard. *Earth Surface Processes and Landforms*, 28, 1125-1142.

Carrière, S. R., Jongmans, D., Chambon, G., Bièvre, G., Lanson, B., Bertello, L., Berti, M., Jaboyedoff, M., Malet, J. P. & Chambers, J. E. 2018. Rheological properties of clayey soils originating from flow-like landslides. *Landslides*.

Cascini, L. 2008. Applicability of landslide susceptibility and hazard zoning at different scales. *Engineering Geology*, 102, 164-177.

Chambers, J. E., Gunn, D. A., Wilkinson, P. B., Meldrum, P. I., Haslam, E., Holyoake, S., Kirkham, M., Kuras, O., Merritt, A. & Wragg, J. 2014. 4D electrical resistivity tomography monitoring of soil moisture dynamics in an operational railway embankment. *Near Surface Geophysics*, 12.

Chambers, J. E., Meldrum, P. I., Wilkinson, P. B., Gunn, D., Uhlemann, S., Kuras, O., Swift, R., Inauen, C. & Butler, S. Remote condition assessment of geotechnical assets using a new low-power ERT monitoring system. 22nd European Meeting of Environmental and Engineering Geophysics, Near Surface Geoscience 2016, 2016.

Chambers, J. E., Meldrum, P. I., Wilkinson, P. B., Ward, W., Jackson, C., Matthews, B., Joel, P., Kuras, O., Bai, L., Uhlemann, S. & Gunn, D. 2015. Spatial monitoring of groundwater drawdown and rebound associated with quarry dewatering using automated time-lapse electrical resistivity tomography and distribution guided clustering. *Engineering Geology*, 193, 412-420.

Chambers, J. E., Wilkinson, P. B., Kuras, O., Ford, J. R., Gunn, D. A., Meldrum, P. I., Pennington, C. V. L., Weller, A. L., Hobbs, P. R. N. & Ogilvy, R. D. 2011. Three-dimensional geophysical anatomy of an active landslide in Lias Group mudrocks, Cleveland Basin, UK. *Geomorphology*, 125, 472-484.

Chambers, K., Kendall, J. M., Brandsberg-Dahl, S. & Rueda, J. 2010. Testing the ability of surface arrays to monitor microseismic activity. *Geophysical Prospecting*, 58, 821-830.

Chatelain, J.-L. 2004. *GUIDELINES FOR THE IMPLEMENTATION OF THE H/V SPECTRAL RATIO TECHNIQUE ON AMBIENT VIBRATIONS*.

Chávez-García, F. J., Natarajan, T., Cárdenas-Soto, M. & Rajendran, K. 2021. Landslide characterization using active and passive seismic imaging techniques: a case study from Kerala, India. *Natural Hazards*, 105, 1623-1642.

Cheng, F., Correa, J., Dou, S., Freifeld, B., Wood, T., Nihei, K., Guerra, D., Birkholzer, J., Chi, B. & Ajo-Franklin, J. 2021. Testing of a permanent orbital surface source and distributed acoustic sensing for monitoring of unconventional reservoirs: Preliminary results from the Eagle Ford Shale. *Geophysics*, 86, P1-P12.

Church, M., Dudill, A., Venditti, J. G. & Frey, P. 2020. Are Results in Geomorphology Reproducible? *Journal of Geophysical Research: Earth Surface*, 125, e2020JF005553.

Cody, E., Draebing, D., Mccoll, S., Cook, S. & Brideau, M.-A. 2020. Geomorphology and geological controls of an active paraglacial rockslide in the New Zealand Southern Alps. *Landslides*, 17, 755-776.

Coe, J. A., Ellis, W. L., Godt, J. W., Savage, W. Z., Savage, J. E., Michael, J. A., Kibler, J. D., Powers, P. S., Lidke, D. J. & Debray, S. 2003. Seasonal movement of the Slumgullion landslide determined from Global Positioning System surveys and field instrumentation, July 1998–March 2002. *Engineering Geology*, 68, 67-101.

Colangelo, G., Lapenna, V., Perrone, A., Piscitelli, S. & Telesca, L. 2006. 2D Self-Potential tomographies for studying groundwater flows in the Varco d'Izzo landslide (Basilicata, southern Italy). *Engineering Geology*, 88, 274-286.

Craig, M. S., Hayashi, K. & Kozacı, Ö. 2021. Active and passive seismic surface wave methods for levee assessment in the Sacramento–San Joaquin Delta, California, USA. *Near Surface Geophysics*, n/a.

Craig, R. F. 2004. *Craig's Soil Mechanics, Seventh Edition*, Taylor & Francis.

Crawford, M. M. & Bryson, L. S. 2018. Assessment of active landslides using field electrical measurements. *Engineering Geology*, 233**,** 146-159.

Cruden, D. M. 1991. A simple definition of a landslide. *Bulletin of the International Association of Engineering Geology - Bulletin de l'Association Internationale de Géologie de l'Ingénieur*, 43**,** 27-29.

Cruden, D. M. & Varnes, D. J. 1996. Landslide Types and Processes.

Dahlin, T. & Zhou, B. 2004. A numerical comparison of 2D resistivity imaging with 10 electrode arrays. *Geophysical Prospecting*, 52**,** 379-398.

Daley, T. M., Solbau, R. D., Ajo-Franklin, J. B. & Benson, S. M. 2007. Continuous active-source seismic monitoring of C O2 injection in a brine aquifer. *GEOPHYSICS*, 72**,** A57-A61.

Dangeard, M., Bodet, L., Pasquet, S., Thiesson, J., Guérin, R., Jougnot, D. & Longuevergne, L. 2018. Estimating picking errors in near-surface seismic data to enable their time-lapse interpretation of hydrosystems. *Near Surface Geophysics*, 16**,** 613-625.

Dangeard, M., Rivière, A., Bodet, L., Schneider, S., Guérin, R., Jougnot, D. & Maineult, A. 2021. River Corridor Model Constrained by Time-Lapse Seismic Acquisition. *Water Resources Research*, 57**,** e2020WR028911.

Dashwood, B., Gunn, D., Curioni, G., Inauen, C., Swift, R., Chapman, D., Royal, A., Hobbs, P., Reeves, H. & Taxil, J. 2019. Surface wave surveys for imaging ground property changes due to a leaking water pipe. *Journal of Applied Geophysics*, 103923.

Daskalakis, E., Evangelidis, C. P., Garnier, J., Melis, N. S., Papanicolaou, G. & Tsogka, C. 2016. Robust seismic velocity change estimation using ambient noise recordings. *Geophysical Journal International*, 205**,** 1926-1936.

Deekshit, V. N., Ramesh, M. V., Indukala, P. K. & Nair, G. J. Smart geophone sensor network for effective detection of landslide induced geophone signals. 2016 International Conference on Communication and Signal Processing (ICCSP), 6-8 April 2016 2016. 1565-1569.

Delay, F., Ackerer, P. & Guadagnini, A. 2011. Theoretical analysis and field evidence of reciprocity gaps during interference pumping tests. *Advances in Water Resources*, 34**,** 592-606.

Delforge, D., Watlet, A., Kaufmann, O., Van Camp, M. & Vanclooster, M. 2021. Time-series clustering approaches for subsurface zonation and hydrofacies detection using a real time-lapse electrical resistivity dataset. *Journal of Applied Geophysics*, 184**,** 104203.

Dijkstra, T. A. & Dixon, N. 2010. Climate change and slope stability in the UK: challenges and approaches. *Quarterly Journal of Engineering Geology and Hydrogeology*, 43**,** 371-385.

Dilley, M. 2005. *Natural Disaster Hotspots: A Global Risk Analysis*, World Bank.

Dinov, I. D. 2018. k-Means Clustering. *Data Science and Predictive Analytics: Biomedical and Health Applications using R*. Cham: Springer International Publishing.

Doetsch, J., Linde, N., Coscia, I., Greenhalgh, S. A. & Green, A. G. 2010. Zonation for 3D aquifer characterization based on joint inversions of multimethod crosshole geophysical data. *GEOPHYSICS*, 75**,** G53-G64.

Dou, S., Lindsey, N., Wagner, A. M., Daley, T. M., Freifeld, B., Robertson, M., Peterson, J., Ulrich, C., Martin, E. R. & Ajo-Franklin, J. B. 2017. Distributed Acoustic Sensing for Seismic Monitoring of The Near Surface: A Traffic-Noise Interferometry Case Study. *Scientific Reports*, 7**,** 11620.

Doyoro, Y. G., Chang, P.-Y., Puntu, J. M., Lin, D.-J., Van Huu, T., Rahmalia, D. A. & Shie, M.-S. 2022. A review of open software resources in python for electrical resistivity modelling. *Geoscience Letters*, 9, 3.

Dziak, J. J., Coffman, D. L., Lanza, S. T., Li, R. & Jermiin, L. S. 2020. Sensitivity and specificity of information criteria. *Brief Bioinform*, 21, 553-565.

Everett, M. E. 2013. *Near-Surface Applied Geophysics*, Cambridge University Press.

Fan, X., Dufresne, A., Whiteley, J., Yunus, A. P., Subramanian, S. S., Okeke, C. a. U., Pánek, T., Hermanns, R. L., Ming, P., Strom, A., Havenith, H.-B., Dunning, S., Wang, G. & Tacconi Stefanelli, C. 2021. Recent technological and methodological advances for the investigation of landslide dams. *Earth-Science Reviews*, 218, 103646.

Fell, R. 1994. Landslide risk assessment and acceptable risk. *Canadian Geotechnical Journal*, 31, 261-272.

Fell, R., Corominas, J., Bonnard, C., Cascini, L., Leroi, E. & Savage, W. Z. 2008. Guidelines for landslide susceptibility, hazard and risk zoning for land use planning. *Engineering Geology*, 102, 85-98.

Fiolleau, S., Jongmans, D., Bièvre, G., Chambon, G., Baillet, L. & Vial, B. 2020. Seismic characterization of a clay-block rupture in Harmalière landslide, French Western Alps. *Geophysical Journal International*, 221, 1777-1788.

Fiolleau, S., Jongmans, D., Bièvre, G., Chambon, G., Lacroix, P., Helmstetter, A., Wathelet, M. & Demierre, M. 2021. Multi-method investigation of mass transfer mechanisms in a retrogressive clayey landslide (Harmalière, French Alps). *Landslides*.

Fiorucci, M., Iannucci, R., Martino, S. & Paciello, A. 2016. DETECTION OF NANOSEISMIC EVENTS RELATED TO SLOPE INSTABILITIES IN THE QUARRY DISTRICT OF CORENO AUSONIO (ITALY). *Italian Journal of Engineering Geology and Environment*, 16, 13.

Flammer, I., Blum, A., Leiser, A. & Germann, P. 2001. Acoustic assessment of flow patterns in unsaturated soil. *Journal of Applied Geophysics*, 46, 115-128.

Fournier, A., Mosegaard, K., Omre, H., Sambridge, M. & Tenorio, L. 2013. Assessing uncertainty in geophysical problems — Introduction. *GEOPHYSICS*, 78, WB1-WB2.

Fox-Strangways, C. & Howell, H. H. 1983. *Sheet 63, York, Solid and Drift*, 1:50000. British Geological Survey.

Francioni, M., Calamita, F., Coggan, J., De Nardis, A., Eyre, M., Miccadei, E., Piacentini, T., Stead, D. & Sciarra, N. 2019. A Multi-Disciplinary Approach to the Study of Large Rock Avalanches Combining Remote Sensing, GIS and Field Surveys: The Case of the Scanno Landslide, Italy. *Remote Sensing*, 11, 1570.

Fredlund, D. G. & Xing, A. 1994. Equations for the soil-water characteristic curve. *Canadian geotechnical journal*, 31, 521-532.

Friedel, S., Thielen, A. & Springman, S. M. 2006. Investigation of a slope endangered by rainfall-induced landslides using 3D resistivity tomography and geotechnical testing. *Journal of Applied Geophysics*, 60, 100-114.

Froude, M. J. & Petley, D. N. 2018. Global fatal landslide occurrence from 2004 to 2016. *Nat. Hazards Earth Syst. Sci.*, 18, 2161-2181.

Gance, J., Bernardie, S., Grandjean, G. & Malet, J. P. 2015. Slope Mechanical Modelling: Contribution of Multi-Geophysical Imagery. *In:* LOLLINO, G., GIORDAN, D., CROSTA, G., COROMINAS, J., AZZAM, R.,

WASOWSKI, J. & SCIARRA, N. (eds.) *Engineering Geology for Society and Territory - Volume 2*. Springer International Publishing.

Gance, J., Malet, J. P., Supper, R., Sailhac, P., Ottowitz, D. & Jochum, B. 2016. Permanent electrical resistivity measurements for monitoring water circulation in clayey landslides. *Journal of Applied Geophysics*, 126, 98-115.

Gariano, S. L. & Guzzetti, F. 2016. Landslides in a changing climate. *Earth-Science Reviews*, 162, 227-252.

Gassmann, F. 1951. *Über die Elastizität Poröser Medien*.

Gauthier, T. D. 2001. Detecting Trends Using Spearman's Rank Correlation Coefficient. *Environmental Forensics*, 2, 359-362.

Geuzaine, C. & Remacle, J.-F. 2009. Gmsh: A 3-D finite element mesh generator with built-in pre- and post-processing facilities. *International Journal for Numerical Methods in Engineering*, 79, 1309-1331.

Gibson, A. D., Culshaw, M. G., Dashwood, C. & Pennington, C. V. L. 2013. Landslide management in the UK—the problem of managing hazards in a 'low-risk' environment. *Landslides*, 10, 599-610.

Gill, J. C. & Malamud, B. D. 2014. Reviewing and visualizing the interactions of natural hazards. *Reviews of Geophysics*, 52, 680-722.

Glendinning, S., Hall, J. & Manning, L. Asset-management strategies for infrastructure embankments. Proceedings of the Institution of Civil Engineers-Engineering Sustainability, 2009. Thomas Telford Ltd, 111-120.

Göktürkler, G., Balkaya, Ç. & Erhan, Z. 2008. Geophysical investigation of a landslide: The Altındağ landslide site, İzmir (western Turkey). *Journal of Applied Geophysics*, 65, 84-96.

Gomberg, J., Bodin, P., Savage, W. Z. & Jackson, M. E. 1995. Landslide faults and tectonic faults, analogs?: The Slumgullion earthflow, Colorado. *Geology*, 23, 41-44.

Gomberg, J., Schulz, W., Bodin, P. & Kean, J. 2011. Seismic and geodetic signatures of fault slip at the Slumgullion Landslide Natural Laboratory. *Journal of Geophysical Research: Solid Earth*, 116, n/a-n/a.

Grandjean, G., Cerdan, O., Richard, G., Cousin, I., Lagacherie, P., Tabbagh, A., Wesemael, B., Stevens, A., Lambot, S., Carré, F., Maftei, R.-M., Hermann, T., Thörnelöf, M., Chiarantini, L., Moretti, S., Ben-Dor, E., Viscarra Rossel, R., Mcbratney, A. & Minasny, B. 2010. *DIGISOIL: An Integrated System of Data Collection Technologies for Mapping Soil Properties*.

Grandjean, G., Hibert, C., Mathieu, F., Garel, E. & Malet, J.-P. 2009. Monitoring water flow in a clay-shale hillslope from geophysical data fusion based on a fuzzy logic approach. *Comptes Rendus Geoscience*, 341, 937-948.

Grelle, G. & Guadagno, F. M. 2009. Seismic refraction methodology for groundwater level determination: "Water seismic index". *Journal of Applied Geophysics*, 68, 301-320.

Guedes, V. J. C. B., Maciel, S. T. R. & Rocha, M. P. 2022. Refrapy: A Python program for seismic refraction data analysis. *Computers & Geosciences*, 159, 105020.

Gunn, D. A., Chambers, J. E., Dashwood, B. E., Lacinska, A., Dijkstra, T., Uhlemann, S., Swift, R., Kirkham, M., Milodowski, A., Wragg, J. & Donohue, S. 2018. Deterioration model and condition monitoring of aged railway embankment using non-invasive geophysics. *Construction and Building Materials*, 170, 668-678.

Gunn, D. A., Chambers, J. E., Hobbs, P. R. N., Ford, J. R., Wilkinson, P. B., Jenkins, G. O. & Merritt, A. 2013. Rapid observations to guide the design of systems for long-term monitoring of a complex landslide in the Upper Lias clays of North Yorkshire, UK. *Quarterly Journal of Engineering Geology and Hydrogeology*, 46, 323-336.

Guzzetti, F., Carrara, A., Cardinali, M. & Reichenbach, P. 1999. Landslide hazard evaluation: a review of current techniques and their application in a multi-scale study, Central Italy. *Geomorphology*, 31, 181-216.

Guzzetti, F., Gariano, S. L., Peruccacci, S., Brunetti, M. T., Marchesini, I., Rossi, M. & Melillo, M. 2020. Geographical landslide early warning systems. *Earth-Science Reviews*, 200, 102973.

Guzzetti, F., Mondini, A. C., Cardinali, M., Fiorucci, F., Santangelo, M. & Chang, K.-T. 2012. Landslide inventory maps: New tools for an old problem. *Earth-Science Reviews*, 112, 42-66.

Hack, R. 2000. Geophysics For Slope Stability. *Surveys in Geophysics*, 21, 423-448.

Hadamard, J. 1902. Sur les problèmes aux dérivées partielles et leur signification physique. *Princeton university bulletin*, 49-52.

Hagedoorn, J. G. 1959. THE PLUS-MINUS METHOD OF INTERPRETING SEISMIC REFRACTION SECTIONS*. *Geophysical Prospecting*, 7, 158-182.

Haines, A. 2021. Resilience of rail infrastructure: Update report to the Secretary of State for Transport following the derailment at Carmont, near Stonehaven. Network Rail Infrastructure Ltd.

Hanafy, S. M., Hoteit, H., Li, J. & Schuster, G. T. 2021. Near-surface real-time seismic imaging using parsimonious interferometry. *Scientific Reports*, 11, 7194.

Handwerger, A. L., Roering, J. J. & Schmidt, D. A. 2013. Controls on the seasonal deformation of slow-moving landslides. *Earth and Planetary Science Letters*, 377–378, 239-247.

Haque, U., Blum, P., Da Silva, P. F., Andersen, P., Pilz, J., Chalov, S. R., Malet, J.-P., Auflič, M. J., Andres, N., Poyiadji, E., Lamas, P. C., Zhang, W., Peshevski, I., Pétursson, H. G., Kurt, T., Dobrev, N., García-Davalillo, J. C., Halkia, M., Ferri, S., Gaprindashvili, G., Engström, J. & Keellings, D. 2016. Fatal landslides in Europe. *Landslides*, 13, 1545-1554.

Harba, P. & Pilecki, Z. 2017. Assessment of time–spatial changes of shear wave velocities of flysch formation prone to mass movements by seismic interferometry with the use of ambient noise. *Landslides*, 14, 1225-1233.

Helmstetter, A. & Garambois, S. 2010. Seismic monitoring of Séchilienne rockslide (French Alps): Analysis of seismic signals and their correlation with rainfalls. *Journal of Geophysical Research: Earth Surface*, 115.

Hen-Jones, R. M., Hughes, P. N., Stirling, R. A., Glendinning, S., Chambers, J. E., Gunn, D. A. & Cui, Y. J. 2017. Seasonal effects on geophysical–geotechnical relationships and their implications for electrical resistivity tomography monitoring of slopes. *Acta Geotechnica*, 12, 1159-1173.

Hibert, C., Malet, J. P., Bourrier, F., Provost, F., Berger, F., Bornemann, P., Tardif, P. & Mermin, E. 2017. Single-block rockfall dynamics inferred from seismic signal analysis. *Earth Surf. Dynam.*, 5, 283-292.

Hilley, G. E., Bürgmann, R., Ferretti, A., Novali, F. & Rocca, F. 2004. Dynamics of Slow-Moving Landslides from Permanent Scatterer Analysis. *Science*, 304, 1952-1955.

Hobbs, P., Jones, L., Kirkham, M., Pennington, C., Morgan, D. & Dashwood, C. 2020. Coastal landslide monitoring at Aldbrough, East Riding of Yorkshire, UK. *Quarterly Journal of Engineering Geology and Hydrogeology*, 53**,** 101-116.

Hobbs, P. R. N., Entwisle, D. C., Northmore, K. J., Sumbler, M. G., Jones, L. D., Kemp, S., Self, S., Barron, M. & Meakin, J. L. 2012. Engineering geology of British rocks and soils : Lias Group. *In:* NORTHMORE, K. J. (ed.).

Holmes, J., Chambers, J., Meldrum, P., Wilkinson, P., Boyd, J., Williamson, P., Huntley, D., Sattler, K., Elwood, D., Sivakumar, V., Reeves, H. & Donohue, S. 2020. Four-dimensional electrical resistivity tomography for continuous, near-real-time monitoring of a landslide affecting transport infrastructure in British Columbia, Canada. *Near Surface Geophysics*, 18**,** 337-351.

Holmes, J., Chambers, J., Wilkinson, P., Meldrum, P., Cimpoiaşu, M., Boyd, J., Huntley, D., Williamson, P., Gunn, D., Dashwood, B., Whiteley, J., Watlet, A., Kirkham, M., Sattler, K., Elwood, D., Sivakumar, V. & Donohue, S. 2022. Application of petrophysical relationships to electrical resistivity models for assessing the stability of a landslide in British Columbia, Canada. *Engineering Geology***,** 106613.

Hruska, J. & Hubatka, F. Landslide investigation and monitoring by a high-performance ground penetrating radar system. 8th International Conference on Ground Penetrating Radar, 2000. SPIE, 6.

Hungr, O., Leroueil, S. & Picarelli, L. 2014. The Varnes classification of landslide types, an update. *Landslides*, 11**,** 167-194.

Huntley, D., Bobrowsky, P., Hendry, M., Macciotta, R., Elwood, D., Sattler, K., Best, M., Chambers, J. & Meldrum, P. 2019. Application of multi-dimensional electrical resistivity tomography datasets to investigate a very slow-moving landslide near Ashcroft, British Columbia, Canada. *Landslides*, 16**,** 1033-1042.

Huntley, D., Holmes, J., Bobrowsky, P., Chambers, J., Meldrum, P., Wilkinson, P., Donohue, S., Elwood, D., Sattler, K., Hendry, M., Macciotta, R. & Roberts, N. J. 2020. Hydrogeological and geophysical properties of the very-slow-moving Ripley Landslide, Thompson River valley, British Columbia. *Canadian Journal of Earth Sciences*, 57**,** 1371-1391.

Hussain, Y., Cardenas-Soto, M., Martino, S., Moreira, C., Borges, W., Hamza, O., Prado, R., Uagoda, R., Rodríguez-Rebolledo, J., Silva, R. C. & Martinez-Carvajal, H. 2019. Multiple Geophysical Techniques for Investigation and Monitoring of Sobradinho Landslide, Brazil. *Sustainability*, 11**,** 6672.

Hutchinson, J. N. & Bhandari, R. K. 1971. Undrained Loading, A Fundamental Mechanism of Mudflows and other Mass Movements. *Géotechnique*, 21**,** 353-358.

Ihamouten, A., Le Bastard, C., Xavier, D., Bosc, F. & Villain, G. 2016. Using machine learning algorithms to link volumetric water content to complex dielectric permittivity in a wide (33–2000 MHz) frequency band for hydraulic concretes. *Near Surface Geophysics*, 14**,** 527-536.

Ikeda, T., Tsuji, T., Nakatsukasa, M., Ban, H., Kato, A., Worth, K., White, D. & Roberts, B. 2018. Imaging and monitoring of the shallow subsurface using spatially windowed surface-wave analysis with a single permanent seismic source. *Geophysics*, 83**,** EN23-EN38.

Ilori, A. O., Okwueze, E. E. & Obianwu, V. I. 2013. Evaluating Compaction Quality Using Elastic Seismic P Wave. *Journal of Materials in Civil Engineering*, 25**,** 693-700.

Imani, P., Tian, G., Hadiloo, S. & El-Raouf, A. A. 2021. Application of combined electrical resistivity tomography (ERT) and seismic refraction tomography (SRT) methods to investigate Xiaoshan District landslide site: Hangzhou, China. *Journal of Applied Geophysics*, 184, 104236.

Imposa, S., Grassi, S., Fazio, F., Rannisi, G. & Cino, P. 2017. Geophysical surveys to study a landslide body (north-eastern Sicily). *Natural Hazards*, 86, 327-343.

Intrieri, E., Gigli, G., Casagli, N. & Nadim, F. 2013. Brief communication "Landslide Early Warning System: toolbox and general concepts". *Nat. Hazards Earth Syst. Sci.*, 13, 85-90.

Intrieri, E., Gigli, G., Mugnai, F., Fanti, R. & Casagli, N. 2012. Design and implementation of a landslide early warning system. *Engineering Geology*, 147, 124-136.

Jaboyedoff, M., Del Gaudio, V., Derron, M.-H., Grandjean, G. & Jongmans, D. 2019. Characterizing and monitoring landslide processes using remote sensing and geophysics. *Engineering Geology*, 105167.

Jaboyedoff, M., Pedrazzini, A., Loye, A., Oppikofer, T., I Pons, M. & Locat, J. 2009. Earth flow in a complex geological environment: the example of Pont Bourquin, Les Diablerets (Western Switzerland). *Landslide Processes, From Geomorphologic Mapping to Dynamic Modelling*, 131-137.

Jenkins, G. O., Jones, L. D. & Gibson, A. D. 2005. Analysis of the Hollin Hill Landslide, Low Mowthorpe, North Yorkshire; Field reconaissance survey and proposed survey recommendations. British Geological Survey.

Jibson, R. W. 1993. Predicting earthquake-induced landslide displacements using Newmark's sliding block analysis. *Transportation Research Record*.

Jomard, H., Lebourg, T., Binet, S., Tric, E. & Hernandez, M. 2007. Characterization of an internal slope movement structure by hydrogeophysical surveying. *Terra Nova*, 19, 48-57.

Jomard, H., Lebourg, T., Guglielmi, Y. & Tric, E. 2010. Electrical imaging of sliding geometry and fluids associated with a deep seated landslide (La Clapière, France). *Earth Surface Processes and Landforms*, 35, 588-599.

Jongmans, D., Baillet, L., Larose, E., Bottelin, P., Mainsant, G., Chambon, G. & Jaboyedoff, M. 2015. Application of Ambient Vibration Techniques for Monitoring the Triggering of Rapid Landslides. *In:* LOLLINO, G., GIORDAN, D., CROSTA, G., COROMINAS, J., AZZAM, R., WASOWSKI, J. & SCIARRA, N. (eds.) *Engineering Geology for Society and Territory - Volume 2*. Springer International Publishing.

Jongmans, D., Bièvre, G., Renalier, F., Schwartz, S., Beaurez, N. & Orengo, Y. 2009. Geophysical investigation of a large landslide in glaciolacustrine clays in the Trièves area (French Alps). *Engineering Geology*, 109, 45-56.

Jongmans, D. & Garambois, S. 2007. Geophysical investigation of landslides : a review. *Bulletin De La Societe Geologique De France*, 178, 101-112.

Juang, C. S., Stanley, T. A. & Kirschbaum, D. B. 2019. Using citizen science to expand the global map of landslides: Introducing the Cooperative Open Online Landslide Repository (COOLR). *PLOS ONE*, 14, e0218657.

Jung, Y. G., Kang, M. S. & Heo, J. 2014. Clustering performance comparison using K-means and expectation maximization algorithms. *Biotechnology, biotechnological equipment*, 28, S44-S48.

Kabanikhin, S. I. 2008. Definitions and examples of inverse and ill-posed problems. 16, 317-357.

Kannaujiya, S., Chattoraj, S. L., Jayalath, D., Champati Ray, P. K., Bajaj, K., Podali, S. & Bisht, M. P. S. 2019. Integration of satellite remote sensing and geophysical techniques (electrical resistivity tomography and

ground penetrating radar) for landslide characterization at Kunjethi (Kalimath), Garhwal Himalaya, India. *Natural Hazards*, 97**,** 1191-1208.

Kao, H., Kan, C.-W., Chen, R.-Y., Chang, C.-H., Rosenberger, A., Shin, T.-C., Leu, P.-L., Kuo, K.-W. & Liang, W.-T. 2012. Locating, monitoring, and characterizing typhoon-linduced landslides with real-time seismic signals. *Landslides*, 9**,** 557-563.

Kearey, P., Brooks, M. & Hill, I. 2001. *An introduction to geophysical exploration*, Malden, MA, Blackwell Science.

Khalaf, A., Camerlynck, C., Florsch, N. & Schneider, A. 2018. Development of an adaptive multi-method algorithm for automatic picking of first arrival times: application to near surface seismic data. *Near Surface Geophysics*, 16**,** 507-526.

Kirschbaum, D., Stanley, T. & Zhou, Y. 2015. Spatial and temporal analysis of a global landslide catalog. *Geomorphology*, 249**,** 4-15.

Kirschbaum, D. B., Adler, R., Hong, Y., Hill, S. & Lerner-Lam, A. 2010. A global landslide catalog for hazard applications: method, results, and limitations. *Natural Hazards*, 52**,** 561-575.

Klose, M., Maurischat, P. & Damm, B. 2016. Landslide impacts in Germany: A historical and socioeconomic perspective. *Landslides*, 13**,** 183-199.

Kremers, S., Zimmermann, K. & Fleer, A. 2015. Geophysical and Geodetical Monitoring of Slope Movements at the Three Gorges Dam Area of the Yangtze River in China. *In:* LOLLINO, G., GIORDAN, D., CROSTA, G., COROMINAS, J., AZZAM, R., WASOWSKI, J. & SCIARRA, N. (eds.) *Engineering Geology for Society and Territory - Volume 2*. Springer International Publishing.

Krzeminska, D. M., Bogaard, T. A., Malet, J. P. & Van Beek, L. P. H. 2013. A model of hydrological and mechanical feedbacks of preferential fissure flow in a slow-moving landslide. *Hydrol. Earth Syst. Sci.*, 17**,** 947-959.

Krzeminska, D. M., Bogaard, T. A., Van Asch, T. W. J. & Van Beek, L. P. H. 2012. A conceptual model of the hydrological influence of fissures on landslide activity. *Hydrol. Earth Syst. Sci.*, 16**,** 1561-1576.

Kuras, O., Pritchard, J. D., Meldrum, P. I., Chambers, J. E., Wilkinson, P. B., Ogilvy, R. D. & Wealthall, G. P. 2009. Monitoring hydraulic processes with automated time-lapse electrical resistivity tomography (ALERT). *Comptes Rendus Geoscience*, 341**,** 868-885.

L'heureux, J.-S. & Long, M. 2017. Relationship between Shear-Wave Velocity and Geotechnical Parameters for Norwegian Clays. *Journal of Geotechnical and Geoenvironmental Engineering*, 143**,** 04017013.

La Brecque, D., Daily, W. & Adkins, P. 2007. Systematic Errors In Resistivity Measurement Systems.

Lacasse, S., Nadim, F. & Kalsnes, B. 2005. Living with landslide risk. *World*.

Lacroix, P. & Helmstetter, A. 2011. Location of Seismic Signals Associated with Microearthquakes and Rockfalls on the Séchilienne Landslide, French Alps. *Bulletin of the Seismological Society of America*, 101**,** 341-353.

Le Breton, M., Bontemps, N., Guillemot, A., Baillet, L. & Larose, É. 2021. Landslide monitoring using seismic ambient noise correlation: challenges and applications. *Earth-Science Reviews*, 103518.

Le Roux, O., Jongmans, D., Kasperski, J., Schwartz, S., Potherat, P., Lebrouc, V., Lagabrielle, R. & Meric, O. 2011. Deep geophysical investigation of the large Séchilienne landslide (Western Alps, France) and calibration with geological data. *Engineering Geology*, 120**,** 18-31.

Lebourg, T., Binet, S., Tric, E., Jomard, H. & El Bedoui, S. 2005. Geophysical survey to estimate the 3D sliding surface and the 4D evolution of the water pressure on part of a deep seated landslide. *Terra Nova*, 17, 399-406.

Lebourg, T., Hernandez, M., Zerathe, S., El Bedoui, S., Jomard, H. & Fresia, B. 2010. Landslides triggered factors analysed by time lapse electrical survey and multidimensional statistical approach. *Engineering Geology*, 114, 238-250.

Lecocq, T., Caudron, C. & Brenguier, F. 2014. MSNoise, a Python Package for Monitoring Seismic Velocity Changes Using Ambient Seismic Noise. *Seismological Research Letters*, 85, 715-726.

Lehmann, P., Gambazzi, F., Suski, B., Baron, L., Askarinejad, A., Springman, S. M., Holliger, K. & Or, D. 2013. Evolution of soil wetting patterns preceding a hydrologically induced landslide inferred from electrical resistivity survey and point measurements of volumetric water content and pore water pressure. *Water Resources Research*, 49, 7992-8004.

Leroueil, S., Vaunat, J., Picarelli, L., Locat, J., Lee, H. & Faure, R. Geotechnical characterisation of slope movements. 7 International Symposium on Landslides, 1996. AA Balkema, 53-74.

Leung, T. M. 2003. Controls of traveltime data and problems of the generalized reciprocal method. *GEOPHYSICS*, 68, 1626-1632.

Loke, M. H. & Barker, R. D. 1996. Rapid least-squares inversion of apparent resistivity pseudosections by a quasi-Newton method 1. *Geophysical prospecting*, 44, 131-152.

Loke, M. H., Chambers, J. E., Rucker, D. F., Kuras, O. & Wilkinson, P. B. 2013. Recent developments in the direct-current geoelectrical imaging method. *Journal of Applied Geophysics*, 95, 135-156.

Loke, M. H., Wilkinson, P. B. & Chambers, J. E. 2010. Fast computation of optimized electrode arrays for 2D resistivity surveys. *Computers & Geosciences*, 36, 1414-1426.

Loke, M. H., Wilkinson, P. B., Chambers, J. E. & Meldrum, P. I. 2017. Rapid inversion of data from 2D resistivity surveys with electrode displacements. *Geophysical Prospecting*, n/a-n/a.

Lotti, A., Saccorotti, G., Fiaschi, A., Matassoni, L., Gigli, G., Pazzi, V. & Casagli, N. 2015. Seismic Monitoring of a Rockslide: The Torgiovannetto Quarry (Central Apennines, Italy). *In:* LOLLINO, G., GIORDAN, D., CROSTA, G., COROMINAS, J., AZZAM, R., WASOWSKI, J. & SCIARRA, N. (eds.) *Engineering Geology for Society and Territory - Volume 2*. Springer International Publishing.

Lu, Z. & Sabatier, J. M. 2009. Effects of Soil Water Potential and Moisture Content on Sound Speed. *Soil Science Society of America Journal*, 73, 1614-1625.

Lucas, D. R., Fankhauser, K. & Springman, S. M. 2017. Application of geotechnical and geophysical field measurements in an active alpine environment. *Engineering Geology*, 219, 32-51.

Luongo, R., Perrone, A., Piscitelli, S. & Lapenna, V. 2012. A Prototype System for Time-Lapse Electrical Resistivity Tomographies. *International Journal of Geophysics*, 2012.

Mainsant, G., Larose, E., Brönnimann, C., Jongmans, D., Michoud, C. & Jaboyedoff, M. 2012. Ambient seismic noise monitoring of a clay landslide: Toward failure prediction. *Journal of Geophysical Research: Earth Surface*, 117, n/a-n/a.

Malet, J. P., Maquaire, O. & Calais, E. 2002. The use of Global Positioning System techniques for the continuous monitoring of landslides: application to the Super-Sauze earthflow (Alpes-de-Haute-Provence, France). *Geomorphology*, 43, 33-54.

Malet, J. P., Van Asch, T. W. J., Van Beek, R. & Maquaire, O. 2005. Forecasting the behaviour of complex landslides with a spatially distributed hydrological model. *Nat. Hazards Earth Syst. Sci.*, 5, 71-85.

Manconi, A. & Giordan, D. 2015. Landslide early warning based on failure forecast models: the example of the Mt. de La Saxe rockslide, northern Italy. *Nat. Hazards Earth Syst. Sci.*, 15, 1639-1644.

Manconi, A. & Giordan, D. 2016. Landslide failure forecast in near-real-time. *Geomatics, Natural Hazards and Risk*, 7, 639-648.

Manconi, A., Picozzi, M., Coviello, V., De Santis, F. & Elia, L. 2016. Real-time detection, location, and characterization of rockslides using broadband regional seismic networks. *Geophysical Research Letters*, 43, 6960-6967.

Marino, P., Peres, D. J., Cancelliere, A., Greco, R. & Bogaard, T. A. 2020. Soil moisture information can improve shallow landslide forecasting using the hydrometeorological threshold approach. *Landslides*, 17, 2041-2054.

Martinez, K., Hart, J. K., Basford, P. J., Bragg, G. M., Ward, T. & Young, D. S. 2017. A geophone wireless sensor network for investigating glacier stick-slip motion. *Computers & Geosciences*, 105, 103-112.

Maurer, H., Curtis, A. & Boerner, D. E. 2010. Recent advances in optimized geophysical survey design. *GEOPHYSICS*, 75, 75A177-75A194.

Mavko, G., Mukerji, T. & Dvorkin, J. 2020. *The rock physics handbook*, Cambridge university press.

Mccann, D. M. & Forster, A. 1990. Reconnaissance geophysical methods in landslide investigations. *Engineering Geology*, 29, 59-78.

Mccollum, E. V. 1952. Quality of geophysical measurements. *Geophysics*, 17, 56-69.

Mcnamara, J. M., Green, R. F. & Olsson, O. 2006. Bayes' theorem and its applications in animal behaviour. *Oikos*, 112, 243-251.

Medina-Cetina, Z. & Nadim, F. 2008. Stochastic design of an early warning system. *Georisk: Assessment and Management of Risk for Engineered Systems and Geohazards*, 2, 223-236.

Merghadi, A., Yunus, A. P., Dou, J., Whiteley, J., Thaipham, B., Bui, D. T., Avtar, R. & Abderrahmane, B. 2020. Machine learning methods for landslide susceptibility studies: A comparative overview of algorithm performance. *Earth-Science Reviews*, 207, 103225.

Merritt, A. 2014. *4D geophysical monitoring of hydrogeological precursors to landslide activation.* PhD, University of Leeds.

Merritt, A. J., Chambers, J. E., Murphy, W., Wilkinson, P. B., West, L. J., Gunn, D. A., Meldrum, P. I., Kirkham, M. & Dixon, N. 2013. 3D ground model development for an active landslide in Lias mudrocks using geophysical, remote sensing and geotechnical methods. *Landslides*, 11, 537-550.

Merritt, A. J., Chambers, J. E., Murphy, W., Wilkinson, P. B., West, L. J., Uhlemann, S., Meldrum, P. I. & Gunn, D. 2018. Landslide activation behaviour illuminated by electrical resistance monitoring. *Earth Surface Processes and Landforms*, n/a-n/a.

Merritt, A. J., Chambers, J. E., Wilkinson, P. B., West, L. J., Murphy, W., Gunn, D. & Uhlemann, S. 2016. Measurement and modelling of moisture—electrical resistivity relationship of fine-grained unsaturated soils and electrical anisotropy. *Journal of Applied Geophysics*, 124, 155-165.

Moghadas, D. & Badorreck, A. 2019. Machine learning to estimate soil moisture from geophysical measurements of electrical conductivity. *Near Surface Geophysics*, 17, 181-195.

Mollaret, C., Wagner, F. M., Hilbich, C., Scapozza, C. & Hauck, C. 2020. Petrophysical joint inversion applied to alpine permafrost field sites to image subsurface ice, water, air, and rock contents. *Frontiers in Earth Science*, 8, -.

Morelli, G. & Labrecque, D. 1996. Advances in ERT inverse modeling. *European Journal of Environmental and Engineering Geophysics*, 1, 171-186.

Moser, T. J. 1991. Shortest path calculation of seismic rays. *GEOPHYSICS*, 56, 59-67.

Mreyen, A.-S., Cauchie, L., Micu, M., Onaca, A. & Havenith, H.-B. 2021. Multiple geophysical investigations to characterize massive slope failure deposits: application to the Balta rockslide, Carpathians. *Geophysical Journal International*, 225, 1032-1047.

Mulargia, F. 2001. Retrospective selection bias (or the benefit of hindsight). *Geophysical Journal International*, 146, 489-496.

Mwakanyamale, K., Slater, L., Binley, A. & Ntarlagiannis, D. 2012. Lithologic imaging using complex conductivity: Lessons learned from the Hanford 300 Area. *GEOPHYSICS*, 77, E397-E409.

Nakamura, Y. 1989. Method for dynamic characteristics estimation of subsurface using microtremor on the ground surface. *Quarterly Report of RTRI (Railway Technical Research Institute) (Japan)*, 30, 25-33.

Neath, A. A. & Cavanaugh, J. E. 2012. The Bayesian information criterion: background, derivation, and applications. *WIREs Computational Statistics*, 4, 199-203.

Niccoli, M. 2014. Geophysical tutorial. *The Leading Edge*, 33, 910-912.

O'sullivan, F. 1986. A Statistical Perspective on Ill-Posed Inverse Problems. *Statistical Science*, 1, 502-518.

Oh, T.-M., Bang, E.-S., Cho, G.-C. & Park, E.-S. 2017. Estimation of undrained shear strength for saturated clay using shear wave velocity. *Marine Georesources & Geotechnology*, 35, 236-244.

Oldenborger, G. A., Routh, P. S. & Knoll, M. D. 2005. Sensitivity of electrical resistivity tomography data to electrode position errors. *Geophysical Journal International*, 163, 1-9.

Olivier, G., Brenguier, F., De Wit, T. & Lynch, R. 2017. Monitoring the stability of tailings dam walls with ambient seismic noise. *Leading Edge*, 36, 350a1-350a6.

Öz, Y. 2015. *Engineering Seismology*.

Ozaki, Y., Mikada, H., Goto, T. N. & Takekawa, J. The 3D self-potential inversion for the estimation of hydraulic parameters. SEG Technical Program Expanded Abstracts, 2014. 4539-4543.

Palis, E., Lebourg, T., Tric, E., Malet, J.-P. & Vidal, M. 2017a. Long-term monitoring of a large deep-seated landslide (La Clapiere, South-East French Alps): initial study. *Landslides*, 14, 155-170.

Palis, E., Lebourg, T., Vidal, M., Levy, C., Tric, E. & Hernandez, M. 2017b. Multiyear time-lapse ERT to study short- and long-term landslide hydrological dynamics. *Landslides*, 14, 1333-1343.

Palmer, D. 1981. An Introduction to the generalized reciprocal method of seismic refraction interpretation. *GEOPHYSICS*, 46, 1508-1518.

Palmer, D. 2012. Uncertainty in Near-Surface Refraction Inversion. *ASEG Extended Abstracts*, 2012, 1-4.

Parasnis, D. S. 1988. Reciprocity theorems in geoelectric and geoelectromagnetic work. *Geoexploration*, 25, 177-198.

Park, C. B. & Miller, R. D. 2008. Roadside Passive Multichannel Analysis of Surface Waves (MASW). *Journal of Environmental and Engineering Geophysics*, 13, 1-11.

Parsekian, A. D., Singha, K., Minsley, B. J., Holbrook, W. S. & Slater, L. 2015. Multiscale geophysical imaging of the critical zone. *Reviews of Geophysics*, 53, 1-26.

Partsinevelos, P., Kritikakis, G., Economou, N., Agioutantis, Z., Tripolitsiotis, A., Mertikas, S. & Vafidis, A. 2016. Integration of seismic and image data processing for rockfall monitoring and early warning along transportation networks. *Natural Hazards*, 83, 133-153.

Pasquet, S., Bodet, L., Bergamo, P., Guérin, R., Martin, R., Mourgues, R. & Tournat, V. 2016a. Small-Scale Seismic Monitoring of Varying Water Levels in Granular Media. *Vadose Zone Journal*, 15.

Pasquet, S., Bodet, L., Longuevergne, L., Dhemaied, A., Camerlynck, C., Rejiba, F. & Guérin, R. 2015. 2D characterization of near-surface V‹inf›P‹/inf›/V‹inf›S‹/inf›: Surface-wave dispersion inversion versus refraction tomography. *Near Surface Geophysics*, 13, 315-331.

Pasquet, S., Holbrook, W. S., Carr, B. J. & Sims, K. W. W. 2016b. Geophysical imaging of shallow degassing in a Yellowstone hydrothermal system. *Geophysical Research Letters*, 43, 12,027-12,035.

Pazzi, V., Morelli, S. & Fanti, R. 2019. A Review of the Advantages and Limitations of Geophysical Investigations in Landslide Studies. *International Journal of Geophysics*, 2019, 1-27.

Pecoraro, G., Calvello, M. & Piciullo, L. 2019. Monitoring strategies for local landslide early warning systems. *Landslides*, 16, 213-231.

Pedregosa, F., Varoquaux, G., Gramfort, A., Michel, V., Thirion, B., Grisel, O., Blondel, M., Prettenhofer, P., Weiss, R., Dubourg, V., Vanderplas, J., Passos, A., Cournapeau, D., Brucher, M., Perrot, M. & Duchesnay, É. 2011. Scikit-learn: Machine Learning in Python. *J. Mach. Learn. Res.*, 12, 2825–2830.

Pennington, C., Boon, D. & Morgan, D. 2012. Burton Bradstock rock fall, Dorset. *BGS website*.

Pennington, C., Foster, C., Chambers, J. & Jenkins, G. 2009. Landslide Research at the British Geological Survey: Capture, Storage and Interpretation on a National and Site-Specific Scale. *Acta Geologica Sinica - English Edition*, 83, 991-999.

Pennington, C., Freeborough, K., Dashwood, C., Dijkstra, T. & Lawrie, K. 2015. The National Landslide Database of Great Britain: Acquisition, communication and the role of social media. *Geomorphology*, 249, 44-51.

Pérez-Díaz, L., Alcalde, J. & Bond, C. E. 2020. Introduction: Handling uncertainty in the geosciences: identification, mitigation and communication. *Solid Earth*, 11, 889-897.

Perrone, A., Canora, F., Calamita, G., Bellanova, J., Serlenga, V., Panebianco, S., Tragni, N., Piscitelli, S., Vignola, L., Doglioni, A., Simeone, V., Sdao, F. & Lapenna, V. 2021. A multidisciplinary approach for landslide residual risk assessment: the Pomarico landslide (Basilicata Region, Southern Italy) case study. *Landslides*, 18, 353-365.

Perrone, A., Iannuzzi, A., Lapenna, V., Lorenzo, P., Piscitelli, S., Rizzo, E. & Sdao, F. 2004. High-resolution electrical imaging of the Varco d'Izzo earthflow (southern Italy). *Journal of Applied Geophysics,* 56**,** 17-29.

Perrone, A., Lapenna, V. & Piscitelli, S. 2014. Electrical resistivity tomography technique for landslide investigation: A review. *Earth-Science Reviews,* 135**,** 65-82.

Pescaroli, G. & Alexander, D. 2015. A definition of cascading disasters and cascading effects: Going beyond the â€œtoppling dominosâ€ metaphor. *Planet@ Risk,* 3.

Petley, D. 2012. Global patterns of loss of life from landslides. *Geology,* 40**,** 927-930.

Planès, T., Mooney, M. A., Rittgers, J. B. R., Parekh, M. L., Behm, M. & Snieder, R. 2016. Time-lapse monitoring of internal erosion in earthen dams and levees using ambient seismic noise. *Géotechnique,* 66**,** 301-312.

Poli, P. 2017. Creep and slip: Seismic precursors to the Nuugaatsiaq landslide (Greenland). *Geophysical Research Letters,* 44**,** 8832-8836.

Provost, F., Hibert, C. & Malet, J. P. 2017. Automatic classification of endogenous landslide seismicity using the Random Forest supervised classifier. *Geophysical Research Letters,* 44**,** 113-120.

Rabby, Y. W. & Li, Y. 2019. An integrated approach to map landslides in Chittagong Hilly Areas, Bangladesh, using Google Earth and field mapping. *Landslides,* 16**,** 633-645.

Raharjo, W., Palupi, I. R., Nurdian, S. W., Giamboro, W. S. & Soesilo, J. 2016. Poisson's ratio analysis (Vp/Vs) on volcanoes and geothermal potential areas in Central Java using tomography travel time method of grid search relocation hypocenter. *Journal of Physics: Conference Series,* 776**,** 012114.

Rahimi, S., Wood, C. M. & Bernhardt-Barry, M. 2021. The MHVSR technique as a rapid, cost-effective, and noninvasive method for landslide investigation: case studies of Sand Gap and Ozark, AR, USA. *Landslides,* 18**,** 2705-2720.

Ramesh, M. V. 2014. Design, development, and deployment of a wireless sensor network for detection of landslides. *Ad Hoc Networks,* 13**,** Part A**,** 2-18.

Ramesh, M. V. & Rangan, V. P. 2014. Data Reduction and Energy Sustenance in Multisensor Networks for Landslide Monitoring. *IEEE Sensors Journal,* 14**,** 1555-1563.

Raykov, Y. P., Boukouvalas, A., Baig, F. & Little, M. A. 2016. What to Do When K-Means Clustering Fails: A Simple yet Principled Alternative Algorithm. *PLOS ONE,* 11**,** e0162259.

Renalier, F., Bievre, G., Jongmans, D., Campillo, M. & Bard, P. Y. 2010a. Clayey Landslide Investigations Using Active and Passive V-S Measurements. *In:* MILLER, R. D., BRADFORD, J. H. & HOLLIGER, K. (eds.) *Advances in near-Surface Seismology and Ground-Penetrating Radar.*

Renalier, F., Jongmans, D., Campillo, M. & Bard, P. Y. 2010b. Shear wave velocity imaging of the Avignonet landslide (France) using ambient noise cross correlation. *Journal of Geophysical Research: Earth Surface,* 115**,** n/a-n/a.

Rodriguez, M. Z., Comin, C. H., Casanova, D., Bruno, O. M., Amancio, D. R., Costa, L. D. F. & Rodrigues, F. A. 2019. Clustering algorithms: A comparative approach. *PLOS ONE,* 14**,** e0210236.

Romero-Ruiz, A., Linde, N., Keller, T. & Or, D. 2018. A Review of Geophysical Methods for Soil Structure Characterization. *Reviews of Geophysics,* 56**,** 672-697.

Ronczka, M., Hellman, K., Günther, T., Wisén, R. & Dahlin, T. 2017. Electric resistivity and seismic refraction tomography: a challenging joint underwater survey at Äspö Hard Rock Laboratory. *Solid Earth*, 8, 671-682.

Rosone, M., Ziccarelli, M., Ferrari, A. & Farulla, C. A. 2018. On the reactivation of a large landslide induced by rainfall in highly fissured clays. *Engineering Geology*, 235, 20-38.

Rosso, R., Rulli, M. C. & Vannucchi, G. 2006. A physically based model for the hydrologic control on shallow landsliding. *Water Resources Research*, 42, n/a-n/a.

Rowbotham, P., Kane, P. & Bentley, M. 2010. Bias in geophysical interpretation–the case for multiple deterministic scenarios. *The Leading Edge*, 29, 590-595.

Rücker, C., Günther, T. & Wagner, F. M. 2017. pyGIMLi: An open-source library for modelling and inversion in geophysics. *Computers & Geosciences*, 109, 106-123.

Rusydy, I., Fathani, T. F., Al-Huda, N., Sugiarto, Iqbal, K., Jamaluddin, K. & Meilianda, E. 2021. Integrated approach in studying rock and soil slope stability in a tropical and active tectonic country. *Environmental Earth Sciences*, 80, 58.

Safeland 2012. Deliverable 4.8: Guidelines for landslide monitoring and early warning systems in Europe - Design and required technology. *Living with landslide risk in Europe: Assessment, effects of global change, and risk management strategies.* Revision 1 ed.

Salvermoser, J., Hadziioannou, C. & Stähler, S. C. 2015. Structural monitoring of a highway bridge using passive noise recordings from street traffic. *The Journal of the Acoustical Society of America*, 138, 3864-3872.

Sambridge, M. & Drijkoningen, G. 1992. Genetic algorithms in seismic waveform inversion. *Geophysical Journal International*, 109, 323-342.

Samyn, K., Travelletti, J., Bitri, A., Grandjean, G. & Malet, J. P. 2012. Characterization of a landslide geometry using 3D seismic refraction traveltime tomography: The La Valette landslide case history. *Journal of Applied Geophysics*, 86, 120-132.

Saneiyan, S., Blanchy, G., Boyd, J. & Binley, A. 2018. *pyR2: an open-source standalone graphical user interface for inversion of electrical resistivity and induced polarization measurements*.

Sastry, R. G. & Mondal, S. K. 2013. Geophysical Characterization of the Salna Sinking Zone, Garhwal Himalaya, India. *Surveys in Geophysics*, 34, 89-119.

Scheidegger, A. E. & Willmore, P. L. 1957. THE USE OF A LEAST SQUARES METHOD FOR THE INTERPRETATION OF DATA FROM SEISMIC SURVEYS. *GEOPHYSICS*, 22, 9-21.

Schrott, L. & Sass, O. 2008. Application of field geophysics in geomorphology: Advances and limitations exemplified by case studies. *Geomorphology*, 93, 55-73.

Schwarz, G. 1978. Estimating the Dimension of a Model. *The Annals of Statistics*, 6, 461-464, 4.

Sheehan, J. R., Doll, W. E. & Mandell, W. A. 2005. An Evaluation of Methods and Available Software for Seismic Refraction Tomography Analysis. *Journal of Environmental and Engineering Geophysics*, 10, 21-34.

Skempton, A. & Hutchinson, J. Stability of natural slopes and embankment foundations. Soil Mech & Fdn Eng Conf Proc/Mexico/, 1969.

Spiker, E. C. & Gori, P. L. 2003. National landslide hazards mitigation strategy : a framework for loss reduction. *Circular.* - ed.

Springman, S. M., Thielen, A., Kienzler, P. & Friedel, S. 2013. A long-term field study for the investigation of rainfall-induced landslides. *Géotechnique*, 63**,** 1177-1193.

Stork, A. L., Allmark, C., Curtis, A., Kendall, J. M. & White, D. J. 2018. Assessing the potential to use repeated ambient noise seismic tomography to detect CO2 leaks: Application to the Aquistore storage site. *International Journal of Greenhouse Gas Control*, 71**,** 20-35.

Sun, M. & Zhang, J. 2020. The near-surface velocity reversal and its detection via unsupervised machine learning. *GEOPHYSICS*, 85**,** U55-U63.

Supper, R., Ottowitz, D., Jochum, B., Kim, J. H., Römer, A., Baron, I., Pfeiler, S., Lovisolo, M., Gruber, S. & Vecchiotti, F. 2014. Geoelectrical monitoring: An innovative method to supplement landslide surveillance and early warning. *Near Surface Geophysics*, 12**,** 133-150.

Supper, R., Romer, A., Kreuzer, G., Jochum, B., Ottowitz, D., Ita, A. & Kauer, S. 2012. *The GEOMON 4D electrical monitoring system: current state and future developments*.

Suriñach, E., Vilajosana, I., Khazaradze, G., Biescas, B., Furdada, G. & Vilaplana, J. M. 2005. Seismic detection and characterization of landslides and other mass movements. *Nat. Hazards Earth Syst. Sci.*, 5**,** 791-798.

Szalai, S. & Szarka, L. 2008. On the classification of surface geoelectric arrays. *Geophysical Prospecting*, 56**,** 159-175.

Telford, W. M., Telford, W. M., Geldart, L. P. & Sheriff, R. E. 1990. *Applied Geophysics*, Cambridge University Press.

Terzaghi, K. 1943. *Theoretical soil mechanics*, J. Wiley and Sons, inc.

Terzaghi, K., Peck, R. B., Mesri, G. & Knovel 1996. *Soil Mechanics in Engineering Practice*, Wiley.

Toll, D. G., Lourenço, S. D. N., Mendes, J., Gallipoli, D., Evans, F. D., Augarde, C. E., Cui, Y. J., Tang, A. M., Rojas, J. C., Pagano, L., Mancuso, C., Zingariello, C. & Tarantino, A. 2011. Soil suction monitoring for landslides and slopes. *Quarterly Journal of Engineering Geology and Hydrogeology*, 44**,** 23-33.

Tomás, R., Abellán, A., Cano, M., Riquelme, A., Tenza-Abril, A. J., Baeza-Brotons, F., Saval, J. M. & Jaboyedoff, M. 2018. A multidisciplinary approach for the investigation of a rock spreading on an urban slope. *Landslides*, 15**,** 199-217.

Tonnellier, A., Helmstetter, A., Malet, J.-P., Schmittbuhl, J., Corsini, A. & Joswig, M. 2013. Seismic monitoring of soft-rock landslides: the Super-Sauze and Valoria case studies. *Geophysical Journal International*, 193**,** 1515-1536.

Trafford, A. & Long, M. 2020. Relationship between Shear-Wave Velocity and Undrained Shear Strength of Peat. *Journal of Geotechnical and Geoenvironmental Engineering*, 146**,** 04020057.

Travelletti, J., Sailhac, P., Malet, J. P., Grandjean, G. & Ponton, J. 2012. Hydrological response of weathered clay-shale slopes: water infiltration monitoring with time-lapse electrical resistivity tomography. *Hydrological Processes*, 26**,** 2106-2119.

Tresoldi, G., Hojat, A., Zanzi, L. & Certo, A. 2020. Introducing G.RE.T.A. – an innovative geo-resistivimeter for long-term monitoring of earthen dams and unstable slopes. *In:* DIGHT, P. M. (ed.) *Proceedings of the 2020 International Symposium on Slope Stability in Open Pit Mining and Civil Engineering.* Online: Australian Centre for Geomechanics.

Tso, C.-H. M., Kuras, O., Wilkinson, P. B., Uhlemann, S., Chambers, J. E., Meldrum, P. I., Graham, J., Sherlock, E. F. & Binley, A. 2017. Improved characterisation and modelling of measurement errors in electrical resistivity tomography (ERT) surveys. *Journal of Applied Geophysics*, 146, 103-119.

Uhlemann, S., Chambers, J., Wilkinson, P., Maurer, H., Merritt, A., Meldrum, P., Kuras, O., Gunn, D., Smith, A. & Dijkstra, T. 2017. Four-dimensional imaging of moisture dynamics during landslide reactivation. *Journal of Geophysical Research: Earth Surface*, 122, 398-418.

Uhlemann, S., Hagedorn, S., Dashwood, B., Maurer, H., Gunn, D., Dijkstra, T. & Chambers, J. 2016a. Landslide characterization using P- and S-wave seismic refraction tomography — The importance of elastic moduli. *Journal of Applied Geophysics*, 134, 64-76.

Uhlemann, S., Smith, A., Chambers, J., Dixon, N., Dijkstra, T., Haslam, E., Meldrum, P., Merritt, A., Gunn, D. & Mackay, J. 2016b. Assessment of ground-based monitoring techniques applied to landslide investigations. *Geomorphology*, 253, 438-451.

Uhlemann, S., Wilkinson, P. B., Chambers, J. E., Maurer, H., Merritt, A. J., Gunn, D. A. & Meldrum, P. I. 2015. Interpolation of landslide movements to improve the accuracy of 4D geoelectrical monitoring. *Journal of Applied Geophysics*, 121, 93-105.

Uyanık, O. 2011. The porosity of saturated shallow sediments from seismic compressional and shear wave velocities. *Journal of Applied Geophysics*, 73, 16-24.

Van Asch, T. W. J., Malet, J.-P., Van Beek, L. P. H. & Amitrano, D. 2007a. Techniques, issues and advances in numerical modelling of landslide hazard. *Bulletin de la Societe Geologique de France*, 178, 65-88.

Van Asch, T. W. J., Malet, J.-P., Van Beek, L. P. H. & Amitrano, D. 2007b. Techniques, issues and advances in numerical modelling of landslide hazard. *Bulletin de la Société Géologique de France*, 178, 65-88.

Van Dam, R. L. 2012. Landform characterization using geophysics—Recent advances, applications, and emerging tools. *Geomorphology*, 137, 57-73.

Van Westen, C. J., Van Asch, T. W. J. & Soeters, R. 2006. Landslide hazard and risk zonation—why is it still so difficult? *Bulletin of Engineering Geology and the Environment*, 65, 167-184.

Vanapalli, S., Fredlund, D., Pufahl, D. & Clifton, A. 1996. Model for the prediction of shear strength with respect to soil suction. *Canadian geotechnical journal*, 33, 379-392.

Wagner, F., Mollaret, C., Günther, T., Kemna, A. & Hauck, C. 2019. Quantitative imaging of water, ice and air in permafrost systems through petrophysical joint inversion of seismic refraction and electrical resistivity data. *Geophysical Journal International*, 219, 1866-1875.

Walter, M., Arnhardt, C. & Joswig, M. 2012. Seismic monitoring of rockfalls, slide quakes, and fissure development at the Super-Sauze mudslide, French Alps. *Engineering Geology*, 128, 12-22.

Walter, M., Gomberg, J., Schulz, W., Bodin, P. & Joswig, M. 2013. Slidequake Generation versus Viscous Creep at Softrock-landslides: Synopsis of Three Different Scenarios at Slumgullion Landslide, Heumoes Slope, and Super-Sauze MudslideSlidequake Generation vs. Viscous Creep at Softrock-landslides. *Journal of Environmental and Engineering Geophysics*, 18, 269-280.

Walter, M. & Joswig, M. 2008. Seismic monitoring of fracture processes generated by a creeping landslide in the Vorarlberg Alps. *First Break*, 26.

Walter, M., Niethammer, U., Rothmund, S. & Joswig, M. 2009. Joint analysis of the Super-Sauze (French Alps) mudslide by nanoseismic monitoring and UAV-based remote sensing. *first break*, 27.

Walter, M., Walser, M. & Joswig, M. 2011. Mapping Rainfall-Triggered Slidequakes and Seismic Landslide-Volume Estimation at Heumoes Slope All rights reserved. No part of this periodical may be reproduced or transmitted in any form or by any means, electronic or mechanical, including photocopying, recording, or any information storage and retrieval system, without permission in writing from the publisher. *Vadose Zone Journal*, 10**,** 487-495.

Wapenaar, K., Draganov, D., Snieder, R., Campman, X. & Verdel, A. 2010. Tutorial on seismic interferometry: Part 1 — Basic principles and applications. *GEOPHYSICS*, 75**,** 75A195-75A209.

Ward, W. O. C., Wilkinson, P. B., Chambers, J. E., Nilsson, H., Kuras, O. & Bai, L. 2016. Tracking tracer motion in a 4-D electrical resistivity tomography experiment. *Water Resources Research*, 52**,** 4078-4094.

Ward, W. O. C., Wilkinson, P. B., Chambers, J. E., Oxby, L. S. & Bai, L. 2014. Distribution-based fuzzy clustering of electrical resistivity tomography images for interface detection. *Geophysical Journal International*, 197**,** 310-321.

Wasowski, J. & Bovenga, F. 2014. Investigating landslides and unstable slopes with satellite Multi Temporal Interferometry: Current issues and future perspectives. *Engineering Geology*, 174**,** 103-138.

Watlet, A., Thirugnanam, H., Singh, B., Kumar, N. M., Brahmanandan, D., Swift, R. T., Inauen, C., Meldrum, P., Uhlemann, S. & Wilkinson, P. B. Deployment of an electrical resistivity monitoring system to monitor a rainfall-induced landslide (Munnar, India). AGU Fall Meeting Abstracts, 2019. H14A-03.

Waxman, M. H. & Smits, L. 1968. Electrical conductivities in oil-bearing shaly sands. *Society of Petroleum Engineers Journal*, 8**,** 107-122.

White, D. J. 1989. Two-Dimensional Seismic Refraction Tomography. *Geophysical Journal International*, 97**,** 223-245.

Whiteley, J., Watlet, A., Uhlemann, S., Boyd, J. P., Wilkinson, P. B., Kendall, J. M. & Chambers, J. E. 2020a. Rapid characterization of landslide hydrogeology through simple clustering of seismic refraction and electrical resistivity surveys.

Whiteley, J., Watlet, A., Uhlemann, S., Meldrum, P., Wilkinson, P. & Chambers, J. 2021a. Recent Advances in High Spatial Resolution Geophysical Monitoring of Moisture-Induced Landslides. *In:* CASAGLI, N., TOFANI, V., SASSA, K., BOBROWSKY, P. T. & TAKARA, K. (eds.) *Understanding and Reducing Landslide Disaster Risk: Volume 3 Monitoring and Early Warning.* Cham: Springer International Publishing.

Whiteley, J. S., Chambers, J. E., Uhlemann, S., Boyd, J., Cimpoiasu, M. O., Holmes, J. L., Inauen, C. M., Watlet, A., Hawley-Sibbett, L. R., Sujitapan, C., Swift, R. T. & Kendall, J. M. 2020b. Landslide monitoring using seismic refraction tomography – The importance of incorporating topographic variations. *Engineering Geology*, 268**,** 105525.

Whiteley, J. S., Chambers, J. E., Uhlemann, S., Wilkinson, P. B. & Kendall, J. M. 2019. Geophysical Monitoring of Moisture-Induced Landslides: A Review. *Reviews of Geophysics*, 57**,** 106-145.

Whiteley, J. S., Watlet, A., Kendall, J. M. & Chambers, J. E. 2021b. Brief communication: The role of geophysical imaging in local landslide early warning systems. *Nat. Hazards Earth Syst. Sci.*, 21**,** 3863-3871.

Whiteley, J. S., Watlet, A., Uhlemann, S., Wilkinson, P., Boyd, J. P., Jordan, C., Kendall, J. M. & Chambers, J. E. 2021c. Rapid characterisation of landslide heterogeneity using unsupervised classification of electrical resistivity and seismic refraction surveys. *Engineering Geology*, 106189.

Whiteley, R. J. & Greenhalgh, S. A. 1979. Velocity inversion and the shallow seismic refraction method. *Geoexploration*, 17, 125-141.

Wilkinson, P., Chambers, J., Uhlemann, S., Meldrum, P., Smith, A., Dixon, N. & Loke, M. H. 2016. Reconstruction of landslide movements by inversion of 4-D electrical resistivity tomography monitoring data. *Geophysical Research Letters*, 43, 1166-1174.

Wilkinson, P. B., Chambers, J. E., Meldrum, P. I., Gunn, D. A., Ogilvy, R. D. & Kuras, O. 2010. Predicting the movements of permanently installed electrodes on an active landslide using time-lapse geoelectrical resistivity data only. *Geophysical Journal International*, 183, 543-556.

Wilkinson, P. B., Loke, M. H., Meldrum, P. I., Chambers, J. E., Kuras, O., Gunn, D. A. & Ogilvy, R. D. 2012. Practical aspects of applied optimized survey design for electrical resistivity tomography. *Geophysical Journal International*, 189, 428-440.

Wilkinson, P. B., Uhlemann, S., Chambers, J. E., Meldrum, P. I. & Loke, M. H. 2015. Development and testing of displacement inversion to track electrode movements on 3-D electrical resistivity tomography monitoring grids. *Geophysical Journal International*, 200, 1566-1581.

Winter, M. G., Shearer, B., Palmer, D., Peeling, D., Harmer, C. & Sharpe, J. 2016. The Economic Impact of Landslides and Floods on the Road Network. *Procedia Engineering*, 143, 1425-1434.

Wyllie, M. R. J., Gregory, A. R. & Gardner, L. W. 1956. Elastic wave velocities in heterogeneous and porous media. *Geophysics*, 21, 41-70.

Xia, K., Hilterman, F. & Hu, H. 2018. Unsupervised machine learning algorithm for detecting and outlining surface waves on seismic shot gathers. *Journal of Applied Geophysics*, 157, 73-86.

Xu, D., Hu, X.-Y., Shan, C.-L. & Li, R.-H. 2016. Landslide monitoring in southwestern China via time-lapse electrical resistivity tomography. *Applied Geophysics*, 13, 1-12.

Xu, S., Sirieix, C., Riss, J. & Malaurent, P. 2017. A clustering approach applied to time-lapse ERT interpretation — Case study of Lascaux cave. *Journal of Applied Geophysics*, 144, 115-124.

Zakaria, M. T., Mohd Muztaza, N., Zabidi, H., Salleh, A. N., Mahmud, N., Samsudin, N., Rosli, F. N., Olugbenga, A. T. & Jia, T. Y. 2021. 2-D Cross-Plot Model Analysis Using Integrated Geophysical Methods for Landslides Assessment. *Applied Sciences*, 11, 747.

Zelt, C. A., Haines, S., Powers, M. H., Sheehan, J., Rohdewald, S., Link, C., Hayashi, K., Zhao, D., Zhou, H., Burton, B. L., Petersen, U. K., Bonal, N. D. & Doll, W. E. 2013. Blind Test of Methods for Obtaining 2-D Near-Surface Seismic Velocity Models from First-Arrival Traveltimes. *Journal of Environmental and Engineering Geophysics*, 18, 183-194.

8 Appendix

8.1 Appendix A: Supplementary tables detailing the case studies identified as part of the literature review (Chapter 2).

Table A.1: Published case studies utilizing geophysical monitoring of landslides since 2006, showing details of the landslide setting of the study.

Authors	Landslide name and location	Approximate depth to slide (m bgl)	Approximate slope angle (°)	Approximate area (m^2)	Movement type (after Hungr et al., 2014)
Brückl and Mertl (2006)	Gradenbach Schober Range, Carinthia, Eastern Alps, Austria			$1.68x10^6$	Mountain slope deformation
Brückl and Mertl (2006)	Hochmais-Atemskopf Ötztaler Alpen, Tyrol, Eastern Alps, Austria			$2.82x10^6$	Mountain slope deformation
Brückl and Mertl (2006)	Niedergallmigg- Matekopf Samnaun Range, Tyrol, Eastern Alps, Austria			$2.64x10^6$	Mountain slope deformation
Colangelo et al. (2006)	Varco d'Izzo Potenza, Basilicata, Southern Apennine, Italy	15 – 25	8 – 16	$1.82x10^5$ – $5.88x10^5$	Composite rotational-translational -flow
Friedel et al. (2006)	Toessegg Banks of Rhine, Rüdlingen, Switzerland	0.6 – 1.5	20 – 30	-	Translational
Amitrano et al. (2007)	Super-Sauze Barcelonette Basin, Southeast Alps, France	5 – 10	25	-	Slide - flow
Jomard et al. (2007)	La Clapière Alpes Maritimes, France	10	40	-	Translational - rotational
Bell et al. (2008)	Lichenstein-Unterhausen Swabian Alps,south Germany				

Walter and Joswig (2008)	Heumoes Vorralberg Alps, Austria		-	$9x10^5$	Slide
Grandjean et al. (2009)	Laval Laval catchment, ORE, Draix, South French Alps	5	30	$4x10^3$	Slide-flow?
Walter et al. (2009)	Super-Sauze Barcelonette Basin, Southeast Alps, France				
Helmstetter and Garambois (2010)	Séchilienne Belledonne massif, French Alps, France	-	35 - 40	-	Rockslide
Lebourg et al. (2010)	Vence Alps Maritimes, South East France	12	12 – 14	$8.75x10^4$	Translational
Renalier et al. (2010a)	Avignonet Trièves area, French Alps, France	5 – 42	8 – 15	$1.5x10^6$	Translational - rotational
Gomberg et al. (2011)	Slumgullion San Juan mountains, Colorado, United States	20	-	$1.17x10^6$	Translational
Lacroix and Helmstetter (2011)	Séchilienne Belledonne massif, French Alps, France	-	35 - 40	-	Rockslide
Walter et al. (2011)	Heumoes Vorralberg Alps, Austria	-	-	$9x10^5$	Slide
Bièvre et al. (2012)	Avignonet Trièves area, French Alps, France	5 – 42	8 – 15	$1.5x10^6$	Translational - rotational
Luongo et al. (2012)	- Picerino region, Basilicata region, Italy	-	-	-	Translational - rotational

Mainsant et al. (2012)	Pont Bourquin Switzerland	"few metres" to 11	-	$8x10^3$ *(potentially* $3x10^4 - 4x10^4$	Active composite earthslide - earthflow
Travelletti et al. (2012)	Laval Laval catchment, ORE, Draix, South French Alps	1 – 6	32	$4x10^3$	Slide-flow?
Walter et al. (2012)	Super-Sauze Barcelonette Basin, Southeast Alps, France	5 – 10	25	-	Slide - flow
Brückl et al. (2013)	Gradenbach Schober Range, Carinthia, Eastern Alps, Austria	-	-	$1.7x10^6$	
Lehmann et al. (2013)	Controlled site Banks of Rhine, Rüdlingen, Switzerland	0.7 – 5.6	38	262.5	Slide?
Tonnellier et al. (2013)	Super-Sauze Barcelonette Basin, Southeast Alps, France	5 – 10	25	-	Slide - flow
Tonnellier et al. (2013)	Valoria Northern Appenines, Dolo River Basin, Italy	15 – 30?	-	$1.6x10^6$	Translational slide?
Walter et al. (2013)	Heumoes Vorralberg Alps, Austria		-	$9x10^5$	Slide
Walter et al. (2013)	Slumgullion San Juan mountains, Colorado, United States				
Walter et al. (2013)	Super-Sauze Barcelonette Basin, Southeast Alps, France				
Supper et al. (2014)	Ampflwang-Hausruck Ampflwang, Hausruck Hills, Austria	20 – 30	-	$4.4x10^3$	Rotational-translational

Supper et al. (2014)	Bagnaschino Torre Mondovì, Casotto Valley, Cuneo/ Piedmont Province, Italy	8	-	1.5 x 10^5	Rotational-translational
Kremers et al. (2015)	Badong China				
Jongmans et al. (2015)	Pont Bourquin Switzerland				
Gance et al. (2016)	Super-Sauze Barcelonette Basin, Southeast Alps, France	~5? "a few metres"	25	-	Slide - flow
Harba and Pilecki (2017)	Just-Tegoborze Nowy Sacz, Southern Poland	10 – 12 and 14 - 17	-	-	-
Xu et al. (2016)	Bank of Zagunao River Lixian County, Sichuan Province, China	30 – 70	25 -35	1.06x10^6	-
Imposa et al. (2017)	- Tripi, north-eastern Siciliy, Italy	3 - 4	-	2.49x10^3	Translational?
Lucas et al. (2017)	- Canton of Valais, Swiss Alps, Switzerland	1 - 3	33 - 43	-	-
Palis et al. (2017a)	La Clapière Alpes Maritimes, France	‹100-200? (Jomard et al., 2010)	-	›8x10^5	Rockslide
Palis et al. (2017b)	Vence Alps Maritimes, South East France	10 - 15	12 - 14	8.75x10^4	Translational (Lebourg et al., 2010)

Provost et al. (2017)	Super-Sauze Barcelonette Basin, Southeast Alps, France	~5? "a few metres"	25	-	Slide - flow
Uhlemann et al. (2017)	Hollin Hill North Yorkshire, UK	2 - 3	12	$3.9x10^4$	Composite earth-slide earth-flow
Crawford and Bryson, 2018	Doe Run Kentucky, USA	<8	-	$2.5x10^3$	Translational
Crawford and Bryson, 2018	Herron Hill Kentucky, USA	<3	-	$3.75x10^4$	Composite rotational transational?
Merritt et al., 2018	Hollin Hill North Yorkshire, UK	2 - 3	12	$3.9x10^4$	Composite earth-slide earth-flow

Table A.2: Published case studies utilizing geophysical monitoring of landslides since 2006, showing details of the geophysical monitoring campaign. ER = Electrical resistivity, SW = Surface wave methods, SP = Self-potential, SR = Seismic refraction, S-EDCL = continuous seismic monitoring, including use of event characterization, detection and location methods, S-H/V = Seismic monitoring utilizing horizontal-to-vertical ratio methods, S-CC = Seismic monitoring utilizing cross-correlation methods, S-ANT = Seismic monitoring utilizing ambient noise tomography methods.

Authors	Geophysical monitoring method	Monitoring type	Dimension	Monitoring period	Number of	Survey design	Notes
Brückl and Mertl (2006)	S-EDCL	Semi-permanent		15	8*		Detected, characterised and located seismic events on the slope-scale at a slowly deforming rock mass.
	S-EDCL	Semi-permanent		1	9*		
	S-EDCL	Semi-permanent		10	8*		
Brückl and Mertl (2006)	S-EDCL	Semi-permanent		?	5*		
	S-EDCL	Semi-permanent		19	2*		
	S-EDCL	Semi-permanent		5	11*		
Brückl and Mertl (2006)	S-EDCL	Semi-permanent		9	5*		
Colangelo et al. (2006)	SP	Controlled test	2D	1	8	1 x 50m profile (11 electrodes at 5m spacing	Only SP monitoring case study. Showed time-lapse SP tomograpic images indicating subsurface flow. The 24 hour monitoring period was part of a longer semi-permanent monitoring campaign.
Friedel et al. (2006)	ER	Transient	2D	336	2	1 x 24.5m profile (50 electrodes at 0.5m spcaing	Comparative analysis of ER tomographic images acquired one year apart showed influence of rainfall.

Amitrano et al. (2007)	S-H/V	Semi-permanent	1D	13	1*	1 seismometer	H/V ratio from a single seismometer shown in response to landslide movement.
Jomard et al. (2007)	ER	Controlled test	2D	2	14	1 x 141m profile (48 electrodes at 3m spacing	Time-lapse ER tomographic images showed moisture changes over period of controlled rainfall experiment.
Bell et al. (2008)							
Walter and Joswig (2008)	S-EDCL	Semi-permanent	1D	7	8	Two tripartite sensor arrays deployed in each period, comprising of 1 x 3-component sensor surrounded by 3 x 1-component sensors	Two monitoring periods in rapid succession (nine days separation) showed increase in nanoseismic activity five to 26 hours after rainfall event.
	S-EDCL	Semi-permanent		7	8		
Grandjean et al. (2009)	ER	Controlled test	2D	2.8	32	1 x 47m profile (48 electrodes at 1m spacing	Controlled rainfall experiment, presented statistical time-laspe images produced from ER and SR data. Same experiment as in (Travelletti et al., 2012).
	SR	Controlled test	2D	2.8	23	1 x 47m profile (48 geophones at 1m spacing	
Walter et al. (2009)							
Helmstetter and Garambois (2010)	S-EDCL	Semi-permanent	1D	715	45	3 x sensor arrays comprising of 6 vertical and 1 3 component arrays (all replaced by broadband sensors in 2009) and an additional 24 channel geophone array installed in 2008.	Two years of seismic event detection, classification and detection showed a weak, but significant, correlation of rockfall events with rainfall, with even 1mm of rain showing an increase in seismically-detected rockfall events, although events still occurred in the absence of rainfall.
Lebourg et al. (2010)	ER	Semi-permanent	2D	90	90	1 x 115m profile (24 electrodes at 5m spacing	Used statistical analysis of resistivity data to correlate with rainfall.

Renalier et al. (2010a)	S-CC	Semi-permanent	2D	944	2*	2 seismometers from larger array	Cross-correlation between seismometer pair demonstrated landslide movement by using seismic arrival times.
Gomberg et al. (2011)	S-EDCL	Semi-permanent	2D	9	88*		Some issues with instrument batteries in achieving full monitoring coverage with complete networ, but at least 2 days complete monitoring achieved. Determined movement occurs both seismically and aseismocally at the Slumgullion landslide.
Lacroix and Helmstetter (2011)	S-EDCL	Semi-permanent	2D	425	45	3 x sensor arrays comprising of 6 vertical and l 3 component arrays (all replaced by broadband sensors in 2009) and an additional 24 channel geophone array installed in 2008.	Focuses on locating seismic events within the Séchilienne rockslide asscoiated with rockfalls and basal movements, the latter causing microearthquakes. Some areas showed aseismic movements.
Walter et al. (2011)	S-EDCL	Semi-permanent		<28	8*	Two tripartite sensor arrays deployed, comprising of 1 x 3-component sensor surrounded by 3 x 1-component sensors	Extension of Walter and Joswig (2008). Monitoring periods of one to four weeks were undertaken in 2005, 2006, 2007 and 2008. Showed continued increase of seimsic activity five to 26 hours after rainfall events, presumed to be linked to moisture-induced failure.
	S-EDCL	Semi-permanent		<28	8*	Two tripartite sensor arrays deployed, comprising of 1 x 3-component sensor surrounded by 3 x 1-component sensors	
	S-EDCL	Semi-permanent		<28	12*	Three tripartite sensor arrays deployed, comprising of 1 x	

						3-component sensor surrounded by 3 x 1-component sensors	
	S-EDCL	Semi-permanent		<28	20*	Five tripartite sensor arrays deployed, comprising of 1 x 3-component sensor surrounded by 3 x 1-component sensors	
Bièvre et al. (2012)	ER	Transient	2D	498	4	1 x 31.5m profile (64 electrodes at 0.5m spacing	Focused on hydrological infiltration through fissures. Fissures identified through time-lapse ER tomographic images, and size of fissures over time assessed using SW methods.
	SW	Transient	1D	198	2	1 x 57.5m profile (24 geophones at 2.5m spacing	
Luongo et al. (2012)	ER	Semi-permanent	2D	146	584	1 x 47m profile (48 electrodes at 1m spacing	Preliminary study of time-lapse ER monitoring instrument on shallow landslide.
Mainsant et al. (2012)	S-CC	Semi-permanent	2D	146	2*	2 seismometers	Used cross-correlation of ambient noise records to detect relative decreases in landslide material strength before failure.
Travelletti et al. (2012)	ER	Controlled test	2D	2.8	32	1 x 47m profile (48 electrodes at 1m spacing	Identified steady-state flow conditions in a controlled rainfall experiment using time-lapse ER tomographic images, and estimated steady-state flow from ER.
Walter et al. (2012)	S-EDCL	Semi-permanent		10	16*	Four tripartite sensor arrays deployed, comprising of 1 x 3-component sensor surrounded by 3 x 1-component sensors	Discriminated between seismic events associated with rock falls, and slide movement ('slidequakes'). Slidequakes were able to be located within the moving body of the landslide, and the highest amplitude events associated with period after rainfall. Signifcant attenuation

							linked to surface fissure development.
Brückl et al. (2013)	S-EDCL	Semi-permanent	1D 2D	212	6*	6 seismometers	Used seismometers to detect seismic events associated with movement, and located events, including events preceding slope failure.
Lehmann et al. (2013)	ER	Controlled test	2D	0.625	18	1 x 47m profile (48 electrodes at 1m spacing	Two controlled rainfall experiments. Compared soil wetting as measured by sesnsors and ER measurements, and showed wetting front evolution through time-lapse images.
	ER	Controlled test	2D	3	77	1 x 47m profile (48 electrodes at 1m spacing	
Tonnellier et al. (2013)	S-EDCL	Semi-permanent		14	7*	One tripartite sensor array deployed , comprising of 1 x 3-component sensor surrounded by 6 x 1-component sensors	First period (14 days) targetted small displacements, second (28 days) targetted moderate displacements. Compared to measuremenst at Valoria (see below). Located quakes associated with moving inshearing zone. Potential slow-slip seismic noise was identified. Low-correlation between increased seismic activity and landslide acceleration, but good corrleation between increased seismic activity and heavier rainfall.
	S-EDCL	Semi-permanent		28	7*		
Tonnellier et al. (2013)	S-EDCL	Semi-permanent		10	14*	Two tripartite sensor arrays deployed , comprising of 1 x 3-component sensor surrounded by 6 x 1-component sensors	Targetted large displacements, and compared to measurements from Super-Sauze (see above). Identified events associated with material deformation. Potential slow-slip seismic noise was identified. Correlated increased seismic activity with increased acceleration of slide.
Walter et al. (2013)	S-EDCL	Semi-permanent		700	12*	Three tripartite sensor arrays deployed , comprising of 1 x 3-component sensor	Comparison of slidquake generation at three different landslide settings. Two of the sites (Super-Sauze and SLumgullion) reproduced data from previous studies, but data

						surrounded by 6 x 1-component sensors	from Heumoes is from long-term permanent array installation installed July 2008, following on from intermittent studies detailed in Walter et al. (2011). Study was able to determine conditions leading to brittle failure in several landslide settings.
Walter et al. (2013)							
Walter et al. (2013)							
Supper et al. (2014)	ER	Semi-permanent	2D	275	1650	1 x 60m profile (61 electrodes at 1m spacing	Showed time-lapse ER tomomgaphic images over periods of varying seasonal rainfall and snow melt.
Supper et al. (2014)	ER	Semi-permanent	2D	239	1434	1 x 224m profiles; varying electrode spacing (1m spacing in centre, increasing at edges	Showed time-lapse ER tomographic images of a movement event.
Kremers et al. (2015)							
Jongmans et al. (2015)							
Gance et al. (2016)	ER	Semi-permanent	2D	284	568	1 x 113m profile (93 electrodes with varying spacings of 0.5m, 1m and 2m	Used time-lapse ER tomographic images to analyse response of subsurface to two natural rainfall events, highlighting importance of thermal exchange in ER monitoring.
Harba and Pilecki (2017)	S-ANT	Transient	2D	167	12*	12 seismometers along two profiles 1 x 75m and 1 x 95m	Inverted ambient noise records to produce tomographic images of shear wave velocity. Comparative image analysis showed changes in slip surface and moisture content.

Xu et al. (2016)	ER	Transient	2D	274	6	3 x 595m profiles (120 electrodes at 5m spacing	Presented time-lapse ER tomographic images to create a hydrogeological model of landslide mass.
Imposa et al. (2017)	S-H/V	Transient	2D	1589	68	34 H/V stations across profiles	Compared H/V profile from a landslide 5 years apart to detect changes in sliding surface.
Lucas et al. (2017)	ER	Transient	2D	62	6	1 x 47m profile (48 electrodes at 1m spacing	Used time-lapse ER tomographic images to compare areas of increasing and decreasing saturation. Compared volumetric water content measured by ER and sensors, and showed slight over estimation from ER meausrements.
Palis et al. (2017a)	ER	Semi-permanent	2D	365	365	1 x 235m profile (48 electrodes at 5m spacing	Seismic monitoring focused on event classification. Apparent ER data clustered identified sliding mass.
	S-ECDL	Semi-permanent	1D	365	1*	1 seismometer	
Palis et al. (2017b)	ER	Semi-permanent	2D	3510	3510	1 x 115m profile (24 electrodes at 5m spacing	Clustered apparent ER data to look at long-term trends of different units in response to rainfall over 9.5 year period.
Provost et al. (2017)	S-EDCL	Semi-permanent		40	8*	Two tripartite sensor arrays deployed , comprising of 1 x 3-component sensor surrounded by 6 x 1-component sensors	Tested automatic classification methods for detection of events associated with movement.
	S-EDCL	Semi-permanent		21	8*		
	S-EDCL	Semi-permanent		68	8*		
Uhlemann et al. (2017)	ER	Semi-permanent	3D	1369	658	5 x 147.25m profiles (32 electrodes at 4.75m spacing and 9.75m between profiles	Presented time-lapse 3D ER tomographic images, and derived gravimetric moisture content from ER data, showing seasonal gravimetric moisture content changes.

Crawford and Bryson, 2018	ER	Transient	2D	350	5	2 x ~56.7m profiles (64 electrodes at 0.91m spacing)	Presented relative changes in resistivity linked to rainfall, and resistivity results linked to shear strength parameters; shear strength plotted to produce shear strength profile.
Crawford and Bryson, 2018	ER	Transient	2D	350	5	3 x ~62.8m profiles (69 electrodes at 0.91m spacing)	Presented relative changes in resistivity linked to rainfall, and resistivity results linked to shear strength parameters.
Merritt et al., 2018	ER	Semi-permanent	1D	1740	695	4 x time-lapse contact resistance points	Contact resistances used, extracted from larger ER monitoring array (Uhlemann et al., 2017).